INVESTIGATION OF THE IMPACTS OF BUILDING AND URBAN PARAMETERS ON URBAN HEAT ISLAND FORMATION IN ANKARA

A THESIS SUBMITTED TO
THE GRADUATE SCHOOL OF NATURAL AND APPLIED SCIENCES
OF
MIDDLE EAST TECHNICAL UNIVERSITY

BY

DİLARA ERKAYA

IN PARTIAL FULFILLMENT OF THE REQUIREMENTS
FOR
THE DEGREE OF MASTER OF SCIENCE
IN
BUILDING SCIENCE IN ARCHITECTURE

JULY 2022

Approval of the thesis:

INVESTIGATION OF THE IMPACTS OF BUILDING AND URBAN PARAMETERS ON URBAN HEAT ISLAND FORMATION IN ANKARA

submitted by **DİLARA ERKAYA** in partial fulfillment of the requirements for the degree of **Master of Science** i**n Building Science in Architecture, Middle East Technical University** by,

Prof. Dr. Halil Kalıpçılar
Dean, Graduate School of **Natural and Applied Sciences** _____

Prof. Dr. Fatma Cânâ Bilsel
Head of the Department, **Architecture** _____

Prof. Dr. Soofia Tahira Elias Ozkan
Supervisor, **Architecture, METU** _____

Examining Committee Members:

Assoc. Prof. Dr. Funda Baş Bütüner
Architecture, METU _____

Prof. Dr. Soofia Tahira Elias Ozkan
Architecture, METU _____

Prof. Dr. Neşe Dikmen
Architecture, ISUBÜ _____

Assoc. Prof. Dr. Ayşegül Tereci
Architecture, KTO Karatay University _____

Assist. Prof. Dr. Rukiye Çetin
Architecture, Yıldırım Beyazıt University _____

Date: 04.07.2022

I hereby declare that all information in this document has been obtained and presented in accordance with academic rules and ethical conduct. I also declare that, as required by these rules and conduct, I have fully cited and referenced all material and results that are not original to this work.

Name Last name: Dilara Erkaya

Signature:

ABSTRACT

INVESTIGATION OF THE IMPACTS OF BUILDING AND URBAN PARAMETERS ON
URBAN HEAT ISLAND FORMATION IN ANKARA

Erkaya, Dilara
Master of Science, Building Science in Architecture
Supervisor: Prof. Dr. Soofia Tahira Elias Ozkan

July 2022, 200 pages

As a result of the urbanization in the last few centuries, green and permeable surface areas have decreased, and surfaces covered with materials with high heat holding capacity have increased. An increase in the environmental temperature caused by excessive heat above the urban areas is called Urban Heat Island (UHI) effect. This study primarily aims to find a correlation between the microclimate change of Ankara and the change in the building and urban surface materials due to expansion of urban areas.

Within the scope of the study, 16 urban blocks with different structural and environmental characteristics were selected within the borders of Ankara. The buildings in the selected blocks and the surrounding urban elements were photographed with both digital and thermal cameras, and the albedo values of the relevant surfaces were calculated. Later, microclimate simulations of three-dimensional modeled areas were made in ENVI-met software and maps showing surface temperature, potential air temperature, wind speed and reflected shortwave radiation values were produced.

The data obtained from the simulation results were compared with the measurements made in the physical environment and it was observed that they showed consistency. According to the results, building and urban characteristics such as building heights, surface albedo values, window to wall ratio, urban layouts and environmental elements affect the microclimatic conditions. In two blocks with very similar structural features, the different urban layout of the buildings primarily changes the wind passage pattern and the wind speed. Building heights also change the wind passage pattern and the area of shadows on the ground, causing changes in sensible temperature.

As the albedo value of a material increases, the surface temperature decreases, and the use of low albedo materials reduce the ambient temperature. On the other hand, materials with low albedo value and high surface temperature have higher radiation energy to their surroundings. In addition, the presence of vegetation and water bodies reduces the potential air temperature by evaporation and absorbing the SW radiation. This effect helps to reduce the air temperature and increase the thermal comfort level of the people.

Keywords: Urban Heat Island (UHI), surface albedo, thermal imagery, ENVI-met, thermal comfort level

ÖZ

ANKARA'DA KENTSEL ISI ADASI OLUŞUMUNDA BİNA VE KENT PARAMETRELERİNİN ETKİSİNİN İNCELENMESİ

Erkaya, Dilara
Yüksek Lisans, Yapı Bilimleri, Mimarlık
Tez Yöneticisi: Prof. Dr. Soofia Tahira Elias Ozkan

Temmuz 2022, 200 sayfa

Son birkaç yüzyılda, sanayi devrimi ile göçler sonucu kırsal alanlardaki nüfus azalmış, şehirler genişlemiş ve kentleşme artmıştır. Bu artışın sonucunda, daha önce geçirgenliği olan doğal ve yeşil yüzey alanları yerine ısı tutma kapasitesi yüksek malzemelerle kaplı yüzeylerin miktarı artmıştır. Kentsel alanların üzerinde aşırı ısının neden olduğu çevre sıcaklığındaki artış Kentsel Isı Adası (KIA) etkisi olarak adlandırılır ve bu etki günümüzde insan sağlığı ve ekosistem için gezegendeki en önemli sorunlardan biridir. Bilindiği üzere son yıllarda Ankara'da da mikro iklim koşullarının değişimi yaşanmakta ve mevsimler de normal koşulların dışına çıkmaktadır. Özellikle, yaz aylarında yaşanan yüksek sıcaklıklar nedeniyle Ankara'da yaşayan insanların ısıl konfor seviyesinde düşüş olduğu gözlemlenmiştir. Bu nedenle, bu çalışma öncelikle Ankara'da gözlemlenen mikro iklim değişikliği ile kentleşmedeki artış ve yüzey malzemelerindeki değişimi arasında bir ilişki kurmayı amaçlamaktadır.

Çalışma kapsamında Ankara sınırları içerisinde farklı yapısal ve çevresel özelliklere sahip 16 adet kentsel blok seçilmiştir. Seçilen bloklardaki binalar ve çevrelerindeki kentsel ögeler hem dijital hem de termal kamera ile fotoğraflandırılmış, ilgili

yüzeylerin albedo değerleri hesaplanmıştır. Daha sonra dijital ortamda üç boyutlu modeli hazırlanan alanlara, fiziksel ortamda elde edilen ölçüm değerleri işlenmiştir. ENVI-met yazılımında bu alanların mikro iklim simülasyonları yapılmıştır ve "yüzey sıcaklığı", "potansiyel hava sıcaklığı", "rüzgâr hızı" ve "yansıyan kısa dalga radyasyonu" değerlerini gösteren haritalar üretilmiştir.

Simülasyon sonuçlarından elde edilen veriler, fiziksel ortamda yapılan ölçümlerle karşılaştırılmış ve tutarlılık gösterdiği gözlemlenmiştir. Elde edilen sonuçlara göre bina yükseklikleri, yüzey albedo değerleri, pencere/duvar oranı, bina yönelimleri ve bitki ve su varlığı gibi çevresel unsurlar mikro iklim koşullarını etkilemektedir. Örneğin, çok benzer yapısal özelliklere sahip iki blokta, binaların alanda farklı yön ve doğrultularda yerleşim göstermesi öncelikle rüzgar geçiş yönünü ve rüzgar hızını değiştirmektedir. Bina yükseklikleri de rüzgar geçiş düzenini ve zemindeki gölge alanlarını değiştirerek hissedilen sıcaklıkların değişmesine sebep olmaktadır.

Elde edilen bir diğer sonuca göre ise bir malzemenin albedo değeri arttıkça yüzey sıcaklığı düşmekte ve düşük albedo değerine sahip malzemelerin kullanılması ortam sıcaklığını düşürmektedir. Albedo değeri düşük ve yüzey sıcaklığı yüksek olan malzemeler ise çevrelerine daha yüksek radyasyon enerjisi yaymaktadır. Ek olarak, bitki ve su kaynaklarının varlığı, çevredeki ısı enerjisi sayesinde buharlaşarak ve güneşten gelen radyasyon enerjisini soğurarak ısıl konfor seviyesinde olumlu artışa sebep olurken, bu ögelerin eksikliği ise hissedilen sıcaklık miktarını artırmaktadır.

Anahtar Kelimeler: Kentsel Isı Adası (KIA), yüzey albedo değerleri, termal görüntüleme, ENVI-met, ısıl konfor seviyesi

To my beloved family and fiancé.

ACKNOWLEDGMENTS

I would like to express my deepest gratitude to my supervisor Prof. Dr. Soofia Tahira Elias Ozkan for her endless mental support and patience, especially during the pandemic. She always encourages me to make more, and she makes things look easier than they are. Her kindness and guidance made me want to keep on working and maintaining my academic life.

I am grateful to all my valuable instructors at METU for helping me find my passion in life. Thanks to them, architecture has become not only a profession for me but also an element that determines my perspective. I would like to thank Dr. Berrin Çakmaklı for supporting me while applying to Building Science Program and helping me determine my study subject.

I am also thankful that Assoc. Prof. Dr. Funda Baş Bütüner, Prof. Dr. Neşe Dikmen, Assoc. Prof. Dr. Ayşegül Tereci, and Assist. Prof. Dr. Rukiye Çetin have accepted to become my Examining Committee Members as I greatly value their opinions on this subject.

I would like to appreciate my family, especially my mother Reyhan, for believing me to be successful since my childhood. They always make me feel that I am special, and they always support me with my decisions.

Also, I would like to thank my best friends Sinem Ecevit, Çağıl Ezgi Aydemir, and Nihan Bulut for helping me when I struggled with my life. I also appreciate the support and hardwork of my best friends from METU Building Science Program: Ayşe Nihan Dağoğlu, Berkay Barış Çalışkan, Kadriye Akdemir Yılmaz and Ege Soyer. That work would not be accomplished if I had not had the people that are around me. I am grateful to each and every one of them for being there, and I know I will be there when they need me.

I am especially thankful to my fiancé Tarık Batıkan Başçıl, for being encouraging, supportive, and helpful during my studies and I am delighted for him to be in my life. He is one of the main reasons that makes me keep going on and I know his love and guidance will always make me a better person than I am.

TABLE OF CONTENTS

ABSTRACT ..... **v**

ÖZ ..... **vii**

ACKNOWLEDGMENTS ..... **xi**

TABLE OF CONTENTS ..... **xiii**

LIST OF TABLES ..... **xvii**

LIST OF FIGURES ..... **xxi**

LIST OF ABBREVIATIONS ..... **xxxiii**

CHAPTERS

1 INTRODUCTION **1**

1.1 Background Information 1

1.2 Problem Statement 2

1.3 Aim and Objectives 5

1.4 Methodology 5

1.5 Disposition 6

2 LITERATURE REVIEW **9**

2.1 Importance of the UHI Phenomenon 9

2.1.1 Negative Effects of UHI on the Ecosystem 10

2.1.2 Energy Consumption and UHI Relationship 11

2.1.3 Effects of Urban Characteristics on UHI 13

2.1.4 Land Type and Use 13

2.1.4.1 Urban Area 13

2.1.4.2 Rural Area 15

2.1.5 Site Density 15
2.1.6 Building Typology and Shading Layout 16
2.1.7 Surface Albedo 20
2.1.7.1 Vertical Surfaces 21
2.1.7.2 Horizontal Surfaces 22
2.1.8 Environmental Elements 27
2.1.8.1 Vegetation Cover 27
2.1.8.2 Water Bodies 28
2.2 Investigation Methods of UHI 28
2.2.1 Weather and Surface Temperature Observations 29
2.2.2 Thermal Camera Imagery 29
2.2.3 Environmental Conditions Simulation 30
3 MATERIALS OF RESEARCH 33
3.1 Study Area 33
3.2 Selected Urban Blocks 37
3.3 Equipment 50
3.4 Software 51
4 RESEARCH METHODOLOGY 55
4.1 Selection of the Case Study Urban Blocks 55
4.2 Albedo Calculation 59
4.3 Thermal Imagery 61
4.4 Microclimate Simulation Software 62
5 RESULTS AND DISCUSSIONS 67
5.1 Analysis of the Selected Urban Block 67

5.1.1 Analysis on Component Scale 69
5.1.2 Analysis on the Urban Scale 74
5.2 Comparison 80
5.2.1 Building Parameters 80
5.2.1.1 Building Heights 81
5.2.1.2 Facade Albedo 90
5.2.1.3 Window to Wall Ratio 100
5.2.2 Urban Parameters 106
5.2.2.1 Urban Layouts 107
5.2.2.2 Horizontal Surfaces Albedo 113
5.2.2.3 Presence of Vegetation 131
5.2.2.4 Presence of Water Body 137
6 CONCLUSION 145
REFERENCES 149
APPENDICES 155
A. Definition of Terms 155
B. Raw Data of Albedo and Temperature Values of Vertical Surfaces 156
C. Charts for Surface Albedo and Temperature 164
D. ENVI-met Microclimate Simulation Results 167

LIST OF TABLES

TABLES

Table 2.1 Different types of structure patterns and their related indicators (Malys et al., 2016)..... 18
Table 3.1. Height Classification Criteria for Study Areas 38
Table 3.2. Properties of Case Study Urban Blocks..... 38
Table 3.3. Albedo calculation formula at Microsoft Excel Software Screenshot... 53
Table 4.1 Weather data on the dates of site visits when thermal camera images and albedo measurements were taken (Data Source: https://weather.com)..... 59
Table 5.1. General Information about the Urban Block 5 - Eryaman 1..... 68
Table 5.2. Data collected on the day of measurement 69
Table 5.3. Wall albedo and temperature values for Urban Block 5 - Eryaman 1 ... 70
Table 5.4. Albedo and temperature values for different horizontal surfaces in Eryaman 1 71
Table 5.5. Albedo and temperature values for grass-covered area in Eryaman 1... 72
Table 5.6. Albedo and temperature values for asphalt in Eryaman 1 73
Table 5.7 Comparison of field parameters of Bahçelievler, Kızılay, and Eryaman 81
Table 5.8 Comparison of field qualifications of the urban blocks İşçi Blokları and Tunus Caddesi..... 91
Table 5.9 Temperature and albedo values of facades comparison between the urban blocks İşçi Blokları and Tunus Caddesi..... 92
Table 5.10. Comparison of field qualifications of Çukurambar 1 and Demetevler 96
Table 5.11. Temperature and albedo values of facades comparison between Çukurambar1 and Demetevler 97
Table 5.12. Comparison of field qualifications of the urban blocks Çukurambar 2, Mevlana Bulvarı, and Eryaman 1 101
Table 5.13. Temperatures of facades comparison among the urban blocks Çukurambar 2, Mevlana Bulvarı, and Eryaman 1..... 102

Table 5.14 Comparison of field qualifications of the urban blocks Hamamönü and İvedik 107
Table 5.15. Temperature and albedo values of facades comparison between Hamamönü and İvedik..... 108
Table 5.16. Temperature and albedo values of horizontal surfaces of Bahçelievler 114
Table 5.17. Temperature and albedo values of horizontal surfaces of Çukurambar 1 115
Table 5.18. Temperature and albedo values of ground surface materials of Çukurambar 2 116
Table 5.19. Temperature and albedo values of horizontal surfaces of Demetevler 117
Table 5.20. Temperature and albedo values of horizontal surfaces of Eryaman 1 118
Table 5.21. Temperature and albedo values of horizontal surfaces of Eryaman 1 119
Table 5.22. Temperature and albedo values of horizontal surfaces of Eryaman2. 120
Table 5.23. Temperature and albedo values of horizontal surfaces of Eryaman2. 121
Table 5.24. Temperature and albedo values of horizontal surfaces of Eskişehir Yolu 122
Table 5.25. Temperature and albedo values of horizontal surfaces of Gölbaşı 123
Table 5.26. Temperature and albedo values of horizontal surfaces of Hamamönü 124
Table 5.27. Temperature and albedo values of horizontal surfaces of İşçi Blokları 125
Table 5.28. Temperature and albedo values of horizontal surfaces of İvedik..... 126
Table 5.29. Temperature and albedo values of horizontal surfaces of Kızılay 127
Table 5.30. Temperature and albedo values of horizontal surfaces of Mevlana Bulvarı 128
Table 5.31. Temperature and albedo values of horizontal surfaces of Sincan 129
Table 5.32. Temperature and albedo values of horizontal surfaces of Tulumtaş.. 130

Table 5.33. Temperature and albedo values of horizontal surfaces of Tunus Caddesi 131
Table 5.34. Comparison of field qualifications of the urban blocks Eryaman 2 and Sincan 132
Table 5.35. Comparison of atmospheric conditions of Gölbaşı and Tulumtaş 137
Table 5.36. Comparison of field qualifications of Gölbaşı and Tulumtaş 138
Table B.1. Data of Building Facade in Bahçelievler 156
Table B.2. Data of Building Facade in Çukurambar 1 156
Table B.3. Data of Building Facade in Çukurambar 2 157
Table B.4. Data of Building Facade in Demetevler 157
Table B.5. Data of Building Facade in Eryaman 1 158
Table B.6. Data of Building Facade in Eryaman 2 158
Table B.7. Data of Building Facade in Eskişehir Yolu 159
Table B.8. Data of Building Facade in Gölbaşı 159
Table B.9. Data of Building Facade in Hamamönü 160
Table B.10. Data of Building Facade in İşçi Blokları 160
Table B.11. Data of Building Facade in İvedik 161
Table B.12. Data of Building Facade in Kızılay 161
Table B.13. Data of Building Facade in Mevlana Bulvarı 162
Table B.14. Data of Building Facade in Sincan 162
Table B.15. Data of Building Facade in Tulumtaş 163
Table B.16. Data of Building Facade in Tunus Caddesi 163
Table C.17. Albedo and Temperature Values for Horizontal Surfaces 164
Table C.18. (Continued) 165
Table C.19 Albedo and Temperature Values for Vertical Surfaces 166

LIST OF FIGURES

FIGURES

Figure 1.1. Average Temperature Anomalies Map of Türkiye for Summer 2020 (MGM, 2020) 2
Figure 1.2. Türkiye Mean Temperature Anomalies in Summer between the years 1971 and 2020. (MGM, 2020) 3
Figure 1.3. Air temperature (a), total precipitation (b), and wind (c) simulations for the city of Ankara in the year 2050 (Bilgili & Şahin, 2013) 4
Figure 2.1. Mortality estimation caused by temperature changes in the future (Heaviside, Vardoulakis & Cai, 2016) 10
Figure 2.2. "Relationship between the electrical energy consumption values and maximum air temperatures of the case study area" (Souza et al., 2009) 12
Figure 2.3. Causes of UHI (Kleerekoper et al., 2012) 14
Figure 2.4. Map of summertime UHI intensity in world cities (Manoli et al., 2019) 16
Figure 2.5. Schematic definition of sky view ratio (Ψsky=cosβ), height, and width ratios on a city canyon. (Çiçek & Doğan, 2005) 17
Figure 2.6. The average temperature in the late afternoon for different building typologies (Sailor, 1998) 17
Figure 2.7. Variations in UHI change according to the amount of vegetation density ratio (VDR), albedo cover (AL), and urban temperature (ΔT) (Kotharkar et al., 2019) 21
Figure 2.8. Visible (A) and infrared (B) images of four selected coatings (S15: uncoated tile, S7: black coating, S8, S5: white reflective coatings) (Santamouris & Yun, 2020) 23
Figure 2.9. Albedo and pavement temperature relationship (Akbari et al., 2001).. 24
Figure 2.10. Spatial distribution of the ambient temperature in the park during a typical summer day, (a) without the cool pavements and (b) with the cool pavements (Santamouris et al., 2012) 25

Figure 2.11. The solar reflectance of the conventional black asphalt and five colored asphalt samples (Synnefa et al., 2011) 26
Figure 2.12. A: Visible images of the samples B: Infrared images of the sample. (Synnefa et al., 2011)..... 26
Figure 2.13. Surface temperatures are shown along measurement lines, and roof asphalt, rock ballast, and green vegetation are compared (Chui et al., 2018). 30
Figure 2.14. The plan (left) and the 3D model (right) of the simulation area (Taleghani et al., 2021)..... 31
Figure 3.1. Location of the study area (Bilgili & Şahin, 2013)..... 34
Figure 3.2. Ankara's total population graph (left) and urban-rural population ratio change (right) (Şensoy et al., 2015)..... 35
Figure 3.3. The macroform structure of Ankara changes according to the plan periods 1924, 1990, and 2023. (Sat et al., 2017)..... 36
Figure 3.4. Cumulative change in the number of buildings in the city of Ankara between the years 2002 and 2019 (TÜİK, 2019)..... 37
Figure 3.5. Case study urban blocks indicated on the map (1-Bahçelievler, 2-Çukurambar1, 3-Çukurambar2, 4-Demetevler, 5-Eryaman1, 6-Eryaman2, 7-Eskişehir Yolu, 8-Gölbaşı, 9-Hamamönü, 10-İşçi Blokları, 11-İvedik, 12-Kızılay, 13-Mevlana Bulvarı, 14-Sincan, 15-Tulumtaş, 16-Tunus Caddesi)..... 39
Figure 3.6. Satellite Image (left) and 3D Model (right) of the selected Urban Block 1 – Bahçelievler..... 40
Figure 3.7. Satellite Image (left) and 3D Model (right) of the selected Urban Block 2 - Çukurambar 1..... 40
Figure 3.8. Satellite Image (left) and 3D Model (right) of the selected Urban Block 3 - Çukurambar 2..... 41
Figure 3.9. Satellite Image (left) and 3D Model (right) of the selected Urban Block 4 – Demetevler..... 42
Figure 3.10. Satellite Image (left) and 3D Model (right) of the selected Urban Block 5 - Eryaman 1 42

Figure 3.11. Satellite Image (left) and 3D Model (right) of the selected Urban Block 6 - Eryaman 2 43
Figure 3.12. Satellite Image (left) and 3D Model (right) of the selected Urban Block 7 - Eskişehir Yolu 44
Figure 3.13. Satellite Image (left) and 3D Model (right) of the selected Urban Block - 8 Gölbaşı 44
Figure 3.14. Satellite Image (left) and 3D Model (right) of the selected Urban Block 9 – Hamamönü 45
Figure 3.15. Satellite Image (left) and 3D Model (right) of the selected Urban Block 10 - İşçi Blokları 46
Figure 3.16. Satellite Image (left) and 3D Model (right) of the selected Urban Block 11 - İvedik 46
Figure 3.17. Satellite Image (left) and 3D Model (right) of the selected Urban Block 12 - Kızılay 47
Figure 3.18. Satellite Image (left) and 3D Model (right) of the selected Urban Block 13 - Mevlana Bulvarı 48
Figure 3.19. Satellite Image (left) and 3D Model (right) of the selected Urban Block 14 - Sincan 48
Figure 3.20. Satellite Image (left) and 3D Model (right) of the selected Urban Block 15 – Tulumtaş 49
Figure 3.21. Satellite Image (left) and 3D Model (right) of the selected Urban Block 16 – Tunus Caddesi 50
Figure 3.22. FLIR E60 Thermal Camera (Source: https://www.flir.eu/) 51
Figure 3.23. Google Earth Software User Interface Screenshot 52
Figure 3.24. ImageJ Software User Interface Screenshot 52
Figure 3.25. SketchUp Pro Software User Interface Screenshot 54
Figure 3.26. Different tabs on the ENVI-met LITE 4.4.6 Software Screenshot 54
Figure 4.1. Temperature Map Based on Digital Elevation Model (DEM) Data (Prepared by Savaş Demiröz) 56

Figure 4.2. Temperature Map Based on Real Weather Station Data (Prepared by Savaş Demiröz) 57
Figure 4.3. 2020 Population Data Based on Districts (TÜİK, 2020) - (Prepared by Savaş Demiröz) 58
Figure 4.4. Determining the mean value of white paper (241.067) and asphalt (104.591) 60
Figure 4.5. Digital image (left) and thermal image (right) of a pavement 61
Figure 4.6. Digital image (left) and thermal image (right) of a building facade 61
Figure 4.7. 3D model version of Hamamönü Block on 50x50x40 grid system on ENVI-met Software 62
Figure 4.8. ENVI-met software interface for identifying material properties for each urban block 63
Figure 4.9. General Simulation Settings Window 63
Figure 4.10. The average temperature, humidity, and radiation data recorded for the 21st of July 64
Figure 4.11. Basic Meteorological Settings Window 64
Figure 4.12. ENVI-met Leonardo User Interface for creating maps 65
Figure 5.1. Satellite Image of the selected Urban Block 5 - Eryaman 1 68
Figure 5.2. Digital (left) and thermal (right) images of the pools in Eryaman 1 74
Figure 5.3. T surface values for Eryaman-1 (°C) at 21.07.2021, 15.00.00, plan view, z=0 meters 75
Figure 5.4. Potential Air Temperature values (°C) for Eryaman-1 at 21.07.2021, 15.00.00, plan view, 2 meters above the ground 76
Figure 5.5. Potential Air Temperature values (°C) for Eryaman-1 at 21.07.2021, 15.00.00, Section AA', cut at y=118 meters 76
Figure 5.6. Wind speed values (m/s) for Eryaman-1 at 21.07.2021, 15.00.00, plan view, 2 meters above the ground 77
Figure 5.7. Wind speed values (m/s) for Eryaman-1 at 21.07.2021, 15.00.00, Section AA', cut at x=190 meters 78

Figure 5.8. Wind speed values (m/s) for Eryaman-1 at 21.07.2021, 15.00.00, Section BB', cut at x=94 meters 78
Figure 5.9. Plan view of Reflected Shortwave Radiation (W/m²) in Eryaman-1 at 21.07.2021, 15.00.00, plan view, 2 meters above the ground..... 79
Figure 5.10. Section view of Reflected Shortwave Radiation (W/m²) in Eryaman-1 at 21.07.2021, 15.00.00, Section AA', cut at y= 82 meters 80
Figure 5.11. Satellite images of the selected urban blocks in Bahçelievler (left), Kızılay (middle), and Eryaman-1 (right) 81
Figure 5.12. T surface values for Bahçelievler (°C) at 21.07.2021, 15.00.00, plan view, z=0 meters 83
Figure 5.13. T surface values for Kızılay (°C) at 21.07.2021, 15.00.00, plan view, z=0 meters 84
Figure 5.14. T surface values for Eryaman-1 (°C) at 21.07.2021, 15.00.00, plan view, z=0 meters 84
Figure 5.15. Wind speed values (m/s) for Bahçelievler at 21.07.2021, 15.00.00, plan view, z=2 meters 85
Figure 5.16. Wind speed values (m/s) for Bahçelievler at 21.07.2021, 15.00.00, Section AA', cut at x=118 meters 86
Figure 5.17. Wind speed values (m/s) for Kızılay at 21.07.2021, 15.00.00, plan view, 2 meters above the ground 87
Figure 5.18. Wind speed values (m/s) for Kızılay at 21.07.2021, 15.00.00, Section AA', cut at x=118 meters 87
Figure 5.19. Wind speed values (m/s) for Eryaman-1 at 21.07.2021, 15.00.00, plan view, 2 meters above the ground..... 88
Figure 5.20. Wind speed values (m/s) for Eryaman-1 at 21.07.2021, 15.00.00, Section AA', cut at x=190 meters 89
Figure 5.21. Wind speed values (m/s) for Eryaman-1 at 21.07.2021, 15.00.00, Section BB', cut at x=94 meters 89
Figure 5.22. Satellite images of the selected blocks in İşçi Blokları (left) and Tunus Caddesi (right)..... 90

Figure 5.23. Reflected Shortwave Radiation (W/m²) in İşçi Blokları at 21.07.2021, 15.00.00, plan view, 2 meters above the ground 93
Figure 5.24. Reflected Shortwave Radiation (W/m²) in İşçi Blokları at 21.07.2021, 15.00.00, Section AA', cut at y=90 meters 94
Figure 5.25. Reflected Shortwave Radiation (W/m²) in Tunus Caddesi at 21.07.2021, 15.00.00, plan view, 2 meters above the ground 94
Figure 5.26. Reflected Shortwave Radiation (W/m²) in Tunus Caddesi at 21.07.2021, 15.00.00, Section BB', cut at y=102 meters 95
Figure 5.27. Satellite images of the selected blocks in Çukurambar-1 (left) and Demetevler (right) 95
Figure 5.28. Reflected Shortwave Radiation (W/m²) in Çukrambar 1 at 21.07.2021, 15.00.00, plan view, 2 meters above the ground 98
Figure 5.29. Reflected Shortwave Radiation (W/m²) in Demetevler at 21.07.2021, 15.00.00, plan view, 2 meters above the ground 98
Figure 5.30. Reflected Shortwave Radiation (W/m²) in Çukurambar 1 Block at 21.07.2021, 15.00.00, Section AA', cut at y=150 meters 99
Figure 5.31. Reflected Shortwave Radiation (W/m²) in Demetevler Block at 21.07.2021, 15.00.00, Section BB', cut at y=86 meters 100
Figure 5.32. Satellite images of the selected urban blocks in Çukurambar 2 (left), Mevlana Bulvarı (middle) and Eryaman-1 (right) 100
Figure 5.33. Reflected Shortwave Radiation (W/m²) in Eryaman-1 Block at 21.07.2021, 15.00.00, plan view, 2 meters above the ground 103
Figure 5.34. Reflected Shortwave Radiation (W/m²) in Eryaman-1 Block at 21.07.2021, 15.00.00, Section AA', cut at y=86 meters 103
Figure 5.35. Reflected Shortwave Radiation (W/m²) in Mevlana Bulvarı Block at 21.07.2021, 15.00.00, plan view, 2 meters above the ground 104
Figure 5.36. Reflected Shortwave Radiation (W/m²) in Mevlana Bulvarı Block at 21.07.2021, 15.00.00, Section AA', cut at x=6 meters 105
Figure 5.37. Reflected Shortwave Radiation (W/m²) in Çukurambar-2 at 21.07.2021, 15.00.00, plan view, 2 meters above the ground 105

Figure 5.38. Reflected Shortwave Radiation (W/m²) in Çukurambar-2 at 21.07.2021, 15.00.00, Section BB', cut at x=66 meters 106
Figure 5.39. Satellite images of the selected blocks in Hamamönü (left) and İvedik (right)..... 107
Figure 5.40. T surface values for Hamamönü (°C) at 21.07.2021, 15.00.00, plan view, z=0 meters 109
Figure 5.41. T surface values for İvedik (°C) at 21.07.2021, 15.00.00, plan view, z=0 meters 110
Figure 5.42. Wind speed values (m/s) for Hamamönü at 21.07.2021, 15.00.00, plan view, z=2 meters 111
Figure 5.43. Wind speed values (m/s) for Hamamönü at 21.07.2021, 15.00.00, Section AA', cut at x=46 meters 111
Figure 5.44. Wind speed values (m/s) for İvedik at 21.07.2021, 15.00.00, plan view, z=2 meters 112
Figure 5.45. Wind speed values (m/s) for İvedik at 21.07.2021, 15.00.00, Section BB', cut at y=82 meters 112
Figure 5.46. Satellite images of the selected blocks in Eryaman-2 (left) and Sincan (right)..... 131
Figure 5.47. T surface values for Eryaman-2 (°C) at 21.07.2021, 15.00.00, plan view, z=0 meters 133
Figure 5.48. Reflected Shortwave Radiation (W/m²) in Eryaman-2 at 21.07.2021, 15.00.00, plan view, z= 3 meters 134
Figure 5.49. Reflected Shortwave Radiation (W/m²) in Eryaman-2 at 21.07.2021, 15.00.00, Section AA', cut at y= 70 meters 134
Figure 5.50. T surface values for Sincan (°C) at 21.07.2021, 15.00.00, plan view, z=0 meters 135
Figure 5.51. Reflected Shortwave Radiation (W/m²) in Sincan at 21.07.2021, 15.00.00, plan view, z= 2 meters 136
Figure 5.52. Reflected Shortwave Radiation (W/m²) in Sincan at 21.07.2021, 15.00.00, Section BB', cut at y= 82 meters 136

Figure 5.53. Satellite images of the selected blocks in Gölbaşı (left) and Tulumtaş (right) 137
Figure 5.54. T surface values for Gölbaşı (°C) at 21.07.2021, 15.00.00, plan view, z=0 meters 139
Figure 5.55. T surface values for Tulumtaş (°C) at 21.07.2021, 15.00.00, plan view, z=0 meters 140
Figure 5.56. Reflected Shortwave Radiation (W/m²) in Gölbaşı at 21.07.2021, 15.00.00, plan view, z=2 meters 141
Figure 5.57. Reflected Shortwave Radiation (W/m²) in Gölbaşı at 21.07.2021, 15.00.00, Section AA', cut at y=62 meters 141
Figure 5.58. Reflected Shortwave Radiation (W/m²) in Tulumtaş at 21.07.2021, 15.00.00, plan view, z=2 meters 142
Figure 5.59. Reflected Shortwave Radiation (W/m²) in Tulumtaş at 21.07.2021, 15.00.00, Section BB', cut at y=22 meters 142
Figure 5.60. Wind speed values (m/s) for Gölbaşı at 21.07.2021, 15.00.00, plan view, z=2 meter 143
Figure 5.61. Wind speed values (m/s) for Gölbaşı at 21.07.2021, 15.00.00, Section CC', cut at y=162 meters 143
Figure 5.62. Wind speed values (m/s) for Tulumtaş at 21.07.2021, 15.00.00, plan view, z=2 meters 144
Figure 5.63. Wind speed values (m/s) for Tulumtaş at 21.07.2021, 15.00.00, Section DD', cut at y=162 meters 144
Figure D.1. T Surface Temperature (°C) of Urban Block 1 - Bahçelivler 167
Figure D.2. T Surface Temperature (°C) of Urban Block 2 - Çukurambar 1 168
Figure D.3. T Surface Temperature (°C) of Urban Block 3 - Çukurambar 2 168
Figure D.4. T Surface Temperature (°C) of Urban Block 4 - Demetevler 169
Figure D.5. T Surface Temperature (°C) of Urban Block 5 - Eryaman 1 169
Figure D.6. T Surface Temperature (°C) of Urban Block 6 - Eryaman 2 170
Figure D.7. T Surface Temperature (°C) of Urban Block 7 - Eskişehir Yolu 170
Figure D.8. T Surface Temperature (°C) of Urban Block 8 – Gölbaşı 171

Figure D.9. T Surface Temperature (°C) of Urban Block 9 - Hamamönü 171
Figure D.10. T Surface Temperature (°C) of Urban Block 10 - İşçi Blokları 172
Figure D.11. T Surface Temperature (°C) of Urban Block 11 - İvedik 172
Figure D.12. T Surface Temperature (°C) of Urban Block 12 - Kızılay 173
Figure D.13. T Surface Temperature (°C) of Urban Block 13 - Mevlana Bulvarı 173
Figure D.14. T Surface Temperature (°C) of Urban Block 14 - Sincan 174
Figure D.15. T Surface Temperature (°C) of Urban Block 15 - Tulumtaş 174
Figure D.16. T Surface Temperature (°C) of Urban Block 16 -Tunus Caddesi ... 175
Figure D.17. Potential Air Temperature (°C) of Urban Block 1 - Bahçelievler ... 176
Figure D.18. Potential Air Temperature (°C) of Urban Block 2 - Çukurambar 1 176
Figure D.19. Potential Air Temperature (°C) of Urban Block 3 - Çukurambar 2 177
Figure D.20. Potential Air Temperature (°C) of Urban Block 4 - Demetevler..... 177
Figure D.21. Potential Air Temperature (°C) of Urban Block 5 - Eryaman 1..... 178
Figure D.22. Potential Air Temperature (°C) of Urban Block 6 -Eryaman 2..... 178
Figure D.23. Potential Air Temperature (°C) of Urban Block 7 - Eskişehir Yolu 179
Figure D.24. Potential Air Temperature (°C) of Urban Block 8 -Gölbaşı..... 179
Figure D.25. Potential Air Temperature (°C) of Urban Block 9 - Hamamönü..... 180
Figure D.26. Potential Air Temperature (°C) of Urban Block 10 - İşçi Blokları . 180
Figure D.27. Potential Air Temperature (°C) of Urban Block 11 - İvedik 181
Figure D.28. Potential Air Temperature (°C) of Urban Block 12 - Kızılay 181
Figure D.29. Potential Air Temperature (°C) of Urban Block 13 - Mevlana 182
Figure D.30. Potential Air Temperature (°C) of Urban Block 14 - Sincan 182
Figure D.31. Potential Air Temperature (°C) of Urban Block 15 - Tulumtaş 183
Figure D.32. Potential Air Temperature (°C) of Urban Block 16 - Tunus Caddesi 183
Figure D.33. Wind Speed (m/s) of Urban Block 1 - Bahçelievler..... 184
Figure D.34. Wind Speed (m/s) of Urban Block 2 - Çukurambar 1 184
Figure D.35. Wind Speed (m/s) of Urban Block 3 - Çukurambar 2 185
Figure D.36. Wind Speed (m/s) of Urban Block 4 - Demetevler 185
Figure D.37. Wind Speed (m/s) of Urban Block 5 - Eryaman 1..... 186

Figure D.38. Wind Speed (m/s) of Urban Block 6 - Eryaman 2 186
Figure D.39. Wind Speed (m/s) of Urban Block 7 - Eskişehir Yolu..... 187
Figure D.40. Wind Speed (m/s) of Urban Block 8 - Gölbaşı 187
Figure D.41. Wind Speed (m/s) of Urban Block 9 - Hamamönü..... 188
Figure D.42. Wind Speed (m/s) of Urban Block 10 - İşçi Blokları..... 188
Figure D.43. Wind Speed (m/s) of Urban Block 11 - İvedik 189
Figure D.44. Wind Speed (m/s) of Urban Block 12 - Kızılay..... 189
Figure D.45. Wind Speed (m/s) of Urban Block 13 - Mevlana Bulvarı..... 190
Figure D.46. Wind Speed (m/s) of Urban Block 14 - Sincan..... 190
Figure D.47. Wind Speed (m/s) of Urban Block 15 - Tulumtaş 191
Figure D.48. Wind Speed (m/s) of Urban Block 16 – Tunus Caddesi 191
Figure D.49. Reflected Shortwave Radiation (W/m²) of Urban Block 1 –Bahçelievler 192
Figure D.50. Reflected Shortwave Radiation (W/m²) of Urban Block 2 - Çukurambar 1 193
Figure D.51. Reflected Shortwave Radiation (W/m²) of Urban Block 3 – Çukurambar 2 193
Figure D.52. Reflected Shortwave Radiation (W/m²) of Urban Block 4 – Demetevler 194
Figure D.53. Reflected Shortwave Radiation (W/m²) of Urban Block 5 - Eryaman 1 194
Figure D.54. Reflected Shortwave Radiation (W/m²) of Urban Block 6 - Eryaman 2 195
Figure D.55. Reflected Shortwave Radiation (W/m²) of Urban Block 7 - Eskişehir Yolu 195
Figure D.56. Reflected Shortwave Radiation (W/m²) of Urban Block 8 - Gölbaşı 196
Figure D.57. Reflected Shortwave Radiation (W/m²) of Urban Block 9 - Hamamönü 196

Figure D.58. Reflected Shortwave Radiation (W/m²) of Urban Block 10 - İşçi Blokları 197
Figure D.59. Reflected Shortwave Radiation (W/m²) of Urban Block 11 - İvedik 197
Figure D.60. Reflected Shortwave Radiation (W/m²) of Urban Block 12 - Kızılay 198
Figure D.61. Reflected Shortwave Radiation (W/m²) of Urban Block 13 – Mevlana Bulvarı 198
Figure D.62. Reflected Shortwave Radiation (W/m²) of Urban Block 14 - Sincan 199
Figure D.63. Reflected Shortwave Radiation (W/m²) of Urban Block 15 - Tulumtaş 199
Figure D.64. Reflected Shortwave Radiation (W/m²) of Urban Block 16 - Tunus Caddesi 200

LIST OF ABBREVIATIONS

ABBREVIATIONS

3D	Three Dimensional
CAD	Computer-Aided Design
DPI	Dots Per Inch
GHG	Green House Gas
MGM	Meteoroloji Genel Müdürlüğü (General Directory of Meteorology)
TOE	Tonnes of Oil Equivalent
TÜİK	Türkiye İstatistik Kurumu (Turkish Statistical Institute)
SVF	Sky View Factor
SW	Short-Wave
UHI	Urban Heat Island

CHAPTER 1

INTRODUCTION

1.1 Background Information

The first known person who tried to explain the causes of temperature differences between urban and rural areas was L. Howard who spent many years measuring temperature changes in London and its surrounding rural area. As a result of his research, he showed that the increasing population and fuel consumption in houses and factories after the industrial revolution are the main reason for the formation of artificial heat in the cities (Mills, 2008).

For more than a century, this claim has been questioned and the characteristics of the excessive heat impact in urban areas have been recorded for numerous settlements, towns, and cities. Consequently, this vast body of information allows us to accept this claim as universal (Oke, 1982).

According to Zhang, Shou, and Dickerson (2011), covering the natural landscape surfaces with impervious materials decreases evapotranspiration and increases runoff. Also, the materials such as concrete used in buildings and pavements absorb solar radiation and have a higher heat retention capacity. Surfaces are re-exposed to solar energy without releasing the heat they hold during the night. Thus, the excess heat on the earth cannot be removed and creates a heat blanket over the cities. The urban area, which is covered with this heat blanket and is warmer than its surrounding rural area, is called Urban Heat Island (UHI).

1.2 Problem Statement

Increasing urbanization due to population growth causes significant changes in the city and its micro-climate. Rising energy consumption due to heating, traffic, industrial activities in cities, surfaces covered with the manufactured product such as asphalt and concrete, city canyons formed by tall buildings and the streets between them, and decreasing green areas cause climatic changes. Many studies on city climatology have revealed that the most apparent effect of urbanization on climate is on temperature. (Çiçek, 2004) We know that built-up areas in cities are finished with materials that have high heat retaining or reflecting properties, which add to the amount of heat contained within the open spaces between the buildings. This is also called the urban heat island (UHI) effect, which is considered to be one of the greatest contributors to hotter micro-climate in cities.

As can be seen from the map of Türkiye shown in Figure 1.1., there are temperature deviations from normal in provinces with a high rate of urbanization. These provinces, where the temperature is 0.98 – 4.14 ºC higher than the seasonal norms, are the areas with the highest population density in the country. (MGM, 2020)

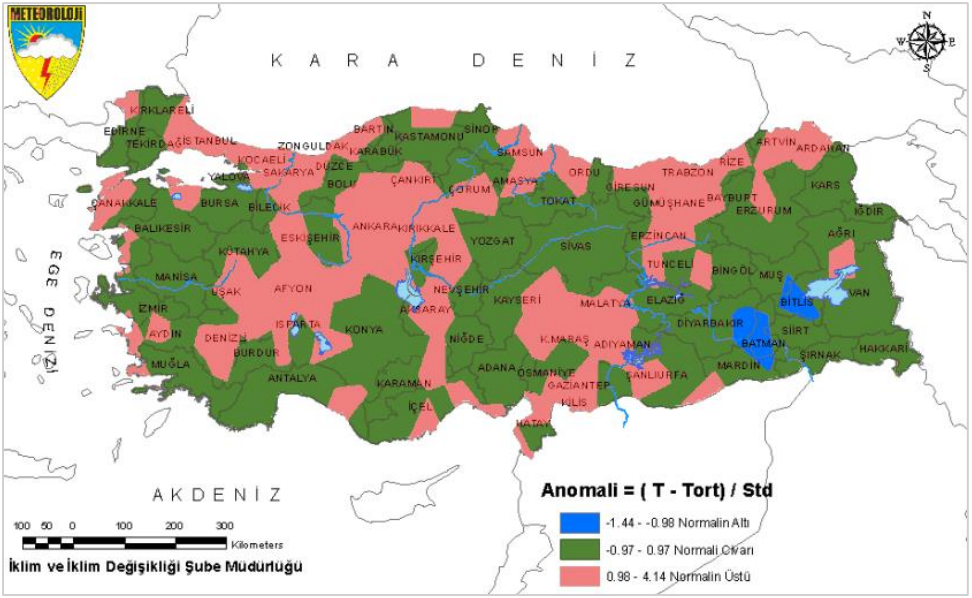

Figure 1.1. Average Temperature Anomalies Map of Türkiye for Summer 2020 (MGM, 2020)

The data provided by the Meteoroloji Genel Müdürlüğü (MGM), i.e. the General Directorate of Meteorology (2020) the average summer temperature in Turkey between 1981 and 2010 was 23.4°C. The average summer temperature in 2020 was 24.3°C, which is 1.1°C above the seasonal normals. (Figure 1.2.)

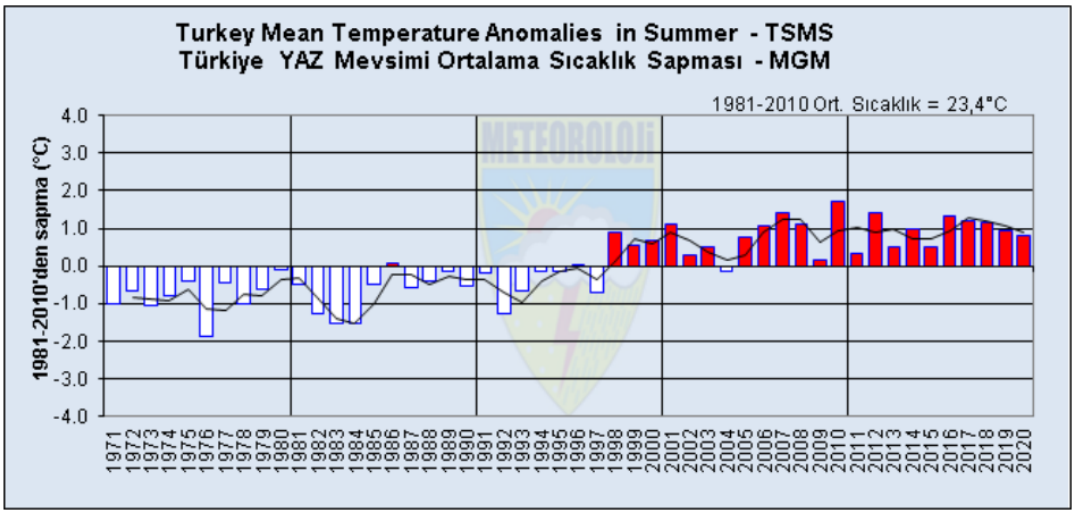

Figure 1.2. Türkiye Mean Temperature Anomalies in Summer between the years 1971 and 2020. (MGM, 2020)

The capital city of Ankara, which is one of the largest cities in Türkiye, has also been undergoing great temperature changes in recent years. Figure 1.3 below shows the climatic maps of the recorded data in 2011 and the simulated data for the year 2050, for the city of Ankara. The maps are presented side by side for comparison; and when the situation of 2011 and the projection of 2050 are compared, it is seen that the temperature in Ankara is expected to increase by an average of 3.8 °C, over time (Bilgili & Şahin, 2013).

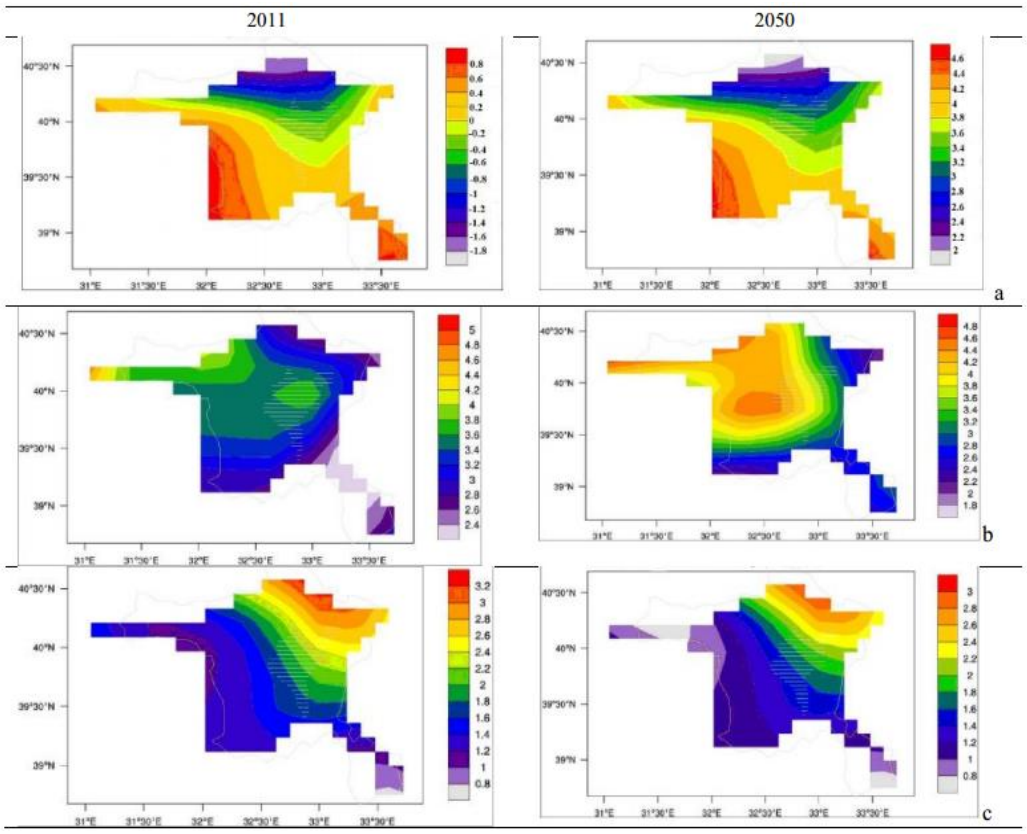

Figure 1.3. Air temperature (a), total precipitation (b), and wind (c) simulations for the city of Ankara in the year 2050 (Bilgili & Şahin, 2013)

Increasing air temperature has brought many climatic problems such as shifts in seasons, floods, increase in the use of air conditioning and energy consumption, drought, and reduction of water in dams. This problem is becoming more evident each year and is expected to increase even more in the future. Therefore, in this research, the problem under scrutiny is the identification of factors that are contributing to the urban heat island effect, which in turn are at the root of the “higher air temperatures than seasonal norms, in Ankara".

1.3 Aim and Objectives

The purpose of this study is to determine whether the cause of drastic temperature changes in Ankara can be associated with the UHI effect due to the use of surface materials having high heat-retaining properties, as a result of excessive urbanization.

Therefore, in this research the aim is to answer the following questions:

- What is the relationship between surface material properties and UHI?
- What is the impact of surface albedo on the temperature of surfaces?
- What is the impact of environmental elements on microclimatic conditions in Ankara?
- How has this microclimatic change affected the thermal comfort level of people in Ankara?

1.4 Methodology

This research aims to relate seasonal changes and excessive heat accumulation in Ankara to changes in the building and urban surface materials. In order to achieve this aim, firstly the study area (Ankara) has been introduced in the materials of the research chapter. Geographical conditions and the expansion of the city borders have been shown through maps due to increased population. The enlarged city borders caused an increase in the urban areas and the change of surface materials from natural permeable materials to human-made heat-absorbing materials. A total of 16 different urban blocks are selected as case study areas among the districts with high population and building density. These areas have also different types of building heights, facade materials, and environmental aspects.

After the urban blocks were determined, the study areas with border dimensions of 200x200 meters were modeled in 3D (three dimensional) in SketchUp Pro software.

Environmental factors such as vegetation and water body were also processed into the models, and trees, if any, were placed in existing locations.

Fieldwork was carried out in each modeled block, and vertical and horizontal surfaces in the areas were photographed with both a digital camera and a FLIR E60 thermal camera. Thermal camera measurements were made on the areas exposed to the sun's rays for the longest time in the cloudless sky in the afternoon. Measured surface temperatures and albedo values have been brought together on Excel tables.

As a third step of the analysis, the collected data of albedo and site conditions were processed into 3D models utilizing ENVI-met software. The processed models were subjected to microclimate simulation by considering the current weather conditions. As a result of the simulations, atmosphere, radiation, surface, and soil data outputs were obtained. Later, these outputs were converted to maps with the visualization tool in the ENVI-met software and saved for analysis.

The results obtained with different methods are mentioned in the results and discussions section.

1.5 Disposition

In the first chapter of this study, background information that contains the definition of UHI, the problem statement, the aim and objectives, and the research methodology are presented.

The second chapter of this study consists of the literature review, which starts with the importance of the UHI phenomenon, and continues with the effects of urban characteristics on UHI through land type and use, site density, building typology, shading layout, and surface albedo, and ends with an overview of investigation methods for determining the UHI phenomenon are explained.

With the literature review, it is aimed to understand better the materials and the methods which are planned to be used in this study, and these parts are the third and

fourth parts of the research paper. Site selection criteria, meteorological data, thermal camera imagery, albedo values calculation via surface photographs, and microclimatic simulation software are the parts of the methodology of this research paper.

In chapter 3 the material of research and details on the case study areas are presented.

Chapter 4 gives details on the research methodology, step by step.

Chapter 5 presents part of the raw data which are collected during the research, while the rest are given in the Appendices. This chapter also presents the results, their analyses, and a relevant discussion of the results obtained.

In the last chapter of the thesis, the conclusions arrived at as a result of the study are given for creating a necessary resource for future studies.

CHAPTER 2

LITERATURE REVIEW

The literature review part of the study is grouped under three headings. The first one is “Importance of the UHI Phenomenon”, the second one is “Effects of Urban Characteristics on UHI” and the last one is “Investigation Methods of UHI”.

2.1 Importance of the UHI Phenomenon

Kim and Baik (2005) state that because of the rapid urbanization and industrialization, various ecological problems have been identified not only on the local scale but also on the global scale. Primarily, changes in temperature, precipitation, wind speed, and humidity levels in the blocks lead to significant climate changes. At the same time, these influences, combined with the city's size, location, morphological structure, and anthropogenic heat factors, begin to affect urban heat island (UHI) intensity to a greater extent.

According to Al-Hafiz, Musy & Hasan (2017), during the summer the surfaces that create the city's structure, trap the radiation from the sun and also increase the total temperature by re-reflecting it to other buildings, their roofs, and urban open spaces. This trapped heat over the cities can harm human health, in the form of heat depression, heat-related diseases, and even death. For example, between 1921 and 1985, in sub-tropical Mexico City, changes in bioclimatic conditions and the accumulation of excess heat in the city have been reported to adversely affect human health (Giridharan & Emmanuel, 2018). A study conducted by Heaviside, Vardoulakis, and Cai (2016) shows that in the future the deaths due to heatwaves will be increased by "… 53 percent in the 2020s, 122 percent in the 2050s, and 209 percent in the 2080s" if the population and the UHI effect increase at the present rate

(Figure 2.1.).

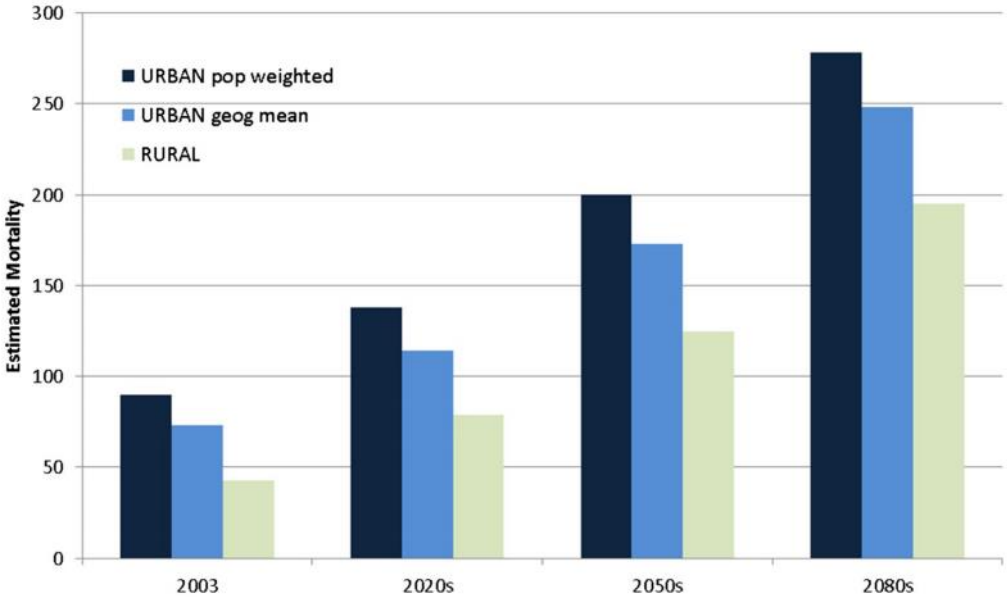

Figure 2.1. Mortality estimation caused by temperature changes in the future (Heaviside, Vardoulakis & Cai, 2016)

When the reasons affecting microclimates are understood, and the negative impacts that cause them are improved, the living conditions of millions of people will change for the better. Emphasizing this issue will increase the number of people who are sensitive to this problem in the future and will enable the design of sustainability. Thanks to the use of renewable energy sources and passive design techniques, both indoor and outdoor human comfort will increase. (Erell, Pearlmutter & Williamson, 2011)

2.1.1 Negative Effects of UHI on the Ecosystem

According to the research that is conducted by Huang, Li, Liu & Seto (2019), the rapid and large expansion of cities causes the overlap of excess heat and rising humidity in tropical/temperate climate areas. Research on UHI shows that the amount of water required for irrigation is increasing day by day, and by 2050, about one billion people will suffer from water shortages. If the needs of scarce regions are

not met in terms of water, cooling by evaporation will not take place and the heating rate will increase further. This overheating will be even greater than the Green House Gas (GHG) effect. In addition, this overheating will result in the deterioration of gray and green infrastructures due to the deterioration of temperature change intervals. These deteriorations will occur due to the cracking of materials and loss of their form due to expansion and contraction movements.

When people build cities, they bring impermeable and heat-imprisoned artificial surfaces instead of the vegetative cover found in nature. The UHI effect created by artificial surfaces primarily affects the original owners, inhabitants of that region before humans. The creatures suffering most from this effect are ectothermic (cold-blooded) animals. Enzyme structures, life, growth, and reproduction cycles of these organisms are directly related to environmental temperature. When the optimum temperature values are exceeded, the life activities of these creatures vary. Reproductive activities of some species of cold-blooded animals slow down, while the breeding activities of species such as the lizard are greatly increased. The over-breeding species begin to dominate others in its habitat and jeopardize the existence of other species. (Battles & Kolbe, 2018)

2.1.2 Energy Consumption and UHI Relationship

Global building energy consumption climbed from 1.4 billion tonnes of oil equivalent (TOE) in 1970 to 3.6 billion TOE in 2010 and was anticipated to increase to 5.5 billion TOE in 2040 due to the ongoing changes in the climate. (Li X. et al., 2019). However, the global building energy consumption value for the year 2022 could not be reached. Excessive energy consumption increases carbon emissions, pollutes the air, and consumes fossil fuels. Therefore, understanding energy consumption in buildings and the patterns of formation along with its reasons has become a highly popular topic in scientific communities. Some of the factors that increase energy consumption in buildings are the reflection and absorption properties

of the surface material, the level of albedo, the height of the building, and the sky view factor (Zhang, Shou & Dickerson, 2012).

Another reason is that climate change in the tropics is one of the consequences of global warming all over the world, and this change is intense in urban areas. While these areas are under more heat stress, they require more cooling energy to ensure human health and comfort. In particular, the use of air conditioning for maintaining the thermal comfort level increases energy consumption and contributes to regional climate change in a vicious cycle, both directly and indirectly (Giridharan & Emmanuel, 2018).

Thermal and energy consumption maps can be created to develop methods that can help in this field. The proposed method matches the map and energy consumption data using Geographic Information Systems (GIS). This way, the data marked on the map can be compared and analyzed. Research has shown a strong relationship between thermal environment and energy consumption. When comparing the maps that are created, as can be seen in Figure 2.2., the areas with the highest UHI intensity consume the highest amount of energy. (Souza, Postigo, Oliveria, Nakata, 2009)

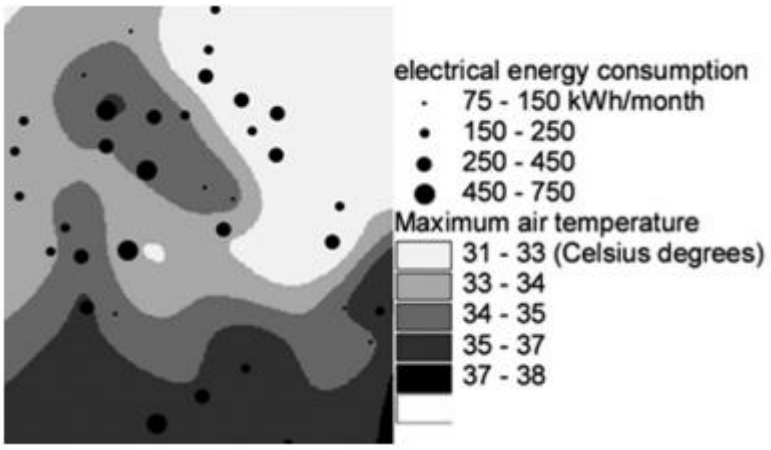

Figure 2.2. "Relationship between the electrical energy consumption values and maximum air temperatures of the case study area" (Souza et al., 2009)

2.1.3 Effects of Urban Characteristics on UHI

As the world's population is continuously growing and people's lifestyles have undergone major changes in the last few centuries, the UHI effect has been created, and this phenomenon has been increasing. According to Li et al. (2018), the city of Lanzhou has undergone rapid urbanization activity in recent years. While the surface area of urban areas reaches 210 km^2, the impermeable surface ratio also increases linearly. In 2016, the city's population reached 3.7 million, which constitutes sixty-five percent of the non-agricultural population. In addition, the rapid construction in this city disrupted the unique climate, caused air pollution, and resulted in the intensification of the UHI effect.

Looking at cities on a large scale, climatic differences, cloud rates, and solar radiation distinguish them from rural areas around them, while on a small scale, we can see that the structure of its own geometry, direction, and material cause temperature differences. Therefore, microclimate has a character that can vary even every few meters (Kleerekoper, van Esch, & Salcedo, 2012).

2.1.4 Land Type and Use

The materials used in buildings and ground in city centers have a very high heat holding capacity due to their characteristic features. During the day, the radiation energy they get from the sun is trapped within their mass, and they are released slowly at night. Due to this basic principle, cities with different land characteristics show different microclimate characteristics from the surrounding areas (Khan & Chatterjee, 2016).

2.1.4.1 Urban Area

Research in 50 different cities shows that radiation energy emitted during the night increases the temperature of cities. In the daytime, UHI is associated with convection

efficiency in the atmosphere, while at night, UHI is related to heat retention capacity and heat release rate of materials that make up the city's structure (Kleerekoper et al., 2012).

In Figure 2.3., the factors that cause UHI are shown. These factors are summarized by Kleerekoper et al. (2012) as follows:

1. The short-wave radiation energy from the sun is struck on the surfaces and reflected, trapped between the building and the street floor.
2. The polluted air in the atmosphere reflects long-wave radiation over the city.
3. Radiation waves that cannot reach the sky due to buildings are released back onto the city.
4. Excess heat generated by people (traffic, industrial activities, etc.) is released into the city.
5. Building surfaces store excess heat in their bodies.
6. Impermeable surfaces prevent evaporation and prevent excessive heat dissipation.
7. Since the wind speed decreases due to buildings, heat dissipation cannot be provided.

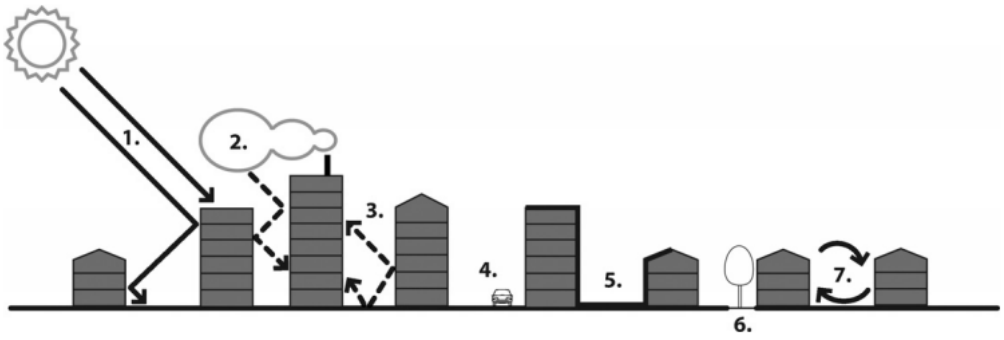

Figure 2.3. Causes of UHI (Kleerekoper et al., 2012)

In order to examine the effect of city texture on UHI, maximum hourly temperature values were recorded for several years. Such a long-term study was found enough to obtain statistical data. This research shows that the texture of the city is an essential source for determining radiation values and reshaping the city design. The increase

in radiation-emitting areas is one of the main sources of excess heat released at night. A strategy to reduce the amount of energy stored will have positive effects on energy consumption and the health of living things (Sobstyl et al., 2018).

2.1.4.2 Rural Area

Martin-Vide, Sarricolea, and Moreno-Garcia (2015) argued that the areas which are selected for urban-rural area comparison should not be very independent of each other. In their research paper, the area referred to as a rural area is not a space taken from any point in the world. Instead of that, the places which are located near the urban area and have similar data collecting methodology for comparison should be counted as rural areas. Moreover, altitude heights should be no more than 10 meters apart, and the water bodies, if there are any, should be similar. Apart from these, the differences in the elements covering the surface are the main comparison item between these two areas. For example, there are impermeable materials such as asphalt and concrete with high heat retention capacity, while the rural ground has natural vegetation. Thanks to the natural vegetation, the water on the surface evaporates easily while using the surrounding heat. Vegetation also keeps less heat for a shorter amount of time than the materials used in the city. Finally, the lack of human activities in the rural area is one of the differences in the UHI effect between the two regions. (Martin-Vide et al., 2015)

2.1.5 Site Density

The global population, as well as excessive population growth, are among the biggest problems of our time. This globally conducted study by Manoli et al. (2019) examines the impact of these two major factors in metropolitan cities around the world and proposes a method to mitigate the effects of these problems. As can be seen in the figure, the UHI effect has accumulated nonlinearly in the most densely populated regions of the world. This increase can be explained by changes in heat

dissipation, surface properties change due to expanding cities as the population increases, and evaporation decreasing gradually.

Human-induced heat release is higher in densely populated and large cities compared to others, and it causes an increase in the measured temperature (Figure 2.4.). In the face of this growing problem, designers and urban planners should incorporate the increasing population factor into their projects. Thus, an effective method can be followed against UHI.

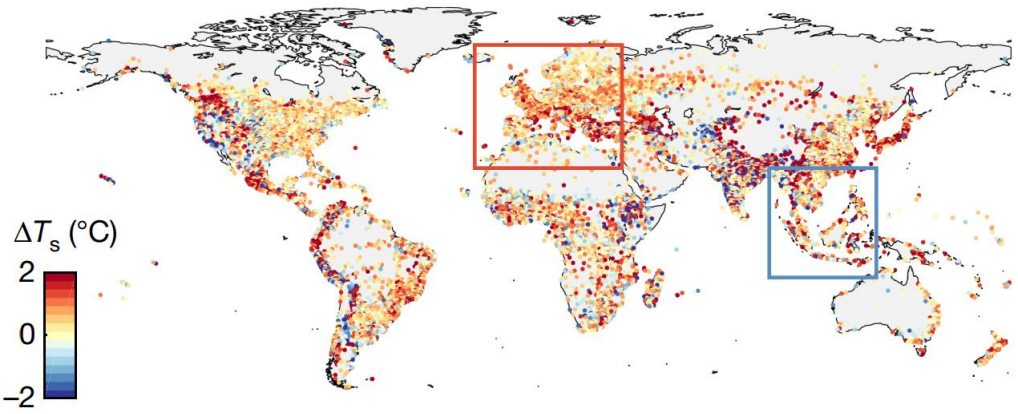

Figure 2.4. Map of summertime UHI intensity in world cities (Manoli et al., 2019)

2.1.6 Building Typology and Shading Layout

In the symmetrical city streets, the three-dimensional geometric shape created by the width of these streets and the height of the buildings is defined as a "canyon". In some North American, European, and Australian cities, the maximum UHI amplitude has been shown to be related to the sky view factor (SVF). The radiation changes caused by the geometry and dimensions of the urban canyon directly affect the amplitude of the UHI. One of the ways of expressing the canyon geometry is the sky view factor, and it is the amount of sky seen from the city canyons and the ratio of the entire sky. As can be seen from Figure 2.5., the SVF is essentially a function of the height-width ratio. Increasing the height of the city canyon decreases the SVF, while the canyon width increases the SVF. (Çiçek & Doğan, 2005)

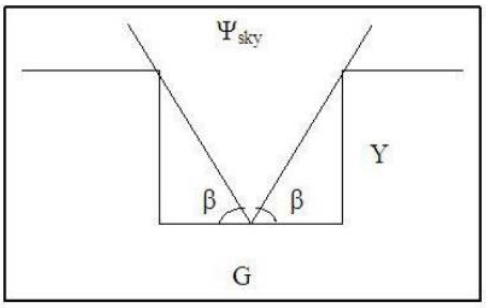

Figure 2.5. Schematic definition of sky view ratio (Ψsky=cosβ), height, and width ratios on a city canyon. (Çiçek & Doğan, 2005)

The urban canyon, which is obtained by the height and width ratio, affects the total solar radiation exposure rate as it changes the amount and shape of the shading on buildings (Cocci Grifoni et al., 2016). In Figure 2.6., it can be seen that different building typologies with different height and width ratios cause different amounts of urban temperatures and thus different UHI effects (Sailor, 1998).

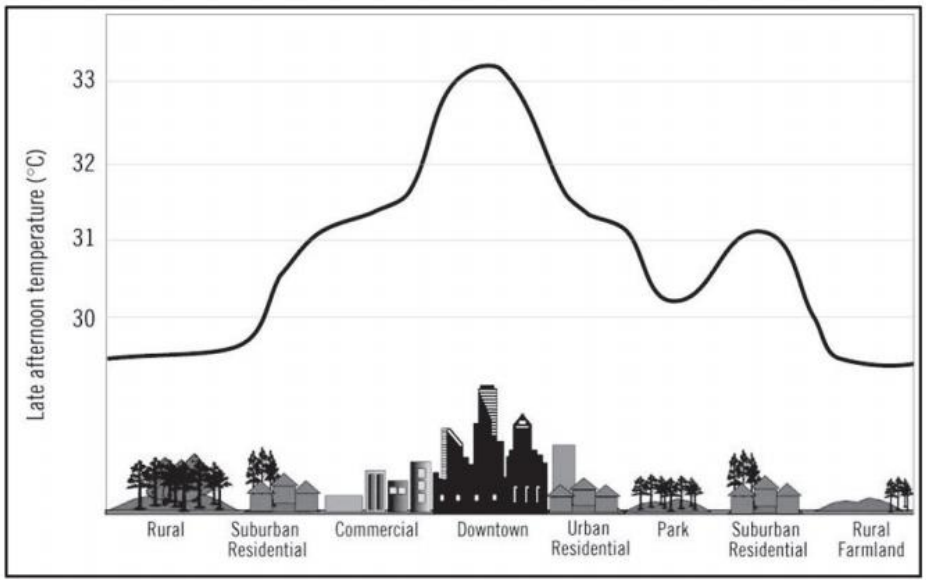

Figure 2.6. The average temperature in the late afternoon for different building typologies (Sailor, 1998)

Studies have shown that the classification of urban forms is achieved through two methods. The first is urban form typology, and the other is morphological indicators.

The values for UHI were calculated by comparing the various form patterns derived from these methods. The scales of the buildings determined for the research range from a single structure to wide and composed urban blocks, as shown in Table 2.1.

Table 2.1 Different types of structure patterns and their related indicators (Malys et al., 2016)

SCALE	FORM PATTERN	RELATED INDICATORS
Single building	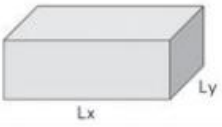	• shape ratio (S/V) • main façade orientation • glazing ratio • ratio of side (Lx/Ly)
Generic built form	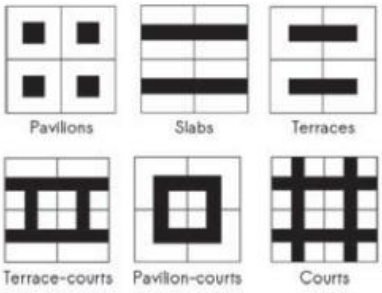 (Ratti et al. 2003)	• plot ratio • site coverage • shape ratio (S/V) • total surface area • sky view factor (SVF)
Street	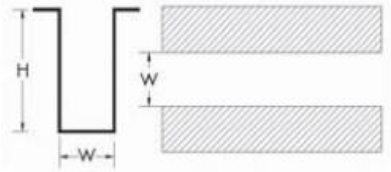	• aspect ratio (H/W) • street orientation
Urban block/district	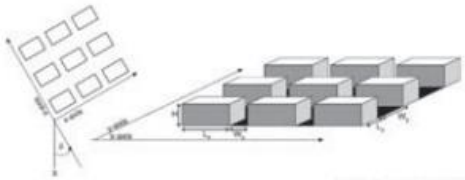 (Panao et al. 2008)	• floor space index (FSI) • grid azimuth (δ) • number of floors (n) • base block dimension (Ly) • building depth ratio (l=Lx/Ly) • directional aspect ratio (H/Wx ; H/Wy) • directional street width ratio (w=Wx/Wy)

In this study conducted by Malys et al., 2016, by modeling the city in 3D the horizontal and vertical surfaces forming the structures and the ground were transferred to digital media in accordance with reality. When utilizing simulation tools, the sky view ratio was found, and the radiation falling on the surface due to the solar movements were determined.

In the first stage of the calculation, the shadows created by the fall of the sun's rays into different geometric shapes created a mask. This shows the effect of the forms of the structures. In the second stage, the solar energy received by each building element was calculated. The direct rays from the sun and the rays reflected from the sky are calculated separately at this stage because the cloudy sky affects the calculation.

According to the simulation results, horizontal surfaces and especially roofs were the areas with the largest SVF (sky view factor). That is, blocks with a large roof surface area have a greater value. As a result of this research, it is understood that in order to reduce the effect of UHI, changes should be made on horizontal surfaces rather than vertical surfaces. In addition, as the solids of buildings rise and become more compact, the UHI effect they give to the environment decreases as the roof surfaces decrease. This study shows that especially urban planners and designers should pay attention to the structure and material properties of horizontal surfaces (Malys et al., 2016).

In another study conducted by Hwang, Lin, and Matzarakis (2011) in central Taiwan, the effects of shading on seasonal and long-term thermal comfort were investigated. For each season, a total of four field studies and simulations of these fields were made with RayMan software. In addition to using 10-year meteorological data for the simulation, thermal comfort levels were tried to be measured by surveys with city residents. As a result of the study, it was found that the presence of shade areas provided a great benefit because it cuts the radiation from the sun. Planting deciduous trees and integrating removable shading systems into the streets can significantly block the heat accumulated in the city and consequently the increased temperature. In addition, the shape of the leaves and crown is more important than the density of these elements because it increases the amount of shading area (McPherson, 1994).

A final example of the shading layout is a case study, which is conducted in an urban district called Pin Sec, France. In this study, a non-insulated and south-facing building has been chosen, and the researchers focused on roofs, green walls, and lawns. When the site is vegetated, the shading effect of the plants and the green walls

as an insulated material helped this case study building to have cooler indoor air in the summertime. This allowed the residents to use less energy to cool the indoor environment. (Malys et al., 2016)

2.1.7 Surface Albedo

Cladding elements used in building envelopes and open area surfaces regulate the microclimatic conditions of cities; because surface temperatures of materials that absorb heat and sunlight are measured high, and the excess heat energy absorbed by the materials is released into the atmosphere during the day.

As a result of new studies and technology, new materials such as "advanced thermochromic, fluorescent, plasmonic and photonic materials" with very high solar reflectivity and low temperature of the surface have started to be produced and used instead of traditional cladding materials. With the use of these innovative materials on building walls, roofs, and pavements, the number of surface albedo increases, and the temperatures of the cities go down from the peak values they reach (Santamouris & Yun, 2020).

According to Kotharkar et al. (2019), the UHI effect is not only due to macroclimate changes but also to factors that change the microclimate properties around it. In Figure 2.7., the 3D graphic shows that when both the albedo value (AL) and the amount of vegetation density ratio (VDR) increase over time, the value of the urban temperature (ΔT) starts to decrease.

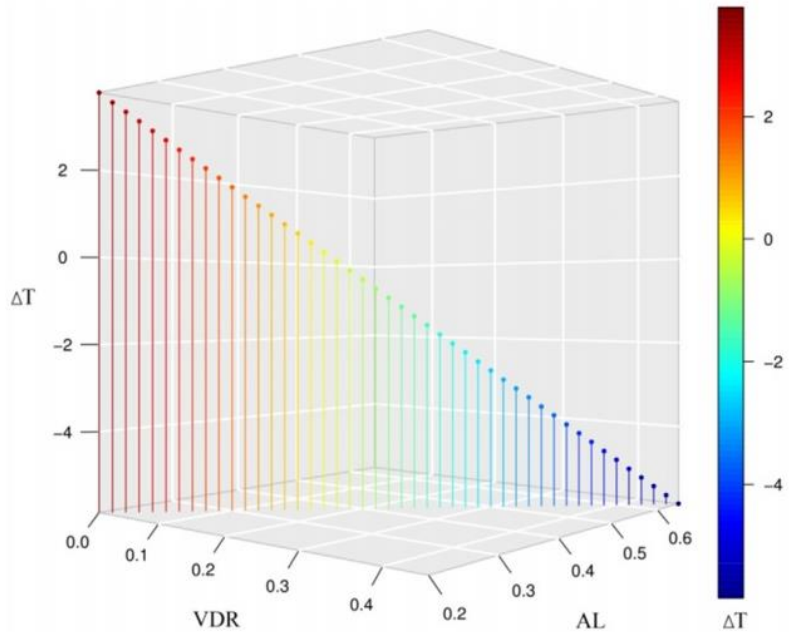

Figure 2.7. Variations in UHI change according to the amount of vegetation density ratio (VDR), albedo cover (AL), and urban temperature (ΔT) (Kotharkar et al., 2019)

2.1.7.1 Vertical Surfaces

Facades play an essential role in the urban context since they are closer to pedestrian level and their surface area exceeds that of the roof and, in certain cases, the street area by thousands of square meters. Furthermore, each side of a building's facade should act in the context of the surrounding environment: both inside and out. Therefore, overheating in the urban area due to climate change and the increase in population is an issue that demands adaptable and responsive facades (Lassandro & Turi, 2017).

“Albedo” is an important thermal parameter that measures a surface's ability to reflect light. Albedo is a dimensionless fraction that is measured on a scale of 0 to 1 and is defined as the ratio of reflected solar radiation to incident solar radiation at the surface. An albedo of 0 indicates that a fully black surface has no reflecting power (no light is reflected, all is absorbed), whereas an albedo of 1 indicates perfect reflection off a perfectly white surface (100 percent reflected) (Li et al., 2013)

Materials with low solar reflectivity values absorb more of the solar radiation instead of reflecting and that excessive radiation cause heat island formation around them.

Some of the solar radiation hitting the building is absorbed by the surface; some is reflected and transferred. According to Mansouri et al. (2017) although heat flux is transferred to the building through the walls by conduction and another form of heat transfer is the convection method, which is through ventilation and infiltration. The glazed surfaces of the windows are also an example of this form of heat transfer. In order to control heat transfer and mitigate excessive heat gain, surface materials should be high albedo materials; i.e. they should not absorb heat. When the outermost layer of the building envelope is made with high albedo materials, it will prevent solar radiation from being absorbed during the day and released during the night. In addition, this research has shown that with the decrease in temperatures due to the high albedo of the building surfaces the comfort levels increase not only for the building occupants in interior spaces but also for the pedestrians on the streets, during summer (Mansouri et al., 2017).

In a study conducted by Uemoto et al. (2010), traditional paints and newly produced "cool paints" with higher reflection properties are applied to building facades for comparison, and the walls are exposed to solar radiation. As a result of the tests, it has been observed that facades painted with "cool paints" reflect the solar radiation more than traditional paint pigments and have approximately 10 degrees lower temperature on the surface than conventional paints. Consequently, when cool paints with high albedo values are applied to the building surfaces, the excess heat accumulated on the surfaces can be reduced, and people's comfort level can be increased.

2.1.7.2 Horizontal Surfaces

Horizontal surfaces such as pavements absorb and reflect radiation from the sun. They transfer heat to the atmosphere, hold the heat in its mass, and transmit it to the ground. According to the climatic conditions, precipitation or icing on the ground

causes heat transfer due to evaporation and condensation. Studies show that the heat energy released on pavements in Tokyo is almost half the heat generated by energy consumption in commercial areas. It can be concluded that pavements are one of the major contributors to the UHI formation (Santamouris, 2013).

In the research by Santamouris & Yun, (2020), various surface coatings were applied to four pieces of tiles made of the same material. Sample S15 was left uncoated in its original state, the black coating was applied on sample S17, and the reflective white coating was applied on S8 and S5 samples. When samples were tested, the ambient air temperature was 34.5 °C, and solar radiation is 880 W per square meter. As shown in Figure 2.8., when thermal infrared photographs of the coated tile samples were taken, a surface temperature difference of 31 °C was observed between the black and white coated surfaces (Santamouris & Yun, 2020).

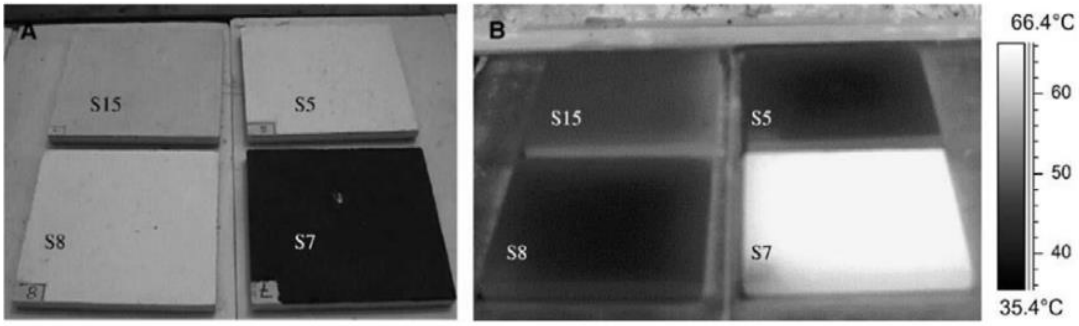

Figure 2.8. Visible (A) and infrared (B) images of four selected coatings (S15: uncoated tile, S7: black coating, S8, S5: white reflective coatings) (Santamouris & Yun, 2020)

When the surface of the pavement materials is dark-colored, the heat retention capacity increases. Forty percent of the urban fabric is considered pavement, so "cool pavements" should be implemented to reduce the UHI effect. Another UHI reduction method is to apply water-repellent cool pavements for roads, walkways, and parking areas. Pavements with this feature absorb radiation to a lesser extent than dry pavements. In addition, thanks to this method, pavements containing water contribute to the reduction of the UHI effect by evaporation using the surrounding

heat (Qin, 2015).

In another study, temperature data of 8 different pavements with various albedo values are collected from two regions of California: Berkeley and San Roman. When the graph in Figure 2.9. is examined, the findings clearly show that considerable changes in pavement temperature are possible: a 10 °C drop decrease in surface temperature for a 0.25 increase in surface albedo. The calculations that follow from these studies show that if cool pavements and other urban heat island mitigation strategies are adopted on a large scale, the national cooling energy demand could be reduced by 20% (Akbari et al., 2001).

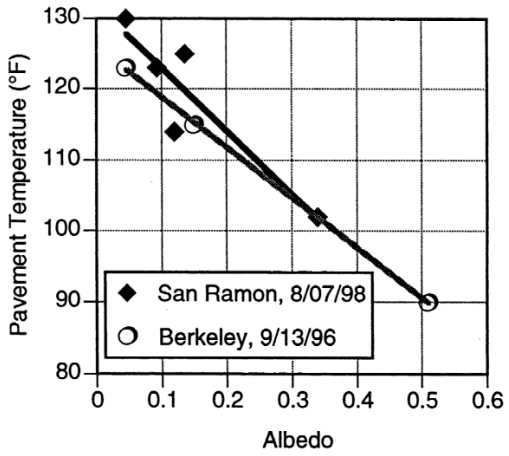

Figure 2.9. Albedo and pavement temperature relationship (Akbari et al., 2001)

For the case study conducted by Santamouris et al. (2012), 4500 square meters of pavement in an urban park located in the city of Athens were replaced with reflective pavement materials. Before the application, the ambient temperature data were collected and compared with the data after the application. As can be seen in Figure 2.10., while there is no significant temperature change in the park areas near the sea, it was observed that there is a temperature difference of 1.9 °C in the parts of the urban park which are closer to the dwellings. The surface temperature of the park decreased by 12 °C, which also increases the thermal comfort conditions of people.

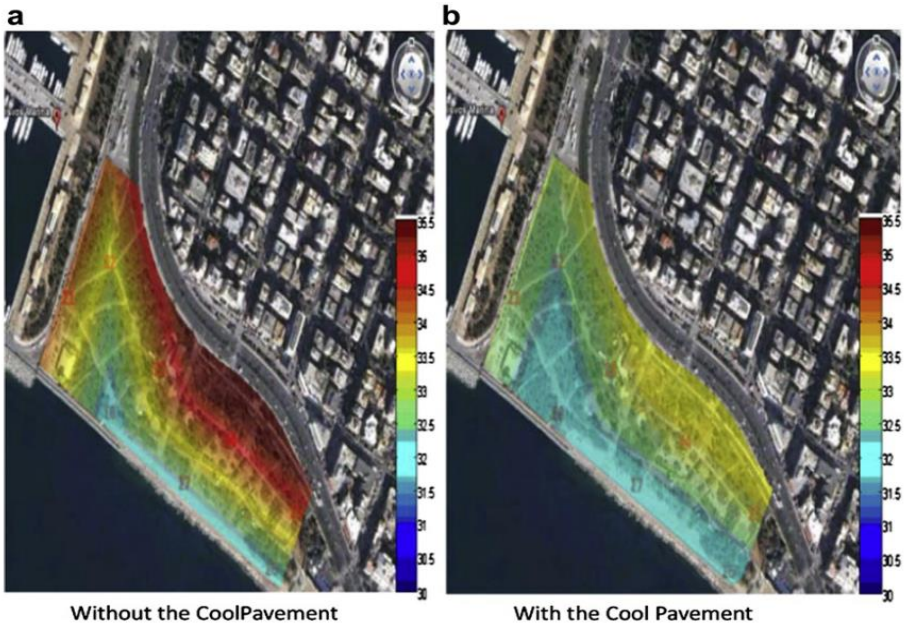

Figure 2.10. Spatial distribution of the ambient temperature in the park during a typical summer day, (a) without the cool pavements and (b) with the cool pavements (Santamouris et al., 2012)

In this study, 5 different colors of paint are applied in a thin layer on conventional asphalt and the surface temperatures of colored samples are compared with the conventional asphalt which is the reference material. As solar reflectance percentages of the samples are shown in Figure 2.11., the off-white colored sample has the highest reflectance percentage with 45% and the conventional black colored sample has the lowest (3%).

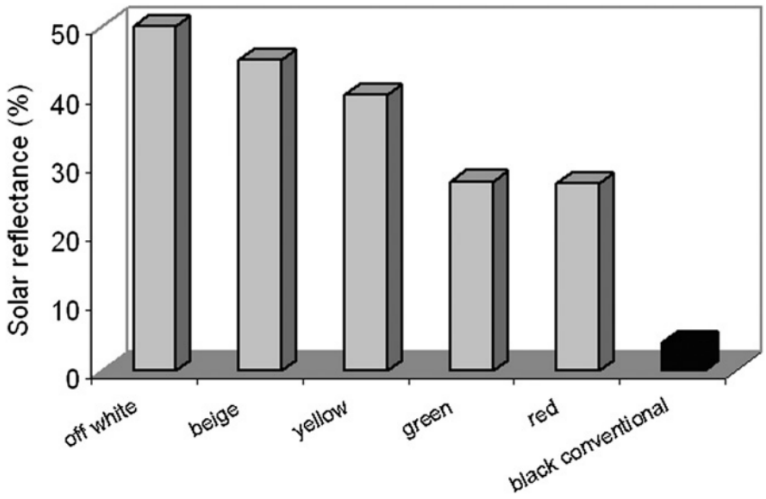

Figure 2.11. The solar reflectance of the conventional black asphalt and five colored asphalt samples (Synnefa et al., 2011)

After being exposed to solar radiation, it can be observed that the higher solar reflecting value the surfaces have, the cooler they are (Figure 2.12.). The off-white sample had the greatest temperature difference from the traditional asphalt, which was equal to 12 °C. The findings of this study show that using a color on a thin layer of asphalt on horizontal surfaces can significantly reduce surface and air temperatures in the cities, hence reducing the heat island effect and its repercussions. (Synnefa et al., 2011)

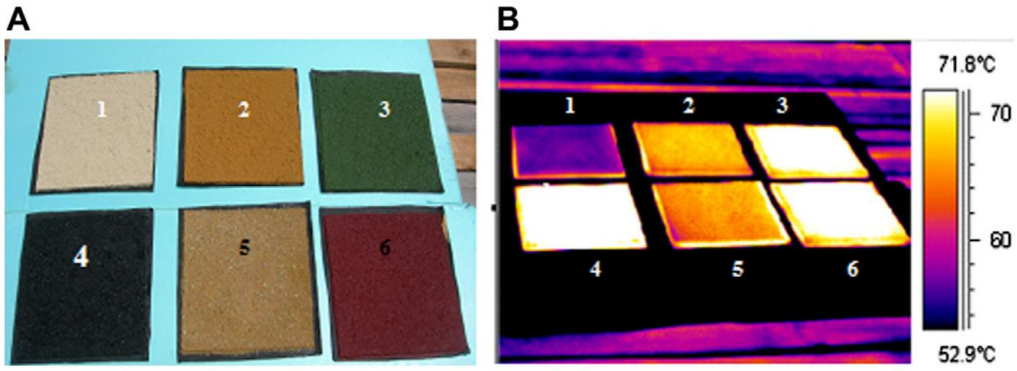

Figure 2.12. A: Visible images of the samples B: Infrared images of the sample. (Synnefa et al., 2011)

2.1.8 Environmental Elements

The UHI effect is not only due to macroclimate changes but also to factors that change the microclimate properties around it. In this section of the literature review, the factors causing the change in the UHI effect will be mentioned. These factors are as follows: “vegetation cover” and “water bodies”.

2.1.8.1 Vegetation Cover

The effect of trees on heat accumulation in the environment has been investigated for many years by many researchers and as a result, it has been shown to be the most effective source for cooling the cities and providing thermal comfort. The vegetation on the surface actively removes excess heat from the environment by evaporation and transpiration, while the shade provided by the vegetation reduces the absorption of short-wave radiation energy. During the night, thanks to the open sky, the heat accumulated during the day is quickly transformed into long-wave radiation and removed from the environment. Green walls help reduce cooling costs and reduce energy consumption by reducing the amount of heat trapped in buildings. These surfaces help to cool the streets in cities. (Kleerekoper et al., 2012)

In the case study which is conducted in an urban district, called Pin Sec, France, a non-insulated and south-facing building has been chosen. The researchers focused on the roof, green walls, and lawns. When the site is vegetated, the shading effect of the plants and the green walls as an insulating material helped this case study building to have cooler indoor air in the summertime. This helped the residents to use less energy to cool the indoor spaces. (Malys et al., 2016)

According to Theodoridou et al. (2017), having green roofs implemented on the existing rooftops in the cities such as Thessaloniki, Greece, the carbon sequestration rates will increase by 2.5 times in comparison. Also, in the same research paper, it is

indicated that the energy consumption which is caused by heating and cooling loads will drop by approximately 16%.

2.1.8.2 Water Bodies

Water evaporates using the heat energy around it and the heat buffer works when the principle is considered for large water bodies. In addition to stagnant water bodies, the use of heat energy can also be seen in flowing waters such as rivers. There is a cooling effect of 1 to 3 degrees celsius in the flow of water for about 30 meters. Water bodies that can help with the cooling effect are more effective when the area grows or flows like waterfalls. The cooling effect as a result of evaporation depends on the speed of the wind passing through the city and other climatic characteristics. Building large water bodies in cities is quite costly. However, when fountains are applied in public areas, streets and squares, they can be cost-effective. (Kleerekoper et al., 2012)

In addition to the cooling effect, the presence of water helps to improve the green infrastructure and thus provides indirect heat control. More green areas, especially in areas with heavy rainfall means more water retention capacity. The multiplicity of green areas also makes the evapotranspiration event more effective. Therefore, the presence of water bodies should be promoted together with the green infrastructure. (Kleerekoper et al., 2012)

2.2 Investigation Methods of UHI

To determine the effect of UHI, several scientific calculations should be made, and with the help of the data obtained, an accurate and effective intervention can be done to the problems that occur in the cities. In this literature review, the explained methods used to investigate the effect of UHI are as followed: "Weather and Surface Temperature Observations", "Thermal Camera Imagery" and "Environmental

Conditions Simulation".

The purpose of this section is to provide information on the collection methods of the data required for conducting this study.

2.2.1 Weather and Surface Temperature Observations

In calm weather where there are not many clouds in the sky, and the wind speed is very low, the evaporation rate also gets low. Also, a low momentum of the wind means that the airflow does not change substantially. As a result of these factors, heat accumulation occurs in cities, and therefore, the weather plays a vital role in determining the amount of UHI.

When determining the amount of UHI, data based on criteria such as air and surface temperatures, wind speed, cloud rate, and air pressure from the sea are recorded every hour. The recorded data can be displayed in daily, monthly, or yearly cycles. For the accuracy of the data, the sensors must be protected against environmental influences and placed at a standard height for each zone. The collected data can then be used for analysis or simulation programs using the UHI calculation. (Wolters & Brandsma, 2012)

2.2.2 Thermal Camera Imagery

Thermal imaging is a technique for analyzing UHIs that necessitates the use of highly accurate equipment, such as a high-resolution infrared camera. To offer the whole thermal properties of the captured object, the thermal imaging camera receives the radiation of a targeted object as well as the emission from the surrounding radiation on the item. The surface temperature of the targeted object can be determined using the object's emission, reflected emission from ambient sources, and atmospheric emission (Elmarakby et al., 2022).

In contrast to air temperature sensors, infrared (IR) cameras have the benefit of greater accuracy and the ability to collect and process large amounts of "scenic data (pixel-level temperature data)" (Chui et al., 2018). For instance, a study conducted by Chui et al. (2018), shows that different surface materials exposed to the same insolation and same climatic conditions have considerable temperature variances (Figure 2.13.) due to different characteristics of the surface materials. Therefore, IR thermography becomes an essential instrument for assessing UHI phenomena since near atmosphere temperature data is not adequate by itself.

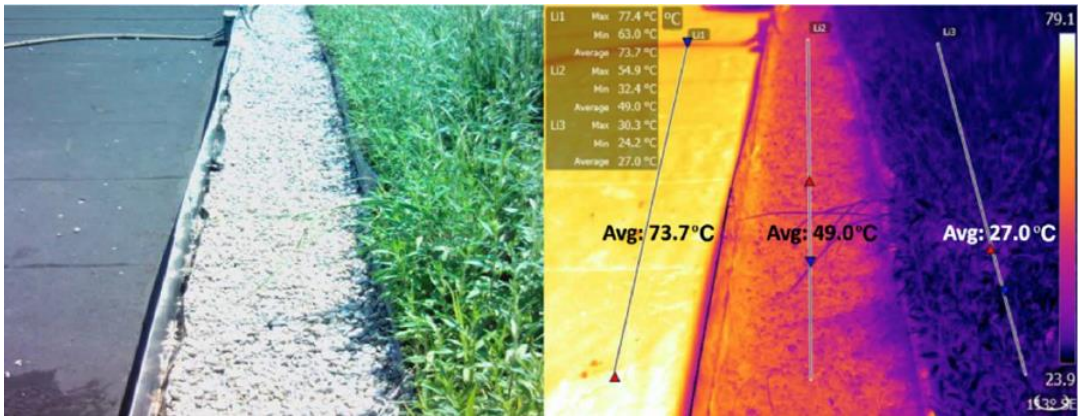

Figure 2.13. Surface temperatures are shown along measurement lines, and roof asphalt, rock ballast, and green vegetation are compared (Chui et al., 2018).

2.2.3 Environmental Conditions Simulation

Throughout history, buildings in cities that have been exposed to sunlight due to climatic conditions have been covered with white paint or plaster. By taking that information, Taleghani et al. (2021) conducted a study to figure out the impact of the facade orientation on the microclimate; therefore, computer simulations had been run using the Climate Simulation program ENVI-met. As can be seen in Figure 2.14., the modeled area contains 16 identical buildings placed on a grid structure as they are considered as detached houses and climate data for the 21st of June is used as it allows the highest amount of sun exposure. After running the simulation, it resulted that east-west canyons are exposed to direct sunlight for 6 hours longer than the

north-south canyons. This result means that east-west canyons have a stronger impact on the UHI formation and pedestrian thermal comfort since the net sun radiation is higher.

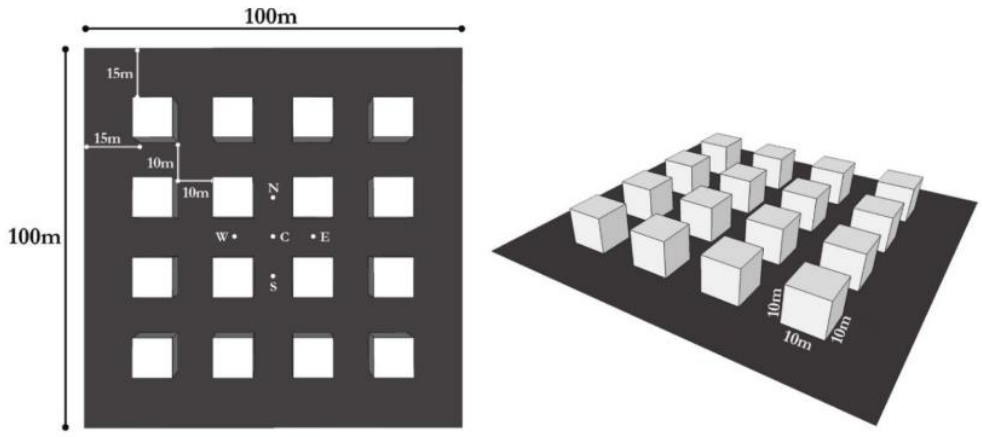

Figure 2.14. The plan (left) and the 3D model (right) of the simulation area (Taleghani et al., 2021)

Although it is estimated that the reflectance and the color values of a building facade are effective in the urban microclimate, a study conducted by Fabbri et al. (2020) by using the environmental simulation software ENVI-met showed that this effect is less than 1 °C. This research process with the software is mainly divided as followed:

- Modeling the subject building and its environment and collecting the necessary data for climate and physical environment,
- Defining the control group and different urban scenarios such as various facade and material configurations,
- Simulating each scenario and then analyzing and comparing the results.

In this study, the simulation results show that pavements, green areas, and vegetation has a far greater impact on the microclimate than building facades since the leaves allow water evaporation from the surface. While water is evaporating, it uses the existing heat around; therefore, the surrounded temperature decreases.

With parametric modeling, different imaginary scenarios about sustainability, energy performance and consumption can be transformed into real life and tested. The

findings can help to make better decisions when they are before the design phase. It also allows governments to devise strategies to take action by developing different scenarios (Cocci Grifoni et al., 2016).

The method which is used can model the thermal properties and operating behavior of future structures. However, this modeling method takes a lot of time and has to be modeled separately for each structure, which reduces the frequency of implementation. Instead, it is more common to make small changes to already built structures and to create alternative solutions. In the early design phase, energy performance measurements of buildings are important factors affecting decisions, and they also help to reduce costs.

Parametric modeling software such as “Honeybee” and “Ladybug” can be connected to “Radiance”, “EnergyPlus”, “Daysim” energy simulation model software, and providing great flexibility to the decision-making process in the early stages of design. Since different results can be seen comparatively when various changes are made to the parameters. The design parameters that can be modified are:

- General geometric form and orientation of the building
- Window-to-wall ratio of openings, amount of daylight and shade
- Wind speed and wind direction
- Thermophysical properties and thicknesses of materials to be used in the facade or partition walls
- Features of units in the HVAC (Heating, Ventilation, and Air Condition) system

Findings from different scenarios can both calculate the existing UHI effect and help to determine how the UHI effect can be determined for future scenarios (Touloupaki & Theodosiou, 2017).

CHAPTER 3

MATERIALS OF RESEARCH

The information and data that are obtained before starting the research are related to:

- Case study areas according to their environmental characteristics.
- The envelope of the residential buildings
- Surface materials of the pavements of the urban areas

In this chapter, materials of the study such as data gathering tools and resources are listed in detail under four subheadings. These are “Study Area”, “Selected Urban Blocks”, “Equipment”, and “Softwares”.

3.1 Study Area

In this research, the city which is chosen for the investigation of the UHI effect is Ankara. It is the capital of Türkiye, and it is located between 39º 50' - 40º 00' north latitudes and 32º 35' and 33º 00' longitudes. (Figure 3.1.) (Bilgili & Şahin, 2013)

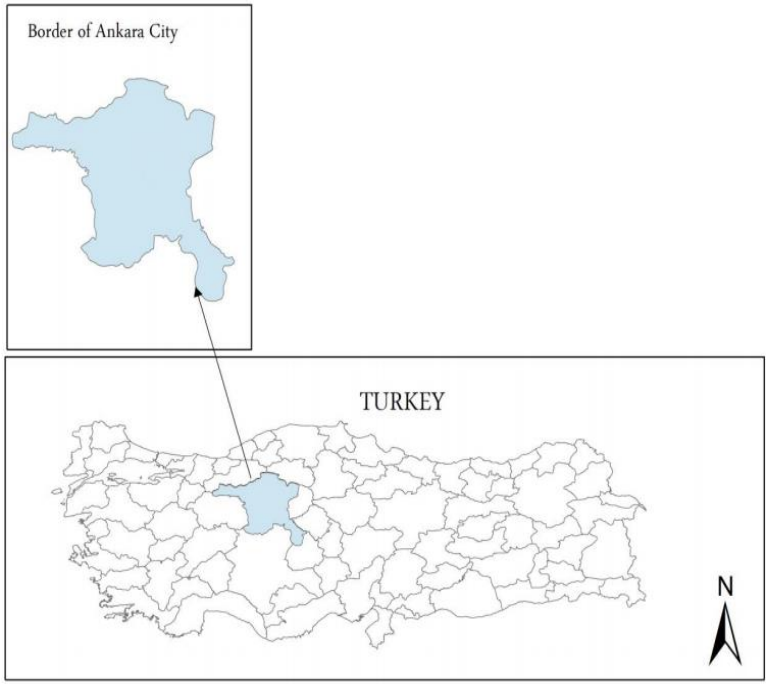

Figure 3.1. Location of the study area (Bilgili & Şahin, 2013)

Figure 3.2. below shows that the population of Ankara was around 1.6 million in the year 1965. However, it has increased more than three times in 50 years and become 5,146,307 in 2014, which means the population underwent significant changes between 1970 and 2007 (Şensoy et al., 2015).

The population change graph (Figure 3.2.) between the years 1965 to 2007 shows that this change is not only an average population growth rate, but there is also a large amount of migration activity from rural areas to the center of Ankara. This migration has put pressure on the urban area, which was not there before. Land use has also changed, and deforestation took place in order to create dwelling areas. Therefore, energy consumption increased as did industrial activities and the traffic load, and waste products are released into the hydrosphere and atmosphere. Ankara's rural population ratio has decreased from 35% to 0, while the urbanization ratio increased from 65% to 100% (Şensoy et al., 2015).

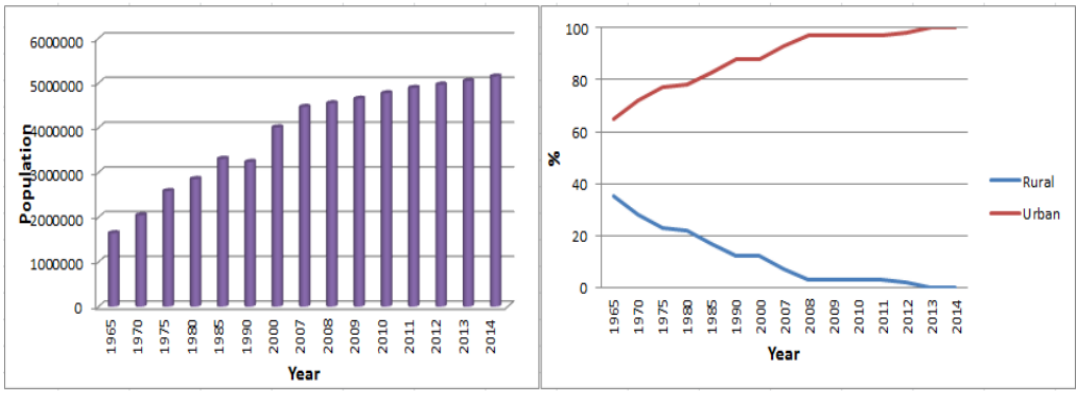

Figure 3.2. Ankara's total population graph (left) and urban-rural population ratio change (right) (Şensoy et al., 2015)

While the city was a small settlement spreading around Ankara Citadel (Kale) and its surroundings in the first years of the Republic, it grew slowly until the 1970s and entered a rapid growth period thereafter, because of the migration movements (Figure 3.3.). The city center was moved in the 1970s and spread over a wider area, towards the west. Until 1985, development was mostly in the north and south directions (Sat et al., 2017); currently, the development in the west direction has increased. After 1990, certain axes of growth were formed, especially on the edges of the intercity roads that offer development potential for new settlements (Çiçek et al., 2013).

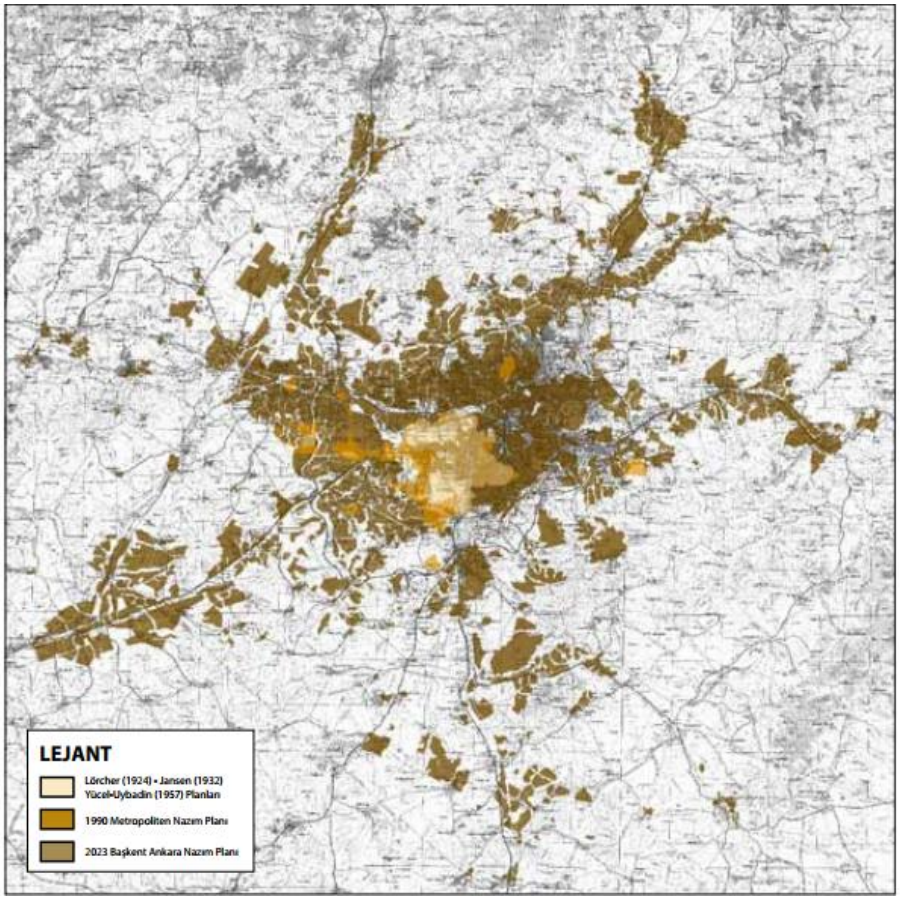

Figure 3.3. The macroform structure of Ankara changes according to the plan periods 1924, 1990, and 2023. (Sat et al., 2017)

When Figure 3.4. is examined, it can be observed that the number of buildings in Ankara is constantly increasing in addition to the information which is previously mentioned. Table 3.1. shows the number of buildings built each year, while Figure 3.4. shows the cumulative total of these buildings. According to the data obtained from TÜİK, the number of newly built buildings in Ankara in the year 2002 is 28,809. By the end of 2019, the number of those buildings in Ankara in 17 years is approximately 1.2 million. These data are supportive compared to the growing trend of city borders since the earlier years of the republic.

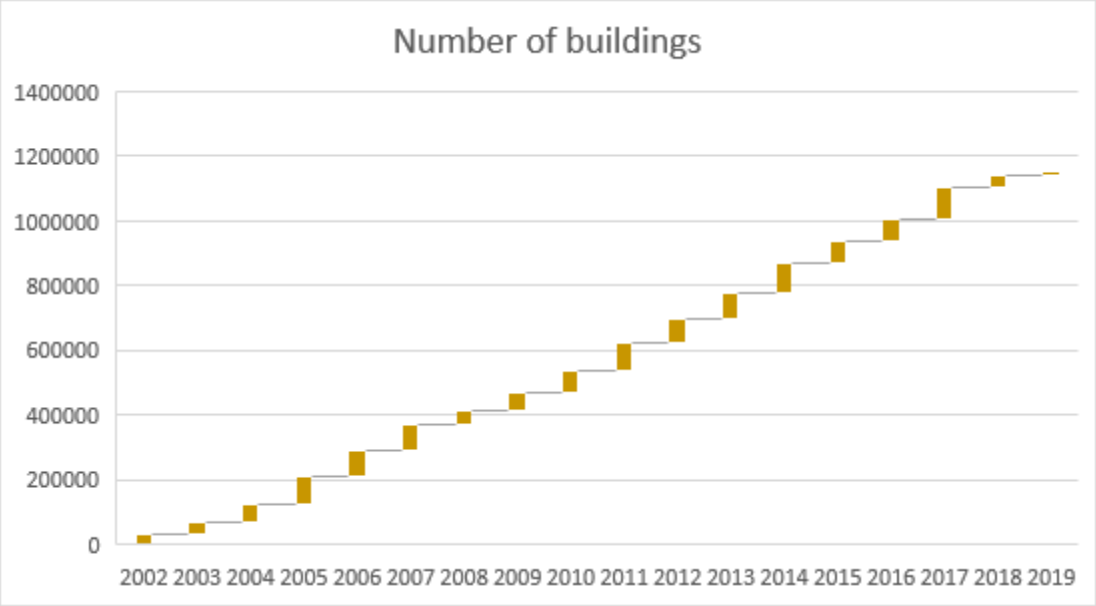

Figure 3.4. Cumulative change in the number of buildings in the city of Ankara between the years 2002 and 2019 (TÜİK, 2019)

3.2 Selected Urban Blocks

In the study, a total of 16 urban blocks are selected among the districts with high populations and building density, and the relationship between urban heat island and surface materials are studied. Since the ENVI-met LITE software allows modeling in 50x50x40 grid dimensions, the selected areas in the regions were created in square blocks with a total area of 200x200 meters (40,000 square meters) with 1 grid = 4 meters. Urban settlements in these areas were determined according to different urban density values, building heights and window-to-wall ratios, and environmental factors.

Urban Density was calculated with the following formula:

Floor Space Ratio (FSR) = Building Area / Land Area

Buildings located in the study areas with different density values have varying heights. Height Classification is determined as shown in table 4.1.

Table 3.1. Height Classification Criteria for Study Areas

Number of Floors	Height Classification
1-5	Low Rise
6-10	Mid Rise
11<	High Rise

Coordinates of case study urban blocks, total areas of different materials on the surface, building density in areas, number of floors, classification of floor heights, and building types are given in Table 4.2. The combined data in this table are used to make comparisons in the following sections.

Table 3.2. Properties of Case Study Urban Blocks

AREA	COORDINATE (x)	COORDINATE (y)	BUILDING AREA (m²)	GRASS AREA (m²)	WATERBODY AREA (m²)	ASPHALT AREA (m2)	PAVEMENT AREA (m²)	SOIL AREA(m²)	TOTAL AREA (m2)	BUILDING DENSITY (%)	FLOORS	BUILDING HEIGHT	BUILDING TYPE
BAHÇELİEVLER	39.92388	32.83140	16470.00	2152.08	0.00	8644.54	12732.53	0.00	40000	41.17	4	LOW	RESIDENTIAL
ÇUKURAMBAR 1	39.90189	32.80395	8962.59	16122.09	0.00	5496.28	9418.31	0.00	40000	22.41	9	MEDIUM	RESIDENTIAL
ÇUKURAMBAR 2	39.90765	32.81289	9513.63	1423.25	0.00	4370.00	17568.12	7125.00	40000	23.78	34	HIGH	OFFICE
DEMETEVLER	39.96566	32.79014	18862.48	0.00	0.00	6059.01	15060.11	0.00	40000	47.16	7	MEDIUM	RESIDENTIAL
ERYAMAN 1	39.99507	32.64448	3943.04	13055.64	911.82	6355.91	15733.59	0.00	40000	9.86	26	HIGH	RESIDENTIAL
ERYAMAN 2	39.97254	32.64766	3463.43	24596.06	0.00	4599.70	6791.02	549.71	40000	8.66	5	LOW	RESIDENTIAL
ESKİŞEHİR YOLU	39.91114	32.79629	2178.58	3756.81	0.00	10869.30	17641.43	5553.88	40000	5.45	24	HIGH	OFFICE
GÖLBAŞI	39.78172	32.78977	737.75	20182.44	5044.12	1235.76	5725.45	7074.47	40000	1.84	2	LOW	OFFICE
HAMAMÖNÜ	39.93468	32.86557	18874.96	1828.17	0.00	2842.26	16454.09	0.00	40000	47.19	2	LOW	RESIDENTIAL
İŞÇİ BLOKLARI	39.89166	32.79720	5719.53	22418.04	0.00	8799.46	2837.42	225.55	40000	14.30	5	LOW	RESIDENTIAL
İVEDİK	39.96112	32.81685	20621.87	1430.36	0.00	6462.25	11485.52	0.00	40000	51.55	5	LOW	RESIDENTIAL
KIZILAY	39.92131	32.85744	15747.58	0.00	0.00	12674.41	11559.38	0.00	40000	39.37	9	MEDIUM	OFFICE
MEVLANA BLV.	39.89926	32.81332	13118.36	4680.70	0.00	8407.87	13793.07	0.00	40000	32.80	26	HIGH	OFFICE
SİNCAN	39.95926	32.57530	11864.57	0.00	0.00	9682.78	18452.65	0.00	40000	29.66	4	LOW	RESIDENTIAL
TULUMTAŞ	39.76287	32.72956	5792.41	21810.74	0.00	4032.04	4580.46	3784.36	40000	14.48	2	LOW	RESIDENTIAL
TUNUS	39.91437	32.85698	13268.75	1530.71	0.00	10694.46	14506.05	0.00	40000	33.17	4	LOW	RESIDENTIAL

16 urban blocks are given numbers in alphabetical order on the Ankara map and the characteristics of these blocks are explained in detail in the following section. (Figure 3.5.)

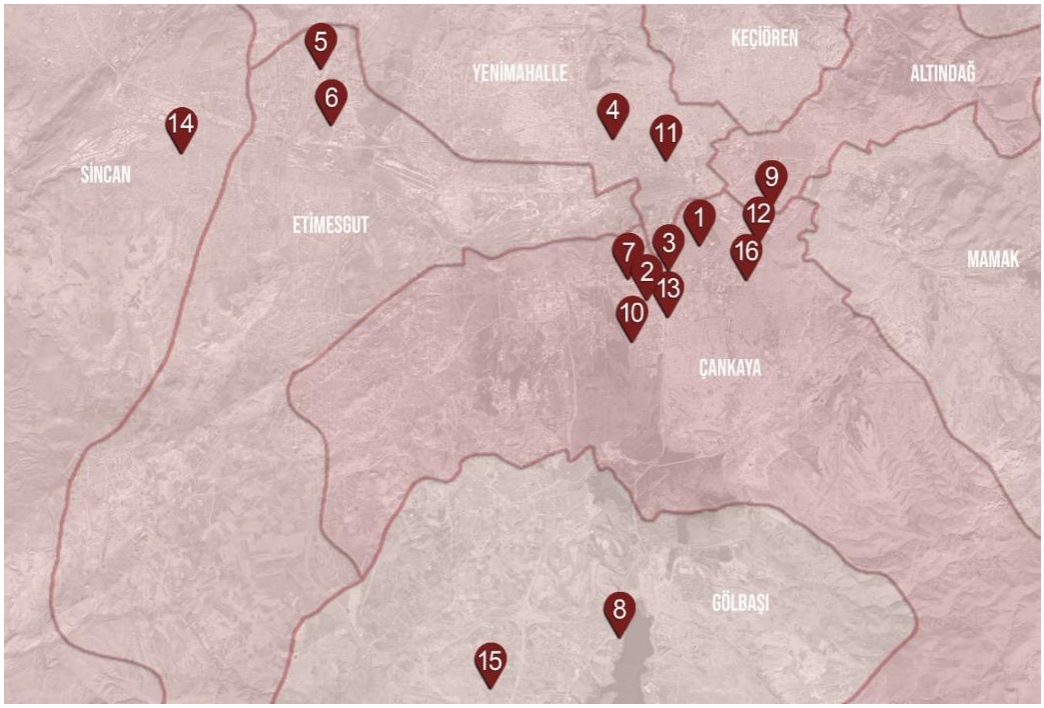

Figure 3.5. Case study urban blocks indicated on the map (1-Bahçelievler, 2-Çukurambar1, 3-Çukurambar2, 4-Demetevler, 5-Eryaman1, 6-Eryaman2, 7-Eskişehir Yolu, 8-Gölbaşı, 9-Hamamönü, 10-İşçi Blokları, 11-İvedik, 12-Kızılay, 13-Mevlana Bulvarı, 14-Sincan, 15-Tulumtaş, 16-Tunus Caddesi)

1) Urban Block 1 - Bahçelievler

The typology of the buildings in the urban block located at 39.923877, 32.831397 coordinates is similar, and the buildings have a height of 4 floors. There is no grass-covered area between these residential buildings, but there is a park (2152.08 m^2) located at the north of the study area. In the streets between the buildings, the plantation can be seen along the sidewalks. (Figure 3.6.)

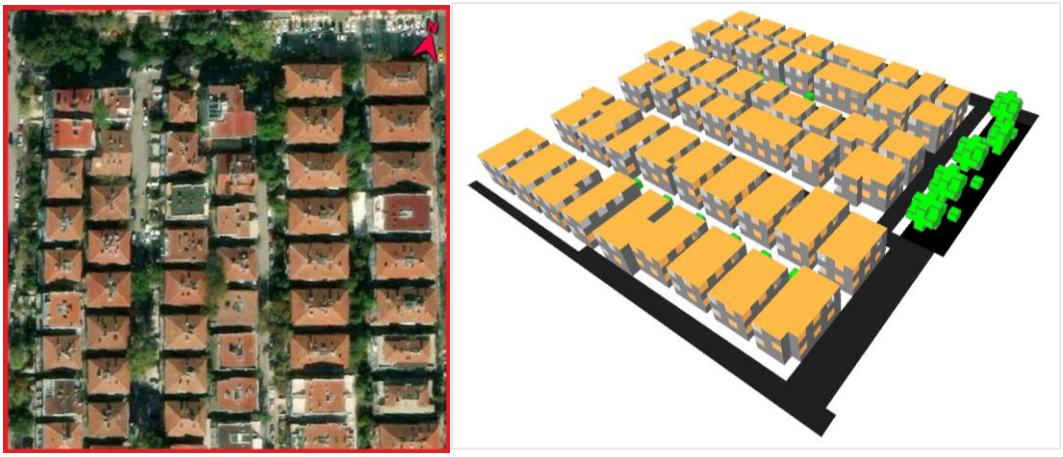

Figure 3.6. Satellite Image (left) and 3D Model (right) of the selected Urban Block 1 – Bahçelievler

2) Urban Block 2 - Çukurambar 1

In this urban block with low building density (22.41%), streets and asphalt cover the largest area. Residential buildings with an average height of 9 floors have their own green areas (16,122.09 m²), but the rate of paved area in the block is also high (9,418.31 m²). (Figure 3.7.)

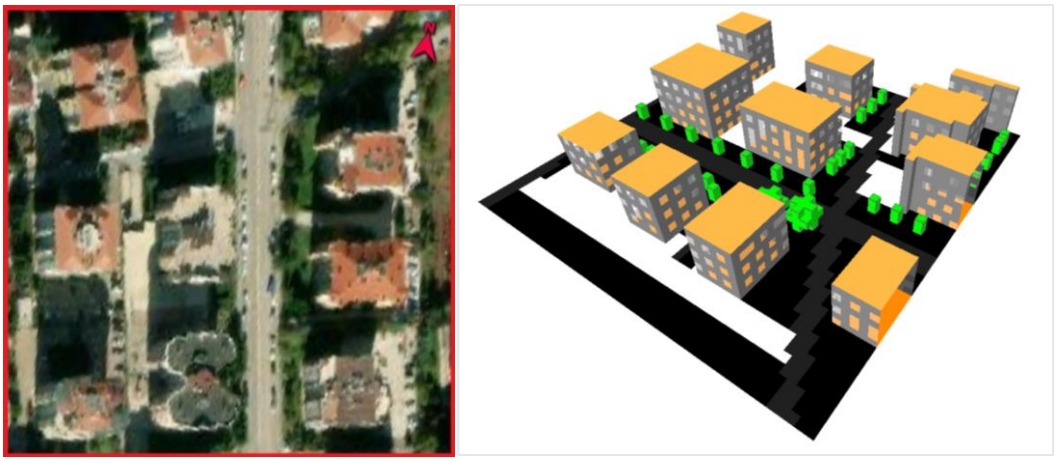

Figure 3.7. Satellite Image (left) and 3D Model (right) of the selected Urban Block 2 - Çukurambar 1

3) Urban Block 3 - Çukurambar 2

In this urban block, which has almost the same building density as Çukurambar 1 (23.78%), the buildings are being used as offices and have a height of up to 34 floors. There is approximately 10% grass cover in the selected block. The exterior materials of the buildings in the block are mirror-like glass, which is a highly reflective material. (Figure 3.8.)

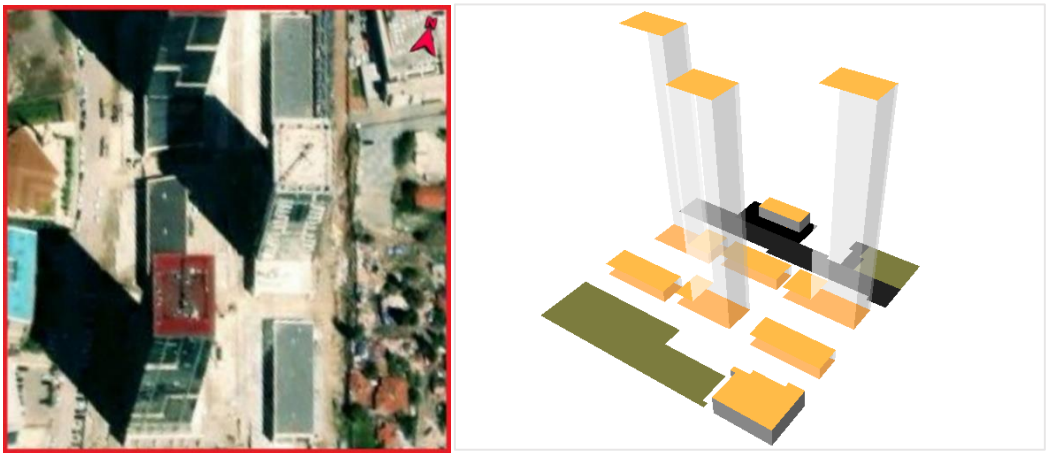

Figure 3.8. Satellite Image (left) and 3D Model (right) of the selected Urban Block 3 - Çukurambar 2

4) Urban Block 4 - Demetevler

In this area with a building density of 47.16% and an average building height of 7 floors, the ground floors of the buildings are used as commercial spaces, while the upper floors are used as residential units. In this block, which has no grass cover, trees that can provide shade are very few. (Figure 3.9.)

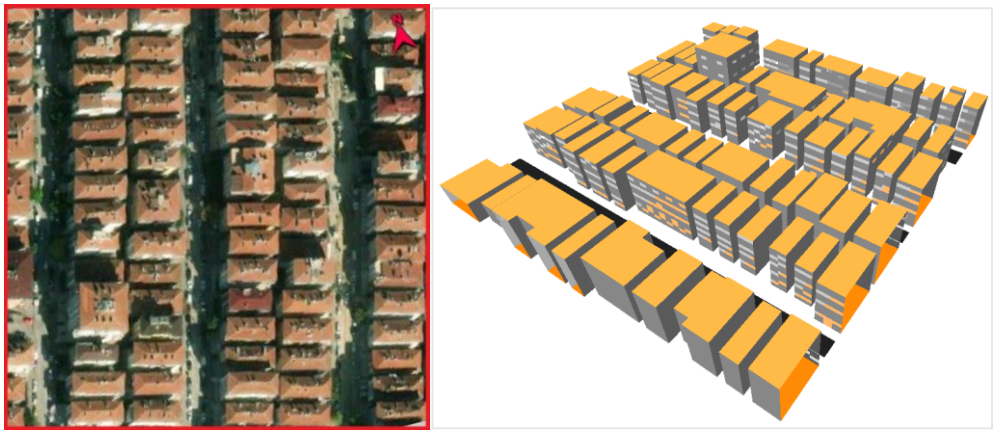

Figure 3.9. Satellite Image (left) and 3D Model (right) of the selected Urban Block 4 – Demetevler

5) Urban Block 5 - Eryaman 1

The buildings in the area are 26 stories high and are used as residential units. In this block with a low building density (9.86%), most of the ground cover materials are grass and pavements made of concrete tiles. Newly planted trees in the area are not able to create shade. (Figure 3.10.)

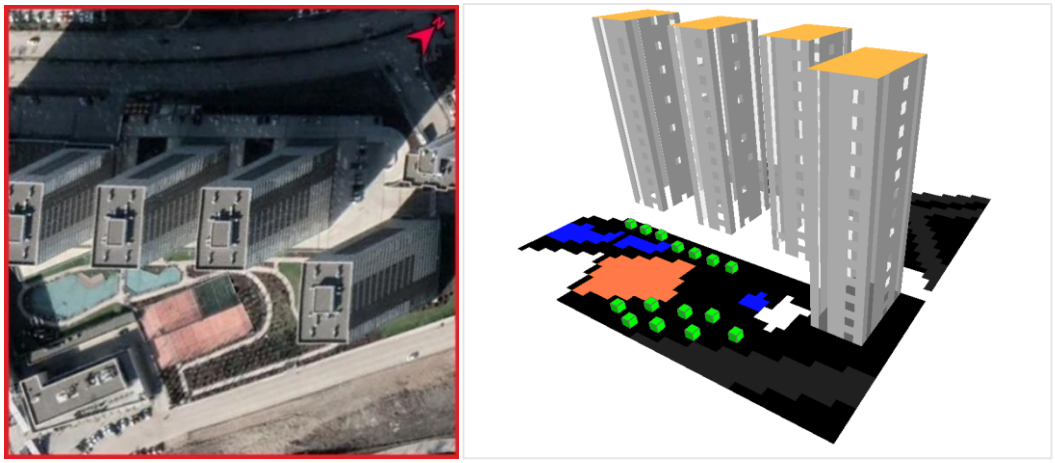

Figure 3.10. Satellite Image (left) and 3D Model (right) of the selected Urban Block 5 - Eryaman 1

6) Urban Block 6 - Eryaman 2

Among the studied areas, it is the area with the highest amount of grass cover (24596,057 m²). At the same time, the building density ratio of the area is low (8.66%). Between the buildings with a height of 5 floors, there are tall trees that provide shade. (Figure 3.11.)

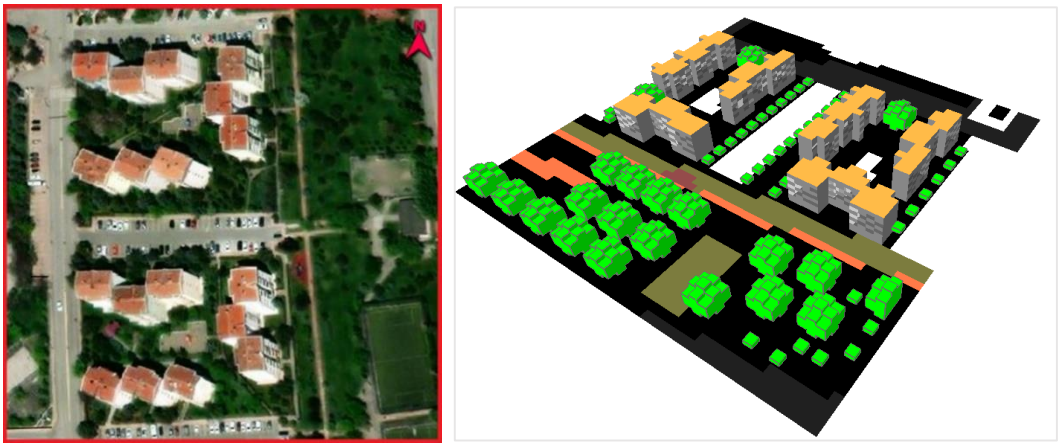

Figure 3.11. Satellite Image (left) and 3D Model (right) of the selected Urban Block 6 - Eryaman 2

7) Urban Block 7 - Eskişehir Yolu

In the area around Eskişehir Yolu, the selected block has a building density of 5.45%, and the building heights are 24 floors. The exterior facades of the buildings that are used as offices have mirrored glazing with highly reflective properties. There are no vegetation or landscape elements that create shade around the pavement, which is open to the pedestrian circulation between the buildings. (Figure 3.12.)

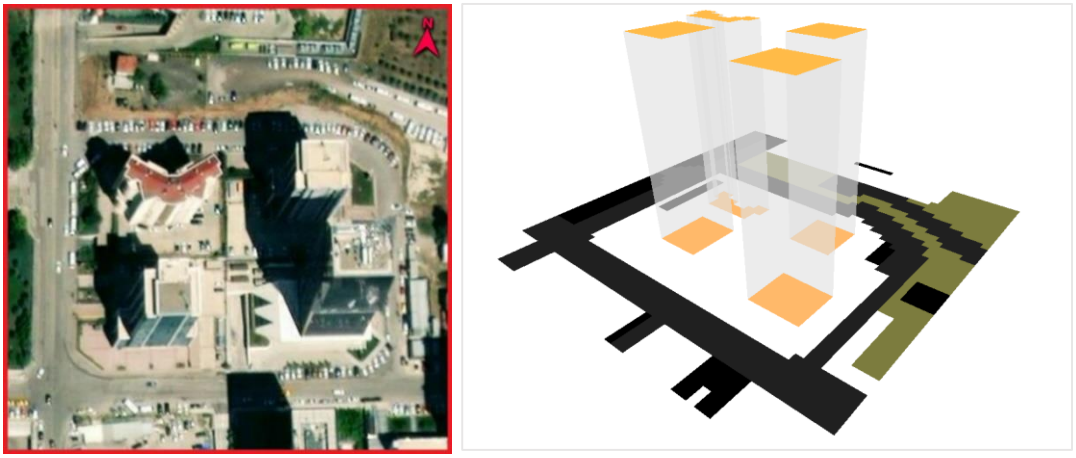

Figure 3.12. Satellite Image (left) and 3D Model (right) of the selected Urban Block 7 - Eskişehir Yolu

8) Urban Block 8 - Gölbaşı

The buildings located in this area bordering Mogan Lake, have a height of 2 floors. Building density is low (1.84%) in this block, which has approximately 50% grass cover and 12.5% water. (Figure 3.13.)

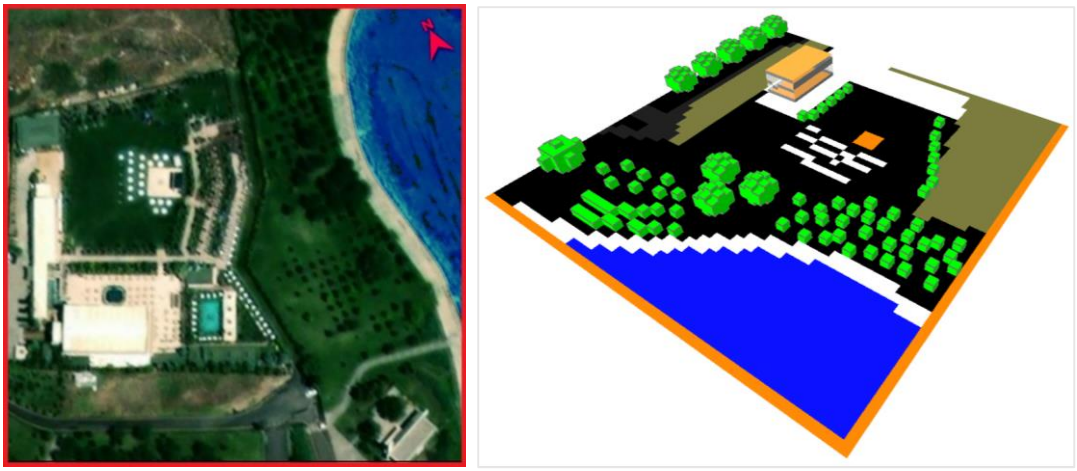

Figure 3.13. Satellite Image (left) and 3D Model (right) of the selected Urban Block - 8 Gölbaşı

9) Urban Block 9 - Hamamönü

The selected area in Hamamönü, which is one of the old and central settlements of Ankara, is one of the blocks with the highest building density (47.19%). Buildings with a height of 2 floors show an irregular layout. Among the buildings, the amount of grass cover is low (1828.17 m²), while the amount of pavement is high (16,454.09 m²). Trees with the feature of creating shadows are not very common in the area. (Figure 3.14.)

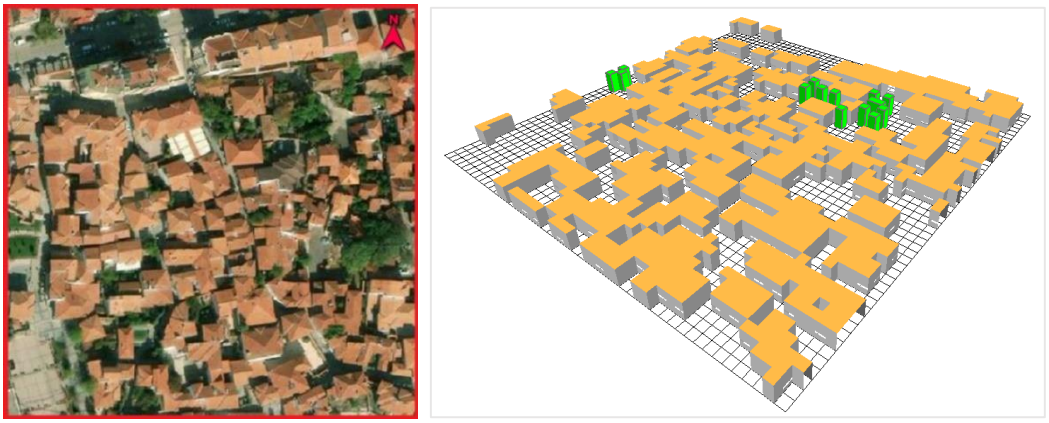

Figure 3.14. Satellite Image (left) and 3D Model (right) of the selected Urban Block 9 – Hamamönü

10) Urban Block 10 - İşçi Blokları

The buildings in this area, which is adjacent to Malazgirt Boulevard, have the same typological characteristics and are 5 stories high. Due to the Malazgirt Boulevard proximity, approximately 25% of the area has asphalt as ground cover. More than 50% of the block has grass and the trees in the area are tall and densely populated. (Figure 3.15.)

Figure 3.15. Satellite Image (left) and 3D Model (right) of the selected Urban Block 10 - İşçi Blokları

11) Urban Block 11 - İvedik

Unlike the building typologies found in other areas in the study, the buildings in this area are attached buildings like row houses. Due to this settlement pattern, long and thin corridors are formed in the block and there are very few spaces that can provide airflow between these parallel corridors. In this block, which has the highest building density (51.55%) among the case study areas, the building heights are 4 floors. Grass cover between the buildings is about 3.5% and there are no trees that can provide shade in the area. (Figure 3.16.)

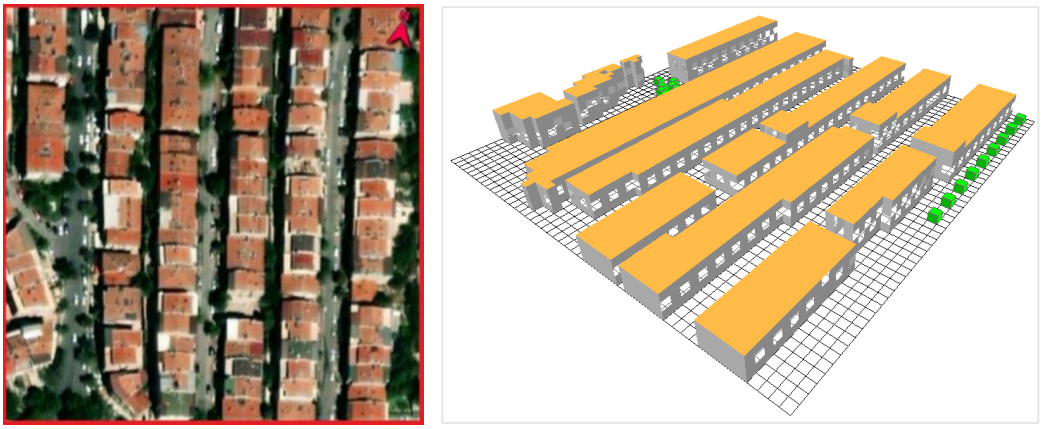

Figure 3.16. Satellite Image (left) and 3D Model (right) of the selected Urban Block 11 - İvedik

12) Urban Block 12 - Kızılay

Buildings with an average height of 9 floors, located in the center of Ankara, have office and commercial functions. For this reason, the glazing ratio is very high on the building facades, especially on the entrance floors. The total amount of asphalt including the street passing through the middle of the area is 12,674 m². In the selected block grass cover is zero, and the trees that may provide shade are at a negligible level. (Figure 3.17.)

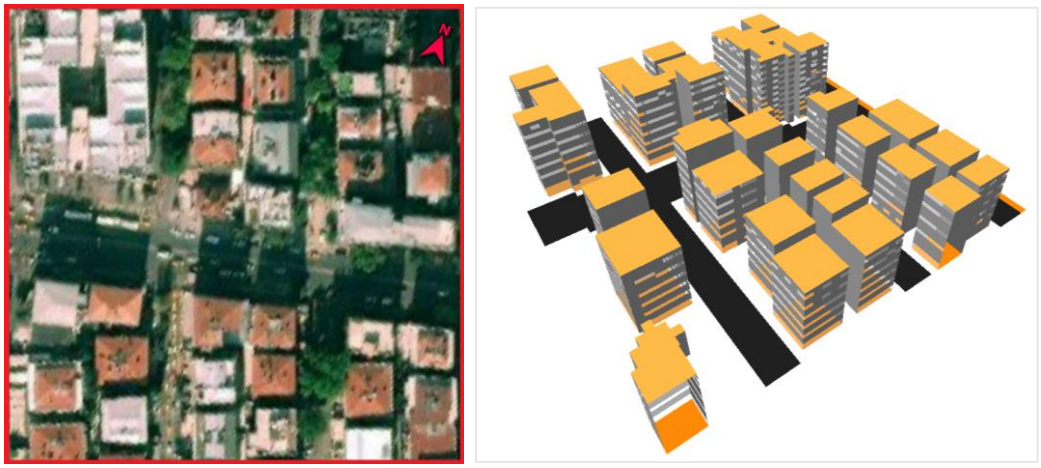

Figure 3.17. Satellite Image (left) and 3D Model (right) of the selected Urban Block 12 - Kızılay

13) Urban Block 13 - Mevlana Bulvarı:

The case study block has been selected from the area touching Mevlana Bulvarı with a width of 10 traffic lanes. The density of the buildings in the block is 32.80%, and the building heights are 26 floors. The facades of buildings with office and commercial functions are made of mirrored glass with high reflective properties. (Figure 3.18.)

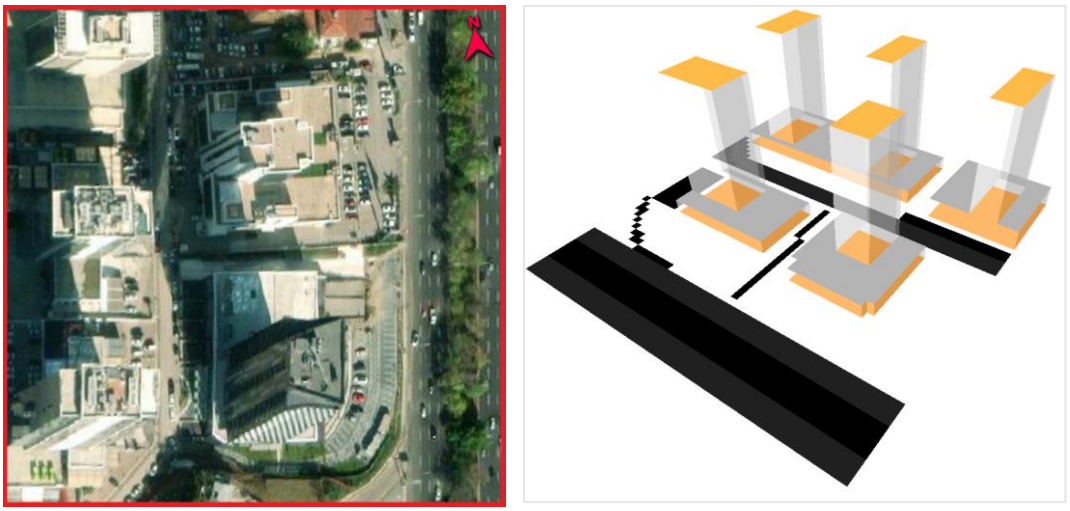

Figure 3.18. Satellite Image (left) and 3D Model (right) of the selected Urban Block 13 - Mevlana Bulvarı

14) Urban Block 14 - Sincan

In this area with no grass cover, the building density is 29.66%. The average floor height is 4. Trees in the area are in negligible and there is no landscaping element in the area that has the quality to cast shadows. (Figure 3.19.)

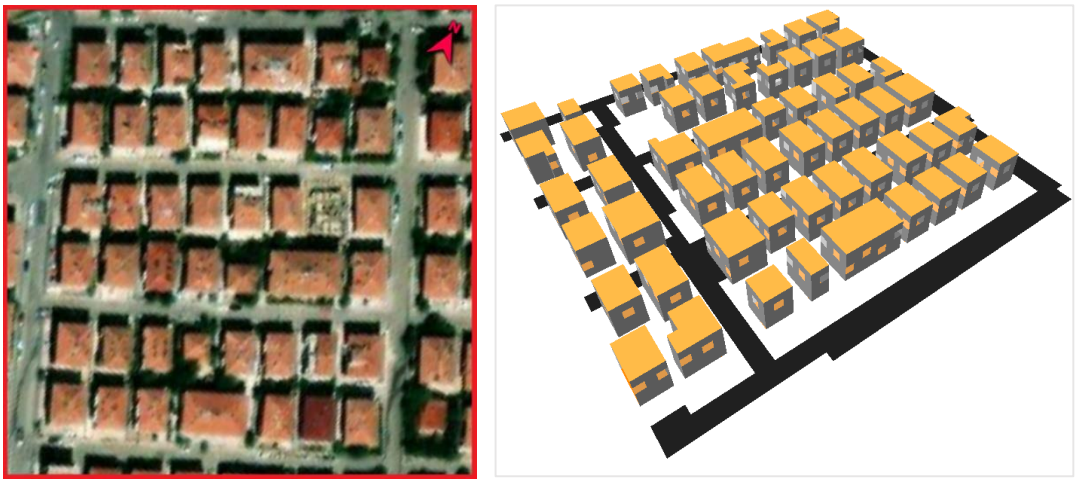

Figure 3.19. Satellite Image (left) and 3D Model (right) of the selected Urban Block 14 - Sincan

15) Urban Block 15 - Tulumtaş

In Tulumtaş, one of the new settlements, the building density is low (14.48%). In this block consisting of 2-story detached houses, the owners have their own gardens. Although the amount of grass is high at 21,810.74 m², the trees planted are still new and do not have the quality to cast a shadow. (Figure 3.20.)

Figure 3.20. Satellite Image (left) and 3D Model (right) of the selected Urban Block 15 – Tulumtaş

16) Urban Block 16 – Tunus Caddesi

The density of the buildings in the study area, which is centrally located in Ankara, is 33.17%, and the average floor height is 4. Although the amount of grass in the area is low (1530.74 m²), the trees planted along the street have high shading qualities. (Figure 3.21.)

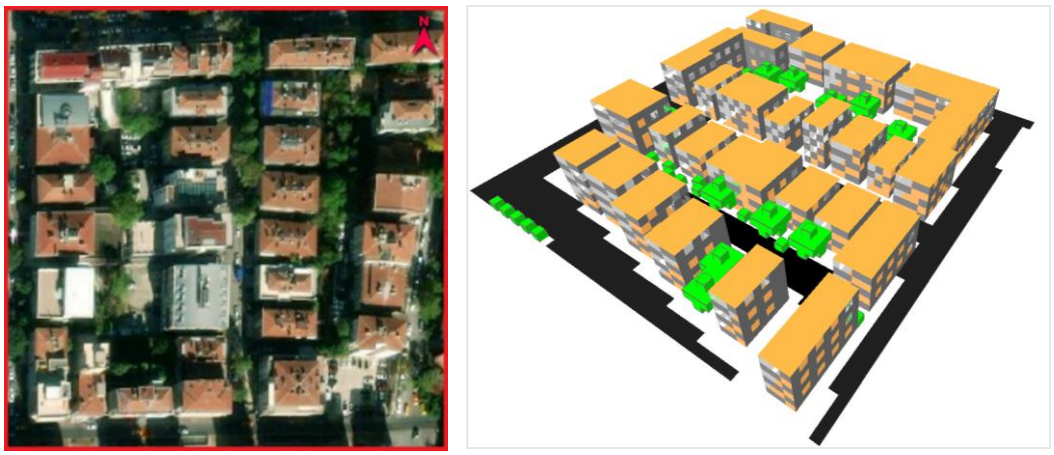

Figure 3.21. Satellite Image (left) and 3D Model (right) of the selected Urban Block 16 – Tunus Caddesi

3.3 Equipment

A number of equipment was needed to obtain data about materials and environmental factors in the selected case study areas. These are described in this section.

a) Digital Camera

During the visits to the case study areas, vertical and horizontal surfaces and surrounding elements were photographed digitally. The equipment used for this process is a digital camera built into the author's smartphone. The photos taken are saved in .jpg format, have 3024x4032 pixel dimensions and the resolution is 72 dots per inch (dpi).

b) Thermal Camera

Figure 3.22. FLIR E60 Thermal Camera (Source: https://www.flir.eu/)

FLIR E60 Thermal Camera was used for capturing thermal imagery of the building facades and ground cover to determine surface temperatures. Thermal images taken from the device, are saved in .jpg format with 320x240 pixel dimensions and the resolution is 72 dpi.

3.4 Software

Various software was needed in order to process the physically obtained data into digital media and to use it in the later stages of the study. In this section, the software used during this study is introduced.

c) Satellite Image Software

Google Earth Pro is a free software for obtaining aerial photographs taken by satellites around the world. After the blocks in the case study areas were determined, high resolution and scaled satellite images of the areas were obtained by this software. (Figure 3.23.)

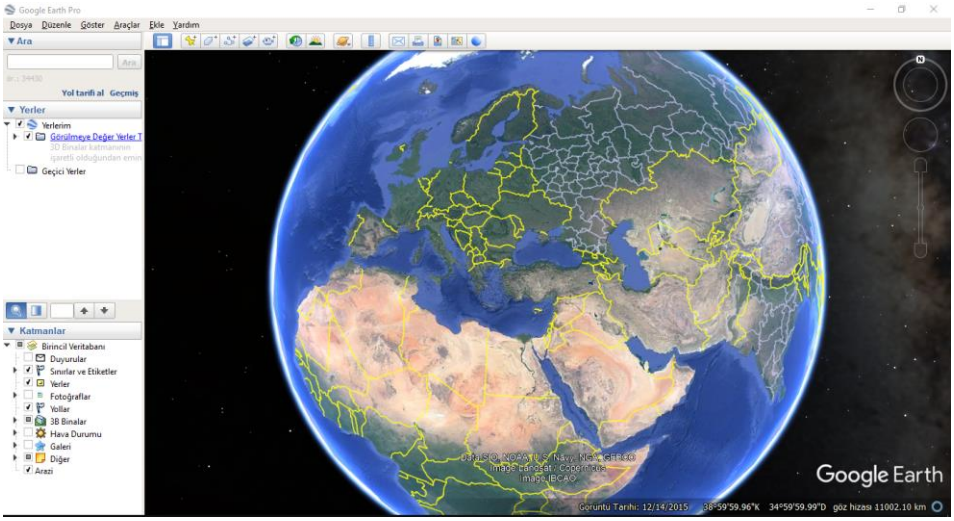

Figure 3.23. Google Earth Software User Interface Screenshot

d) Albedo Calculation Software

ImageJ is an open-source image processing and analysis program. Color and light analysis required to make albedo calculations were obtained in the "histogram" tab of this software. (Figure 3.24.)

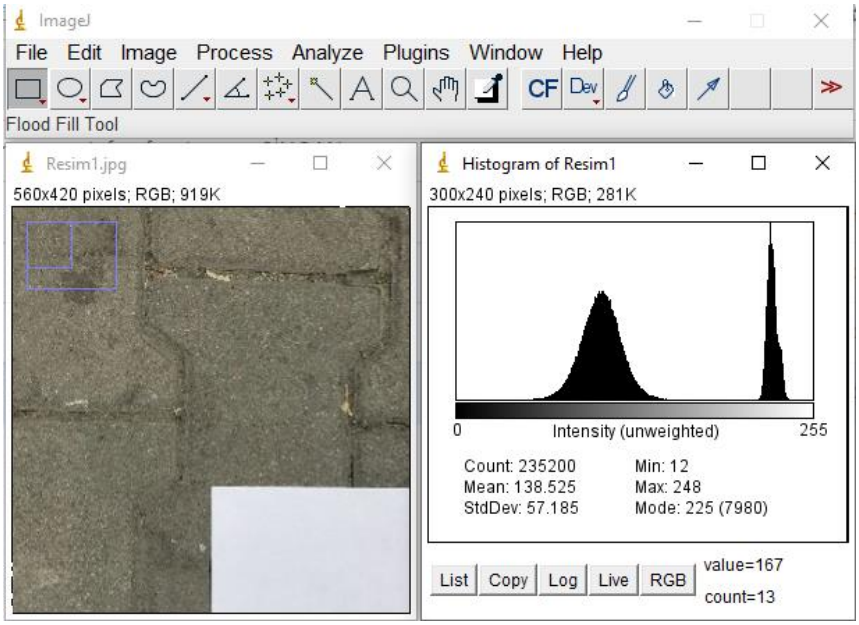

Figure 3.24. ImageJ Software User Interface Screenshot

e) Microsoft Excel

The formula used to calculate the albedo values was entered in the excel table and the albedo values of all materials were obtained in this way. Additionally, photographs taken in the field and thermal camera images are also added to the tables in this software. (Figure 3.25.)

Table 3.3. Albedo calculation formula at Microsoft Excel Software Screenshot

MATERIAL	HAMAMÖNÜ PAVEMENT	İVEDİK PAVEMENT
ALBEDO PHOTOGRAPHY		
MEAN VALUE (PAPER ALBEDO)	241.289	240.917
MEAN VALUE (SURFACE ALBEDO)	133.257	113.889
SURFACE ALBEDO VALUE (%)	=(J5/J4)*0.65	**0.307275327**

f) CAD Software

The CAD (Computer-Aided Design) software used to model workspaces is SketchUp Pro 2020. The structures and other environmental elements on the scaled satellite images are modeled in 3D. These models were then used for the simulation phase. (Figure 3.25.)

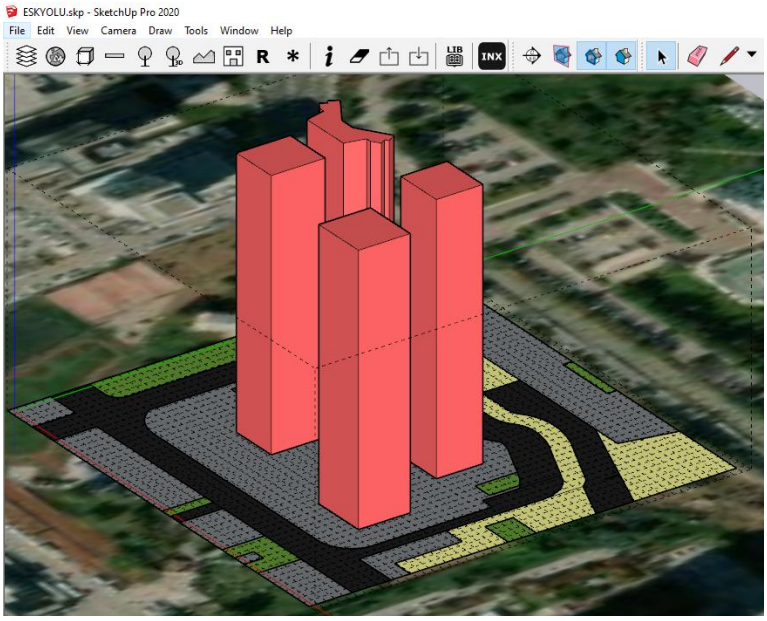

Figure 3.25. SketchUp Pro Software User Interface Screenshot

g) Microclimate Simulation Software

ENVI-met LITE 4.4.6 is the software used to process all the data collected in the previous stages onto the field models and perform microclimate simulations. There are different tasks in the tabs within this software: The collected material data is processed on the 3D model from the "Spaces" tab, the climate data required for the simulation is set in the "ENVI-Guide" tab, and the microclimate simulation process is carried out from the "ENVI-Core" tab, and finally, simulation results are visualized as various maps from the "Leonardo" tab. (Figure 3.26.)

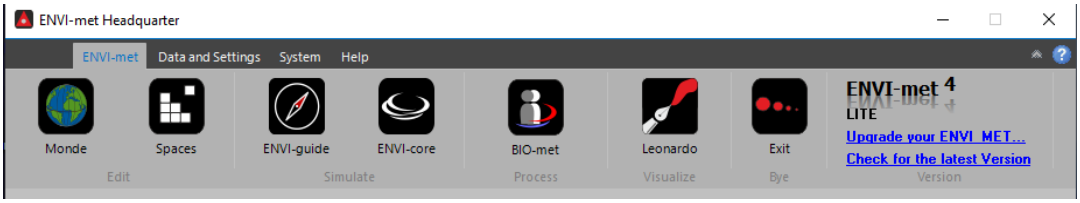

Figure 3.26. Different tabs on the ENVI-met LITE 4.4.6 Software Screenshot

CHAPTER 4

RESEARCH METHODOLOGY

In the first section of this chapter, the selection criteria of the case study areas are explained in detail and a preliminary step is provided for the other stages. The approximate locations of the areas were determined on the satellite images and site visits were made to draw the definite borders of the urban blocks to be analyzed. According to these borders, 3D models of the case study areas were prepared.

Secondly, digital camera images were used for calculating the albedo values of the building facades and the pavements around the buildings.

Thirdly, thermal camera and digital camera images of different surfaces were taken at the site. Thermal imagery shows the temperature of the specific points on surfaces.

Lastly, material and albedo values were input to 3D models on ENVI-met Microclimate Simulation Software in order to simulate climate scenarios for these 16 urban blocks, which contain different materials and building typologies and have different environmental factors.

4.1 Selection of the Case Study Urban Blocks

As it is mentioned in the problem statement section of the study, the effects of urbanization on the climate have reached a level that can be noticed by city-dwellers. The expansion of settlements in Ankara to peripheral districts over the years has been taken into consideration; therefore, not only the first settlements but also the later migrated areas were included in the scope of the study.

If there was no human activity in Ankara and the temperature data were distributed according to the Digital Elevation Model (DEM) i.e. the altitude data, there should have been a temperature distribution among the districts as shown in Figure 4.1.

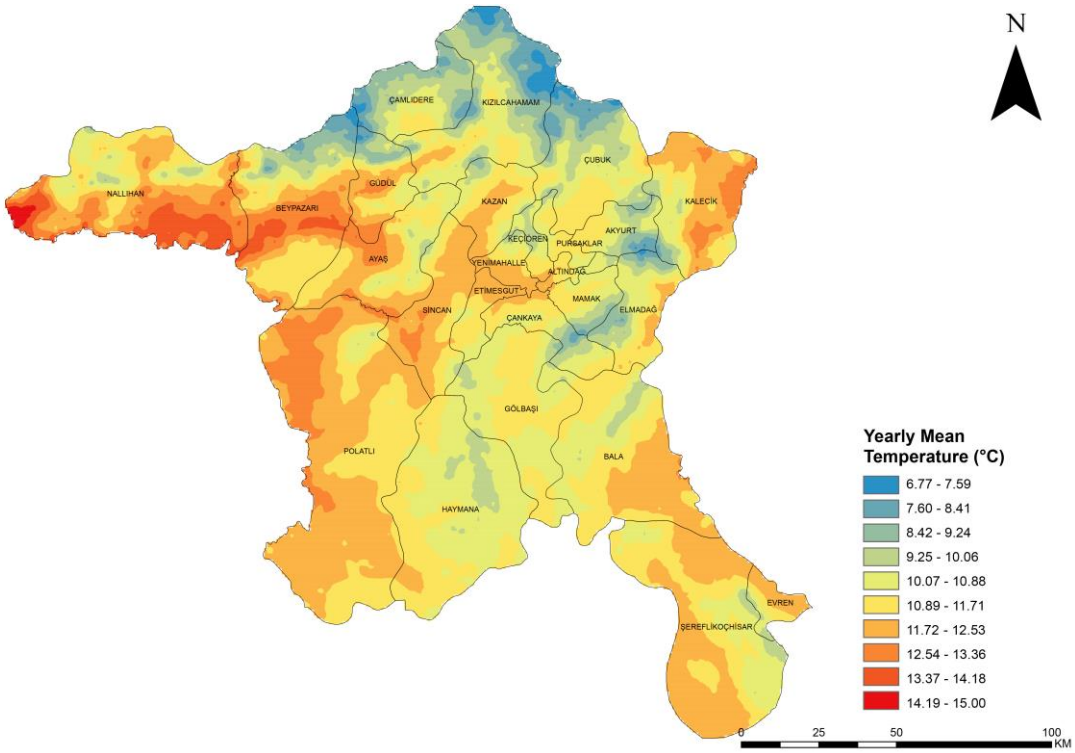

Figure 4.1. Temperature Map Based on Digital Elevation Model (DEM) Data (Prepared by Savaş Demiröz)

However, when the data obtained from the real weather stations in the district centers are processed on the map, it can be observed that the temperature data results are different from the DEM temperature map. (Figure 4.2.)

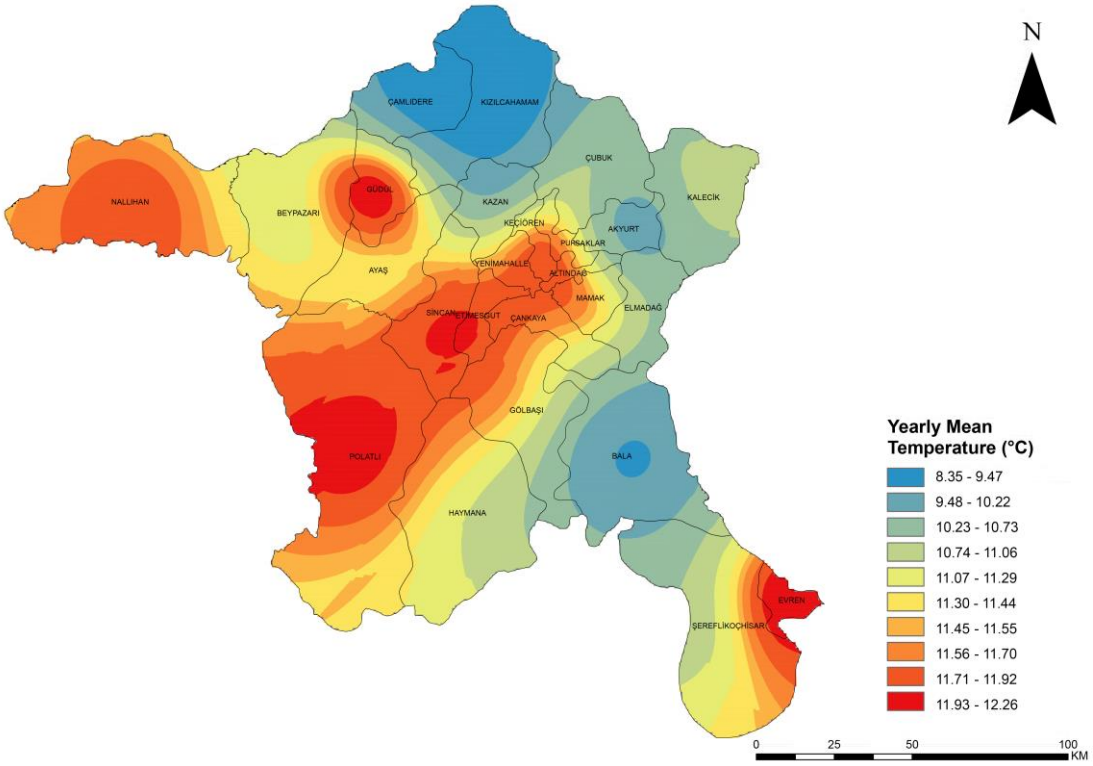

Figure 4.2. Temperature Map Based on Real Weather Station Data (Prepared by Savaş Demiröz)

When the 2020 population data based on districts from TÜİK are shown on the map (Figure 4.3.), it is seen that the registered population data is especially high in Çankaya, Etimesgut, Keçiören, Yenimahalle, and Sincan. These areas with a high registered population also have a high rate of urban settlement. That is the main reason for selecting the previously mentioned 16 urban blocks in different locations in Ankara.

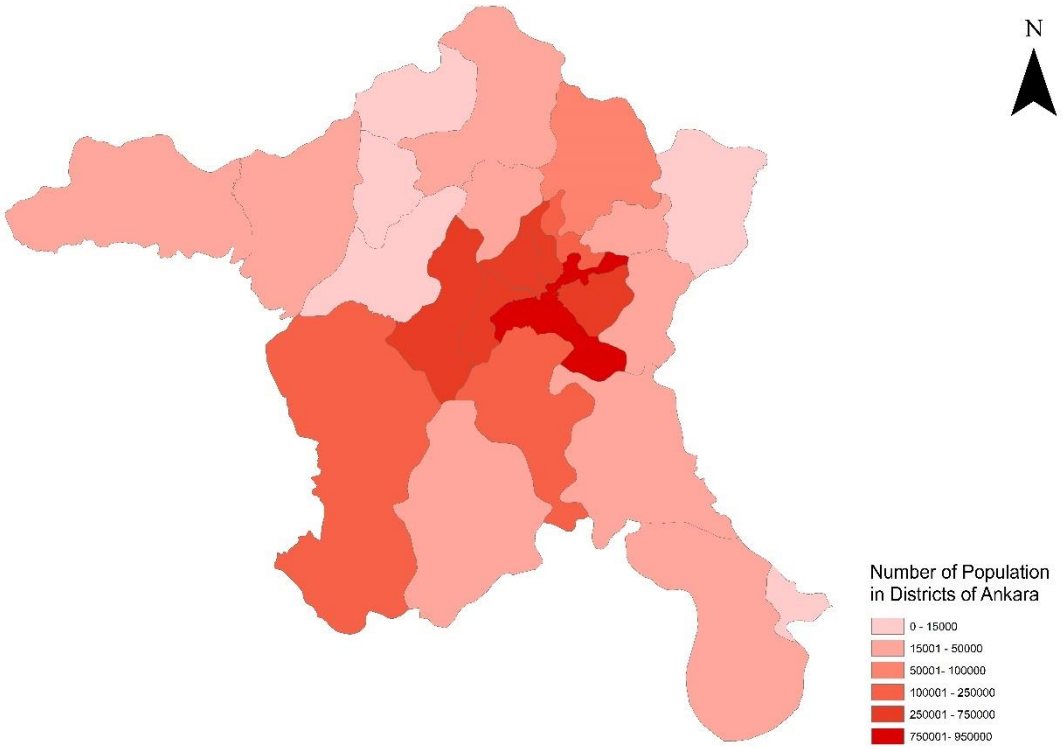

Figure 4.3. 2020 Population Data Based on Districts (TÜİK, 2020) - (Prepared by Savaş Demiröz)

All recorded data of the studied urban blocks are shown in Table 4.1. The date when measurements were taken, the time range of taking digital and thermal photographs, and climatic conditions of that moment are recorded.

Table 4.1 Weather data on the dates of site visits when thermal camera images and albedo measurements were taken (Data Source: https://weather.com)

	AREA	MEASUREMENT DATE	TIME RANGE	TEMPERATURE (°C)	HUMIDITY (%)	WIND DIRECTION	WIND SPEED (km/h)	PRECIPITATION (cm)	PRESSURE (hPa)	SIGHT DISTANCE (km)	UV INDEX
1	BAHÇELİEVLER	24.07.2021	13:45	27	25	NE	8	0	1007	16.1	9
2	ÇUKURAMBAR 1	22.07.2021	14:10	29	25	NNE	5	0	1006	16.1	8
3	ÇUKURAMBAR 2	24.07.2021	14:50	28	23	N	10	0	1012	9.7	7
4	DEMETEVLER	22.07.2021	13:00-13:21	28	26	NW	18	0	1013	9.7	9
5	ERYAMAN 1	21.07.2021	13:21-13:51	32	29	WSW	11	0	1012	9.7	9
6	ERYAMAN 2	28.07.2021	13:00-13:21	30	23	NE	11	0	1018	9.7	9
7	ESKİŞEHİR YOLU	23.07.2021	13:00-13:15	28	30	NNE	10	0	1007	16.1	9
8	GÖLBAŞI	26.07.2021	13:20-13:40	28	28	NW	14	0	1017	9.7	9
9	HAMAMÖNÜ	22.07.2021	14:00-14:20	29	31	NNE	11	0	1005	16.1	8
10	İŞÇİ BLOKLARI	22.07.2021	14:25	28	31	NNW	21	0	1012	9.7	7
11	İVEDİK	24.07.2021	14:30	28	23	N	10	0	1012	9.7	7
12	KIZILAY	23.07.2021	13:55-14:20	28	30	NNE	10	0	1007	16.1	9
13	MEVLANA BLV.	24.07.2021	14:50	28	23	N	10	0	1012	9.7	7
14	SİNCAN	28.07.2021	13:55-14:20	31	22	NE	11	0	1018	9.7	9
15	TULUMTAŞ	26.07.2021	13:50-14:10	28	27	NW	14	0	1017	9.7	9
16	TUNUS	23.07.2021	13:20-13:45	28	30	NNE	10	0	1007	16.1	9

4.2 Albedo Calculation

Albedo value is an important criterion in determining the amount of light and heat energy reflected by a surface. After the surface temperatures were measured and recorded with a thermal camera, the albedo values of the same surfaces were calculated.

In the method used to measure albedo values, first of all, a white sheet of paper is placed on the various surfaces and their photographs are taken with the digital camera. After the photos are taken, the photos are opened on the ImageJ program. The “mean values” of the material and white paper whose albedo value is to be

measured are displayed on the "histogram" tab. Then, the obtained data are placed in the formula:

$$\frac{\text{mean value of the material}}{\text{mean value of the white paper}} \times \text{white paper albedo value } (0.65) = \text{albedo of the material}$$

Since the albedo value of the white paper is 0.65, when it is substituted in the equation, the albedo value of the studied material is determined. The values of floor and facade materials were recorded with this method in all selected urban blocks during the site visits conducted on the 21st, 22nd, 23rd, 24th, 26th, and 28th of July, 2021 as shown in Table 1.1. in Chapter 1.

For instance, a white sheet of paper was placed on the asphalt surface and a photograph was taken. When this photograph was analyzed with the ImageJ Software, the mean value of white printing paper was found as 241.067 and the mean value of asphalt surface was determined as 104.591 (Figure 4.4.). Using the following formula, the albedo value of the asphalt surface was calculated to be 0.2820.

$$\frac{104.591}{241.067} \times 0.65 \text{ (white paper albedo value} = 0.2820 \text{ (albedo of the material)}$$

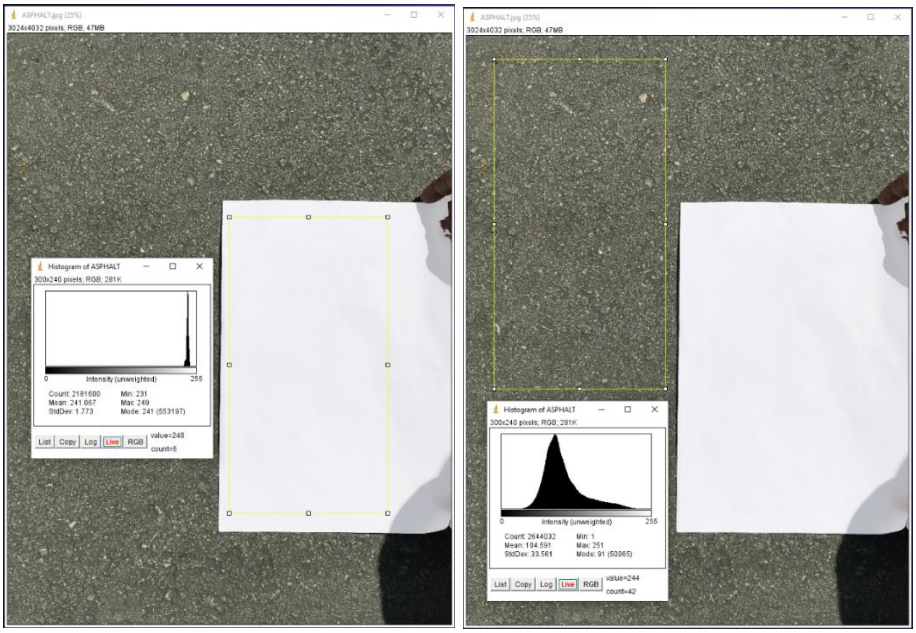

Figure 4.4. Determining the mean value of white paper (241.067) and asphalt (104.591)

4.3 Thermal Imagery

While taking images with the FLIR thermal camera, it was recognized that there are similar conditions in different districts. For this reason, measurements were made within the same time intervals and weather conditions in every area visited.

Thermal imagery photographs were taken at the hours 13:00-15:00, between the dates 20-28 July 2021, when there was no precipitation. Because of gaining direct sunlight, facades facing the south direction are taken into consideration and the surfaces which are overshadowed were neglected.

Temperature data of horizontal and vertical surfaces of the blocks are both measured. While the thermal camera photograph is taken, the digital photograph of the same surface is also recorded (Figures 4.5. and 4.6.).

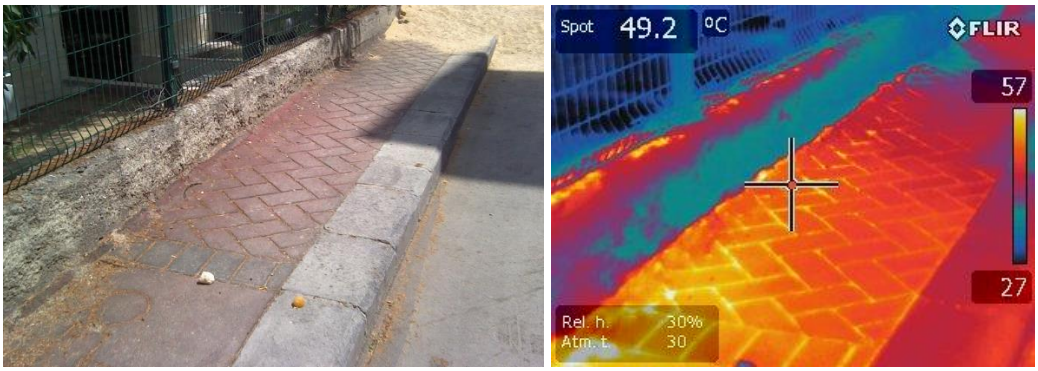

Figure 4.5. Digital image (left) and thermal image (right) of a pavement

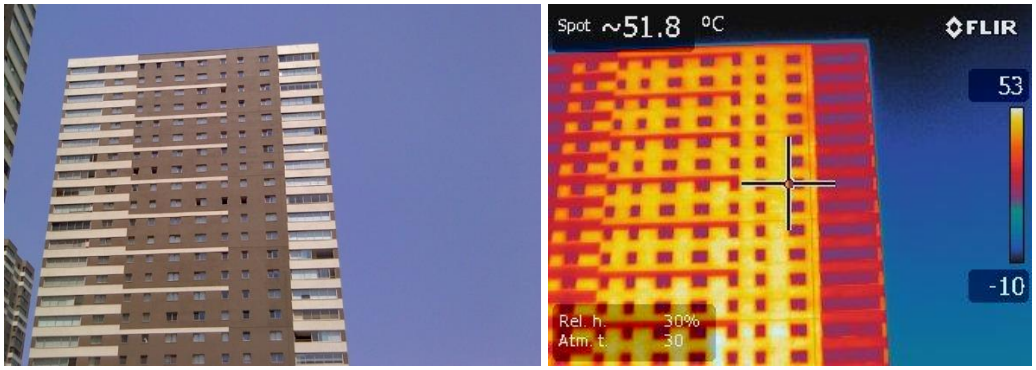

Figure 4.6. Digital image (left) and thermal image (right) of a building facade

4.4 Microclimate Simulation Software

ENVI-met Simulation Software allows users to have maximum of 50x50x40 grid dimensions in the LITE version (Figure 4.7.). For this reason, these dimensions were considered when determining the building boundaries and 3D modeling in the areas to be studied.

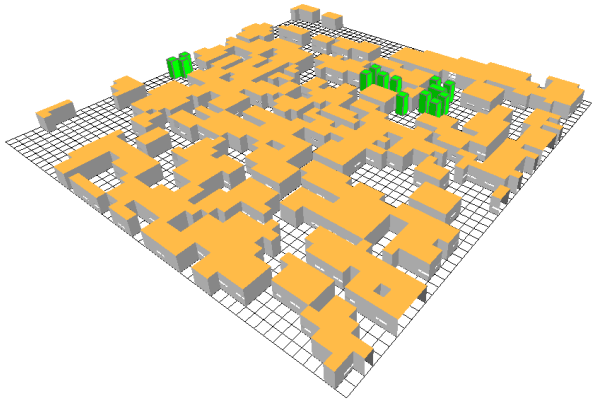

Figure 4.7. 3D model version of Hamamönü Block on 50x50x40 grid system on ENVI-met Software

Location, weather and site conditions, vegetation, water mass, the orientation of the buildings, building heights, building densities, vertical and horizontal surface elements, real albedo values, and window-to-wall ratio were input for the simulations in ENVI-met Software. The collected data are processed into necessary parts in the software and the model is prepared for the simulation. (Figure 4.8.).

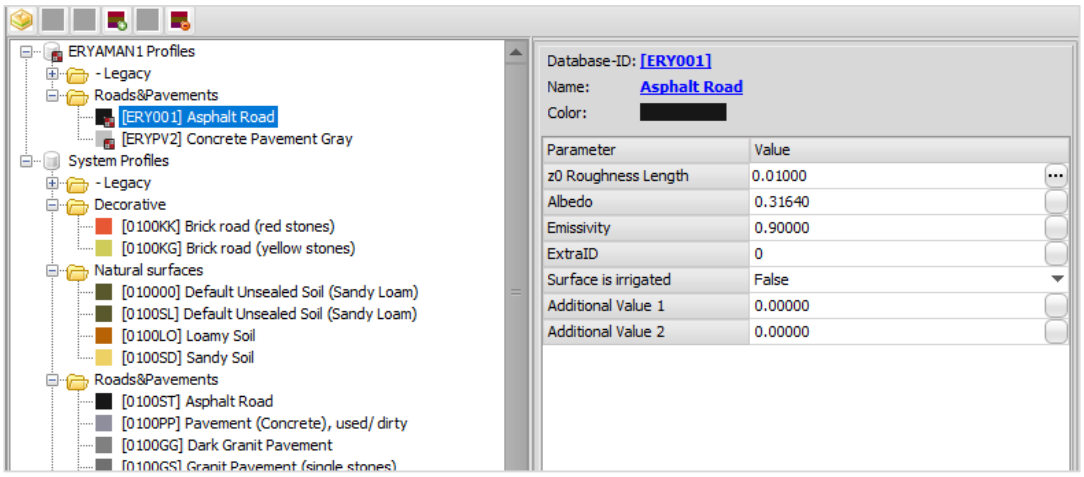

Figure 4.8. ENVI-met software interface for identifying material properties for each urban block

The results calculated for the hours 15:00 (3 PM), when the sun is the most intense, are discussed. In order to obtain these results, the simulation program was run between 12:00 and 16:00 hours, because the situation before and after the critical hour for the study should be considered to obtain the temperatures at the desired time. (Figure 4.9.)

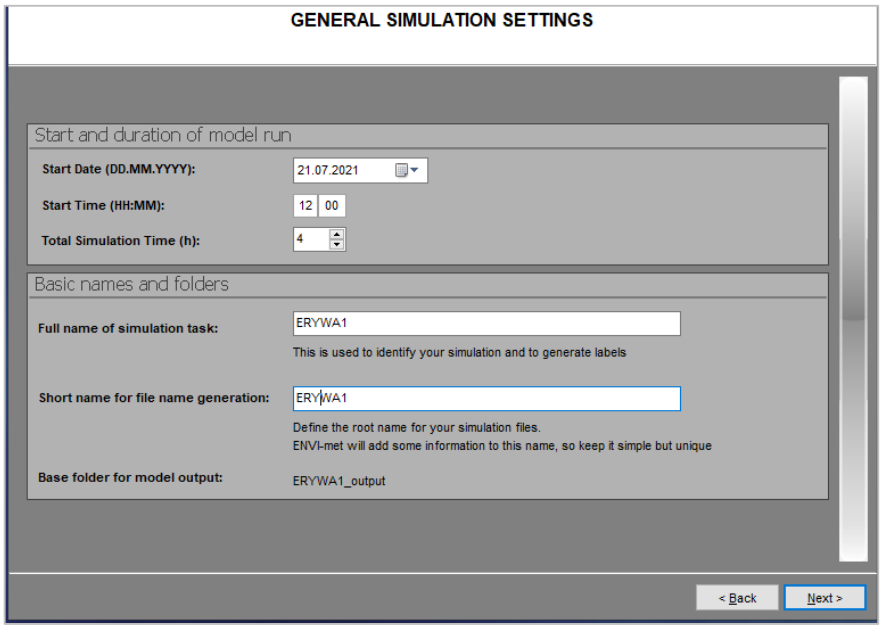

Figure 4.9. General Simulation Settings Window

The average temperature, humidity, and radiation data recorded for the 21st of July (Figure 4.10.) are entered in the necessary places in the basic meteorological settings window. (Figure 4.11.)

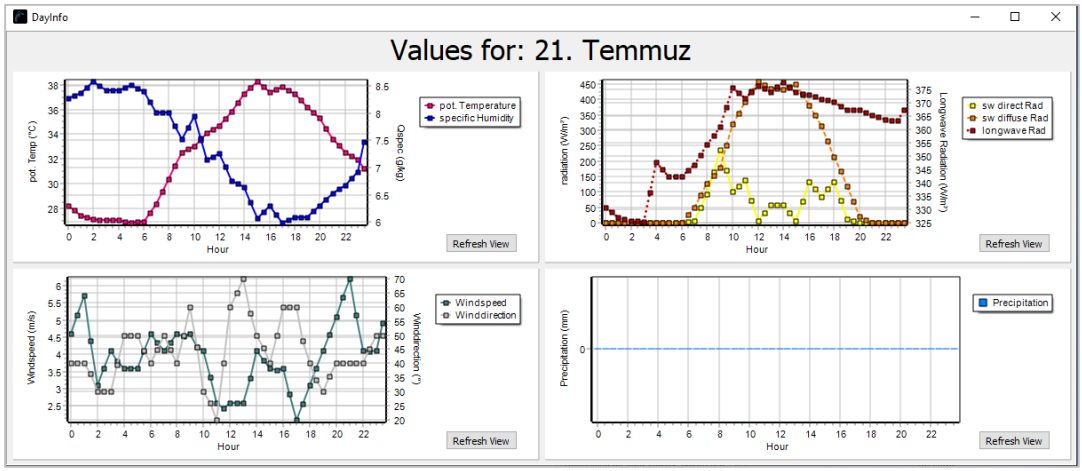

Figure 4.10. The average temperature, humidity, and radiation data recorded for the 21st of July

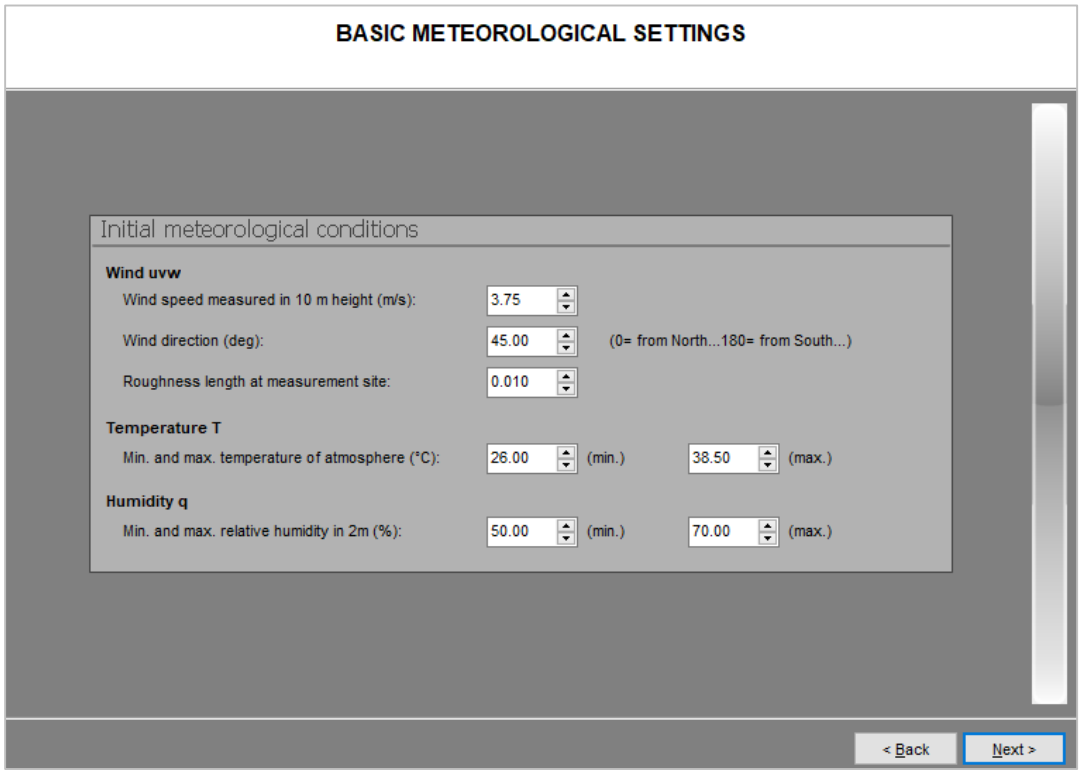

Figure 4.11. Basic Meteorological Settings Window

ENVI-met LITE software only allows users to have the following outputs: atmosphere, inflow, radiation, soil, and surface. Buildings, receptors, and vegetation outputs are obtained in the professional version of the software.

After simulations were conducted, “Leonardo” which is a visualization software application already built into ENVI-met was used to get the different types of maps and graphical presentations of the output data. Legends of the maps are selected specifically for each area for showing the regional value differences within one study area. Therefore, each map has different values for its legends. (Figure 4.12.)

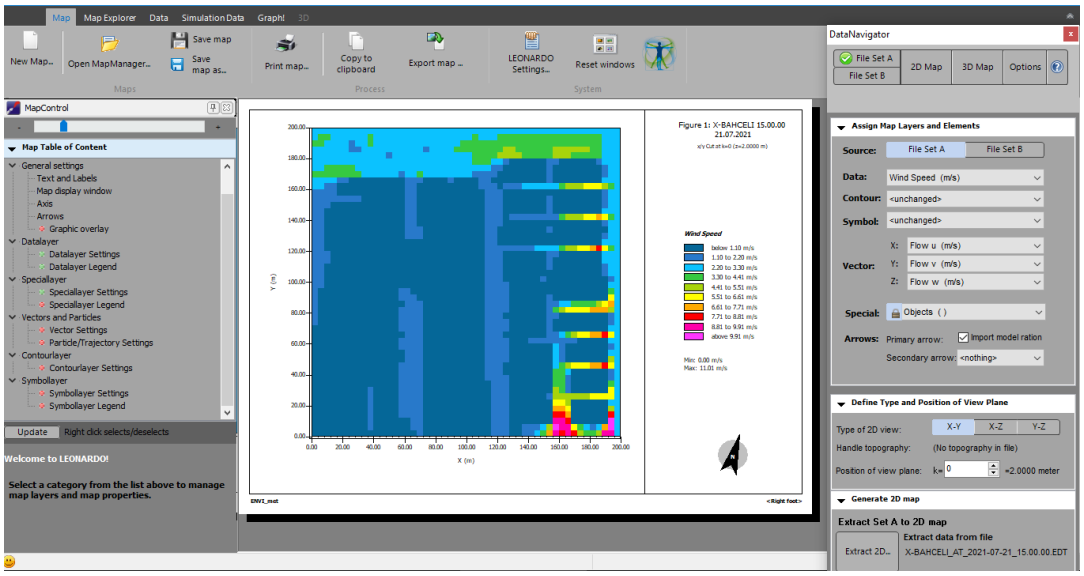

Figure 4.12. ENVI-met Leonardo User Interface for creating maps

CHAPTER 5

RESULTS AND DISCUSSIONS

In this chapter, all the information collected will be described in detail and the results of the study will be discussed.

In the first part of the chapter, one of the selected urban blocks, which is Eryaman-1 Block, is explained as an example in order to understand the working method and to demonstrate the actions taken within the scope of the study step by step.

In the second part of this chapter, all study areas were compared among themselves according to building parameters and urban parameters. By separating the scales under the title of building and urban, it is aimed to make the effects of different surface materials on the microclimate more coherent.

5.1 Analysis of the Selected Urban Block

Urban Block 5 - Eryaman 1 (Figure 5.1.) is the block with the highest variety of materials within the scope of the studies. The high material diversity and the characteristic features of the area were frequently used when making comparisons in the later stages of the study.

Under this title, all studies of the Eryaman-1 Block are examined and how building materials, environmental factors, and structures affect the microclimatic properties of this block is explained.

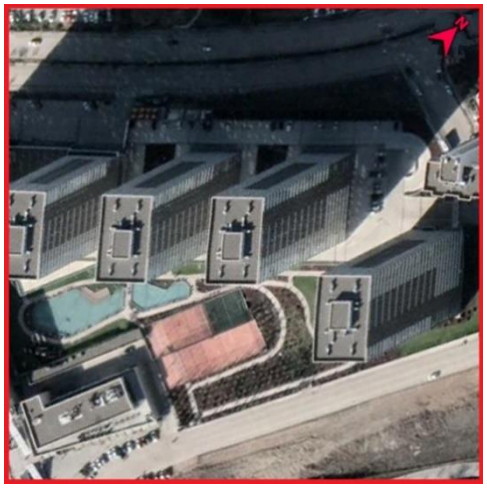

Figure 5.1. Satellite Image of the selected Urban Block 5 - Eryaman 1

There are 4, 26-story residential blocks in Eryaman 1 with an area of 40,000 sqm, located at coordinates 39.9995 and 32.6444. (Table 5.1). These blocks cover 9.86% of the total area and their window ratio is 26%, that is, approximately one-fourth of the facades of a building consist of windows, and the other three-quarters are walls. Although it is known that the structural system of the buildings is the tunnel concrete system, the walls on the outer surfaces are pumice blocks without load-bearing properties. The next layers are the thermal insulation layer, the outer plaster, and the paint, respectively. Dark-colored exterior paint was preferred in the blocks, and decorative pattern work was carried out with light-colored paints along the floor moldings.

Table 5.1. General Information about the Urban Block 5 - Eryaman 1

URBAN BLOCK 5 - ERYAMAN 1	
COORDINATE (x)	39.99507354
COORDINATE (y)	32.64447927
BUILDING AREA (m²)	3943.43
GRASS AREA (m²)	13055.64
WATER AREA (m²)	911.82
ASPHALT AREA (m²)	6355.91
PAVEMENT (m²)	15733.59

Table 5.1. (Continued)

SOIL (m²)	0.00
TOTAL AREA (m²)	40000.00
BUILDING DENSITY (%)	9.86
VEGETATION	YES
FLOOR NUMBER	26
BUILDING HEIGHT	HIGH
BUILDING TYPE	RESIDENTIAL
WINDOW RATIO (%)	26

Data collected from the selected block in Eryaman is given in Table 5.2 below. Measurements in the field were made on 21 July 2021, between 13:21 and 13:51. The current air temperature was 32 °C and the relative humidity in the air was 29%. The wind was blowing from the West-Southwest direction at a speed of 11 km/h. The sky was clear, and the sight distance was 9.7 kilometers.

Table 5.2. Data collected on the day of measurement

URBAN BLOCK	ERYAMAN 1
MEASUREMENT DATE	21.07.2021
TIME RANGE	13:21-13:51
TEMPERATURE (°C)	32
HUMIDITY (%)	29
WIND DIRECTION	WSW
WIND SPEED (km/h)	11
PRECIPITATION (cm)	0
PRESSURE (hPa)	1012
SIGHT DISTANCE (km)	9.7
UV INDEX	9

5.1.1 Analysis on Component Scale

The horizontal and vertical surfaces had different materials, textures, and colors. These differences were viewed with the FLIR Thermal camera, and photographs were taken to analyze the thermal behavior of the surfaces; e.g. it was observed that there is a temperature difference of 15 centigrade degrees between the surfaces of

different colors of the building walls. Additionally, albedo calculations of the surface materials were made after putting a white sheet of paper on the walls of different colors and photographs thus taken were uploaded to ImageJ software. The albedo value of the dark-colored wall was found to be lower (0.292) and the temperature was higher (64.6 °C), while the albedo value of the light-colored wall was higher (0.533) and the temperature value was lower (50.2 °C). With respect to the measurements, an inversely proportional relationship was observed between the albedo values and the surface temperatures, as expected. (Table 5.3.)

Table 5.3. Wall albedo and temperature values for Urban Block 5 - Eryaman 1

MATERIAL	WALL1	WALL2
ALBEDO PHOTOGRAPHY		
MEAN VALUE (PAPER ALBEDO)	242.209	211.928
MEAN VALUE (SURFACE ALBEDO)	108.869	174.021
SURFACE ALBEDO VALUE (%)	**0.292164412**	**0.533736222**
DIGITAL PHOTOGRAPHY		
THERMAL IMAGERY	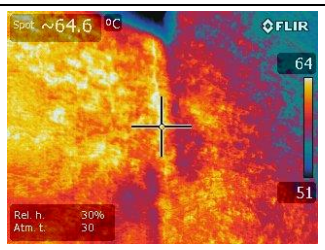	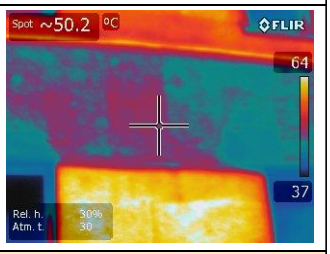
TEMPERATURE (°C)	**64.6**	**50.2**

There are various horizontal surface materials with different properties in the area (Table 5.4.). Walking paths, basketball field, and floors between buildings are classified under the title of “pavement”. The total surface area of these areas is 1573.59 square meters. Walkways are indicated as “Pavement 1” in the table. There are light and dark-colored floor tiles together on the walkways. In the images taken with the thermal camera, the temperature of the part with the red color in the tiles is 45.9 °C, and the temperature of the darker floor is 50.5 °C. It has been observed that the temperatures of the two materials made of the same material and in contact with each other differ according to their albedo value.

Table 5.4. Albedo and temperature values for different horizontal surfaces in Eryaman 1

MATERIAL	PAVEMENT1	PAVEMENT2	PAVEMENT3	BASKETBALL FIELD
ALBEDO PHOTOGRAPHY	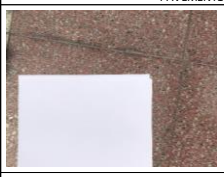			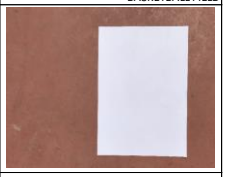
MEAN VALUE (PAPER ALBEDO)	235.819	230.271	236.831	229.942
MEAN VALUE (SURFACE ALBEDO)	119.351	149.480	84.980	114.964
SURFACE ALBEDO VALUE (%)	0.32897328	0.421946315	0.233233825	0.324980212
DIGITAL PHOTOGRAPHY				
THERMAL IMAGERY	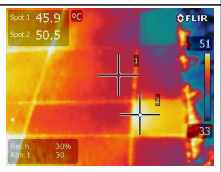	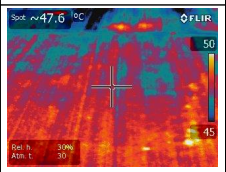	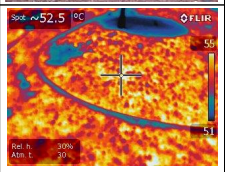	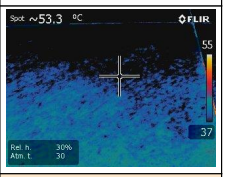
TEMPERATURE (°C)	45.9	47.6	52.5	53.3

The main material that fills the sections between the buildings is named “Pavement 2” and is made of concrete blocks. The albedo value of this material is measured as approximately 0.422, and the surface temperature is observed as 47.6 °C.

The albedo value of the basketball court (Pavement 4) in the area is 0.325 and the surface temperature is 53.3 °C. On the other hand, the surface temperature of the material called “Pavement 3” is 52.5 °C, but its albedo value is 0.233. The fact that there are two materials with almost the same temperature and different albedo values

shows that the temperature does not depend only on the albedo value, but that the different structural properties of the material affect the temperature value also.

13055.64 square meters of the area is covered with grass. There are trees up to 5 years old in the green area but these trees are not able to provide shade. Although the albedo value of the grass was 0.206, which is the lowest albedo value calculated in the area, the surface temperature was measured at 30.3 °C. Therefore, it can be seen that factors such as the high water-holding capacity of the grass and the fact that they give out water vapor through photosynthesis cause the surface temperature to decrease. (Table 5.5.)

Table 5.5. Albedo and temperature values for grass-covered area in Eryaman 1

MATERIAL	GRASS
ALBEDO PHOTOGRAPHY	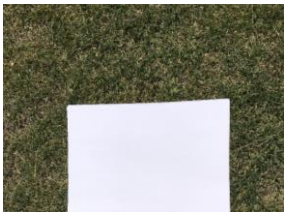
MEAN VALUE (PAPER ALBEDO)	241.997
MEAN VALUE (SURFACE ALBEDO)	76.909
SURFACE ALBEDO VALUE (%)	0.206576321
DIGITAL PHOTOGRAPHY	
THERMAL IMAGERY	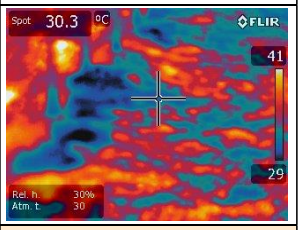
TEMPERATURE (°C)	30.3

Another main ground material with high density in the area is asphalt. Covering an area of 6355.91 square meters, asphalt is located at the back of the buildings. When the images were taken with the thermal camera, the surface temperature of the asphalt

was measured at 52.5 °C and it was determined that it was the material with the highest surface temperature among all horizontal surfaces. The albedo value of asphalt was calculated as approximately 0.3164. (Table 5.6.)

Table 5.6. Albedo and temperature values for asphalt in Eryaman 1

MATERIAL	ASPHALT
ALBEDO PHOTOGRAPHY	
MEAN VALUE (PAPER ALBEDO)	230.362
MEAN VALUE (SURFACE ALBEDO)	112.153
SURFACE ALBEDO VALUE (%)	0.316456056
DIGITAL PHOTOGRAPHY	
THERMAL IMAGERY	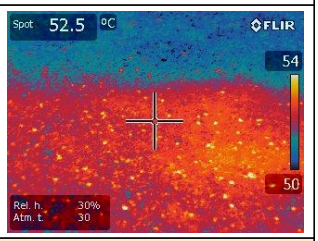
TEMPERATURE (°C)	52.5

The last horizontal surface on the area with a different characteristic than other horizontal surfaces is the pool. There are 3 pools in the area, located closely and the total horizontal surface area of the pools is 911.82 square meters. The pools in the area are not deep swimming pools, but shallow ornamental pools. The albedo value of the water cannot be calculated, but the material properties are processed in the model. In the ENVI-met software, the depth of the pools is specified in order to obtain accurate microclimate data in simulations.

In the digital photograph seen in Figure 5.2., the sun rays reflecting on the pool can be seen. When the same area is photographed with a thermal camera, the instantaneous temperature values on the water vary depending on the reflections of the sun's rays. Although the water temperature is not high in mass, the surface temperature of the pool is recorded as 58 °C, but this value is seen at the points where the sun rays are reflected; hence this is not a representative value.

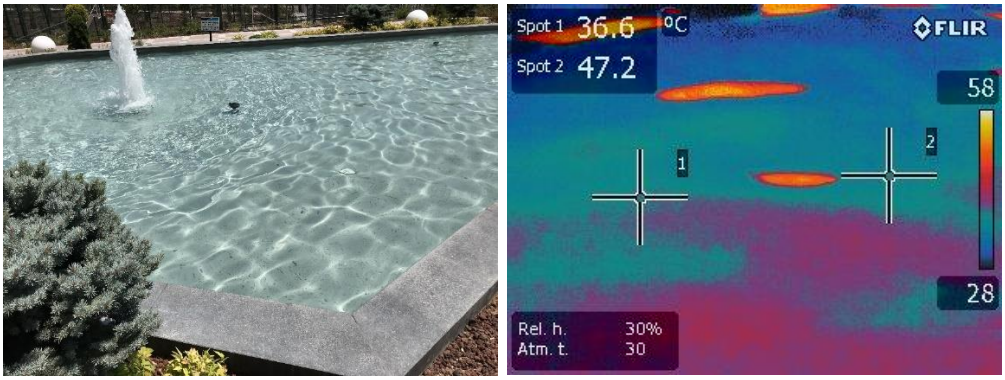

Figure 5.2. Digital (left) and thermal (right) images of the pools in Eryaman 1

5.1.2 Analysis on the Urban Scale

With SketchUp Pro, 3D models of the structures in the area were prepared and the material types of the structures were shown. The data of material properties obtained from field measurements were processed into these 3D models through the ENVI-met software. Then, simulation was taken under the climatic conditions specified in the materials and methodology section of the study.

When the given map (Figure 5.3.) is examined, it can be seen that the parts with the highest temperature values (above 44 °C) are the areas shown with the color fuchsia. These areas are roads covered with asphalt material. Then the areas indicated in red color are covered with “pavement 2” material, which is made of concrete. Although there is the same material in the area between the high blocks, the reason why the temperature of those areas appears below 28 °C is due to the shade from the buildings on the ground.

Another low-temperature area in the block is the areas with pools and lawns. Since the water in the pools takes a longer time to warm up and cool down, it can be deduced that this is the reason why the temperature does not rise much during the day. Similarly, green areas, although low in albedo values, can cause the surroundings to get cold as they give off water vapor throughout the day.

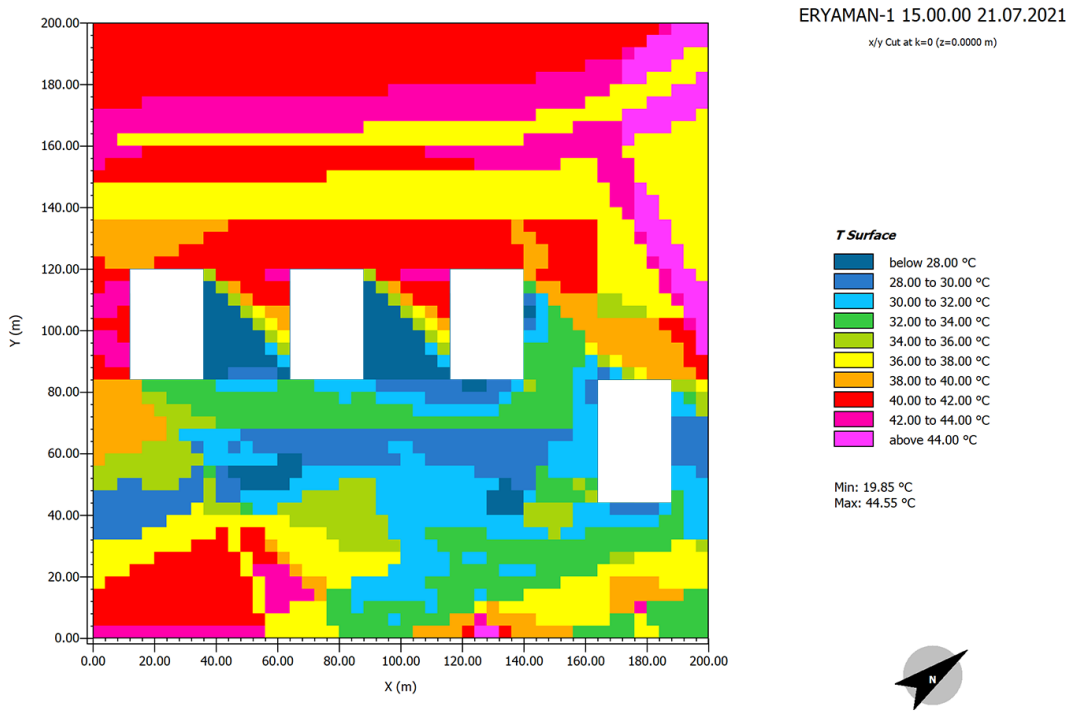

Figure 5.3. T surface values for Eryaman-1 (°C) at 21.07.2021, 15.00.00, plan view, z=0 meters

Although the surface temperatures show great variations, no great differences are observed between the hottest and coldest values when "potential air temperature" mapping is created. It can be said that the potential air temperature value is approximately 2.5 °C less in areas where the buildings create shadows, and the surface temperatures are relatively low. (Figure 5.4.)

The section A formed when the plan view is cut from y=118 meters is given in Figure 5.5. According to this section, it is seen that the potential air temperature value does not vary much between the buildings.

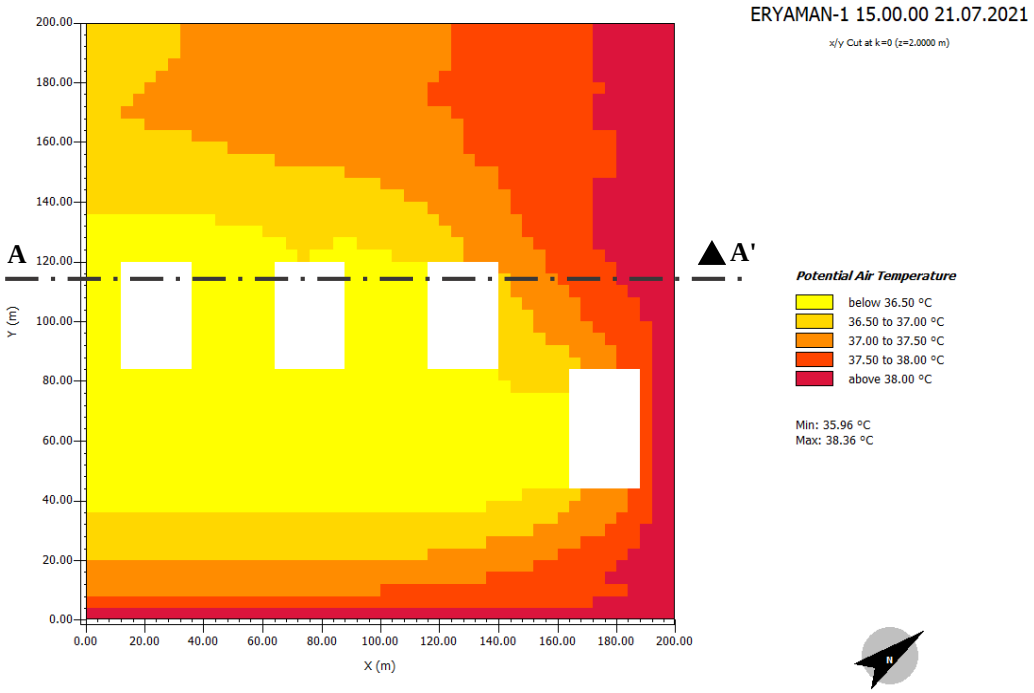

Figure 5.4. Potential Air Temperature values (°C) for Eryaman-1 at 21.07.2021, 15.00.00, plan view, 2 meters above the ground

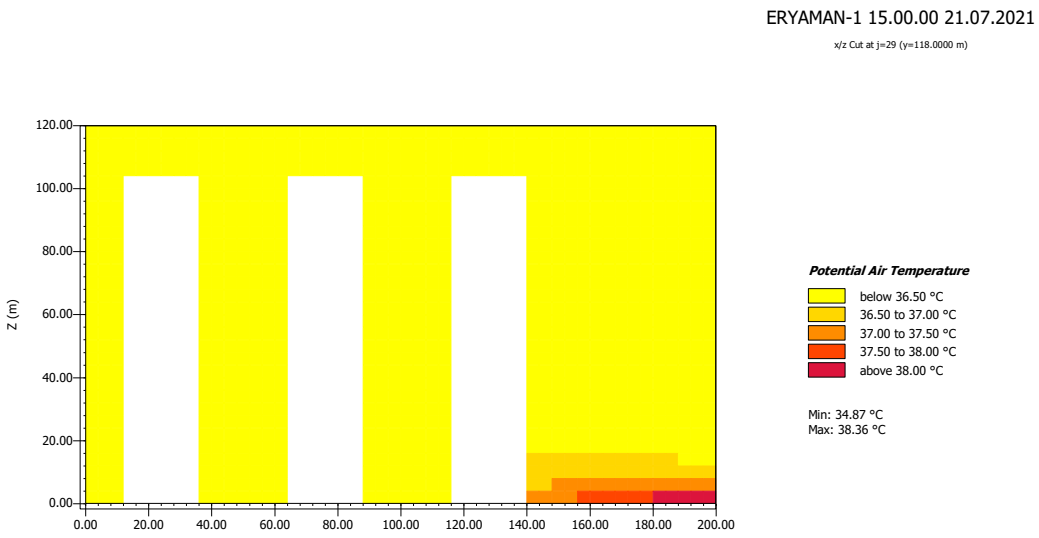

Figure 5.5. Potential Air Temperature values (°C) for Eryaman-1 at 21.07.2021, 15.00.00, Section AA', cut at y=118 meters

Despite the fact that there are no big differences between the air temperatures when the wind speed analysis between the buildings is made, it has been observed that the wind speed between the buildings is below 1.35 m/s (Figure 5.6.). There is a wind wave starting from the right side of the building on the far right within the boundaries of the study area and the wind hitting the building directly accelerated before spreading (Figure 5.7.). Between the other 3 blocks, the wind speed between the buildings decreased as the buildings were positioned perpendicular to the wind direction (Figure 5.8.).

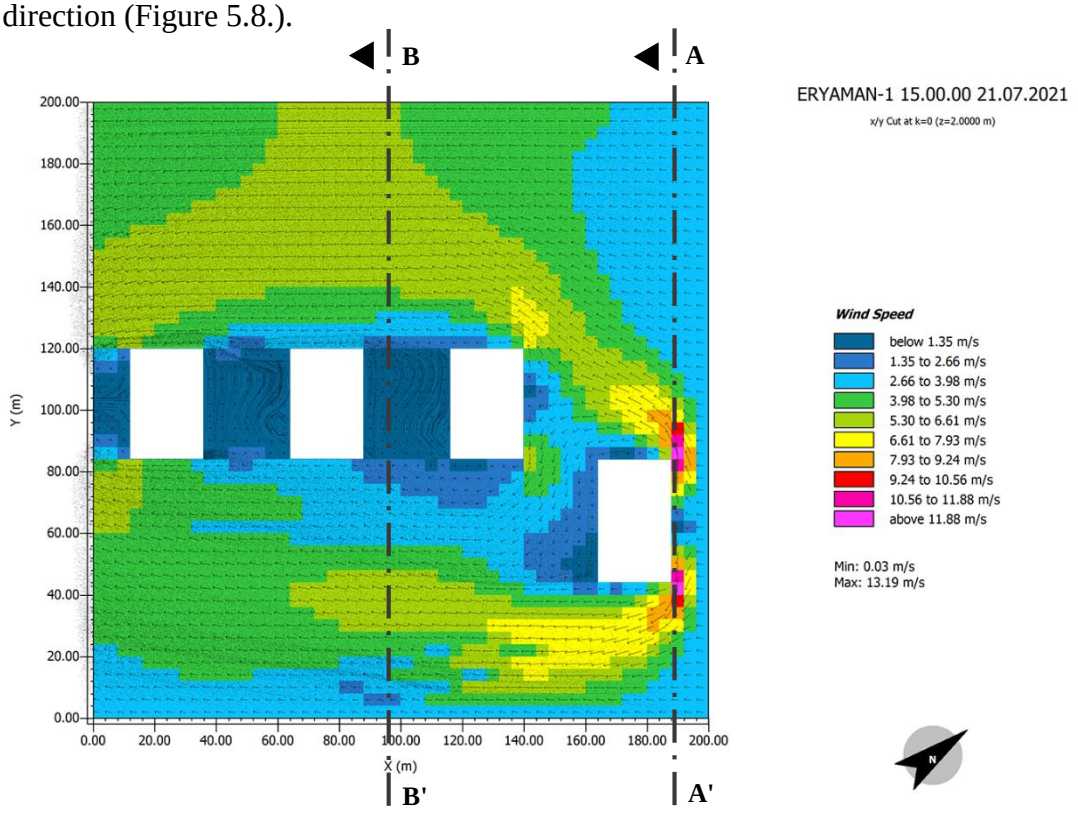

Figure 5.6. Wind speed values (m/s) for Eryaman-1 at 21.07.2021, 15.00.00, plan view, 2 meters above the ground

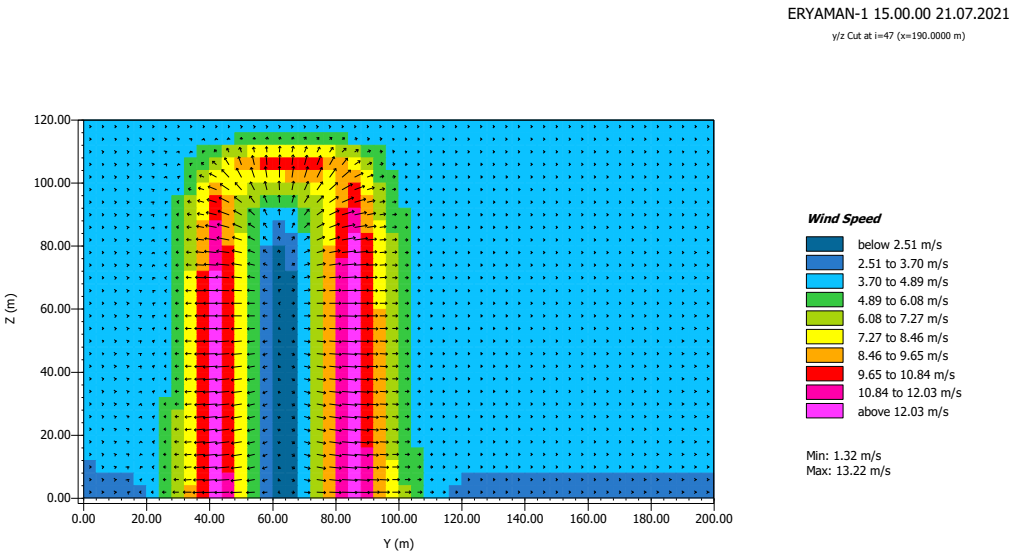

Figure 5.7. Wind speed values (m/s) for Eryaman-1 at 21.07.2021, 15.00.00, Section AA', cut at x=190 meters

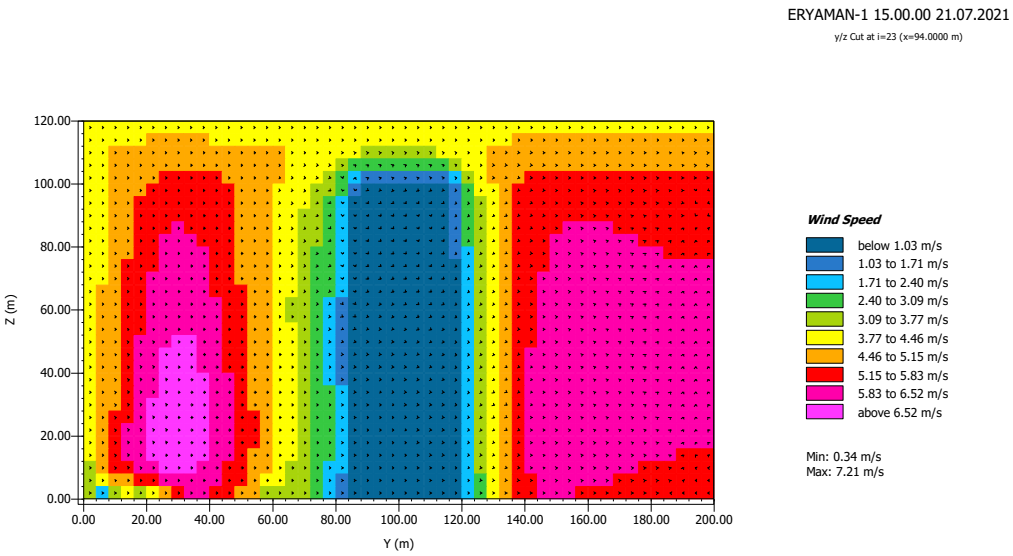

Figure 5.8. Wind speed values (m/s) for Eryaman-1 at 21.07.2021, 15.00.00, Section BB', cut at x=94 meters

The largest masses in the block are 4 buildings with an area of 3943.43 square meters and a height of approximately 100 meters. When the shortwave radiation plans are examined, it is observed that the rays coming from the sun are trapped on the building facades and reflected to the outside. The fact that the materials used on the facades

of these buildings have low albedo values and high irradiation capacities can explain the reason why these shortwave radiation values on the facades are higher than the surrounding environment. Especially, reflected shortwave radiation values around the vegetation and trees are much lower than in the environment. (Figure 5.9.)

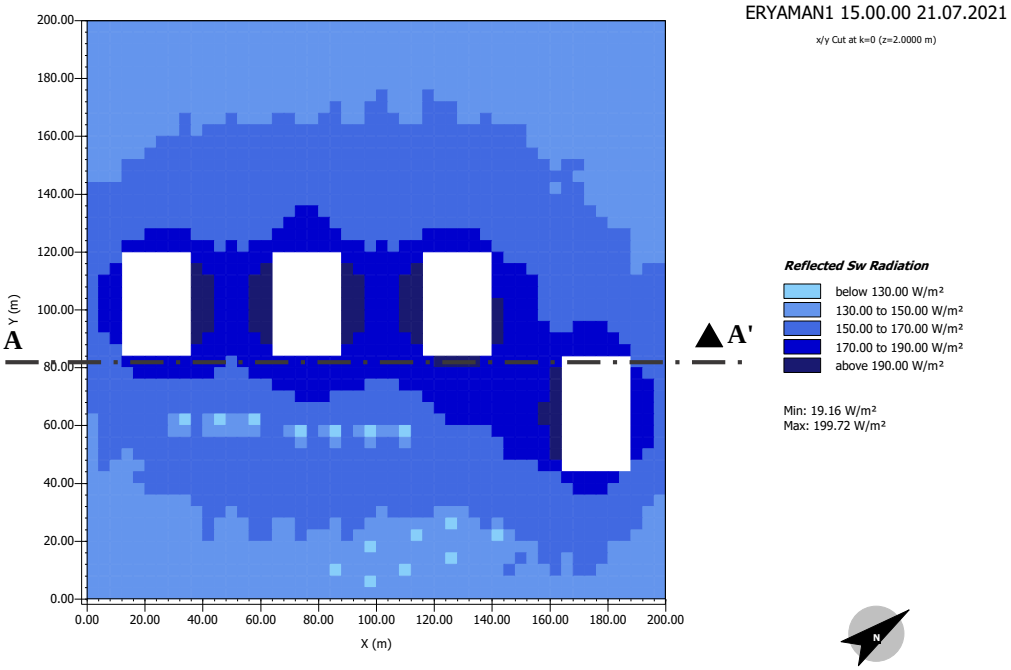

Figure 5.9. Plan view of Reflected Shortwave Radiation (W/m²) in Eryaman-1 at 21.07.2021, 15.00.00, plan view, 2 meters above the ground

The section view taken from the 82nd meter in the y coordinate in the plan coincides with the front facade of 3 buildings; therefore, shortwave radiation values on the front facades can be seen. Values on the sections are consistent with the ones on the plans and it is thought that heat-absorbing facade materials played a role in the formation of these values. (Figure 5.10.)

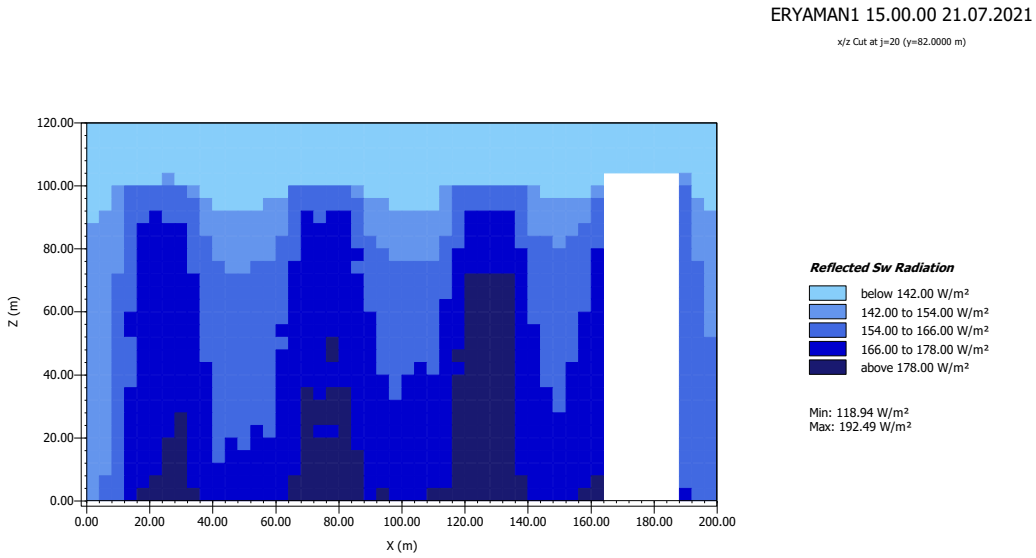

Figure 5.10. Section view of Reflected Shortwave Radiation (W/m²) in Eryaman-1 at 21.07.2021, 15.00.00, Section AA', cut at y= 82 meters

5.2 Comparison

Under this title, the comparison of the data obtained in the urban blocks studied according to various factors is presented. The comparison criteria are grouped as follows: Building Parameters such as Building Heights, Facade Albedo, and Window to Wall Ratio; and Urban Parameters such as Urban Layouts, Presence of Vegetation, Presence of Water Body, and Horizontal Surfaces Albedo.

5.2.1 Building Parameters

The building parameters that are influential in creating or mitigating the UHI effect are building heights, facade albedo, and window-to-wall ratio. The effects of these parameters in the buildings of the case study areas are explained in detail as follows.

5.2.1.1 Building Heights

Figure 5.11. Satellite images of the selected urban blocks in Bahçelievler (left), Kızılay (middle), and Eryaman-1 (right)

In this first comparison criterion, it is aimed to observe the effect of building heights on microclimate. Within the scope of the study, the heights of the buildings are divided into 3 different categories: 1-5 floors are classified as low, 6-10 floors are classified as medium, and 11 and above are categorized as high. The selected urban blocks are Bahçelievler, Kızılay, and Eryaman 1 (Figure 5.11.), whose detailed information is given in Table 5.7. The reason for choosing these study areas is that while their heights differ, the difference between other data is negligible.

Table 5.7 Comparison of field parameters of Bahçelievler, Kızılay, and Eryaman

URBAN BLOCK	BAHÇELİEVLER	KIZILAY	ERYAMAN 1
COORDINATE (x)	39.923877	39.921306	39.995074
COORDINATE (y)	32.831397	32.857436	32.644479
BUILDING AREA (m²)	16470.00	15747.58	3943.04
GRASS AREA (m²)	2152.08	0.00	13055.64
WATER (m²)	0.00	0.00	911.82
ASPHALT AREA (m2)	8644.54	12674.41	6355.91
PAVEMENT (m²)	12732.53	11559.38	15733.59
TOTAL AREA (m2)	40000.00	40000.00	40000.00
BUILDING DENSITY (%)	41.17	39.37	9.86
FLOORS	4	9	26
BUILDING HEIGHT	LOW	MEDIUM	HIGH
BUILDING TYPE	RESIDENTIAL	OFFICE	RESIDENTIAL

According to the planned areas zoning regulation valid in Türkiye, certain rules are followed when designing buildings (Planlı Alanlar İmar Yönetmeliği, 2017). Some rules in this regulation are as follows:

a) The distances between the gardens coinciding with the front garden and the roadside and the garden distances adjacent to the public spaces are at least 5.00 meters.
b) Side and backyard distances are at least 3.00 meters.
c) For side and backyard distances, it is increased by 0.50 meters for each floor above 4 floors in buildings with more than four floors, including basements above natural or leveled ground.
d) Unless otherwise stated in the implementation zoning plan, the apparent height of the building at the lowest elevation on the natural ground or leveled ground is 60.50 meters or more; At least 15.00 meters must be withdrawn from the front, side, and rear parcel borders. For each floor increasing after 60.50 meters of height, 1.00 meters is added to the front, side, and back garden distances.

In other words, by force of the regulation that the distance between buildings should be increased as the height of the building increases, the building density in the area is controlled. According to the calculations made on the scaled satellite imagery, the structures in the selected urban block also comply with these rules.

According to the simulation results, T surface temperature maps were analyzed first. According to the temperature data obtained at 15.00 hours, the places where the shadows of the buildings fall have a much lower temperature than the surrounding surfaces. While the shadows of 4-story (low-rise) buildings are shorter in Bahçelievler (Figure 5.12.), the shadows of 26-story (high-rise) buildings in Eryaman-1 block (Figure 5.14.) are much longer. This affects the area of shadows on the ground and causes the ground temperatures to differ. While the rate of exposure to the sun is higher around shorter buildings, as the height of the building

increases, the amount of shadow around them increases and therefore the amount of temperature felt in those areas decreases.

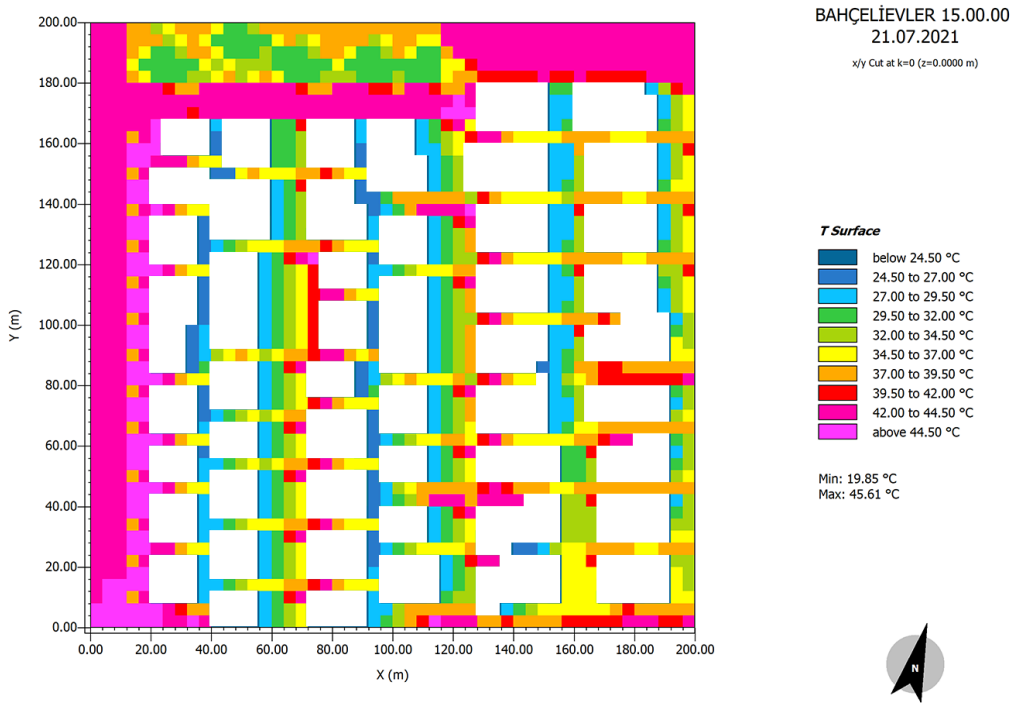

Figure 5.12. T surface values for Bahçelievler (°C) at 21.07.2021, 15.00.00, plan view, z=0 meters

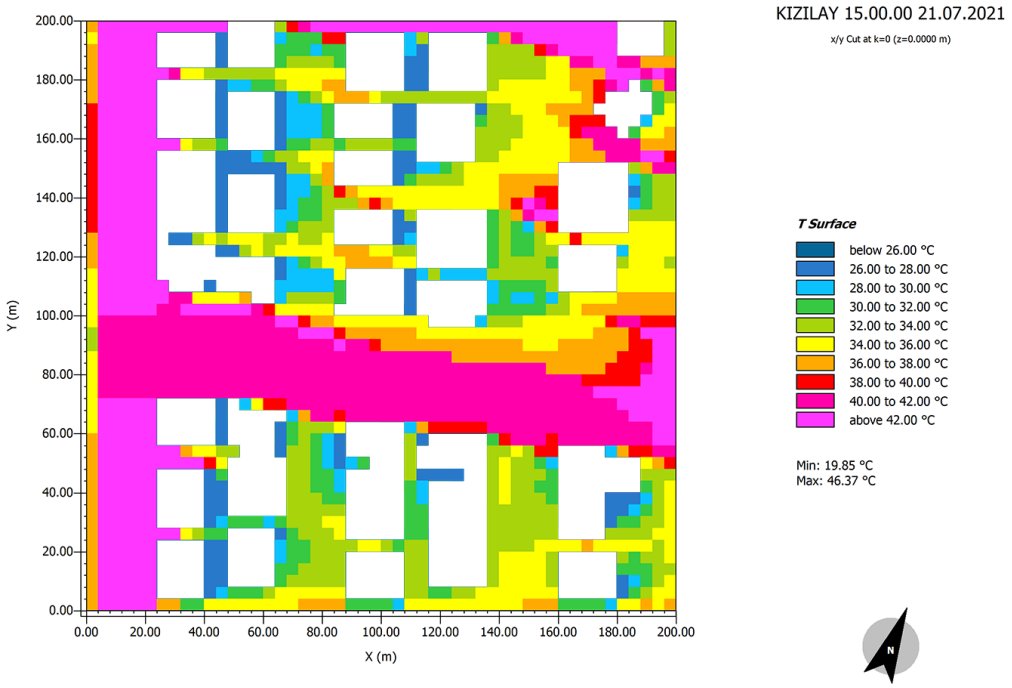

Figure 5.13. T surface values for Kızılay (°C) at 21.07.2021, 15.00.00, plan view, z=0 meters

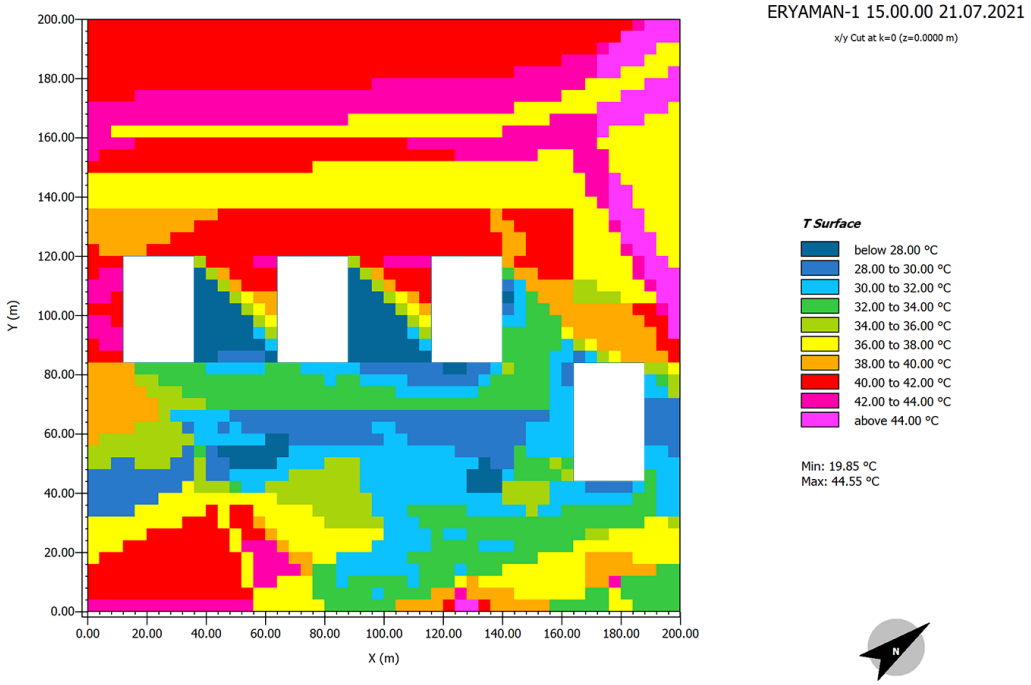

Figure 5.14. T surface values for Eryaman-1 (°C) at 21.07.2021, 15.00.00, plan view, z=0 meters

As mentioned before, according to the planned areas regulation, the different heights of the buildings determine the distance between the buildings. The distance between buildings is one of the important factors affecting wind speed. It is observed that different micro-climate characteristics occur in areas subject to the same climate data on the same date, depending on the structures of the buildings. When the Bahçelievler study area, which has low-rise and tightly positioned structures, is mapped from 2 meters above the ground, the wind speeds are seen in Figure 5.15. below. It is seen that the wind moves along the long corridors formed between the buildings and the wind speed decreases to 0.92 m/s (Figure 5.16.). The tight positioning of the structures cuts the wind to a great extent.

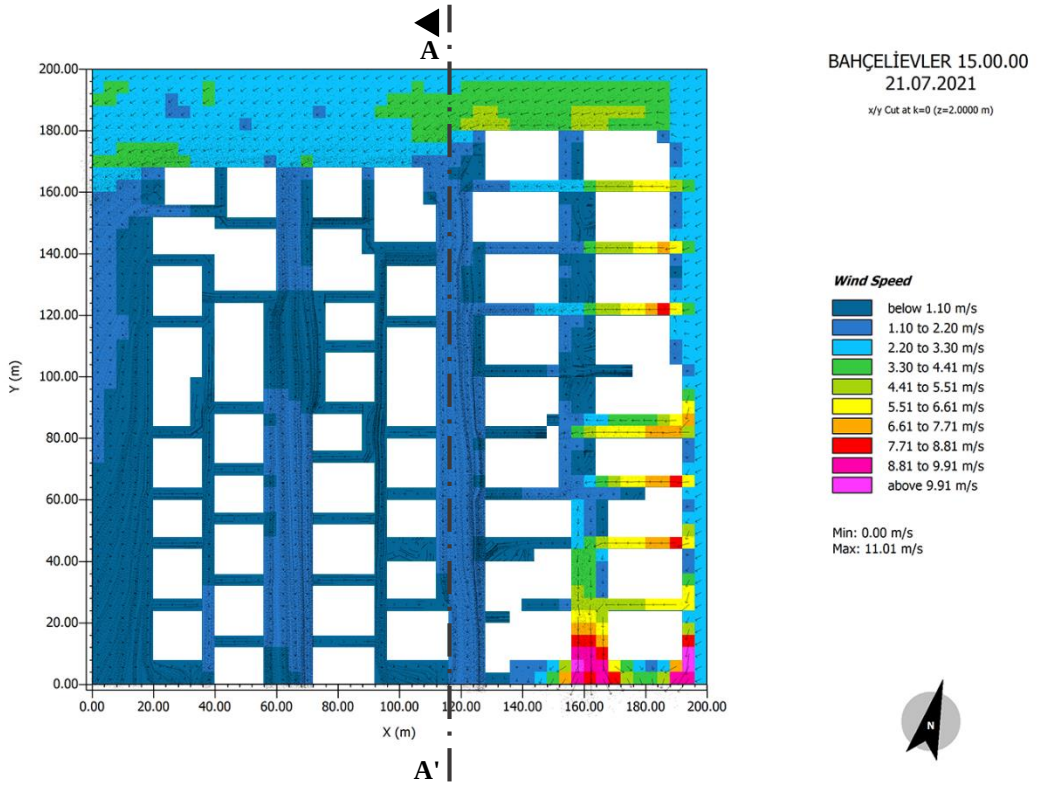

Figure 5.15. Wind speed values (m/s) for Bahçelievler at 21.07.2021, 15.00.00, plan view, z=2 meters

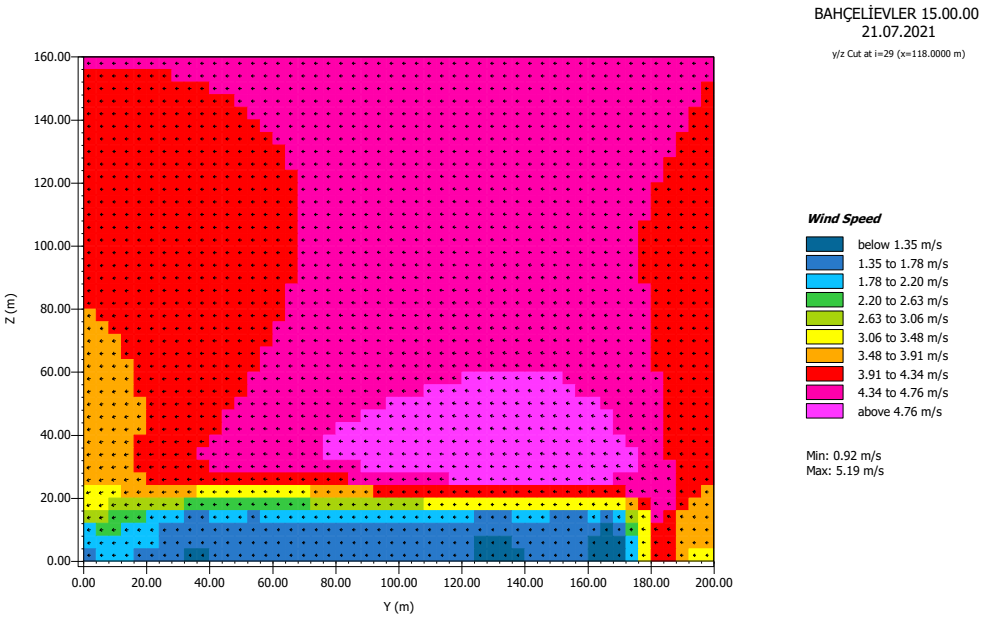

Figure 5.16. Wind speed values (m/s) for Bahçelievler at 21.07.2021, 15.00.00, Section AA', cut at x=118 meters

In the study area in Kızılay, it is seen that the buildings reduce the wind speed to a great extent and the wind speed decreases to 0.90 m/s (Figure 5.17.). On the other hand, when looking at a street where there are no buildings, a wind corridor is formed because the wind is not blocked by any obstacles. The wind speed in this corridor reaches up to 6.05 m/s (Figure 5.18.). Although it is not in the shade, the increase in wind speed can cause a decrease in the temperature felt.

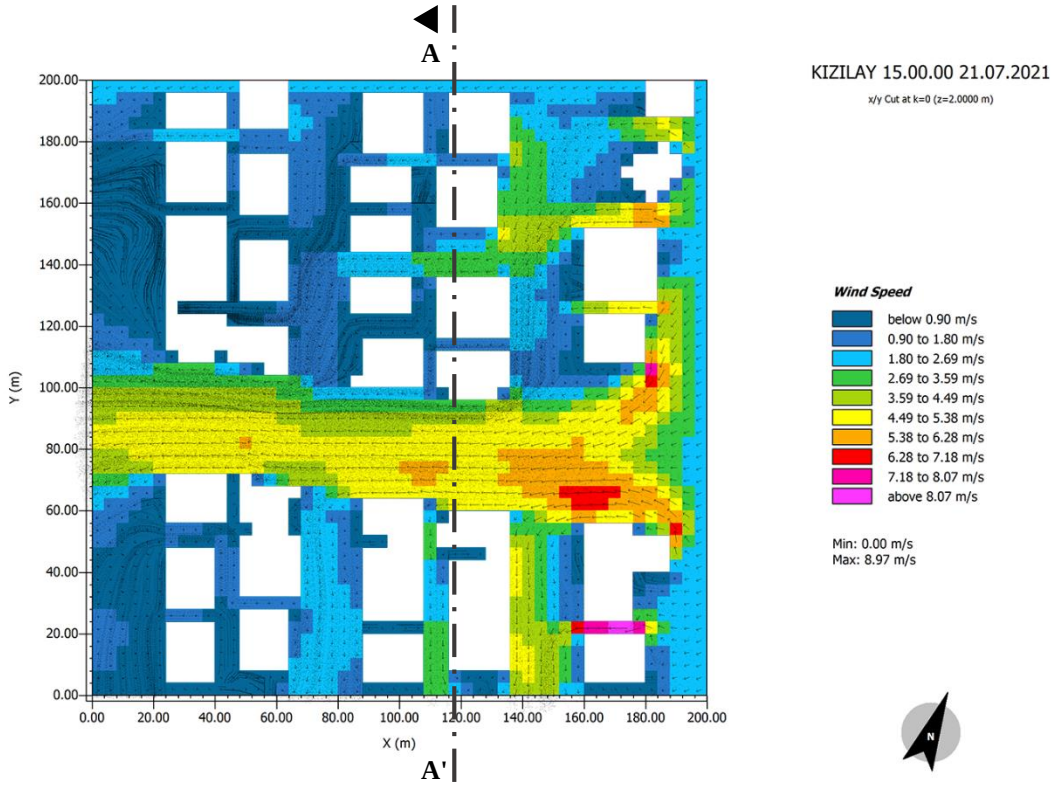

Figure 5.17. Wind speed values (m/s) for Kızılay at 21.07.2021, 15.00.00, plan view, 2 meters above the ground

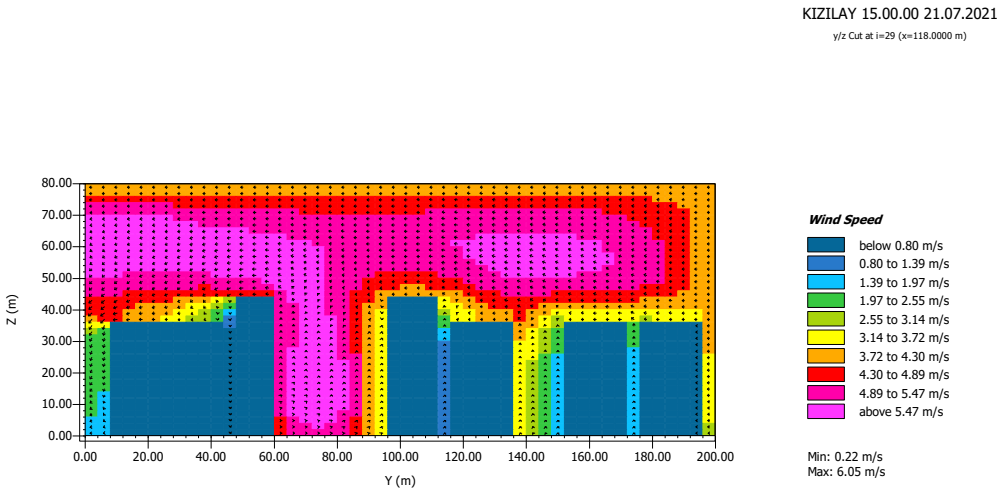

Figure 5.18. Wind speed values (m/s) for Kızılay at 21.07.2021, 15.00.00, Section AA', cut at x=118 meters

When the wind map emerging for the Eryaman-1 area is examined and compared with the previous examples, it is observed that the wide openings between the

buildings increase the wind speed (Figure 5.19.). When cutting at the x=190 meters from the plan on the map, it can be seen that the wind hitting the structure accelerates (above 11.88 m/s) and spreads to the environment (Figure 5.20.). When building shadows and wind speeds are considered together, long and spaced positioning of structures can be considered as an effect that increases the level of thermal comfort on the ground.

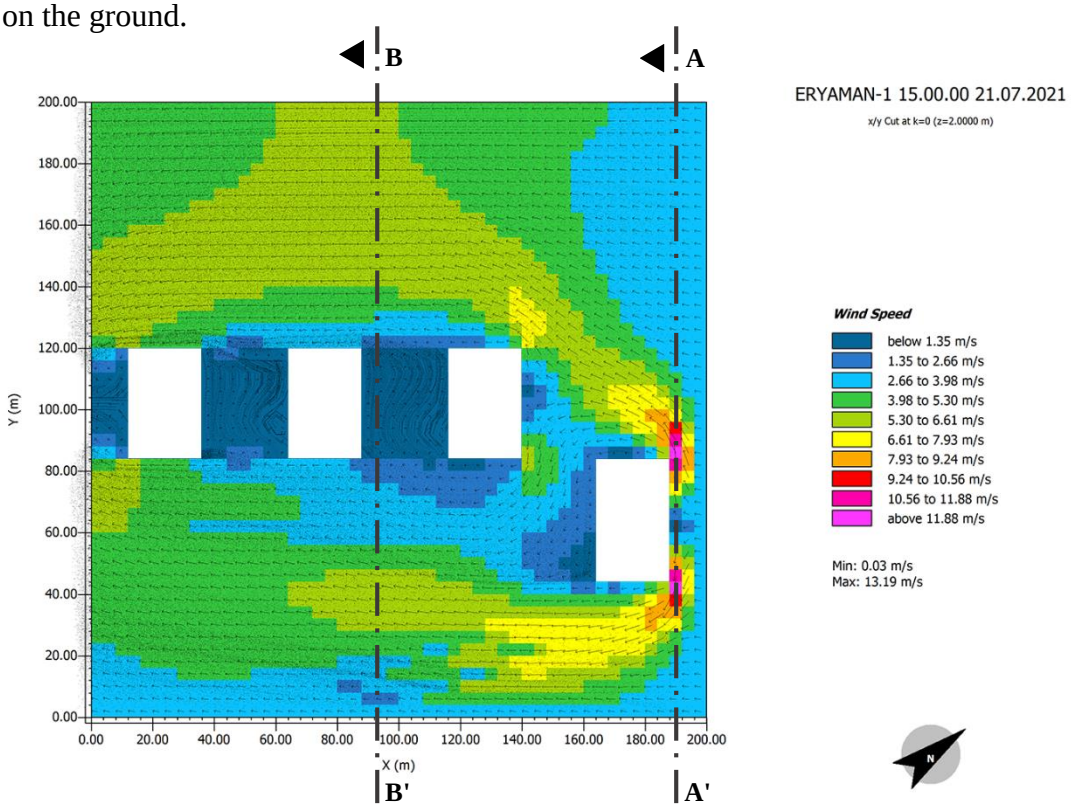

Figure 5.19. Wind speed values (m/s) for Eryaman-1 at 21.07.2021, 15.00.00, plan view, 2 meters above the ground

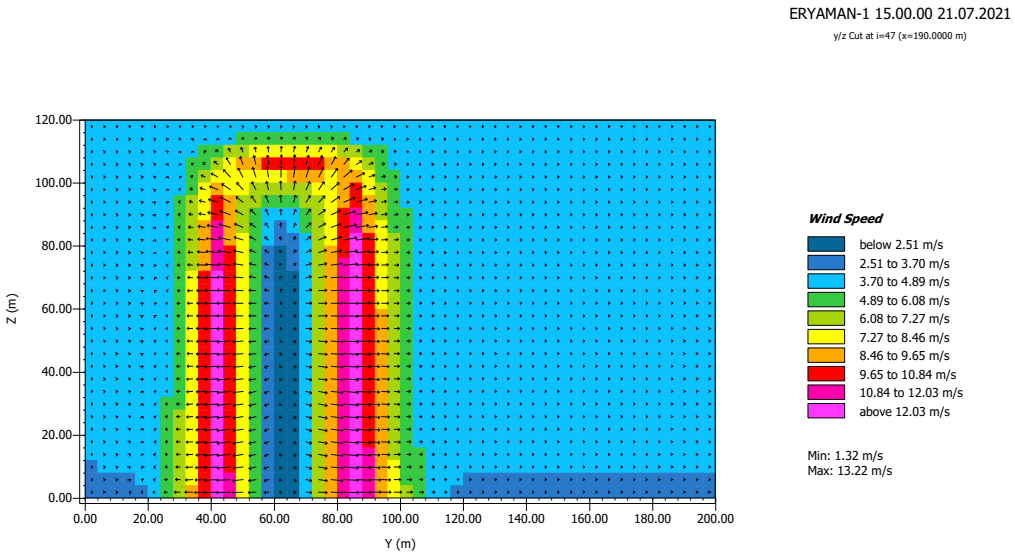

Figure 5.20. Wind speed values (m/s) for Eryaman-1 at 21.07.2021, 15.00.00, Section AA', cut at x=190 meters

When the cross-section is taken from the x=94 meter level in the plan, it is seen that the wind speed decreases in the sections between the buildings. (Figure 5.21.)

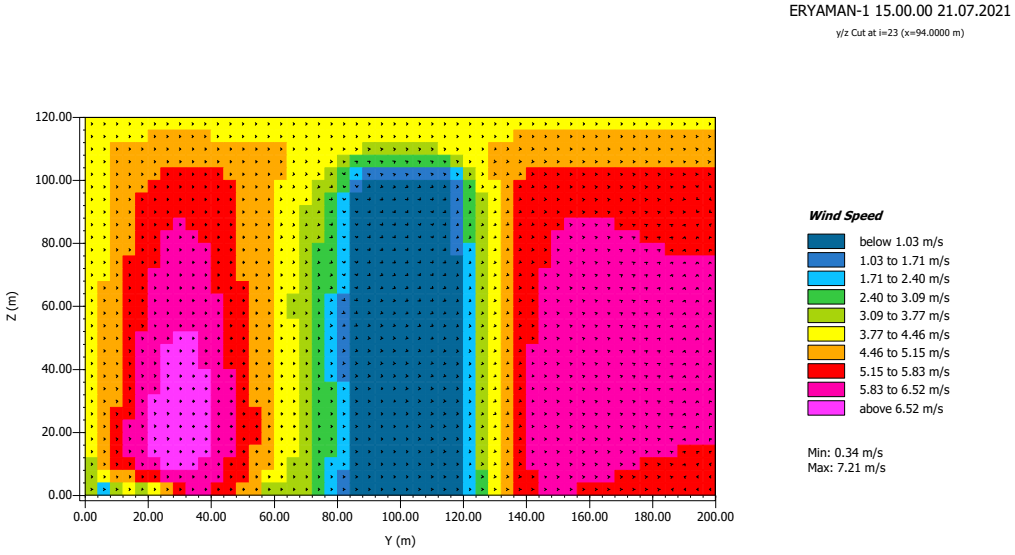

Figure 5.21. Wind speed values (m/s) for Eryaman-1 at 21.07.2021, 15.00.00, Section BB', cut at x=94 meters

5.2.1.2 Facade Albedo

For this type of comparison, areas with similar structural and environmental characteristics were selected. In this way, the only parameter that changes when making a comparison is the albedo values of the facade materials and the surface temperatures that vary accordingly. The first two urban blocks to be compared are İşçi Blokları and Tunus Caddesi, and the other two urban blocks are Çukurambar 1 and Demetevler.

a) İşçi Blokları vs. Tunus Caddesi

Figure 5.22. Satellite images of the selected blocks in İşçi Blokları (left) and Tunus Caddesi (right)

İşçi Blokları and Tunus Caddesi urban blocks, which have similar typological and environmental characteristics, were chosen for facade albedo comparison (Figure 5.22.). The buildings in İşçi Blokları are 5 stories and residential, while the buildings in Tunus Caddesi have an average of 4 floors and also have residential properties. The buildings are positioned in a discrete order. The detailed characteristics of the blocks selected for comparison are shown in Table 5.8.

Table 5.8 Comparison of field qualifications of the urban blocks İşçi Blokları and Tunus Caddesi

URBAN BLOCK	İŞÇİ BLOKLARI	TUNUS CADDESİ
COORDINATE (x)	39.891657	39.914369
COORDINATE (y)	32.797199	32.856980
BUILDING AREA (m²)	5719.53	13268.75
GRASS AREA (m²)	22418.04	1530.71
ASPHALT AREA (m2)	8799.46	10694.46
PAVEMENT (m²)	2837.42	14506.05
SOIL (m²)	225.55	0.00
TOTAL AREA (m2)	40000.00	40000.00
BUILDING DENSITY (%)	14.30	33.17
VEGETATION	YES	YES
FLOORS	5	4
BUILDING HEIGHT	LOW	LOW
BUILDING TYPE	RESIDENTIAL	RESIDENTIAL
WINDOW RATIO	0.349752622	0.459079431

While the albedo value of the exterior cladding of the buildings in İşçi Blokları block is about 0.597, the exterior paints of the buildings in Tunus Caddesi are generally dark in color and their albedo value is about 0.273. The surface temperature of the walls with an albedo value of 0.597 was measured as 31.8 °C, while the surface temperature of the walls with an albedo value of 0.273 was measured as 42.5 °C. (Table 5.9.)

Table 5.9 Temperature and albedo values of facades comparison between the urban blocks İşçi Blokları and Tunus Caddesi

MATERIAL	İŞÇİ BLOKLARI WALL	TUNUS WALL
ALBEDO PHOTOGRAPHY		
MEAN VALUE (PAPER ALBEDO)	201.718	228.717
MEAN VALUE (SURFACE ALBEDO)	185.261	96.177
SURFACE ALBEDO VALUE (%)	**0.596970275**	**0.273329267**
DIGITAL PHOTOGRAPHY		
THERMAL IMAGERY	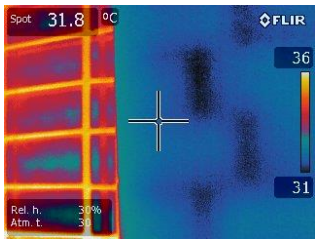	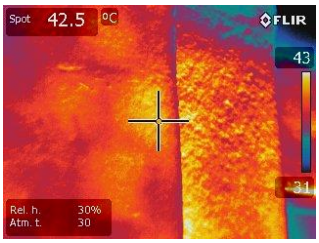
TEMPERATURE (°C)	**31.8**	42.5

Building facades absorb some of the rays coming from the sun to their surfaces, while they reflect the remaining rays. Albedo value can also be expressed as the reflectivity rate of a material. The higher this amount is, can be an indication that the radiation energy from the sun is reflected around the building and therefore the excess rays that cannot be absorbed are emitted to the environment.

After the areas are modeled in 3D and analyzed with the simulation program, how much of the radiation energy from the sun on the exterior rebounds from the surface is shown in the plans.

Considering the northern directions in the plans, the amount of shortwave radiation reflected back by the building facade along the north-south directions around the buildings can be observed.

The amount of shortwave (SW) radiation reflected by the facade materials of the İşçi Blokları, which have a much higher albedo value than buildings on Tunus Caddesi block, is above 172.18 W/m² (Figures 5.23. and 5.24.) On the other hand, the maximum amount of reflected SW radiation emitted from building facades in Tunus Caddesi is above 132.00 W/m² (Figures 5.25. and 5.26.) The fact that the buildings in the İşçi Blokları do not trap the radiation energy in their structure but reflect it outside can be shown as the reason for the low facade temperatures as expected.

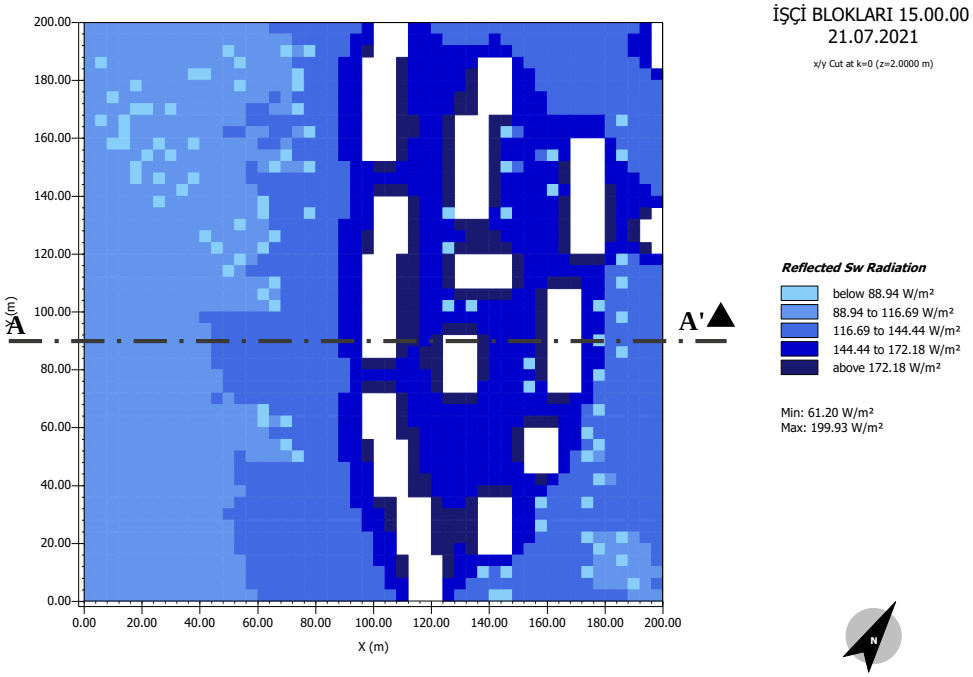

Figure 5.23. Reflected Shortwave Radiation (W/m²) in İşçi Blokları at 21.07.2021, 15.00.00, plan view, 2 meters above the ground

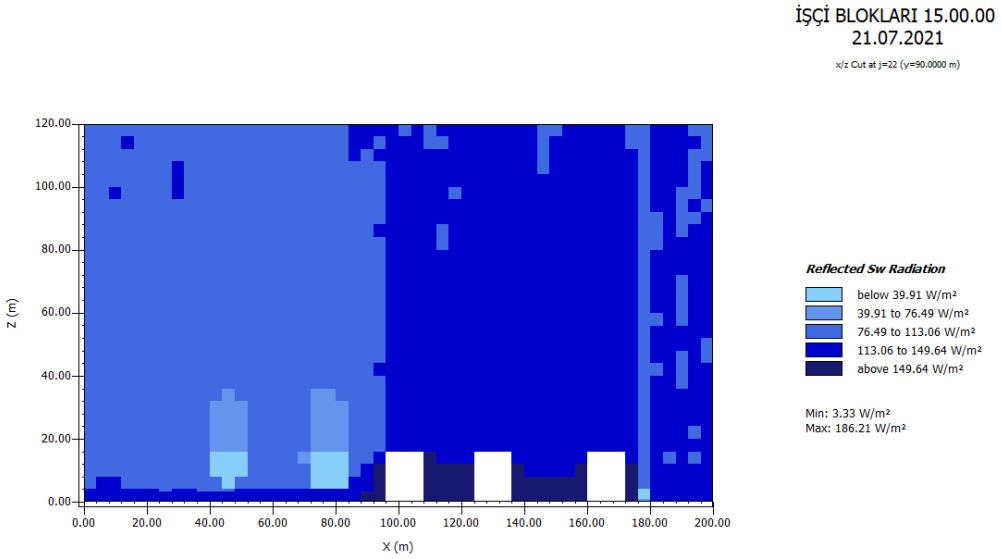

Figure 5.24. Reflected Shortwave Radiation (W/m²) in İşçi Blokları at 21.07.2021, 15.00.00, Section AA', cut at y=90 meters

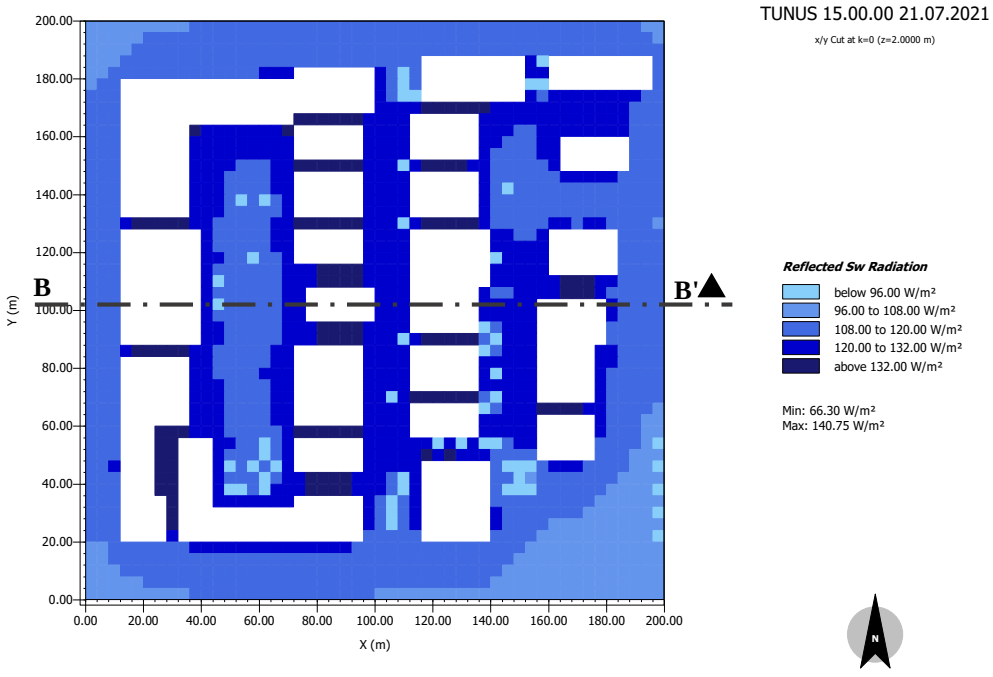

Figure 5.25. Reflected Shortwave Radiation (W/m²) in Tunus Caddesi at 21.07.2021, 15.00.00, plan view, 2 meters above the ground

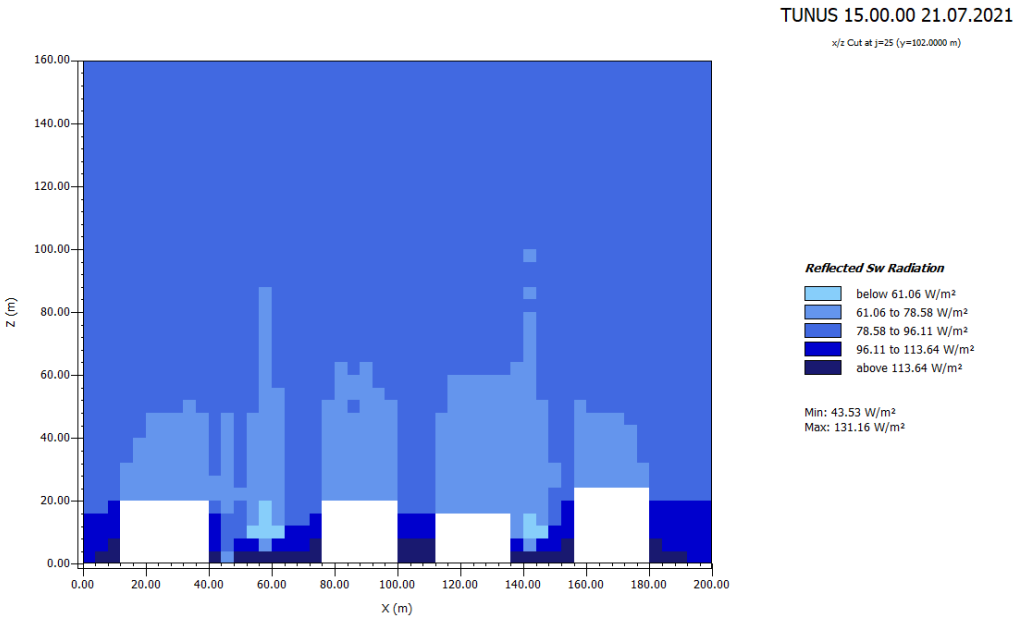

Figure 5.26. Reflected Shortwave Radiation (W/m²) in Tunus Caddesi at 21.07.2021, 15.00.00, Section BB', cut at y=102 meters

b) Çukurambar 1 vs. Demetevler

Figure 5.27. Satellite images of the selected blocks in Çukurambar-1 (left) and Demetevler (right)

Other blocks where the facade albedo values are compared are Çukurambar1 and Demetevler (Figure 5.27.). Similar to the previous example, these buildings are chosen for this comparison because the structures have similar heights and other criteria were ignored for comparison. In both urban blocks, the buildings' heights can be classified as medium-rise, and the buildings are used as residences. (Table 5.10.)

Table 5.10. Comparison of field qualifications of Çukurambar 1 and Demetevler

URBAN BLOCK	ÇUKURAMBAR 1	DEMETEVLER
COORDINATE (x)	39.901893	39.965662
COORDINATE (y)	32.803953	32.790145
BUILDING AREA (m²)	8962.59	18862.48
GRASS AREA (m²)	16122.09	0.00
ASPHALT AREA (m2)	5496.28	6059.01
PAVEMENT (m²)	9418.31	15060.11
TOTAL AREA (m2)	40000.00	40000.00
BUILDING DENSITY (%)	22.41	47.16
VEGETATION	YES	NO
FLOORS	9	7
BUILDING HEIGHT	MEDIUM	MEDIUM
BUILDING TYPE	RESIDENTIAL	RESIDENTIAL
WINDOW RATIO	0.25194059	0.337374895

The buildings in Çukurambar1 block have their own gardens and have similar colors in terms of exterior features. The temperature value of the exterior walls, whose albedo values are approximately 0.489, was measured as 35.7 °C. The albedo value of the measured building facades in Demetevler was determined as approximately 0.269, and the temperature value of this wall was measured as 42.7 °C. (Table 5.11.)

Table 5.11. Temperature and albedo values of facades comparison between Çukurambar1 and Demetevler

MATERIAL	ÇUKURAMBAR 1 WALL	DEMETEVLER WALL
ALBEDO PHOTOGRAPHY		
MEAN VALUE (PAPER ALBEDO)	207.191	252.531
MEAN VALUE (SURFACE ALBEDO)	156.173	104.847
SURFACE ALBEDO VALUE (%)	**0.489946**	**0.2698700**
DIGITAL PHOTOGRAPHY		
THERMAL IMAGERY	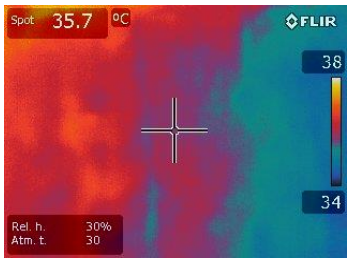	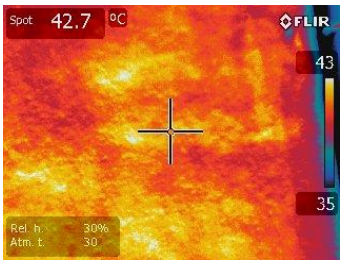
TEMPERATURE (°C)	**35.7**	**42.7**

Reflected shortwave radiation graphs, which are similar to the previous example, are given below. The maximum reflected shortwave radiation value measured on the building walls at Çukurambar 1, which has an albedo value of 0.4899, is 166.20 W/m² (Figure 5.28.). The maximum reflected shortwave radiation value measured on the building walls at Demetevler, whose albedo value was calculated as 0.2698, was found to be 104.28 W/m² (Figure 5.29.). This result shows that the radiation energy coming from the sun is more absorbed by the dark-colored Demetevler wall; therefore, it reflects less radiation to the outside.

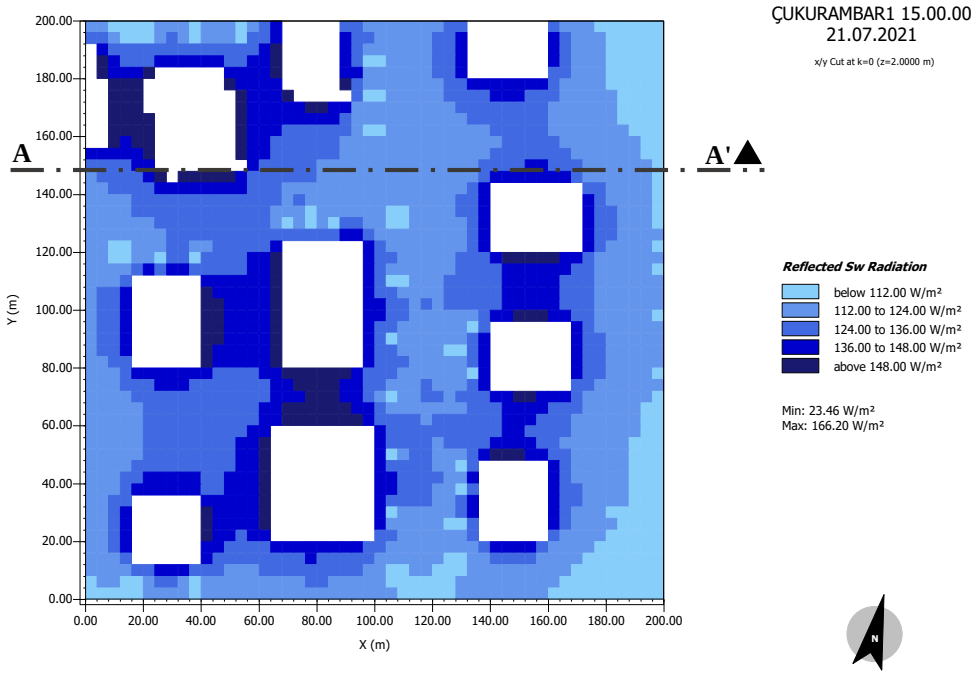

Figure 5.28. Reflected Shortwave Radiation (W/m²) in Çukrambar 1 at 21.07.2021, 15.00.00, plan view, 2 meters above the ground

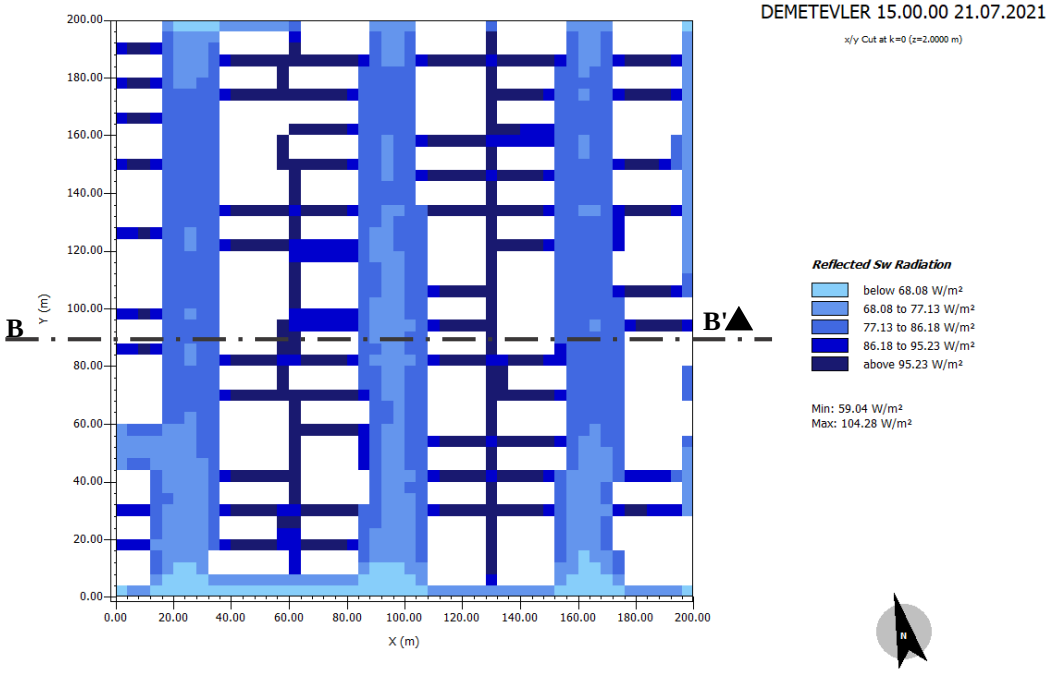

Figure 5.29. Reflected Shortwave Radiation (W/m²) in Demetevler at 21.07.2021, 15.00.00, plan view, 2 meters above the ground

When the given sections are examined, it is seen how much radiation energy is emitted from the building perimeters and roofs. The radiation amounts on the facades of the buildings can be seen when a section is taken from the Çukurambar 1 block at y=150 meters. In the section in Figure 5.30, the radiation reflected from the facade was measured as a maximum of 144.83 W/m². It is seen that the radiation values in the section passing through the vegetation are below 100.29 W/m². Therefore, it can be interpreted that the rays coming from the sun are absorbed by the plants and the amount of reflected energy decreases accordingly.

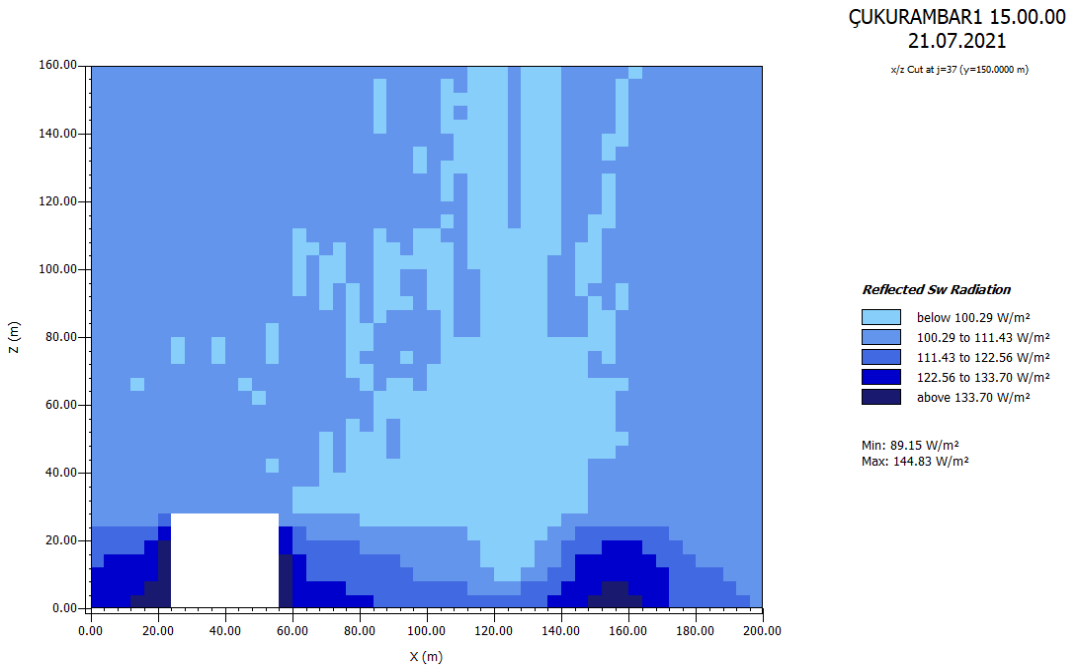

Figure 5.30. Reflected Shortwave Radiation (W/m²) in Çukurambar 1 Block at 21.07.2021, 15.00.00, Section AA', cut at y=150 meters

When the section passing through y=86 meters in Demetevler is examined, the maximum reflected shortwave radiation value on the building facades is 104.11 W/m², which is lower than the facades at Çukurambar 1. (Figure 5.31.)

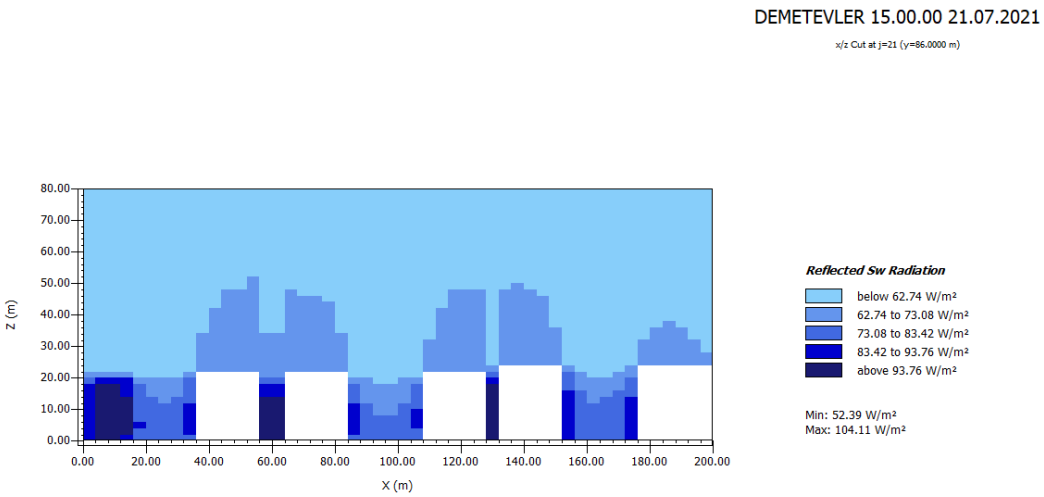

Figure 5.31. Reflected Shortwave Radiation (W/m²) in Demetevler Block at 21.07.2021, 15.00.00, Section BB', cut at y=86 meters

5.2.1.3 Window to Wall Ratio

Figure 5.32. Satellite images of the selected urban blocks in Çukurambar 2 (left), Mevlana Bulvarı (middle) and Eryaman-1 (right)

Along with the opaque materials on the exterior cladding of the buildings, there are also windows that will allow the light to enter. The number of windows may vary according to the design of the building facade. Especially in buildings used as offices, there are buildings whose exteriors are completely covered with glass in order to increase daylight intake.

In this section, the buildings in Çukurambar 2 and Mevlana Bulvarı, which have a window-to-wall ratio of 1 on the exterior, and the Eryaman1 blocks are compared. The reason for choosing Eryaman 1, is that the heights of the buildings in this block are close to the heights of the offices compared. (Figure 5.32.)

The window-to-wall ratio of the buildings in Eryaman1 is 26%, that is, approximately one-fourth of each facade is covered with windows, while the remaining materials have an albedo value of 0.2921. (Table 5.12.)

Table 5.12. Comparison of field qualifications of the urban blocks Çukurambar 2, Mevlana Bulvarı, and Eryaman 1

URBAN BLOCK	ÇUKURAMBAR 2	MEVLANA BULV	ERYAMAN 1
COORDINATE (x)	39.907654	39.899263	39.995074
COORDINATE (y)	32.812890	32.813324	32.644479
BUILDING AREA (m²)	9513.63	13118.36	3943.04
GRASS AREA (m²)	1423.25	4680.70	13055.64
WATER (m²)	0.00	0.00	911.82
ASPHALT AREA (m2)	4370.00	8407.87	6355.91
PAVEMENT (m²)	17568.12	13793.07	15733.59
SOIL (m²)	7125.00	0.00	0.00
TOTAL AREA (m2)	40000.00	40000.00	40000.00
BUILDING DENSITY (%)	23.78	32.80	9.86
VEGETATION	NO	YES	YES
FLOORS	34	26	26
BUILDING HEIGHT	HIGH	HIGH	HIGH
BUILDING TYPE	OFFICE	OFFICE	RESIDENTIAL
WINDOW RATIO (%)	100	100	26

When the comparison table (Table 5.13.) is examined, the surface temperatures of the facades of all 3 buildings exposed to the sun are observed. According to thermal camera measurements, when Çukurambar 2 and Mevlana Bulvarı buildings, which are covered with 100% glass, are compared, it can be seen that they have similar surface temperatures. On the other hand, the surface temperature of the buildings in the Eryaman 1 block, which has a window ratio of only 26%, was measured to be approximately 25 °C higher.

However, when a building has a high window-to-wall ratio, the sun's rays are reflected in various directions, making it difficult to determine the accurate temperature of the facade using a thermal camera. The temperature in the urban areas surrounding the buildings rises and the level of thermal comfort declines as a result of the excessive sun radiation.

Table 5.13. Temperatures of facades comparison among the urban blocks Çukurambar 2, Mevlana Bulvarı, and Eryaman 1

URBAN BLOCK	ÇUKURAMBAR 2	MEVLANA BOULEVARD	ERYAMAN 1
DIGITAL PHOTO			
THERMAL IMAGERY	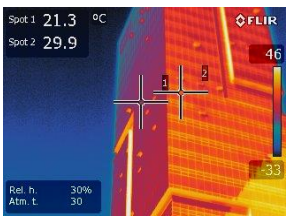	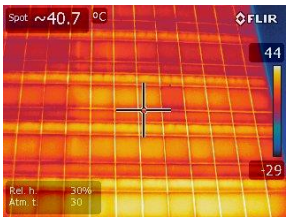	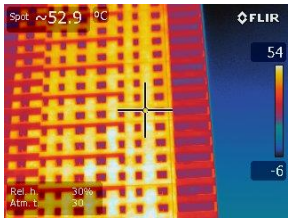
FACADE TEMPERATURE (°C)	29.9	40.7	52.9

When the reflected shortwave radiation maps of the 3 urban blocks are examined below, it is seen that the maximum value seen in the Eryaman-1 block is 199.72 W/m². (Figures 5.33. and 5.34.)

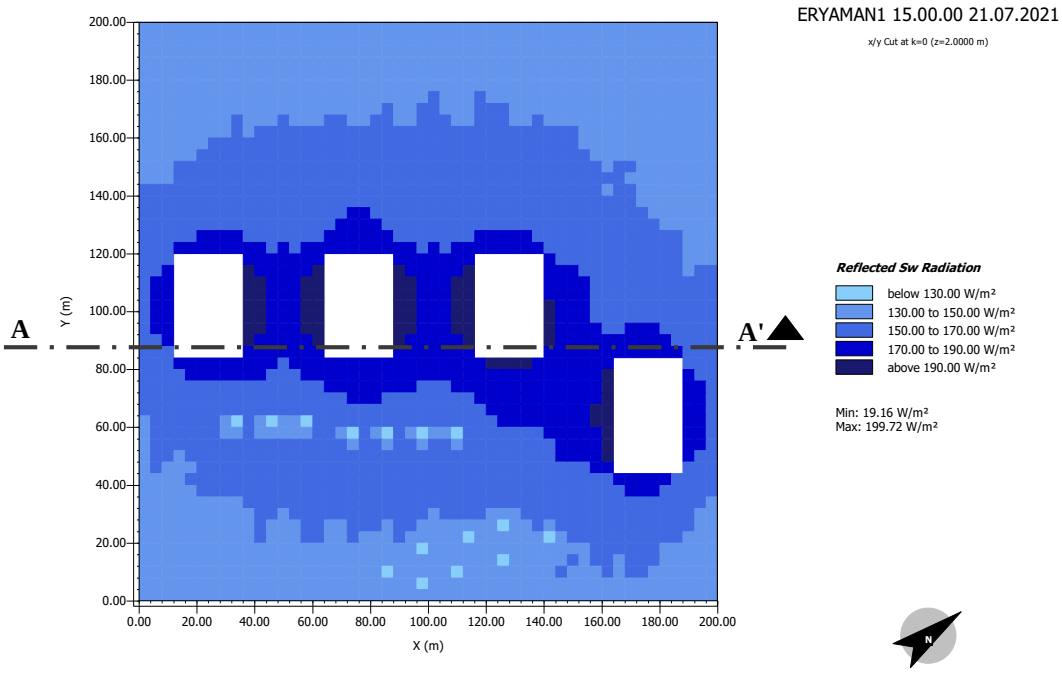

Figure 5.33. Reflected Shortwave Radiation (W/m²) in Eryaman-1 Block at 21.07.2021, 15.00.00, plan view, 2 meters above the ground

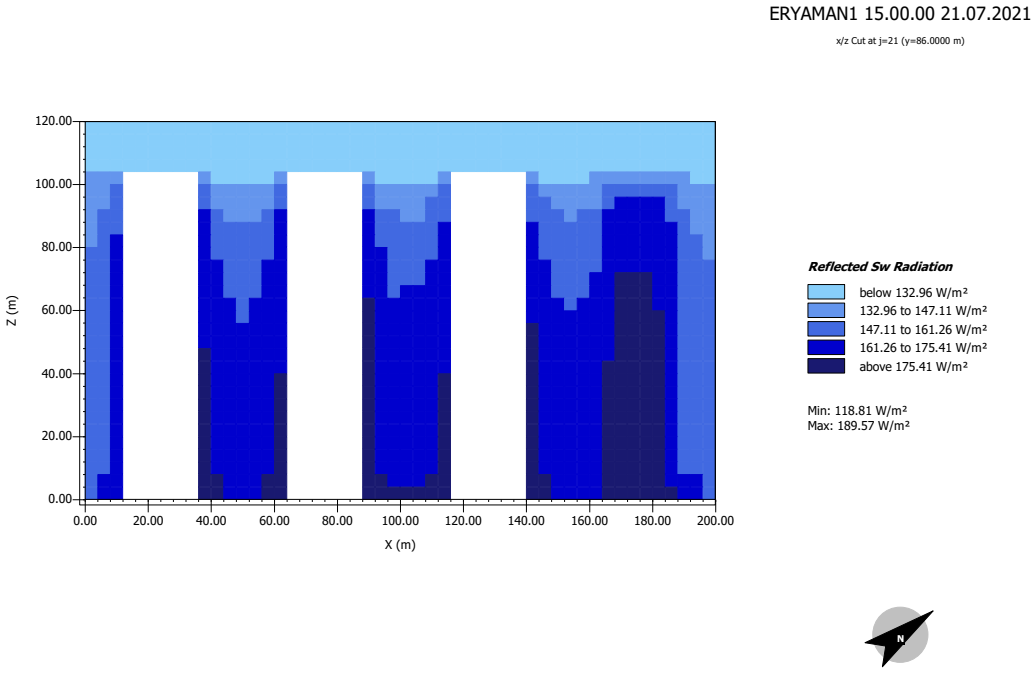

Figure 5.34. Reflected Shortwave Radiation (W/m²) in Eryaman-1 Block at 21.07.2021, 15.00.00, Section AA', cut at y=86 meters

In Mevlana Bulvarı (Figures 5.35. and 5.36.) and Çukurambar 2 (Figures 5.37. and 5.38.) urban blocks, the reflected SW radiation values have lower values on the facades compared to their surroundings. The same situation is better understood in the cross-sections. The facades that allow the sun's rays to pass into the building caused the radiation on the surface to have lower values.

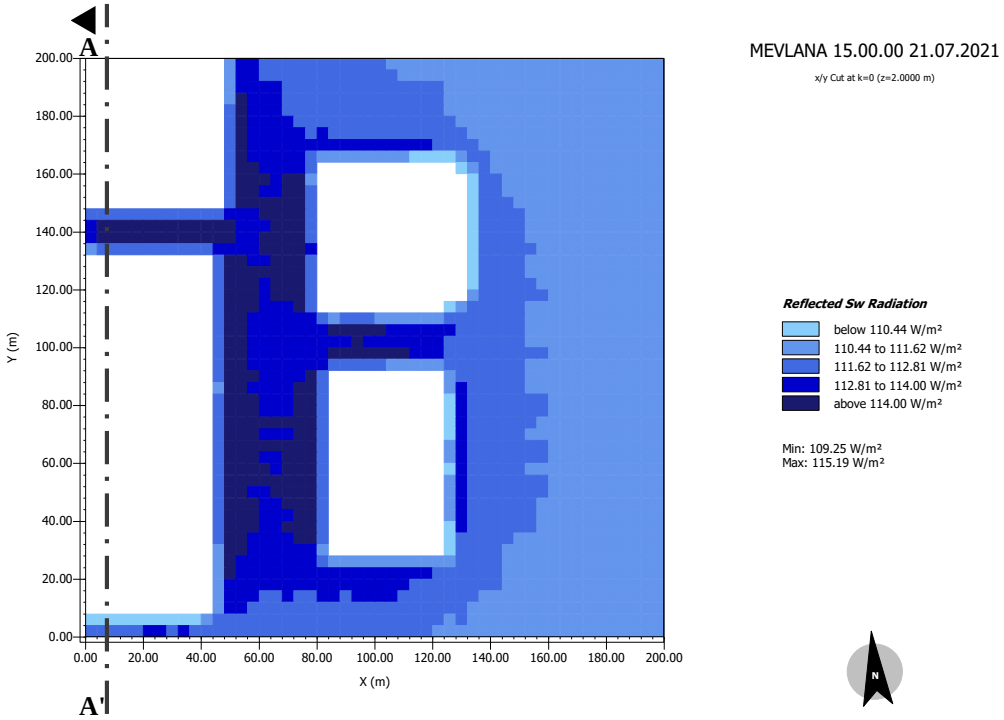

Figure 5.35. Reflected Shortwave Radiation (W/m²) in Mevlana Bulvarı Block at 21.07.2021, 15.00.00, plan view, 2 meters above the ground

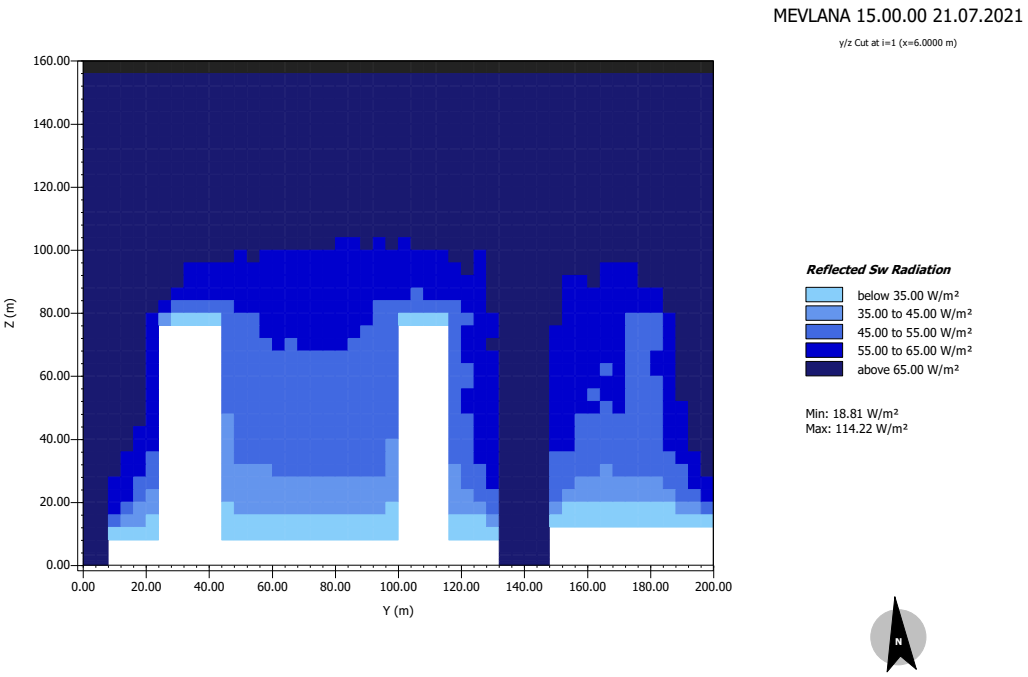

Figure 5.36. Reflected Shortwave Radiation (W/m²) in Mevlana Bulvarı Block at 21.07.2021, 15.00.00, Section AA', cut at x=6 meters

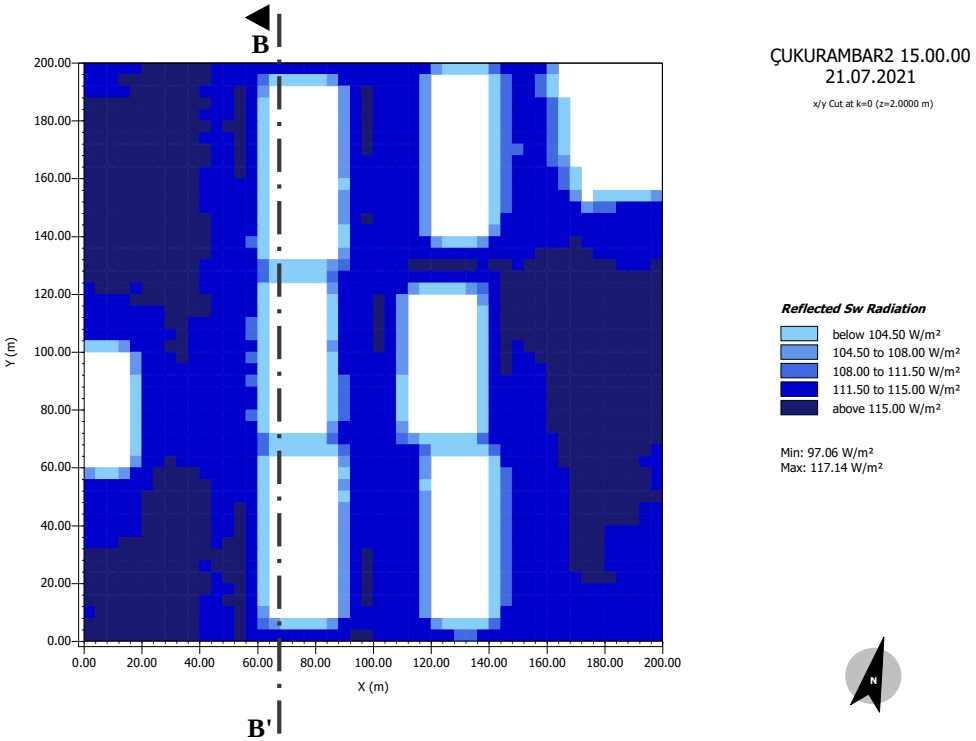

Figure 5.37. Reflected Shortwave Radiation (W/m²) in Çukurambar-2 at 21.07.2021, 15.00.00, plan view, 2 meters above the ground

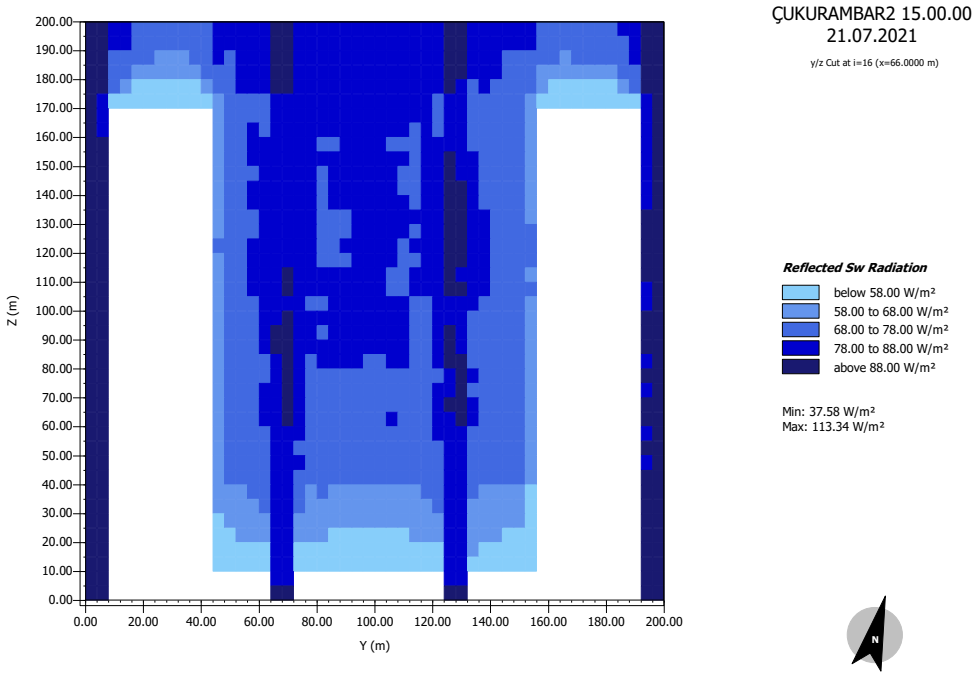

Figure 5.38. Reflected Shortwave Radiation (W/m²) in Çukurambar-2 at 21.07.2021, 15.00.00, Section BB', cut at x=66 meters

5.2.2 Urban Parameters

The urban parameters that are influential in creating or mitigating the UHI effect are urban layouts, presence of vegetation, presence of water body, and horizontal surfaces albedo. The effects of these parameters on the microclimate of the case study areas are explained in detail as follows.

5.2.2.1 Urban Layouts

Figure 5.39. Satellite images of the selected blocks in Hamamönü (left) and İvedik (right)

When the data of case study blocks in Hamamönü and İvedik (Figure 5.39.) among the case study areas are put into a table, it can be seen that they have very similar structural and environmental factors (Table 5.14.). In both urban blocks, the building densities in the area are close to each other. Also, buildings in both blocks are low-rise and used for residential purposes.

Table 5.14 Comparison of field qualifications of the urban blocks Hamamönü and İvedik

URBAN BLOCK	HAMAMÖNÜ	İVEDİK
COORDINATE (x)	39.934680	39.961119
COORDINATE (y)	32.865574	32.816854
BUILDING AREA (m²)	18874.96	20621.87
GRASS AREA (m²)	1828.17	1430.36
ASPHALT AREA (m2)	2842.26	6462.25
PAVEMENT (m²)	16454.09	11485.52
TOTAL AREA (m2)	40000.00	40000.00
BUILDING DENSITY (%)	**47.19**	**51.55**
VEGETATION	**YES**	**YES**
FLOORS	**2**	**5**
BUILDING HEIGHT	**LOW**	**LOW**
BUILDING TYPE	**RESIDENTIAL**	**RESIDENTIAL**

The facade features of the buildings in both blocks are similar. When the albedo values of the exterior facades of the buildings in Hamamönü are calculated, the value of 0.5381 is reached, while the albedo value of the light color, which is predominantly used on the facades of the buildings in İvedik, is 0.5727. (Table 5.15.)

Table 5.15. Temperature and albedo values of facades comparison between Hamamönü and İvedik

MATERIAL	HAMAMÖNÜ WALL	İVEDİK WALL
ALBEDO PHOTOGRAPHY		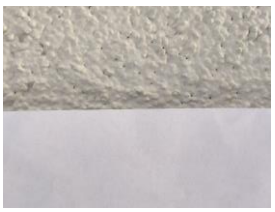
MEAN VALUE (PAPER ALBEDO)	192.116	199.174
MEAN VALUE (SURFACE ALBEDO)	159.050	175.516
SURFACE ALBEDO VALUE (%)	**0.538125403**	**0.572792634**
DIGITAL PHOTOGRAPHY		
THERMAL IMAGERY	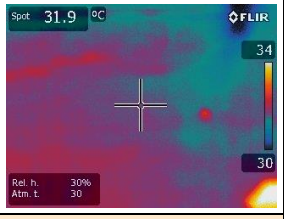	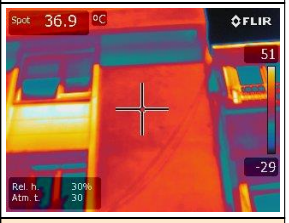
TEMPERATURE (°C)	**31.9**	**36.9**

Despite the structural similarities in the areas, there are differences in the distribution of buildings in the area. In Hamamönü, the buildings are mostly adjacent, but they are organic and unevenly distributed on the ground. In İvedik, on the other hand, the buildings are placed geometrically and forming long corridors. However, there are no gaps to allow passage between these corridors.

When the two urban blocks are modeled and subjected to microclimate simulation, the T surface temperature graphs are obtained. Since the buildings in the Hamamönü block are not arranged regularly, some spaces are exposed to shade while others are

exposed to the sun all day long. The temperature is around 24.5 °C on pavement surfaces in the shade and 42-44.5 °C on non-shaded areas. (Figure 5.40.)

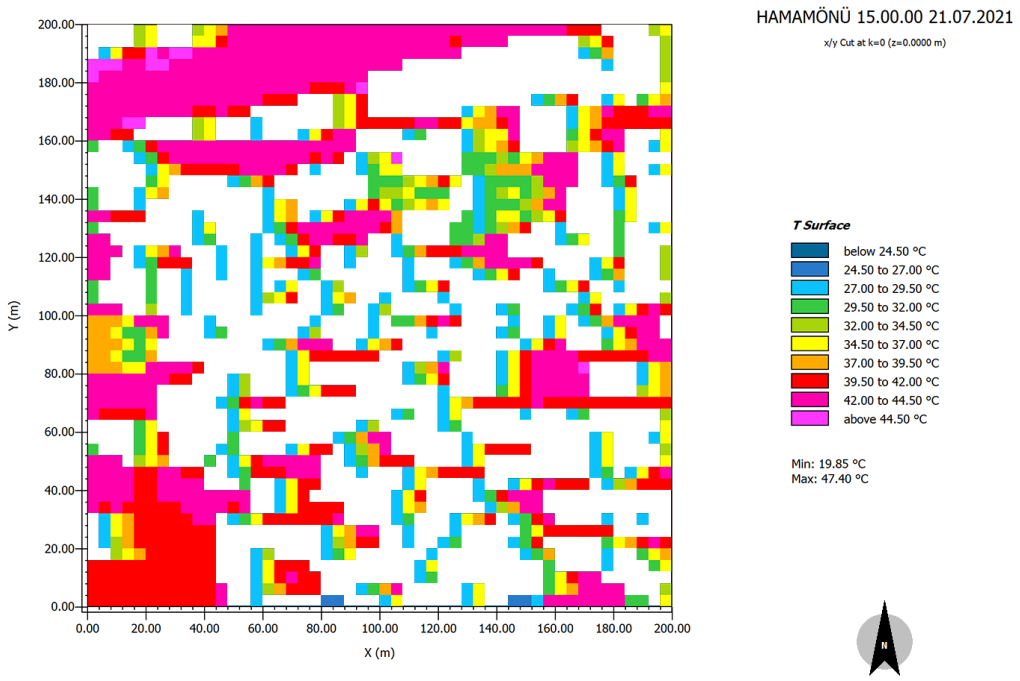

Figure 5.40. T surface values for Hamamönü (°C) at 21.07.2021, 15.00.00, plan view, z=0 meters

The flat and long corridors of the buildings in the İvedik block caused the ground to be continuously exposed to shade, and for this reason, the temperature values were homogeneously distributed throughout the streets. (Figure 5.41.)

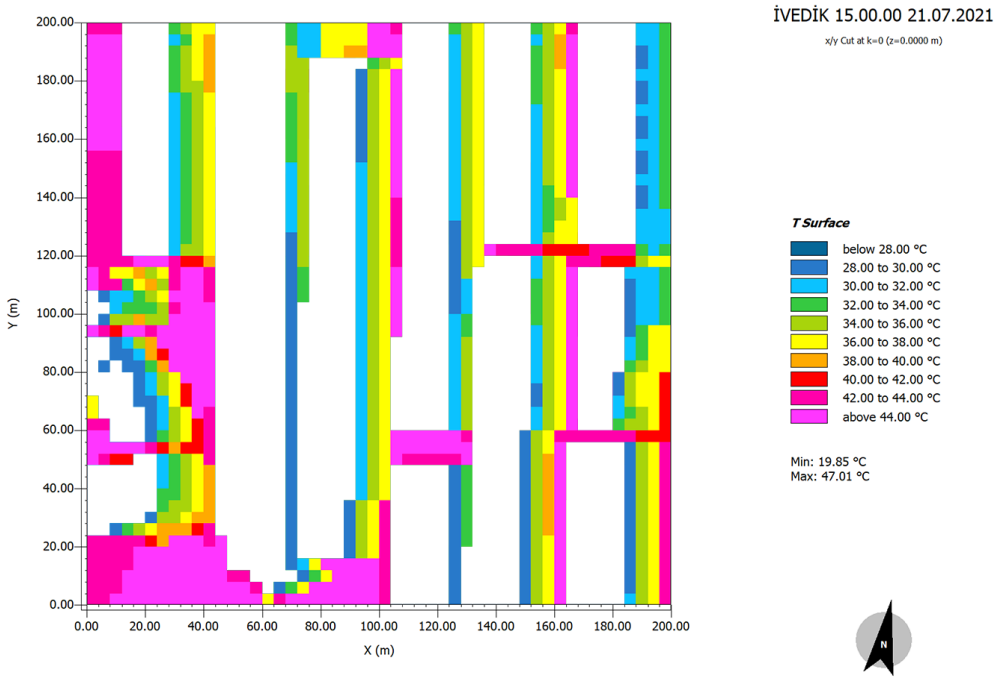

Figure 5.41. T surface values for İvedik (°C) at 21.07.2021, 15.00.00, plan view, z=0 meters

Another factor that building forms affect is wind speed. The organic layout in the Hamamönü block caused the wind to be cut by the buildings (Figure 5.42.). Therefore, the wind speed between the structures decreases to 0.38 m/s (Figure 5.43.).

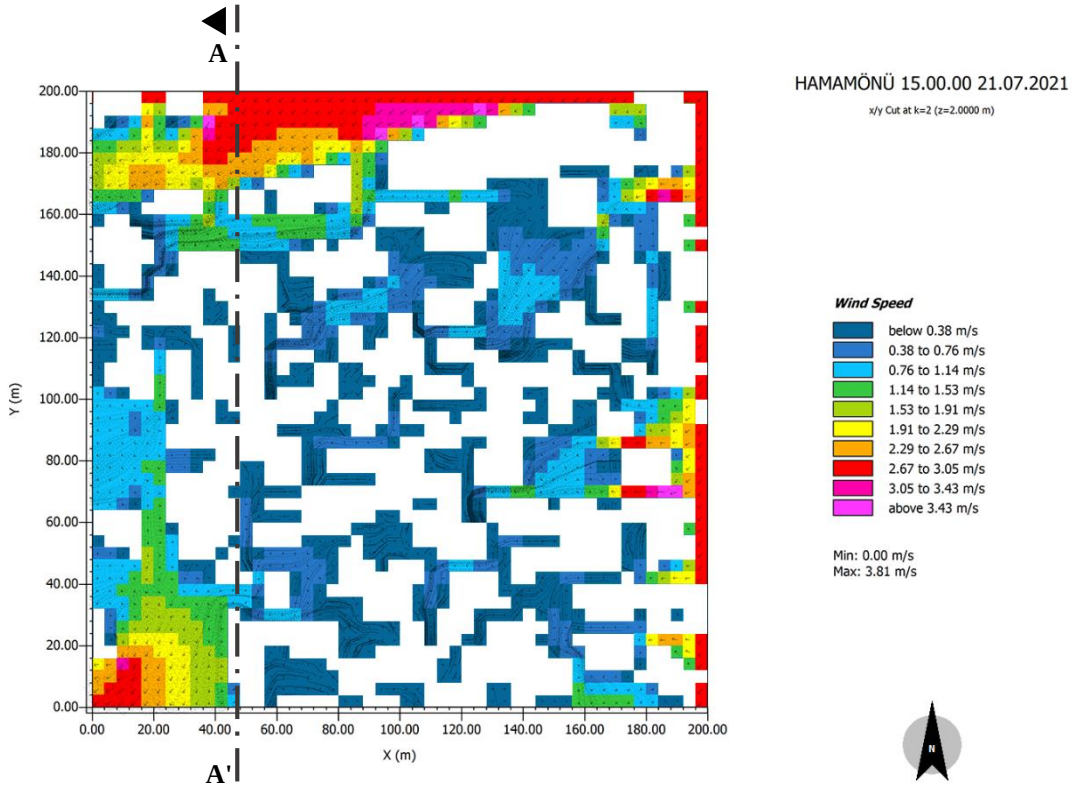

Figure 5.42. Wind speed values (m/s) for Hamamönü at 21.07.2021, 15.00.00, plan view, z=2 meters

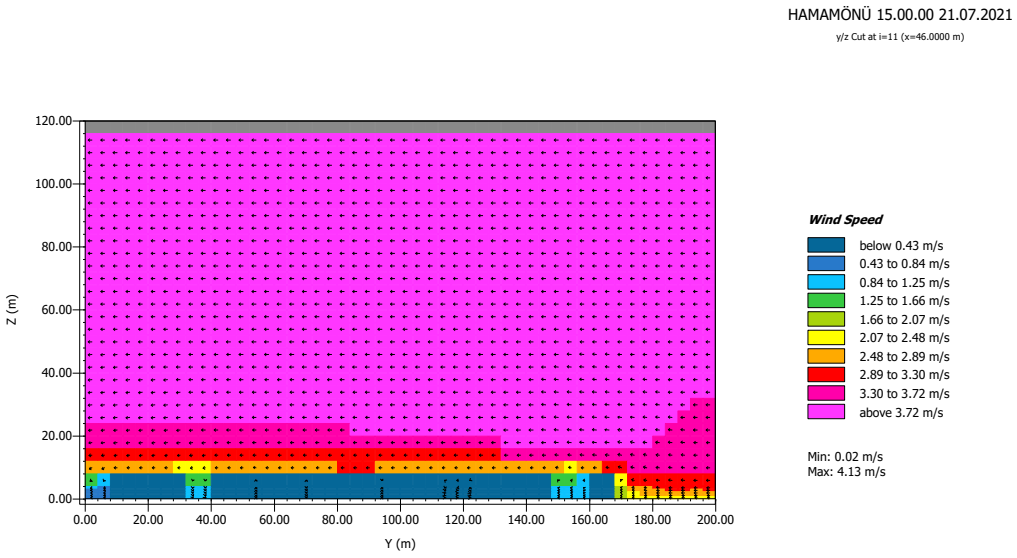

Figure 5.43. Wind speed values (m/s) for Hamamönü at 21.07.2021, 15.00.00, Section AA', cut at x=46 meters

The regular layout in İvedik, on the other hand, enabled the wind to move uninterruptedly along the corridors and because of the venturi effect, the wind is accelerated. In these areas, the wind speed starts from 0.53 m/s and reaches up to 3.17 m/s. (Figure 5.44. and Figure 5.45.)

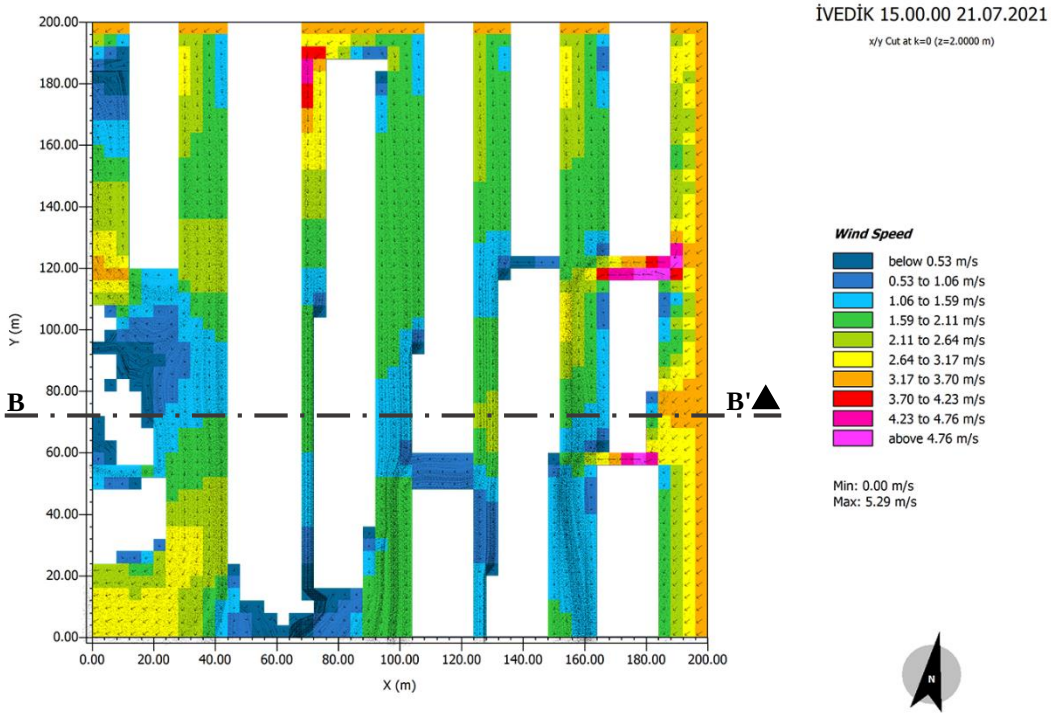

Figure 5.44. Wind speed values (m/s) for İvedik at 21.07.2021, 15.00.00, plan view, z=2 meters

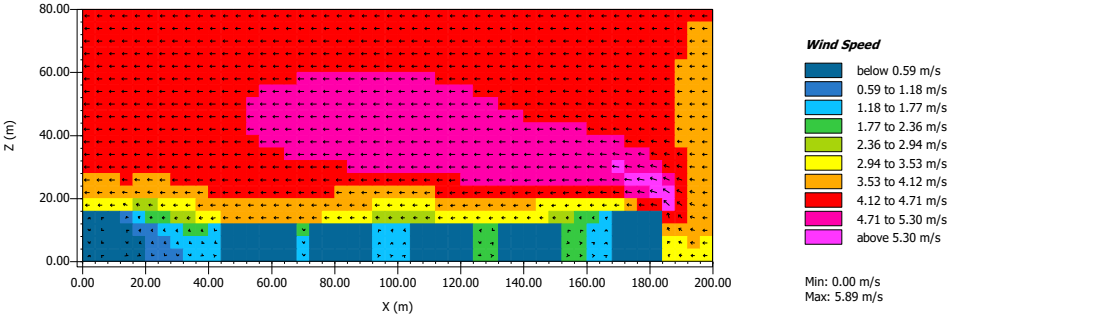

Figure 5.45. Wind speed values (m/s) for İvedik at 21.07.2021, 15.00.00, Section BB', cut at y=82 meters

5.2.2.2 Horizontal Surfaces Albedo

Finally, in this part of the study, the albedo values of the horizontal materials in the urban blocks and the temperature differences due to these values are examined. Then, the horizontal surface materials of each block are compared among themselves.

a) Urban Block 1 - Bahçelievler

Two types of materials are used on the ground in Bahçelievler. The first of these is asphalt roads made for vehicle crossings, and the other is pavements made for pedestrian crossings. The albedo percentages are calculated for both surfaces and the images taken with the thermal camera of the asphalt with an albedo value of about 0.2698 can be seen in Table 5.16. The temperature of the asphalt does not show a homogeneous distribution on the surface. The reason for this distribution may be the heating of the floor as a result of the friction of the vehicles passing over it or the wetness on the floor. According to the thermal camera measurements taken right in the middle of the road, the surface temperature is determined as 51.7 °C.

The material of the sidewalks where pedestrians walk is asphalt, and a herringbone pattern mold has been printed on it. The albedo value of the pavements, which are then covered with a dark red paint layer, is measured as 0.2823. Sidewalks with a surface temperature of 50.7 °C have almost the same temperature as asphalt. These results infer those materials with close albedo values also have similar surface temperatures.

Table 5.16. Temperature and albedo values of horizontal surfaces of Bahçelievler

BAHÇELİEVLER	MATERIALS	
24.07.2021 - (27 °C)	ASPHALT	PAVEMENT
ALBEDO PHOTOGRAPHY		
MEAN VALUE (PAPER ALBEDO)	239.835	238.561
MEAN VALUE (SURFACE ALBEDO)	99.580	100.880
SURFACE ALBEDO VALUE (%)	0.26988138	0.27486471
DIGITAL PHOTO		
THERMAL IMAGERY	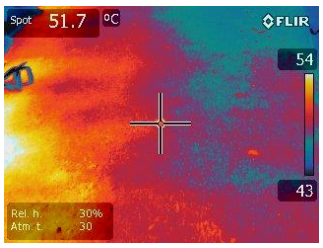	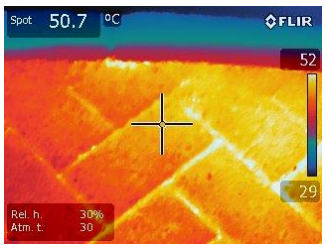
TEMPERATURE (°C)	51.7	50.7

b) Urban Block 2 - Çukurambar 1

In the study area in Çukurambar 1egion, the ground is covered with 3 different types of materials. The first of these materials is asphalt with an albedo value of 0.3333, and the other is a keystone pavement with an albedo value of 0.3593, made of concrete material. These materials, which have very close albedo values, have similar surface temperatures (~50°C). (Table 5.17.)

The surface temperature of the third material, grass, which has a much lower albedo (0.1967) than asphalt and paving tiles, is approximately 36.4 °C. Since plants are

alive, they perform respiration and photosynthesis to continue their lives, and as a result of these actions, the water molecules around them are displaced. By evaporation and transpiration, ground surface vegetation actively removes excessive heat from the environment.

Table 5.17. Temperature and albedo values of horizontal surfaces of Çukurambar 1

ÇUKURAMBAR1	MATERIALS		
22.07.2021 - (29 °C)	ASPHALT	PAVEMENT	GRASS
ALBEDO PHOTOGRAPHY		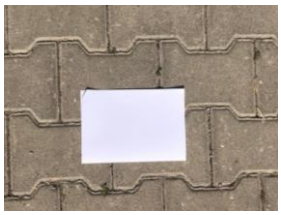	
MEAN VALUE (PAPER ALBEDO)	247.007	237.956	233.723
MEAN VALUE (SURFACE ALBEDO)	126.687	131.551	70.734
SURFACE ALBEDO VALUE (%)	0.333377	0.359344	0.196716
DIGITAL PHOTO			
THERMAL IMAGERY	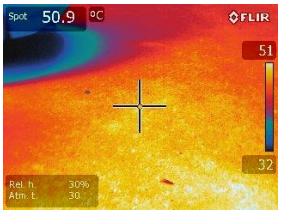	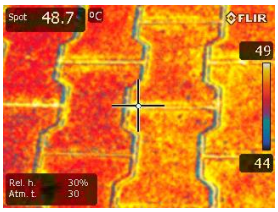	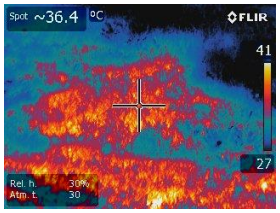
TEMPERATURE (°C)	50.9	48.7	36.4

c) Urban Block 3 - Çukurambar 2

In Çukurambar 2 block, there is a keystone pavement made of concrete and asphalt on the ground. While the surface temperature of the asphalt with an albedo value of 0.3352 is approximately 50.7 °C, the temperature of the pavement with an albedo value of 0.3501 is measured as approximately 52.5 °C. The temperatures of the

surfaces with close albedo values are measured close to each other and the results are in line with the inferences. (Table 5.18.)

Table 5.18. Temperature and albedo values of ground surface materials of Çukurambar 2

ÇUKURAMBAR2	MATERIALS	
24.07.2021 - (28 °C)	ASPHALT	PAVEMENT
ALBEDO PHOTOGRAPHY		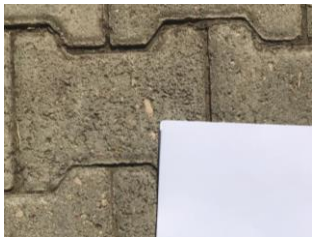
MEAN VALUE (PAPER ALBEDO)	241.519	234.373
MEAN VALUE (SURFACE ALBEDO)	124.567	126.267
SURFACE ALBEDO VALUE (%)	**0.335247**	**0.350183**
DIGITAL PHOTO		
THERMAL IMAGERY	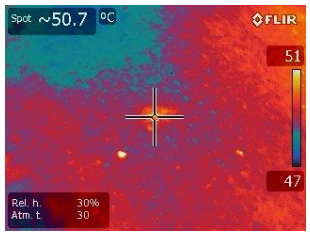	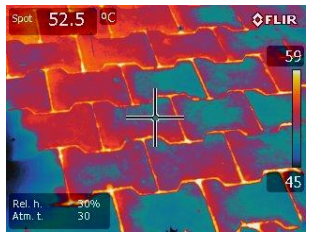
TEMPERATURE (°C)	**50.7**	**52.5**

d) Urban Block 4 - Demetevler

It has been observed that there are 2 different types of pavements on the ground in the Demetevler district. The albedo value of the first of these is calculated as 0.3022, while the albedo value of the second is calculated as 0.3858. Similar to previous inferences, Pavement 1 material with a lower albedo value has a higher surface temperature (51°C), while Pavement 2 material with a higher albedo value, that is, more reflective of light, has a lower surface temperature (46.6°C). The albedo value

of asphalt (0.3054) is slightly higher than pavement 1; therefore, the 2.5 °C difference between the surface temperatures can be considered close. (Table 5.19.)

Table 5.19. Temperature and albedo values of horizontal surfaces of Demetevler

DEMETEVLER	MATERIALS		
22.07.2021 - (28 °C)	ASPHALT	PAVEMENT	PAVEMENT2
ALBEDO PHOTOGRAPHY			
MEAN VALUE (PAPER ALBEDO)	231.930	228.229	231.671
MEAN VALUE (SURFACE ALBEDO)	108.984	106.140	137.534
SURFACE ALBEDO VALUE (%)	0.3054353	0.3022885	0.3858795
DIGITAL PHOTO			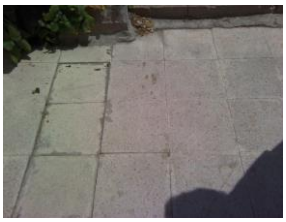
THERMAL IMAGERY	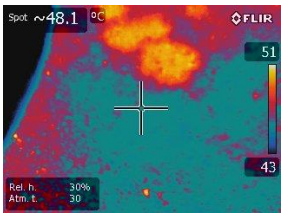		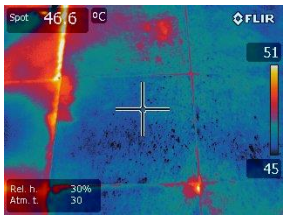
TEMPERATURE (°C)	48.1	51.6	46.6

e) Urban Block 5 - Eryaman 1

As mentioned in the previous parts of the study, Eryaman 1 block is one of the areas with the most material diversity. This high diversity has increased the possibility of making comparisons in the urban block and has enabled albedo values to be interpreted from different perspectives.

The albedo values of both asphalt roads and basketball fields are very close to each other. The surface temperature of the asphalt with an albedo value of 0.3164 was measured at 52.5 °C, while the surface temperature of the basketball field with an

albedo value of 0.3249 was measured as 53.3 °C. It has been observed that the surface temperatures of the areas with close albedo values are also very close to each other. On the other hand, the surface temperature of grass with a much lower albedo (0.2065) was expected to be higher than the other two ground materials, while a value below this expectation (30.3°C) was measured. This is because, as mentioned before, the evaporation and transpiration experienced on the surfaces decreased the temperature values of the surface. At the same time, plants do not absorb all the radiation energy from the sun and reflect most of it back. (Table 5.20.)

Table 5.20. Temperature and albedo values of horizontal surfaces of Eryaman 1

ERYAMAN2	MATERIALS		
28.07.2021 - (30°C)	ASPHALT	GRASS	BASKETBALL FIELD
ALBEDO PHOTOGRAPHY		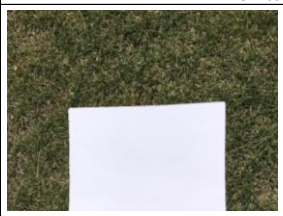	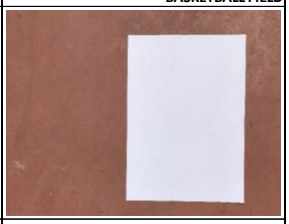
MEAN VALUE (PAPER ALBEDO)	230.362	241.997	229.942
MEAN VALUE (SURFACE ALBEDO)	112.153	76.909	114.964
SURFACE ALBEDO VALUE (%)	0.316456056	0.206576321	0.324980212
DIGITAL PHOTO			
THERMAL IMAGERY	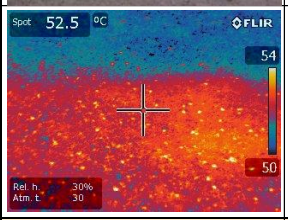	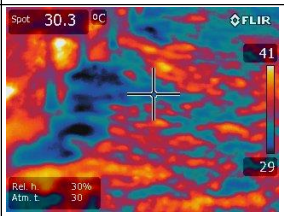	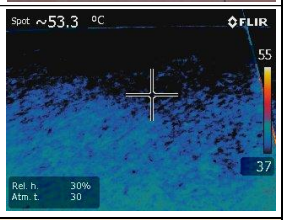
TEMPERATURE (°C)	52.5	30.3	53.3

Other floor materials in the area are specified as Pavement 1, Pavement 2, and Pavement 3. When the Table 5.21. is examined, it is seen that there are color variations in the floor tiles specified as Pavement 1. The temperature differences on the surfaces of the tiles made of the same material also show consistency with the

colors. For lighter colored tiles, the temperature was measured close to 33°C. Moreover, the temperature value marked as spot1 is 45.9°C, and the temperature value marked as spot 2 is 50.5°C.

The temperatures of the ground surface material Pavement 2, made of concrete, fluctuate across the surface. The albedo value of Pavement 2, which shows a surface temperature change between 45°C and 50°C, was calculated as 0.4219.

The temperature value of Pavement 3 material, which has a different albedo value (0.2332), is also similar to Pavement 1 and 2 (52.5 °C). The fact that these three surfaces with different albedo values have similar temperatures shows that the albedo value is not the only factor affecting the surface temperature. The structures of the elements that make up the materials and the variety of roughness on the surfaces of the materials may also have played a role in the differentiation of these values.

Table 5.21. Temperature and albedo values of horizontal surfaces of Eryaman 1

ERYAMAN2	MATERIALS		
28.07.2021 - (30°C)	PAVEMENT1	PAVEMENT2	PAVEMENT3
ALBEDO PHOTOGRAPHY			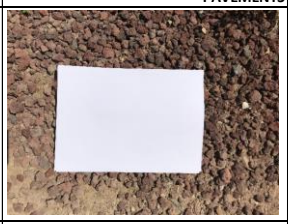
MEAN VALUE (PAPER ALBEDO)	235.819	230.271	236.831
MEAN VALUE (SURFACE ALBEDO)	119.351	149.480	84.980
SURFACE ALBEDO VALUE (%)	0.32897328	0.421946315	0.233233825
DIGITAL PHOTO	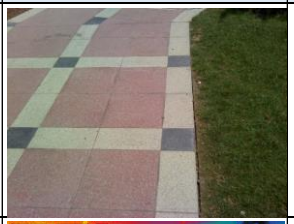		
THERMAL IMAGERY	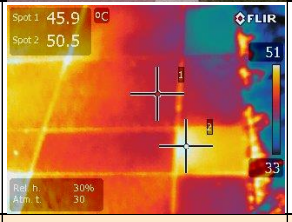	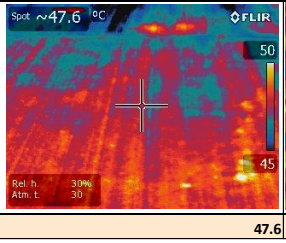	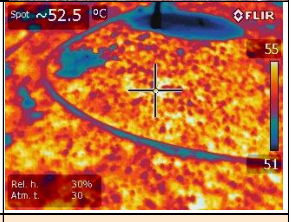
TEMPERATURE (°C)	45.9	47.6	52.5

f) Urban Block 6 - Eryaman 2

Another urban block with a very high material diversity is Eryaman 2. When Grass 1 and Grass 2 are shown in Table 5.22. are compared, it is seen that there is a serious difference between surface temperatures. The reason for this difference is that although the albedo values are close, the plants in the area designated as grass 1 are more alive and can exchange water vapor with the outside. The temperature range seen in the thermal camera is much wider, as the grass in the area designated as Grass 2 is not lively enough and there are only certain spots alive in between. In this area, the surface temperatures of non-living plant parts can reach up to 63°C.

The albedo value (0.2405) of the material specified as the Playground and laid under the children's toys is similar to Grass 1 and Grass 2. However, the highest surface temperature in the block was also measured in this area (72.9°C).

Table 5.22. Temperature and albedo values of horizontal surfaces of Eryaman2

ERYAMAN2	MATERIALS			
28.07.2021 - (30°C)	GRASS1	GRASS2	HIKING TRAIL	PLAYGROUND
ALBEDO PHOTOGRAPHY				
MEAN VALUE (PAPER ALBEDO)	237.119	236.657	242.192	237.047
MEAN VALUE (SURFACE ALBEDO)	72.247	90.250	124.117	87.731
SURFACE ALBEDO VALUE (%)	0.19804634	0.247879843	0.333107824	0.24056474
DIGITAL PHOTO				
THERMAL IMAGERY	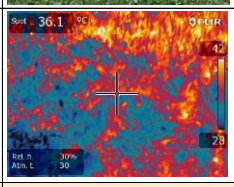	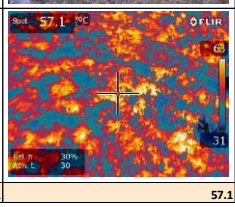	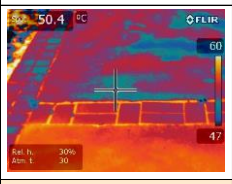	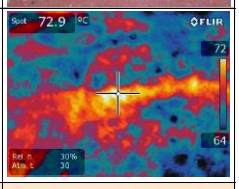
TEMPERATURE (°C)	36.1	57.1	50.4	72.9

The albedo values and surface temperatures of the areas designated as Asphalt and Pavement 1 are close to each other. However, although the albedo value of the area

designated as Pavement 2 is the exact average of the values of these two areas, the surface temperature is approximately 10°C lower. The reason for this may be that the material structure consists of too many elements and the roughness ratio on the surface. The rough areas reflect the sun in different directions and the sun rays cannot spread homogeneously over the whole area. (Table 5.23.)

Table 5.23. Temperature and albedo values of horizontal surfaces of Eryaman2

ERYAMAN2	MATERIALS		
28.07.2021 - (30°C)	ASPHALT	PAVEMENT1	PAVEMENT2
ALBEDO PHOTOGRAPHY		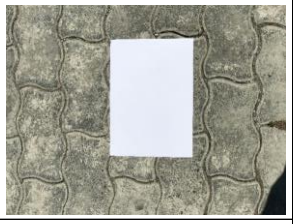	
MEAN VALUE (PAPER ALBEDO)	236.754	239.241	234.785
MEAN VALUE (SURFACE ALBEDO)	115.548	139.322	122.860
SURFACE ALBEDO VALUE (%)	0.317233077	0.37852751	0.340136721
DIGITAL PHOTO			
THERMAL IMAGERY	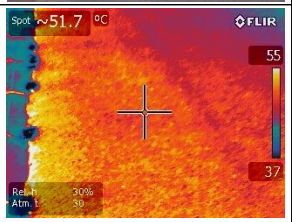	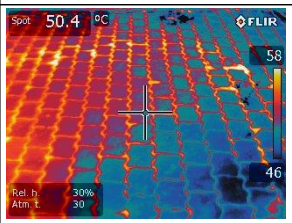	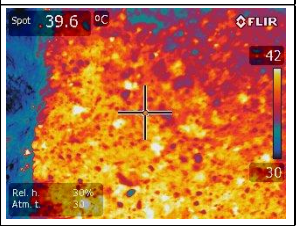
TEMPERATURE (°C)	51.7	50.4	39.6

g) Urban Block 7 - Eskişehir Yolu

Soil materials do not vary in the Eskişehir Yolu urban block. Vehicle roads in the area are asphalt, and pedestrian pavements are keystones made of concrete. The surface temperature of the asphalt with an albedo value of 0.2623 varies between 56-64°C. The temperature of the pavement surface, which has a higher albedo value

(0.3802), varies between 24-49°C. The reason for this diversity on the pavement surface can be explained by the inhomogeneity of the color distribution on the surface. When digital photography and thermal imagery are compared, it can be determined that lighter-colored stones have lower temperature values. (Table 5.24.)

Table 5.24. Temperature and albedo values of horizontal surfaces of Eskişehir Yolu

ESKİŞEHİR YOLU	MATERIALS	
23.07.2021 - (28°C)	ASPHALT	PAVEMENT
		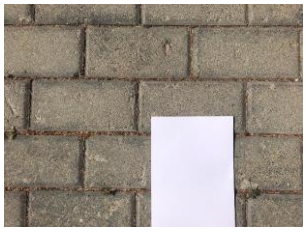
MEAN VALUE (PAPER ALBEDO)	240.587	240.44
MEAN VALUE (SURFACE ALBEDO)	97.098	140.641
SURFACE ALBEDO VALUE (%)	**0.262332**	**0.380206**
DIGITAL PHOTO		
THERMAL IMAGERY	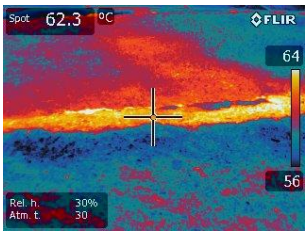	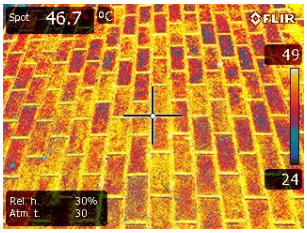
TEMPERATURE (°C)	**62.3**	**46.7**

h) Urban Block 8 - Gölbaşı

Horizontal surfaces in the Gölbaşı urban block are covered with 4 different types of materials (Table 5.25.). The first of these is asphalt with a value of 0.3333 and the surface temperature was measured as 53.5°C. It has been observed that the surface temperature of the soil surface (0.3336), which has almost the same albedo value as asphalt, is 45.9°C. There are parts of low temperature in the soil and live plants can

be found in these low-temperature areas. At the same time, the surface temperature may be measured less than the asphalt surface, since it may be more humid due to the soil structure.

Another surface material is the keystone pavement. The surface temperature of this material, which has a close albedo value (0.3039) to the other two surfaces, was measured as 44.1°C. When thermal camera images are examined, it is observed that the surface does not have a homogeneous temperature distribution. The reason for this may be that there are different humidity rates in the parts where the paving stones touch the ground. It can be deduced that the temperature value decreases at the points where the paving stones, which are a concrete material, carry the moisture in the soil to the surface through the capillary cracks.

The last surface material found in the area is grass. Likewise, green and dry parts on grass surfaces do not show homogeneous distribution. While the surface temperature in arid areas can reach up to 73°C, the surface temperatures in green and lively areas with moisture were measured as 33.8°C.

Table 5.25. Temperature and albedo values of horizontal surfaces of Gölbaşı

GÖLBAŞI	MATERIALS			
26.07.2021 - (28°C)	ASPHALT	PAVEMENT	GRASS	SOIL
ALBEDO PHOTOGRAPHY				
MEAN VALUE (PAPER ALBEDO)	243.816	226.958	233.723	247.201
MEAN VALUE (SURFACE ALBEDO)	125.057	106.140	70.734	126.883
SURFACE ALBEDO VALUE (%)	0.333395	0.303981	0.196716	0.333631
DIGITAL PHOTO				
THERMAL IMAGERY	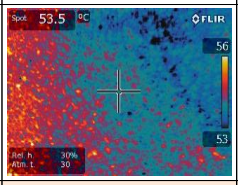	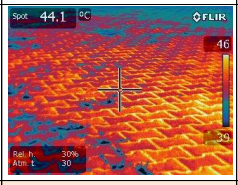	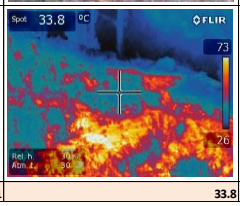	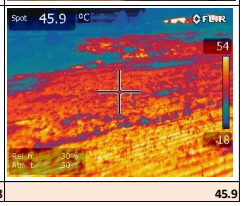
TEMPERATURE (°C)	53.5	44.1	33.8	45.9

i) Urban Block 9 - Hamamönü

Among the floor materials between the buildings in the Hamamönü block, there is only paving stone made of concrete. The albedo value of these stones is calculated as 0.3589. Although it is the same material in the block, the reason for the various surface temperature values when measured from different points may be the shadows that the structures cast on these floors. Therefore, the area marked as Spot 1 is measured at 28.9°C, while the area exposed to sunlight and marked as Spot 2 is measured at 38.8°C.

The albedo value of the asphalt located at the north of the buildings is calculated as 0.2834. This flooring material, which has a lower albedo value than pavement, has a higher surface temperature (52.5 °C). Likewise, the part with a surface temperature independent of the albedo value is grass. Even though the albedo values are lower than all other materials, they do not cause an increase in the surface temperature, since the plants are alive and radiate the radiation from the sun's rays to the environment. (Table 5.26.)

Table 5.26. Temperature and albedo values of horizontal surfaces of Hamamönü

HAMAMÖNÜ	MATERIALS			
22.07.2021 - (29°C)	ASPHALT	PAVEMENT	PAVEMENT	GRASS1
ALBEDO PHOTOGRAPHY				
MEAN VALUE (PAPER ALBEDO)	236.318	241.289	241.289	239.654
MEAN VALUE (SURFACE ALBEDO)	103.050	133.257	133.257	75.652
SURFACE ALBEDO VALUE (%)	0.283442226	0.358976373	0.358976373	0.205186644
DIGITAL PHOTO		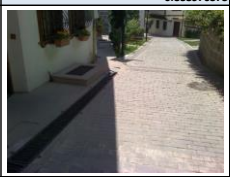		
THERMAL IMAGERY	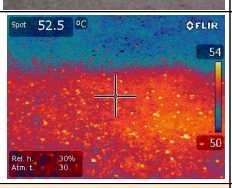	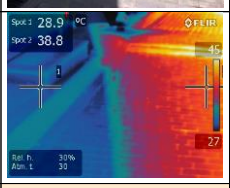		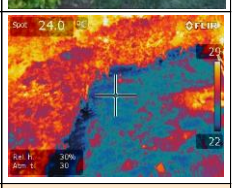
TEMPERATURE (°C)	52.5	28.9	31.9	24

j) Urban Block 10 - İşçi Blokları

Since the albedo value of asphalt (0.2860) in İşçi Blokları block and the albedo value of Pavement 1 (0.2714), which was also made of asphalt and painted over, are close to each other and their temperature values are almost the same (49°C). Unlike these two materials, the albedo value of the material called Pavement 2 is lower (0.2343). Due to its lower albedo value, the temperature of Pavement 2 material is measured higher (58.7°C) than the other two materials.

There are dead spots on the grass surface, which is another ground material in the area. These areas caused the temperature on the grass surface to be heterogeneously distributed. Hence, the temperature values on the same surface vary between 33°C and 54°C. (Table 5.27.)

Table 5.27. Temperature and albedo values of horizontal surfaces of İşçi Blokları

İŞÇİ BLOKLARI	MATERIALS			
22.07.2021 - (28°C)	ASPHALT	PAVEMENT1	PAVEMENT2	GRASS
ALBEDO PHOTOGRAPHY				
MEAN VALUE (PAPER ALBEDO)	220.136	215.084	225.859	241.997
MEAN VALUE (SURFACE ALBEDO)	96.887	89.816	81.436	76.909
SURFACE ALBEDO VALUE (%)	0.286080196	0.271430697	0.234364803	0.206576321
DIGITAL PHOTO				
THERMAL IMAGERY	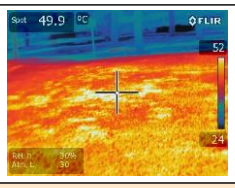	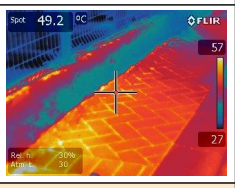	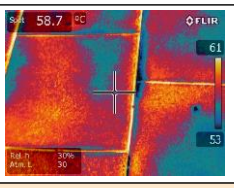	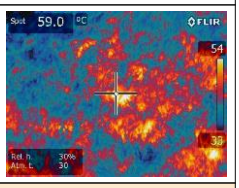
TEMPERATURE (°C)	49.9	49.2	58.7	33-59

k) Urban Block 11 - İvedik

The materials called Pavement 1 and Pavement 2 in the İvedik urban block are shaped as a result of molding on the asphalt floor and opened for pedestrian use. The fact that the raw material of all materials is asphalt, and the albedo values are calculated close to each other can be explained as the reason for the close surface temperatures. (Table 5.28.)

Table 5.28. Temperature and albedo values of horizontal surfaces of İvedik

İVEDİK	MATERIALS		
24.07.2021 - (28°C)	ASPHALT	PAVEMENT1	PAVEMENT2
ALBEDO PHOTOGRAPHY			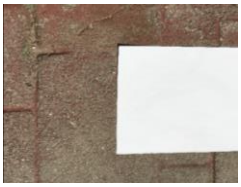
MEAN VALUE (PAPER ALBEDO)	238.551	239.305	240.211
MEAN VALUE (SURFACE ALBEDO)	113.777	110.431	109.457
SURFACE ALBEDO VALUE (%)	0.310017774	0.299952571	0.296185645
DIGITAL PHOTO			
THERMAL IMAGERY	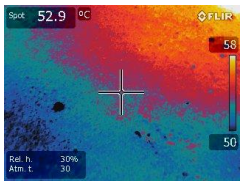	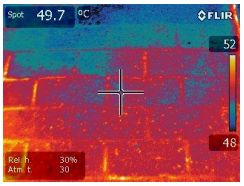	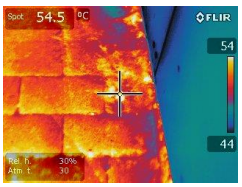
TEMPERATURE (°C)	52.9	49.7	54.5

l) Urban Block 12 - Kızılay

There are asphalt and pavement materials on the floors in the Kızılay urban block. (Table 5.29.) The albedo values of both materials are very close to each other. While the surface temperature of the asphalt is measured as 52.9, the surface temperatures of the pavement tiles vary between 43.2 °C and 51 °C. The reason for the temperature

differences on the ground may be that the sun exposure times differ due to the shadows of the buildings on the ground. While shadows rarely fall on the asphalt surface, the duration of sunbathing on the pavements changes according to the direction of the sun.

Table 5.29. Temperature and albedo values of horizontal surfaces of Kızılay

KIZILAY	MATERIALS	
23.07.2021 - (28°C)	ASPHALT	PAVEMENT
ALBEDO PHOTOGRAPHY		
MEAN VALUE (PAPER ALBEDO)	233.225	234.234
MEAN VALUE (SURFACE ALBEDO)	100.015	95.421
SURFACE ALBEDO VALUE (%)	0.278742631	0.26479354
DIGITAL PHOTO		
THERMAL IMAGERY	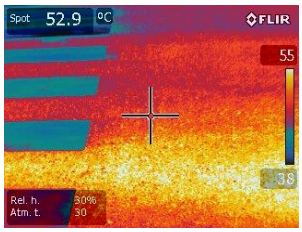	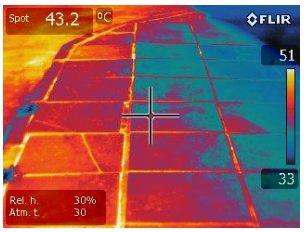
TEMPERATURE (°C)	52.9	43.2 - 51.0

m) Urban Block 13 - Mevlana Bulvarı

The albedo values of the two surface materials in Mevlana Bulvarı are calculated as 0.3087 and they are almost the same result. This similarity led to close results in surface temperatures as well. (Table 5.30.)

Table 5.30. Temperature and albedo values of horizontal surfaces of Mevlana Bulvarı

MEVLANA BULVARI	MATERIALS	
24.07.2021 - (28°C)	ASPHALT	PAVEMENT
ALBEDO PHOTOGRAPHY		
MEAN VALUE (PAPER ALBEDO)	236.702	234.632
MEAN VALUE (SURFACE ALBEDO)	112.444	111.434
SURFACE ALBEDO VALUE (%)	0.308778971	0.308705121
DIGITAL PHOTO		
THERMAL IMAGERY	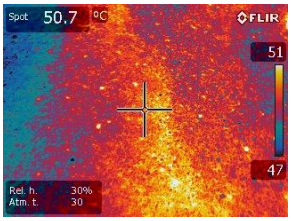	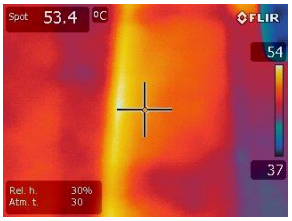
TEMPERATURE (°C)	50.7	53.4

n) Urban Block 14 - Sincan

Another urban block whose materials yield very close results is Sincan. There is a minor difference of approximately 0.9°C between the surface temperature values of asphalt and pavement materials, which have almost the same albedo values. (Table 5.31.)

Table 5.31. Temperature and albedo values of horizontal surfaces of Sincan

SİNCAN	MATERIALS	
28.07.2021 - (31°C)	ASPHALT	PAVEMENT
ALBEDO PHOTOGRAPHY		
MEAN VALUE (PAPER ALBEDO)	246.457	230.741
MEAN VALUE (SURFACE ALBEDO)	126.765	119.515
SURFACE ALBEDO VALUE (%)	0.334327	0.336675103
DIGITAL PHOTO		
THERMAL IMAGERY	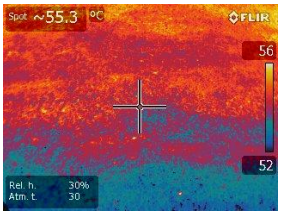	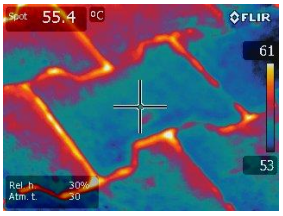
TEMPERATURE (°C)	55.3	55.4

o) Urban Block 15 - Tulumtaş

In the Tulumtaş urban block, the presence of 3 main materials has been determined in the ground (Table 5.32.) The albedo value of asphalt, which is the first of these, is calculated as 0.3896 and the surface temperature is measured as 47.1°C.

There are two types of tiles in Pavement material. The albedo value of the dark pavement tile is calculated as 0.2807, while the albedo value of the light-colored one is calculated as 0.3395. When looking at the thermal imagery, temperature differences are observed between light and dark-colored tiles. The contrasts in colors are also reflected in the thermal camera images. Hence, the surface temperature of the dark-colored tiles reaches up to 46 °C, as opposed to the light-colored tiles whose surface temperature starts at 36°C.

The last surface material in the urban block is the grass found in the gardens of the buildings. The grasses in this block do not show a homogeneous distribution in terms of color and structure. Therefore, the temperatures of grass surfaces, which are alive and dry in places, also vary (26°C-38°C) due to these differences.

Table 5.32. Temperature and albedo values of horizontal surfaces of Tulumtaş

TULUMTAŞ	MATERIALS			
26.07.2021 - (28°C)	ASPHALT	PAVEMENT (DARK)	PAVEMENT (LIGHT)	GRASS
ALBEDO PHOTOGRAPHY				
MEAN VALUE (PAPER ALBEDO)	220.587	224.664	224.664	245.652
MEAN VALUE (SURFACE ALBEDO)	101.263	97.054	117.362	96.743
SURFACE ALBEDO VALUE (%)	0.298389978	0.280797547	0.339552843	0.255983871
DIGITAL PHOTO				
THERMAL IMAGERY	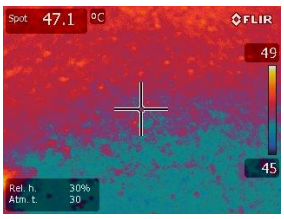	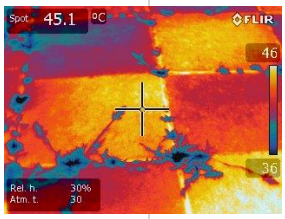		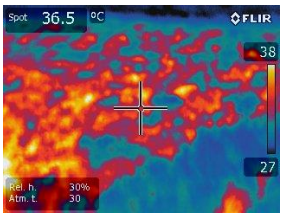
TEMPERATURE (°C)	47.1	45.1	>36	36.5

p) Urban Block 16 - Tunus Caddesi

The last urban block where surface material analysis is conducted is Tunus Caddesi. There is one type of asphalt and three types of pavements in the area. The albedo values of all materials covering the floor are calculated as approximately 0.29. The temperatures of these surface materials, which have very close albedo values, are also very close to each other. (Table 5.33.)

Table 5.33. Temperature and albedo values of horizontal surfaces of Tunus Caddesi

TUNUS	MATERIALS			
23.07.2021 - (28°C)	ASPHALT	PAVEMENT1	PAVEMENT2	PAVEMENT3
ALBEDO PHOTOGRAPHY				
MEAN VALUE (PAPER ALBEDO)	232.241	232.722	231.581	243.817
MEAN VALUE (SURFACE ALBEDO)	103.728	100.318	104.657	110.577
SURFACE ALBEDO VALUE (%)	0.290315663	0.280191387	0.293750567	0.29479097
DIGITAL PHOTO	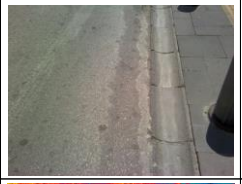			
THERMAL IMAGERY	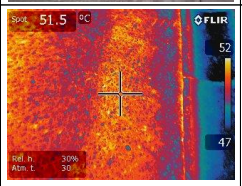	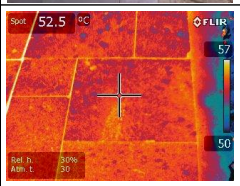	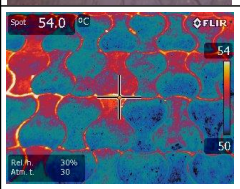	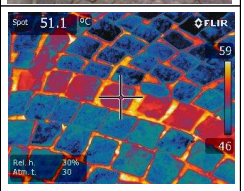
TEMPERATURE (°C)	51.5	52.5	54	51.1

5.2.2.3 Presence of Vegetation

Figure 5.46. Satellite images of the selected blocks in Eryaman-2 (left) and Sincan (right)

The selected urban blocks to compare the effect of plant density on environmental temperature are Eryaman 2 and Sincan (Figure 5.46.). In both blocks, the building

height is classified as low and the window ratios on the facades of buildings used as residential are very close. In Eryaman 2 block, the total area of the ground covered with grass with trees that will provide shade is 24596.06 square meters. On the other hand, there is no grass-covered ground area in the selected block in Sincan. In addition, the plants in that block are at negligible level. (Table 5.34.)

Table 5.34. Comparison of field qualifications of the urban blocks Eryaman 2 and Sincan

URBAN BLOCK	ERYAMAN 2	SİNCAN
COORDINATE (x)	39.972536	39.959261
COORDINATE (y)	32.647660	32.575300
BUILDING AREA (m²)	3463.43	11864.57
GRASS AREA (m²)	**24596.06**	**0.00**
ASPHALT AREA (m2)	4599.70	9682.78
PAVEMENT (m²)	6791.02	18452.65
SOIL (m²)	549.71	0.00
TOTAL AREA (m2)	40000.00	40000.00
BUILDING DENSITY (%)	8.66	29.66
VEGETATION	YES	NO
FLOORS	5	4
BUILDING HEIGHT	LOW	LOW
BUILDING TYPE	RESIDENTIAL	RESIDENTIAL
WINDOW RATIO (%)	16.75	14.52

According to the simulation results, T surface temperature values are given primarily. As can be seen on the Eryaman-2 map (Figure 5.47.), the temperatures of asphalt surfaces are approximately 44°C, while in green areas this temperature drops to 34°C. There are also temperature differences caused by the shadows of the buildings in the area, and this value is below 30 °C.

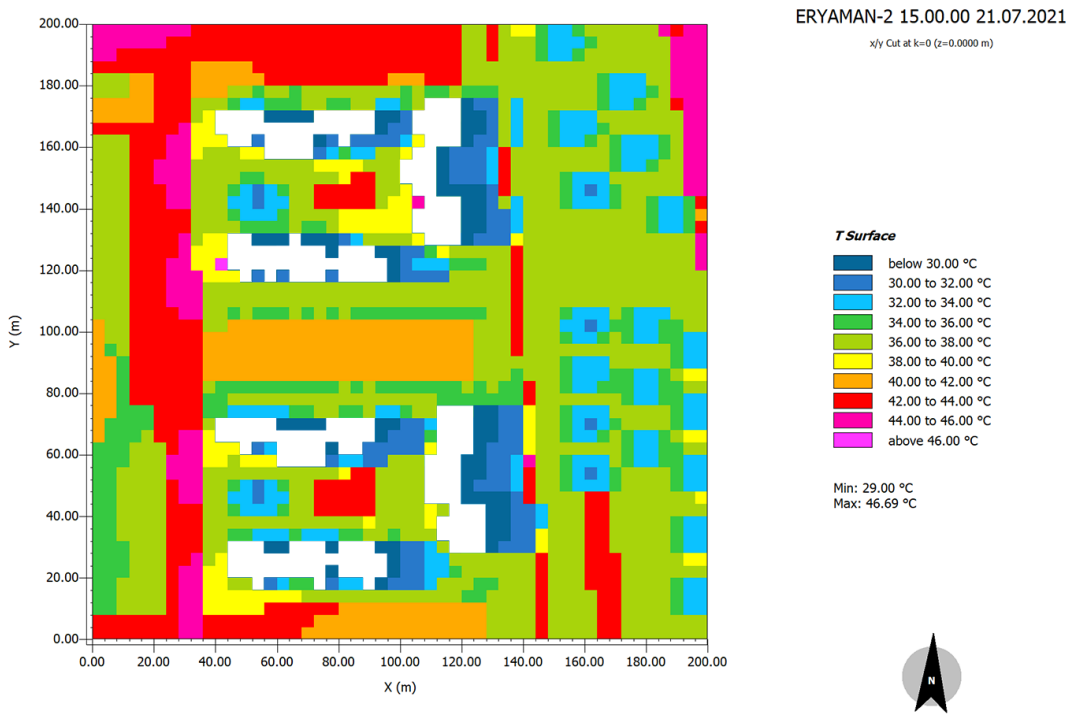

Figure 5.47. T surface values for Eryaman-2 (°C) at 21.07.2021, 15.00.00, plan view, z=0 meters

When the reflected SW radiation map of the area is examined, it is seen that the radiation amount emitted from the building facades reaches a maximum value of 190.56 (W/m²). In the area where the plants are located in the plan, the reflected radiation values can fall below 134 W/m² (Figure 5.48.). This map shows that the radiation rays from the sun are absorbed by plants and reflect less on the environment. When the Eryaman-2 map plan is cut around y=70 meters, the cross-section can be seen in Figure 5.49. While the amount of reflected shortwave radiation on building facades is above 156.75 W/m², this value reaches below 63.69 W/m² in plants seen between x=150-200 coordinates. Vegetation reduces the absorption of short-wave radiation energy. The heat that builds up during the day is rapidly converted into long-wave radiation and expelled from the environment with the help of an open sky.

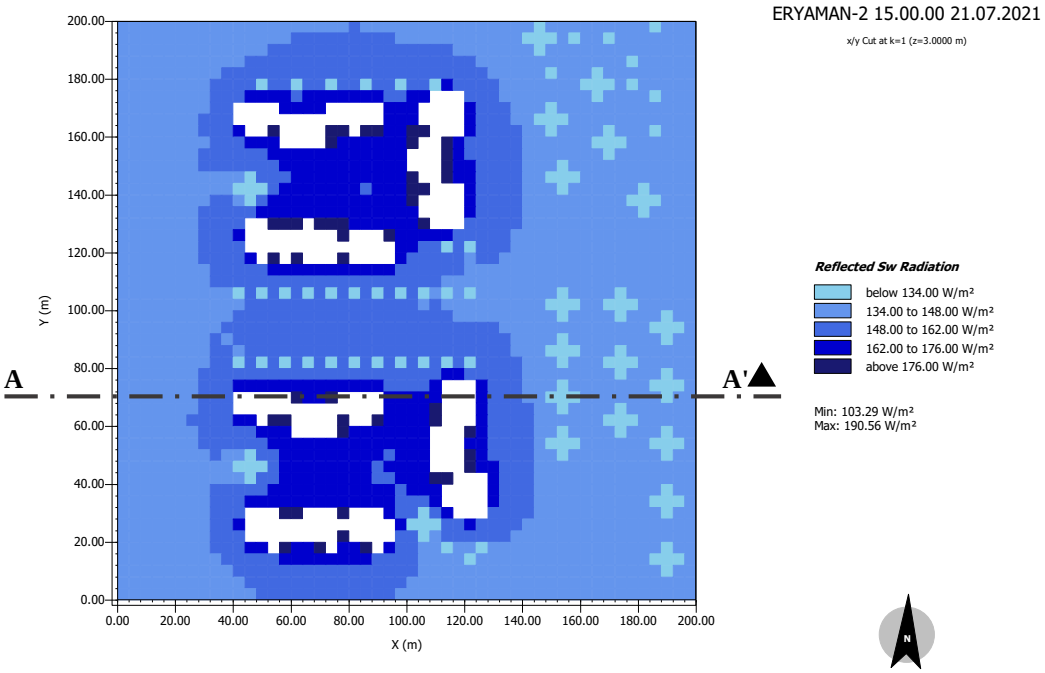

Figure 5.48. Reflected Shortwave Radiation (W/m²) in Eryaman-2 at 21.07.2021, 15.00.00, plan view, z= 3 meters

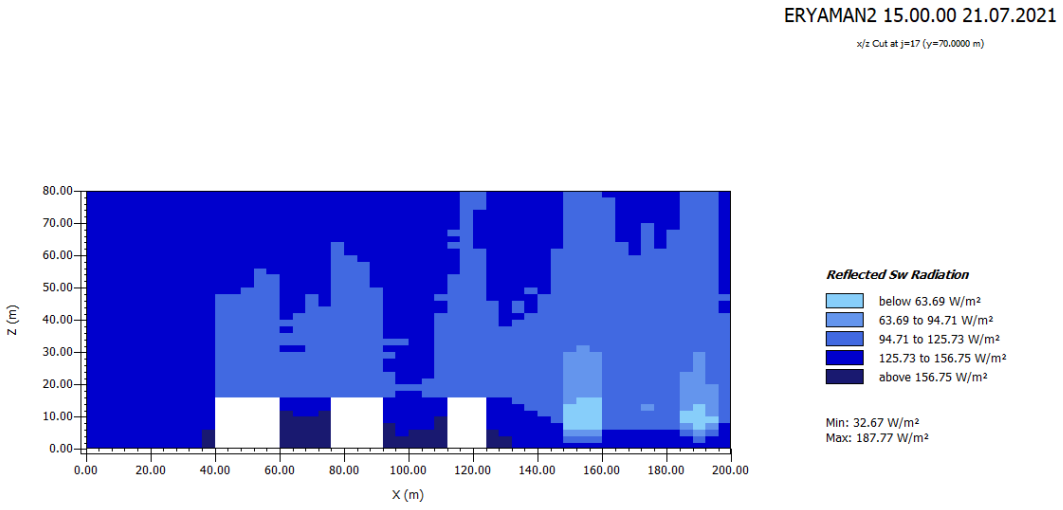

Figure 5.49. Reflected Shortwave Radiation (W/m²) in Eryaman-2 at 21.07.2021, 15.00.00, Section AA', cut at y= 70 meters

When the T surface temperature map created for Sincan is examined (Figure 5.50.), it is seen that the majority of the area consists of asphalt surfaces and the temperature values of these areas can reach up to 46°C. There is no vegetation or green area that may cause this temperature decrease.

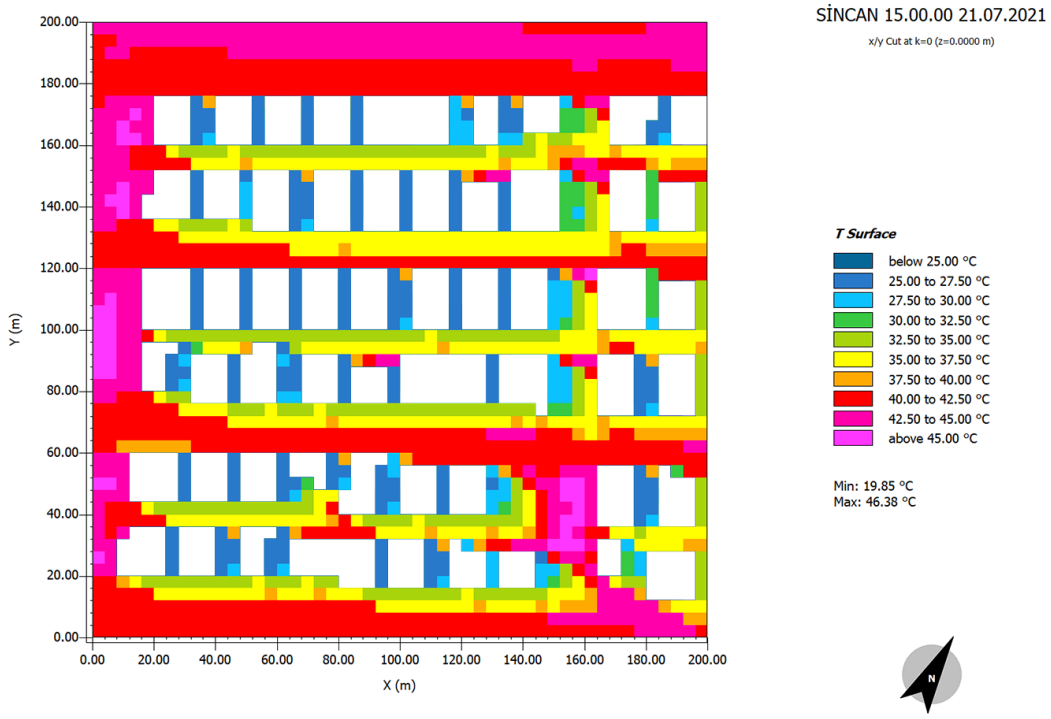

Figure 5.50. T surface values for Sincan (°C) at 21.07.2021, 15.00.00, plan view, z=0 meters

The amount of SW radiation reflected by the building facades of the Sincan Block is above 157.79 W/m² (Figure 5.51). In the section taken from y=82 meters in Sincan, the amount of SW radiation reflected from the buildings reaches 154.52 W/m². There is no plant that will absorb the radiation from the sun and reduce the amount emitted to the environment. (Figure 5.52.)

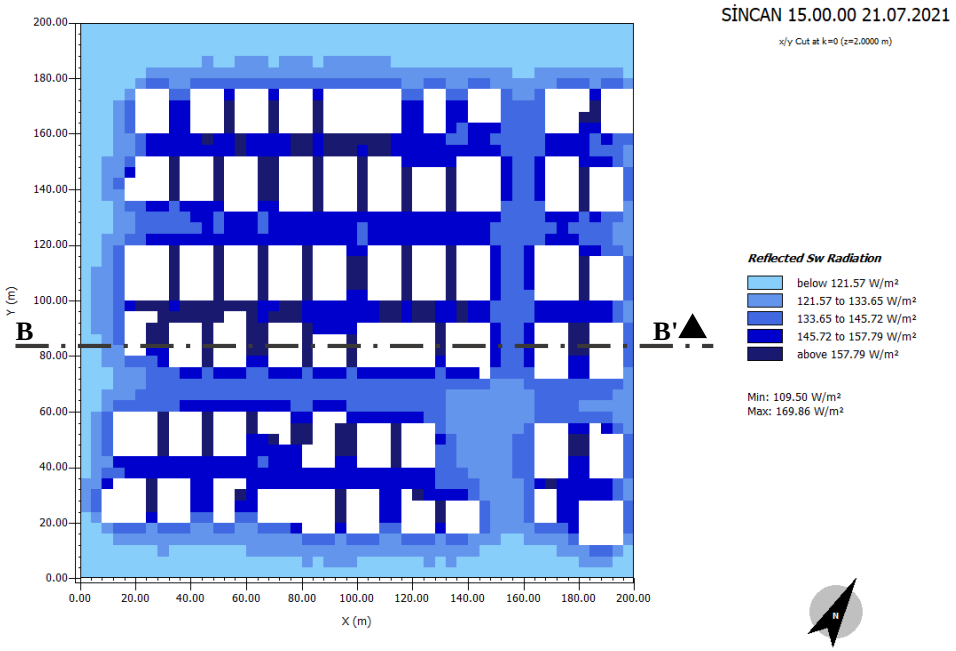

Figure 5.51. Reflected Shortwave Radiation (W/m²) in Sincan at 21.07.2021, 15.00.00, plan view, z= 2 meters

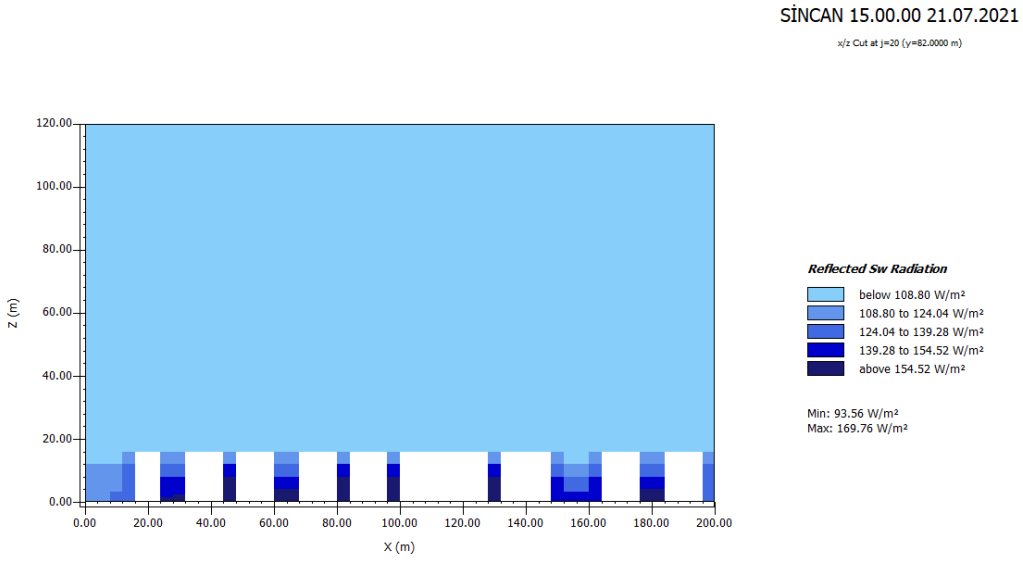

Figure 5.52. Reflected Shortwave Radiation (W/m²) in Sincan at 21.07.2021, 15.00.00, Section BB', cut at y= 82 meters

5.2.2.4 Presence of Water Body

Figure 5.53. Satellite images of the selected blocks in Gölbaşı (left) and Tulumtaş (right)

Gölbaşı is the only urban block with a large water body among the case study blocks (Figure 5.53.). There is a water body covering an area of 5044.12 square meters in the block. Another urban block with similar characteristics to this one is Tulumtaş. Since these two blocks are geographically close to each other, they were exposed to the same weather conditions during the measurement (Table 5.35.)

Table 5.35. Comparison of atmospheric conditions of Gölbaşı and Tulumtaş

URBAN BLOCK	GÖLBAŞI	TULUMTAŞ
MEASUREMENT DATE	26.07.2021	26.07.2021
TIME RANGE	13:20-13:40	13:50-14:10
TEMPERATURE (°C)	28	28
HUMIDITY (%)	28	27
WIND DIRECTION	NW	NW
WIND SPEED (km/h)	14	14
PRECIPITATION (cm)	0	0
PRESSURE (hPa)	1017	1017
SIGHT DISTANCE (km)	9.7	9.7
UV INDEX	9	9

In both Gölbaşı and Tulumtaş urban blocks, 50% of the total area is covered with grass. The buildings in the area have 2 floors. (Table 5.36.) The major difference between these two areas is the presence of a body of water. The water mass with an area of 5044 m² caused a decrease in the average surface temperature in the area.

Table 5.36. Comparison of field qualifications of Gölbaşı and Tulumtaş

URBAN BLOCK	GÖLBAŞI	TULUMTAŞ
COORDINATE (x)	39.781716	39.762866
COORDINATE (y)	32.789775	32.729564
BUILDING AREA (m²)	737.75	5792.41
GRASS AREA (m²)	20182.44	21810.74
WATER (m²)	5044.12	0.00
ASPHALT AREA (m2)	1235.76	4032.04
PAVEMENT (m²)	5725.45	4580.46
SOIL (m²)	7074.47	3784.36
TOTAL AREA (m2)	40000.00	40000.00
BUILDING DENSITY (%)	1.84	14.48
VEGETATION	YES	YES
FLOORS	2	2
BUILDING HEIGHT	LOW	LOW
BUILDING TYPE	OFFICE	RESIDENTIAL

When the T surface temperature map is examined, the surface temperature of the large water body in the Gölbaşı block emerged as 29-31 °C. The surface temperature of the water body is approximately 11°C lower than the temperatures of other surrounding ground materials such as pavement and asphalt. The reason for this might be that the large water mass evaporates by using the heat energy nearby. Another reason might be the water body reflects the rays from the sun and water bodies heat up and cool down later than land.

The remaining areas are covered with grass and these surfaces have temperatures of approximately 35-37 °C. (Figure 5.54.)

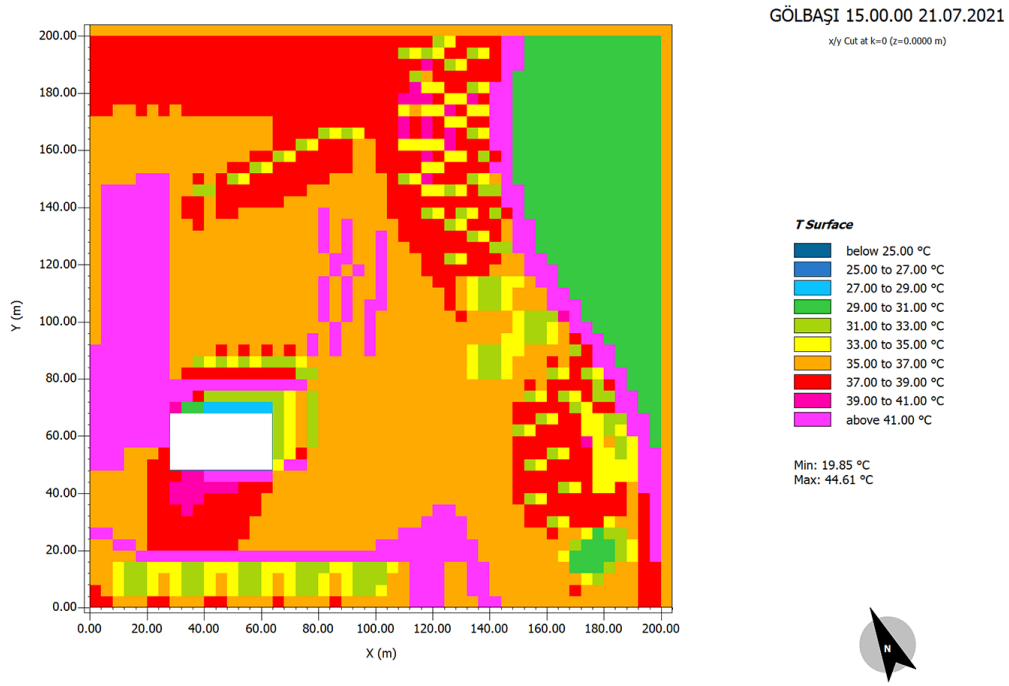

Figure 5.54. T surface values for Gölbaşı (°C) at 21.07.2021, 15.00.00, plan view, z=0 meters

In the Tulumtaş block, the majority of the surface is covered with green areas, but asphalt and construction density are also noteworthy. Grass-covered areas have a similar temperature (35°C) to the Gölbaşı block. (Figure 5.55.)

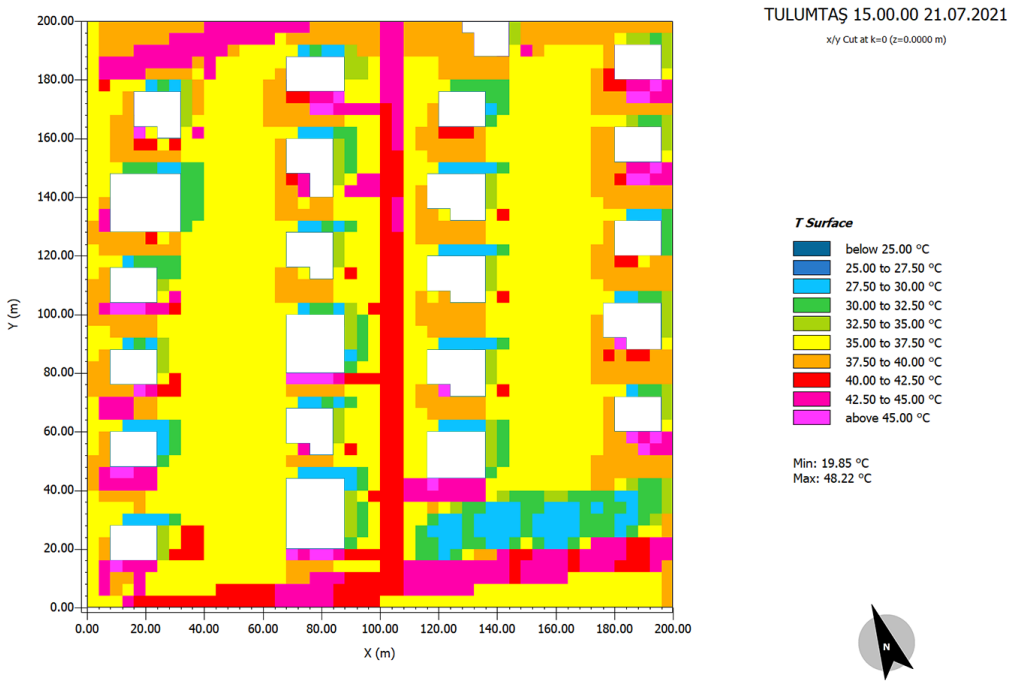

Figure 5.55. T surface values for Tulumtaş (°C) at 21.07.2021, 15.00.00, plan view, z=0 meters

When the reflected SW radiation maps (both plan and section) of the blocks are examined, it is seen that the plants in the Gölbaşı block absorb the radiation from the sun and reflect less of it to its surroundings. (Figure 5.56. and 5.57.)

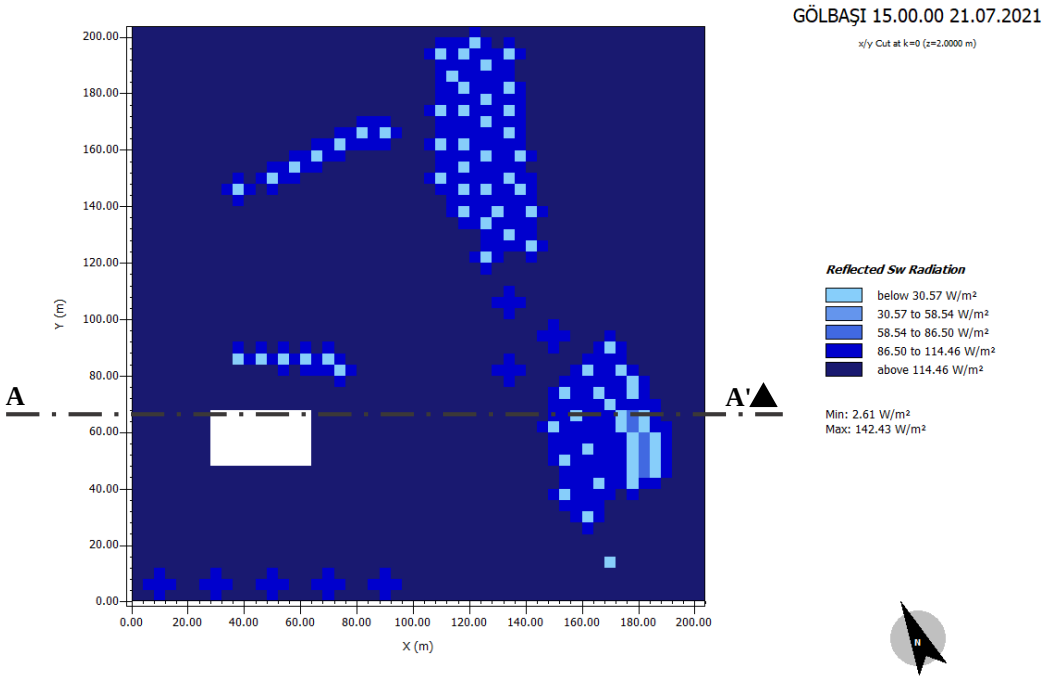

Figure 5.56. Reflected Shortwave Radiation (W/m²) in Gölbaşı at 21.07.2021, 15.00.00, plan view, z=2 meters

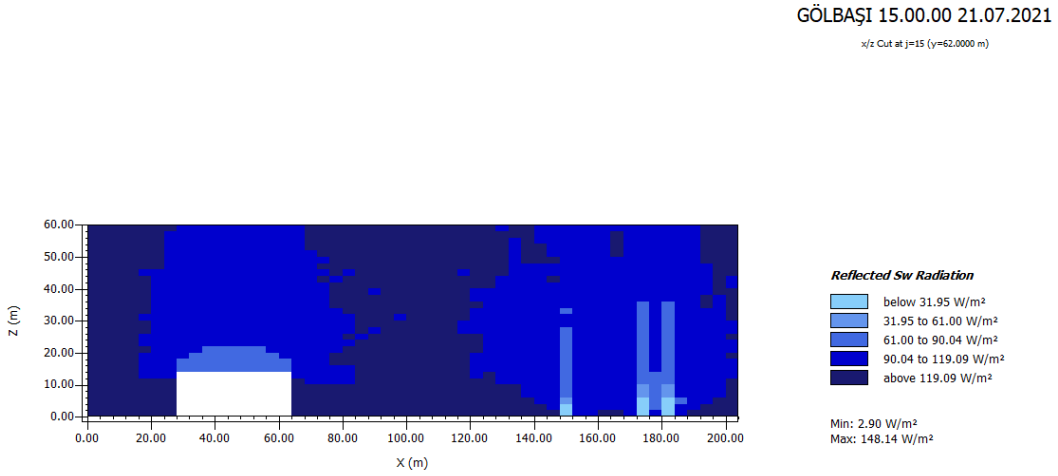

Figure 5.57. Reflected Shortwave Radiation (W/m²) in Gölbaşı at 21.07.2021, 15.00.00, Section AA', cut at y=62 meters

In Tulumtaş, on the other hand, although there is a green surface area, the rate of absorbing SW radiation from the sun is less since there are a smaller number of trees. (Figures 5.58. and 5.59.)

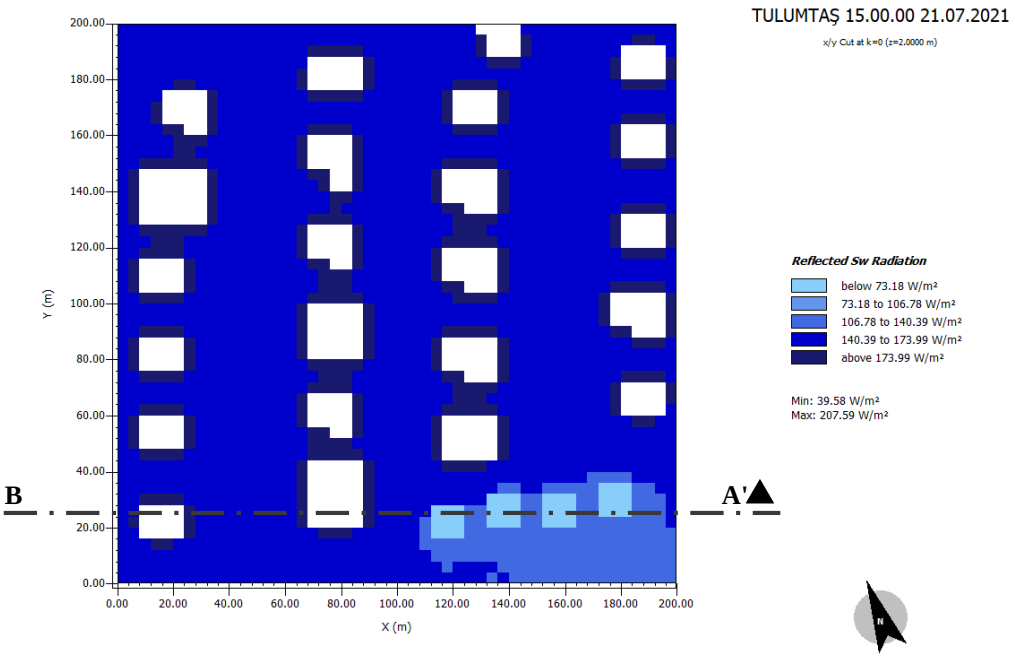

Figure 5.58. Reflected Shortwave Radiation (W/m²) in Tulumtaş at 21.07.2021, 15.00.00, plan view, z=2 meters

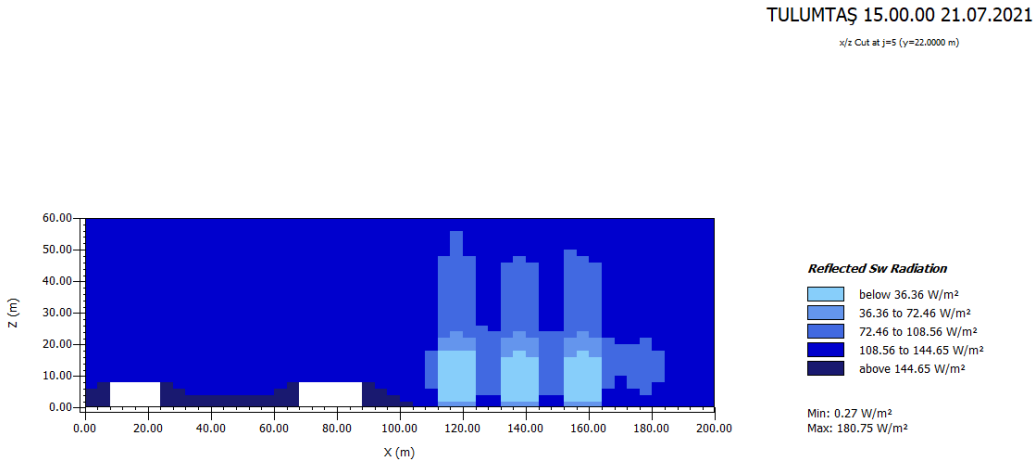

Figure 5.59. Reflected Shortwave Radiation (W/m²) in Tulumtaş at 21.07.2021, 15.00.00, Section BB', cut at y=22 meters

In Gölbaşı Block, the presence of a water body of 5044 square meters has been one of the important factors providing the passage of the wind. When the wind speed map (Figure 5.60. and 5.61.) created for the area is examined, it is seen that the wind speed is higher than 2.81 m/s in most of the area. It can be said that the presence of

a large body of water in the area indirectly increases the thermal comfort level since the wind reduces the temperature in the environment with convective heat transfer.

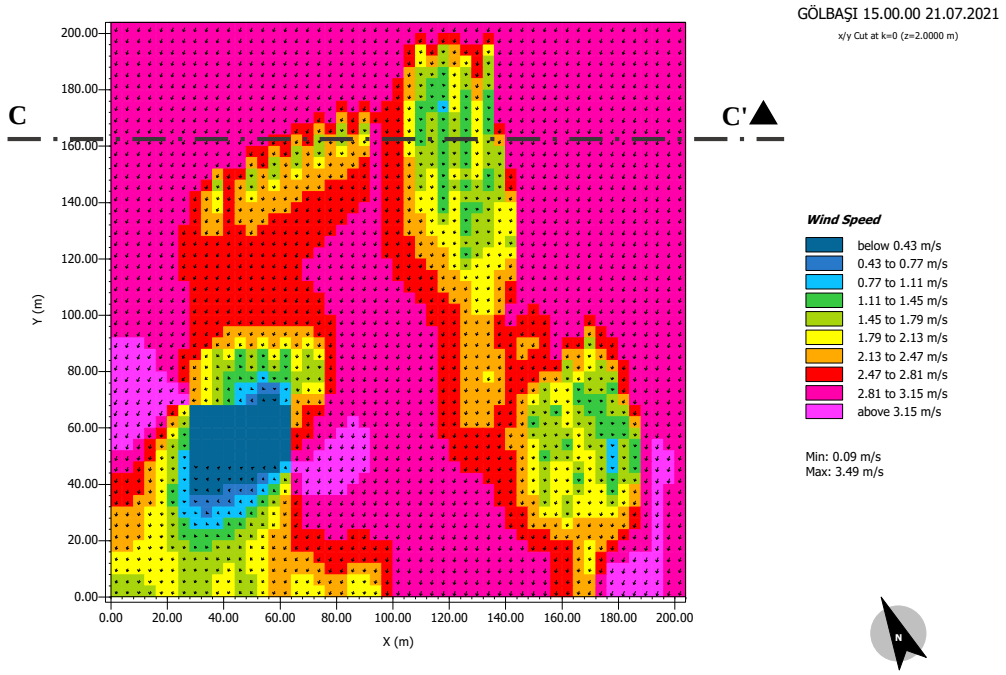

Figure 5.60. Wind speed values (m/s) for Gölbaşı at 21.07.2021, 15.00.00, plan view, z=2 meter

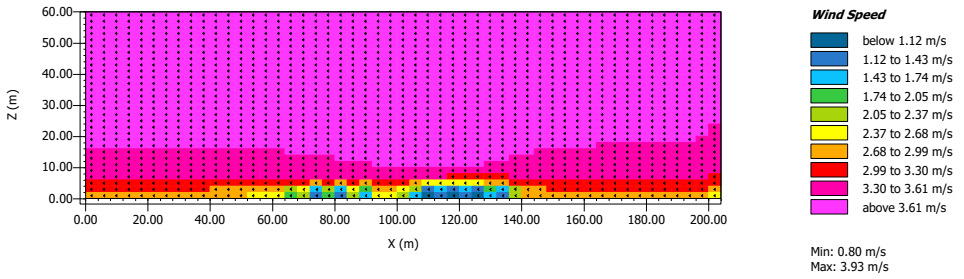

Figure 5.61. Wind speed values (m/s) for Gölbaşı at 21.07.2021, 15.00.00, Section CC', cut at y=162 meters

The fact that Tulumtaş block has a higher density of buildings than Gölbaşı block and that these structures are arranged in a single direction has been a factor preventing wind passage. Wind corridors have been formed in the spaces between

the buildings and the wind speed in this area varies between 2.65 and 3.18 m/s. (Figures 5.62. and 5.63.)

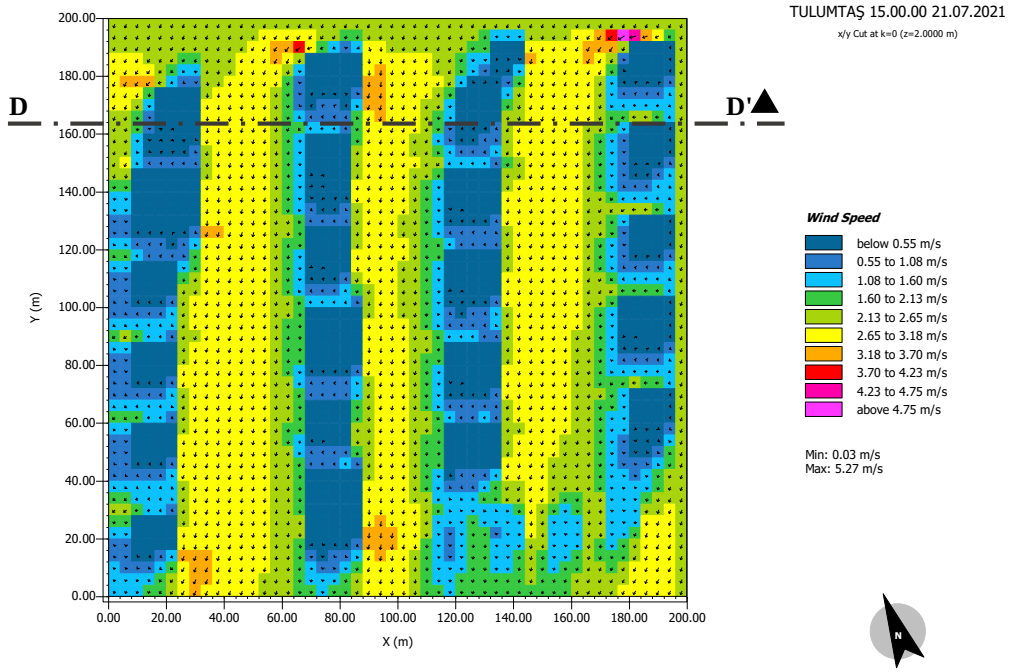

Figure 5.62. Wind speed values (m/s) for Tulumtaş at 21.07.2021, 15.00.00, plan view, z=2 meters

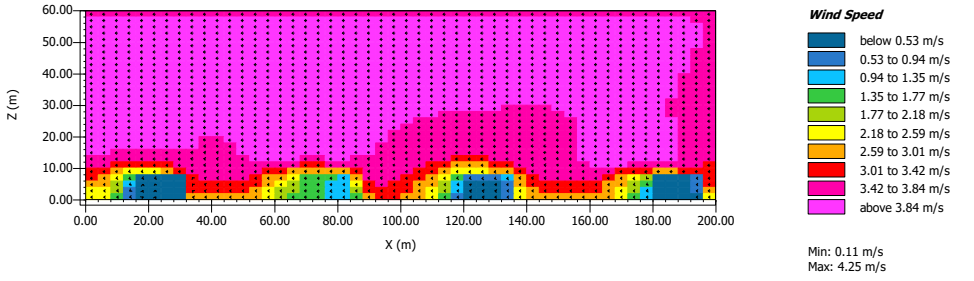

Figure 5.63. Wind speed values (m/s) for Tulumtaş at 21.07.2021, 15.00.00, Section DD', cut at y=162 meters

CHAPTER 6

CONCLUSION

The whole world has come under the influence of global warming, and many studies on this subject have shown that global warming has occurred because of human activities in the last 100 years. Based on these inferences, this research aims to relate seasonal changes and excessive heat accumulation in Ankara to the expansion of urban areas and changes in the building and urban surface materials.

Within the scope of the study, 16 urban blocks with grid dimensions of 200x200 meters were modeled in districts of Ankara, and albedo calculations, thermal camera measurements, and environmental conditions simulations were made.

The results obtained from this study are as follows:

- According to the zoning regulations, as the height of the buildings increases, the distance between them must also be increased. In this way, the building density in the area can be controlled. When the blocks with different building heights are compared, it is seen that they have different microclimatic properties. For instance, shorter buildings in a high-density urban fabric reduce the wind speed, while taller and more spaced located structures allow the wind to accelerate. Although the shadow lengths of shorter buildings are shorter, the shading effect they create for people walking on the street is also lesser. Tall structures, on the other hand, can create a thermal comfort zone for people outside during the day in summer, by creating a shadow in the larger ground area.
- The albedo is a value between 0 and 1, and is defined as “an expression of the ability of surfaces to reflect solar radiation”. Within the scope of the study, the albedo values of the horizontal and vertical surfaces were calculated and the

relationship of these values with the surface temperatures was examined. Accordingly, light-colored surfaces with an albedo value close to the albedo value of a white sheet of paper (0.65) have lower surface temperatures than dark-colored surfaces with a lower albedo value. At the same time, the reflected shortwave (SW) radiation values of the surfaces with lower albedo values were also lower than the surfaces with high values. The reason for this is that these surfaces absorb the radiation energy from the sun and reflect a small amount to the outside. On the contrary, surfaces with a high albedo value reflect most of the radiation outside. Therefore, it can be shown as the reason for the low facade temperatures as expected.

- When the window-to-wall ratio is high in a building, the temperature of the facades cannot be measured accurately with a thermal camera since the rays from the sun are reflected in different directions. Due to the excessive radiated solar radiation, the temperature in the urban areas around the buildings increases, and the thermal comfort level of the people around is adversely affected.

- Another factor affecting microclimatic conditions is the urban layout. In two blocks with very similar structural features, the different positioning and orientation of the buildings primarily change the wind passage pattern. In the blocks with organic layouts and irregularly oriented buildings, the wind is constantly caught in the obstruction and cannot be accelerated. However, in the other area, which is positioned in regular and adjacent order, wind corridors have been formed and the wind speed has accelerated due to the venturi effect. Therefore, the thermal comfort level of the pedestrians increases in summertime. In addition, since the shadows falling on the ground are at different angles in the block that has an irregular building layout, temperature differences have occurred on the ground even though it is covered with the same materials.

- The presence of vegetation is one of the main factors that affect the microclimate of a region. Although grass has a low albedo value, they help control air temperature by evaporation and transpiration. Field investigations and thermal

camera measurements show that having grass-covered areas compared to other pavement materials reduces the surface temperature more than 10 °C. The presence of various plants in the area beside the grass prevents the SW radiation from the sun to be absorbed and released into the environment. For instance, in the Urban Block 6 – Eryaman2, where the reflected SW radiation value on the building facades is 156.75 W/m² when it comes to the area where the trees are located, the reflected SW value that appears in the simulation decreased to 32.67 W/m². Thus, the effect of radiation from the sun decreases and the thermal comfort level of pedestrians increases.

- Only one of the case study urban blocks, which is Gölbaşı, has a large body of water. It has been observed that the surface temperature of the water body is approximately 11°C lower than the temperatures of other surrounding ground materials. This may be because the water surface reflects the rays from the sun and water bodies heat up and cool down later than land. Furthermore, since the wind passing over the water body leaves its heat energy to the water and moves forward its temperature decreases. These factors may increase the thermal comfort level by reducing the sensible temperature.

As a result of all the studies, the questions in the aim and objectives part were tried to be answered:

- Different properties of surface materials also affect their ability to retain and diffuse heat. When the urban area is covered with materials that are high heat retaining, have a low albedo, and have low water permeability, excessive heat accumulates in cities, and it is not easily dispersed. For this reason, a relationship has been established between surface materials and UHI formation. When designing new settlements, paying attention to the properties of materials can prevent the formation of UHI in cities.

- As the albedo value of a material increases, the surface temperature decreases. In order to reduce the ambient temperatures, materials with high albedo values can be used more on horizontal and vertical surfaces.
- The presence of vegetation and water bodies reduces the potential air temperature by evaporation and absorbing the SW radiation. This effect helps to reduce the air temperature and increase the thermal comfort level of the people.

In conclusion, in this study, the reason for the microclimate changes observed in Ankara was questioned and it was tried to investigate the factors causing this microclimate change.

While investigating this situation, different methodologies were used, and these elements were compared with each other. As a result, it has been observed that microclimate changes cannot be due to a single factor and that more than one variable affects an area at the same time. For this reason, when conducting future studies, a holistic approach should be adopted instead of considering the parameters affecting the microclimate separately.

REFERENCES

Akbari, H., Pomerantz, M., & Taha, H. (2001). Cool surfaces and shade trees to reduce energy use and improve air quality in urban areas. Solar Energy, 70(3), 295–310. https://doi.org/10.1016/s0038-092x(00)00089-x

Al-hafiz, B., Musy, M., & Hasan, T. (2017). A Study on the Impact of Changes in the Materials Reflection Coefficient for Achieving Sustainable Urban Design. Procedia Environmental Sciences, 38, 562–570. https://doi.org/10.1016/j.proenv.2017.03.126

Aylık Sıcaklık Analizi. (2020). Meteoroloji Genel Müdürlüğü. https://www.mgm.gov.tr/veridegerlendirme/sicaklik-analizi.aspx

Bilgili, B. C., & Şahin, Ş. (2013). Evaluation of Urban Green Areas on "The City Climate; Case Study of Ataturk Forest Farm. International Caucasian Forestry Symposium.

Chui, A. C., Gittelson, A., Sebastian, E., Stamler, N., & Gaffin, S. R. (2018). Urban heat islands and cooler infrastructure – Measuring near-surface temperatures with hand-held infrared cameras. Urban Climate, 24, 51–62. https://doi.org/10.1016/j.uclim.2017.12.009

Çiçek, İ. (2004). Ankara'da Şehirleşmenin Yağış Üzerine Etkisi. Fırat University Journal of Social Science, 14(1), 1–17.

Çiçek, İ., & Doğan, U. (2005). Ankara'da Şehir Isı Adasının İncelenmesi, Detection of Urban Heat Island in Ankara, Türkiye. Coğrafi Bilimler Dergisi, 3(1), 57–72. https://doi.org/10.1501/cogbil_0000000049

Çiçek, İ., Yılmaz, E., Türkoğlu, N., & Çalışkan, O. (2013). Seasonal Variation of Surface Temperature Based On Land Cover in Ankara. International Journal of Human Sciences, 10(1), 621–640.

Cocci Grifoni, R., D'Onofrio, R., Sargolini, M., & Pierantozzi, M. (2016). A

Parametric Optimization Approach to Mitigating the Urban Heat Island Effect: A Case Study in Ancona, Italy. Sustainability, 8(9), 896. https://doi.org/10.3390/su8090896

Elmarakby, E., Khalifa, M., Elshater, A., & Afifi, S. (2022). Tailored methods for mapping urban heat islands in Greater Cairo Region. Ain Shams Engineering Journal, 13(2), 101545. https://doi.org/10.1016/j.asej.2021.06.030

Erell, E., Pearlmutter, D., & Williamson, T. J. (2011). Urban Microclimate – Designing the Spaces between Buildings. City Weathers: Meteorology and Urban Design 1950-2010, Manchester Architecture Research Centre (MARC).

Fabbri, K., Gaspari, J., Bartoletti, S., & Antonini, E. (2020). Effect of facade reflectance on outdoor microclimate: An Italian case study. Sustainable Cities and Society, 54, 101984. https://doi.org/10.1016/j.scs.2019.101984

Giridharan, R., & Emmanuel, R. (2018). The impact of urban compactness, comfort strategies and energy consumption on tropical urban heat island intensity: A review. Sustainable Cities and Society, 40, 677–687. https://doi.org/10.1016/j.scs.2018.01.024

Heaviside, C., Vardoulakis, S., & Cai, X.-M. (2016). Attribution of mortality to the urban heat island during heatwaves in the West Midlands, UK. Environmental Health, 15(S1). https://doi.org/10.1186/s12940-016-0100-9

Hwang, R.-L., Lin, T.-P., & Matzarakis, A. (2011). Seasonal effects of urban street shading on long-term outdoor thermal comfort. Building and Environment, 46(4), 863–870. https://doi.org/10.1016/j.buildenv.2010.10.017

Khan, A., & Chatterjee, S. (2016). Numerical simulation of urban heat island intensity under urban–suburban surface and reference site in Kolkata, India. Modeling Earth Systems and Environment, 2(2). https://doi.org/10.1007/s40808-016-0119-5

Kim, Y.-H., & Baik, J.-J. (2005). Spatial and Temporal Structure of the Urban Heat Island in Seoul. Journal of Applied Meteorology, 44(5), 591–605. https://doi.org/10.1175/jam2226.1

Kleerekoper, L., van Esch, M., & Salcedo, T. B. (2012). How to make a city climate-proof, addressing the urban heat island effect. Resources, Conservation and Recycling, 64, 30–38. https://doi.org/10.1016/j.resconrec.2011.06.004

Kotharkar, R., Bagade, A., & Ramesh, A. (2019). Assessing urban drivers of canopy layer urban heat island: A numerical modeling approach. Landscape and Urban Planning, 190, 103586. https://doi.org/10.1016/j.landurbplan.2019.05.017

Lassandro, P., & Di Turi, S. (2017). Facade retrofitting: from energy efficiency to climate change mitigation. Energy Procedia, 140, 182–193. https://doi.org/10.1016/j.egypro.2017.11.134

Li, G., Zhang, X., Mirzaei, P. A., Zhang, J., & Zhao, Z. (2018). Urban heat island effect of a typical valley city in China: Responds to the global warming and rapid urbanization. Sustainable Cities and Society, 38, 736–745. https://doi.org/10.1016/j.scs.2018.01.033

Li, H., Harvey, J., & Kendall, A. (2013). Field measurement of albedo for different land cover materials and effects on thermal performance. Building and Environment, 59, 536–546. https://doi.org/10.1016/j.buildenv.2012.10.014

Li, X., Zhou, Y., Yu, S., Jia, G., Li, H., & Li, W. (2019). Urban heat island impacts on building energy consumption: A review of approaches and findings. Energy, 174, 407–419. https://doi.org/10.1016/j.energy.2019.02.183

Malys, L., Musy, M., & Inard, C. (2016). Direct and Indirect Impacts of Vegetation on Building Comfort: A Comparative Study of Lawns, Green Walls and Green Roofs. Energies, 9(1), 32. https://doi.org/10.3390/en9010032

Manoli, G., Fatichi, S., Schläpfer, M., Yu, K., Crowther, T. W., Meili, N., Burlando, P., Katul, G. G., & Bou-Zeid, E. (2019). Magnitude of urban heat islands largely explained by climate and population. Nature, 573(7772), 55–60. https://doi.org/10.1038/s41586-019-1512-9

Mansouri, O., Belarbi, R., & Bourbia, F. (2017). Albedo effect of external surfaces on the energy loads and thermal comfort in buildings. Energy Procedia, 139(2017), 571–577. https://doi.org/10.1016/j.egypro.2017.11.255

Martin-Vide, J., Sarricolea, P., & Moreno-Garcia, M. C. (2015). On the definition of urban heat island intensity: the "rural" reference. Frontiers in Earth Science, 3. https://doi.org/10.3389/feart.2015.00024

McPherson, E. G. (1994). The Ecological City: Preserving and Restoring Urban Biodiversity (pp. 153–171). University Of Massachusetts Press.

Mills, G. (2008). Luke Howard and The Climate of London. Weather, 63(6), 153–157. https://doi.org/10.1002/wea.195

Nüfus ve Demografi. (2020). Türkiye İstatistik Kurumu. https://data.tuik.gov.tr/

Oke, T. R. (1982). The energetic basis of the urban heat island. Quarterly Journal of the Royal Meteorological Society, 108(455), 1–24. https://doi.org/10.1002/qj.49710845502

Qin, Y. (2015). A review on the development of cool pavements to mitigate urban heat island effect. Renewable and Sustainable Energy Reviews, 52, 445–459. https://doi.org/10.1016/j.rser.2015.07.177

Planlı Alanlar İmar Yönetmeliği, 30113 (2017). https://www.resmigazete.gov.tr/eskiler/2017/07/20170703-8.htm

Sailor, D. J. (1998). Simulations of annual degree day impacts of urban vegetative augmentation. Atmospheric Environment, 32(1), 43–52. https://doi.org/10.1016/s1352-2310(97)00178-7

Santamouris, M. (2013). Using cool pavements as a mitigation strategy to fight urban heat island—A review of the actual developments. Renewable and Sustainable Energy Reviews, 26, 224–240. https://doi.org/10.1016/j.rser.2013.05.047

Santamouris, M., Gaitani, N., Spanou, A., Saliari, M., Giannopoulou, K., Vasilakopoulou, K., & Kardomateas, T. (2012). Using cool paving materials to improve microclimate of urban areas – Design realization and results of the flisvos project. Building and Environment, 53, 128–136. https://doi.org/10.1016/j.buildenv.2012.01.022

Santamouris, M., & Yun, G. Y. (2020). Recent development and research priorities on cool and super cool materials to mitigate urban heat island. Renewable Energy, 161(2020), 792–807. https://doi.org/10.1016/j.renene.2020.07.109

Sat, N. A., Güler Üçler, Z. A., Varol, Ç., & Yenigül, S. B. (2017). Sürdürülebilir Kentler İçin Çok Merkezli Gelişme: Ankara Metropoliten Kenti İçin Bir Değerlendirme. Journal of Ankara Studies, 5(1), 98–107.

Şensoy, S., Türkoğlu, N., Çiçek, İ., Demircan, M., Arabacı, H., & Bölük, E. (2015). Urbanization Effect On Trends Of Extreme Temperature Indices In Ankara. VII. Uluslararası Katılımlı Atmosfer Bilimleri Sempozyumu, İstanbul, Türkiye.

Sobstyl, J. M., Emig, T., Qomi, M. J. A., Ulm, F.-J. ., & Pellenq, R. J.-M. (2018). Role of City Texture in Urban Heat Islands at Nighttime. Physical Review Letters, 120(10). https://doi.org/10.1103/physrevlett.120.108701

Souza, L. C. L., Postigo, C. P., Oliveira, A. P., & Nakata, C. M. (2009). Urban heat islands and electrical energy consumption. International Journal of Sustainable Energy, 28(1–3), 113–121. https://doi.org/10.1080/14786450802453249

Synnefa, A., Karlessi, T., Gaitani, N., Santamouris, M., Assimakopoulos, D. N., & Papakatsikas, C. (2011). Experimental testing of cool colored thin layer

asphalt and estimation of its potential to improve the urban microclimate. Building and Environment, 46(1), 38–44. https://doi.org/10.1016/j.buildenv.2010.06.014

Taleghani, M., Swan, W., Johansson, E., & Ji, Y. (2020). Urban cooling: which facade orientation has the most impact on a microclimate? Sustainable Cities and Society, 102547. https://doi.org/10.1016/j.scs.2020.102547

Theodoridou, I., Karteris, M., Mallinis, G., Tsiros, E., & Karteris, A. (2017). Assessing the Benefits from Retrofitting Green Roofs in Mediterranean, Using Environmental Modelling, GIS and Very High Spatial Resolution Remote Sensing Data: The Example of Thessaloniki, Greece. Procedia Environmental Sciences, 38, 530–537. https://doi.org/10.1016/j.proenv.2017.03.117

Touloupaki, E., & Theodosiou, T. (2017). Optimization of Building form to Minimize Energy Consumption through Parametric Modelling. Procedia Environmental Sciences, 38, 509–514. https://doi.org/10.1016/j.proenv.2017.03.114

Uemoto, K. L., Sato, N. M. N., & John, V. M. (2010). Estimating thermal performance of cool colored paints. Energy and Buildings, 42(1), 17–22. https://doi.org/10.1016/j.enbuild.2009.07.026

Wolters, D., & Brandsma, T. (2012). Estimating the Urban Heat Island in Residential Areas in the Netherlands Using Observations by Weather Amateurs. Journal of Applied Meteorology and Climatology, 51(4), 711–721. https://doi.org/10.1175/jamc-d-11-0135.1

Zhang, D.-L., Shou, Y.-X., Dickerson, R. R., & Chen, F. (2011). Impact of Upstream Urbanization on the Urban Heat Island Effects along the Washington–Baltimore Corridor. Journal of Applied Meteorology and Climatology, 50(10), 2012–2029. https://doi.org/10.1175/jamc-d-10-05008.1

APPENDICES

A. Definition of Terms

Albedo: the measure of the diffuse reflection of solar radiation out of the total solar radiation and measured on a scale from 0, corresponding to a black body that absorbs all incident radiation, to 1, corresponding to a body that reflects all incident radiation.

Heat Flux: a flow of energy per unit of area per unit of time. (W/m2)

Potential Air Temperature: the temperature that a sample of air would have if it were brought dry-adiabatically to a pressure of 1000 hPa.

Short Wave (SW) Radiation: a radiant energy produced by the sun with wavelengths ranging from infrared through visible to ultraviolet.

Urban Heat Island (UHI): an urban or metropolitan area that is significantly warmer than its surrounding rural areas due to human activities.

Venturi Effect: the reduction in fluid pressure that results when a fluid flows through a constricted section (or choke) of a pipe.

B. Raw Data of Albedo and Temperature Values of Vertical Surfaces

Table B.1. Data of Building Facade in Bahçelievler

BAHÇELİEVLER	24.07.2021 - (27 °C)	ALBEDO PHOTOGRAPHY	MEAN VALUE (PAPER ALBEDO)	MEAN VALUE (SURFACE ALBEDO)	SURFACE ALBEDO VALUE (%)	DIGITAL PHOTO	THERMAL IMAGERY	TEMPERATURE (°C)
	WALL		237.253	143.112	0.39208271		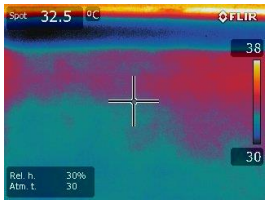	32.5

Table B.2. Data of Building Facade in Çukurambar 1

ÇUKURAMBAR1	22.07.2021 - (29 °C)	ALBEDO PHOTOGRAPHY	MEAN VALUE (PAPER ALBEDO)	MEAN VALUE (SURFACE ALBEDO)	SURFACE ALBEDO VALUE (%)	DIGITAL PHOTO	THERMAL IMAGERY	TEMPERATURE (°C)
	WALL		247.007	126.687	0.333377		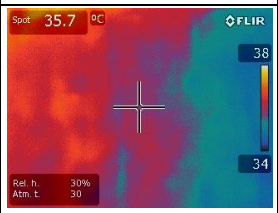	35.7

Table B.3. Data of Building Facade in Çukurambar 2

ÇUKURAMBAR2	GLASS		
DIGITAL PHOTO			
THERMAL IMAGERY	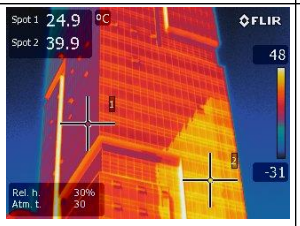		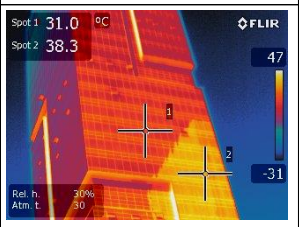
TEMPERATURE (°C)	SPOT1: 24.9 SPOT2: 39.9	SPOT1: 22.2 SPOT2: 38.2	SPOT1: 31.0 SPOT2: 38.3

Table B.4. Data of Building Facade in Demetevler

DEMETEVLER	22.07.2021 - (28 °C)	ALBEDO PHOTOGRAPHY	MEAN VALUE (PAPER ALBEDO)	MEAN VALUE (SURFACE ALBEDO)	SURFACE ALBEDO VALUE (%)	DIGITAL PHOTO	THERMAL IMAGERY	TEMPERATURE (°C)
	WALL		252.531	104.847	0.269870		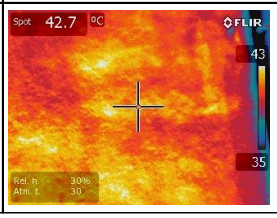	42.7

Table B.5. Data of Building Facade in Eryaman 1

ERYAMAN 1	21.07.2021 - (32 °C)	ALBEDO PHOTOGRAPHY	MEAN VALUE (PAPER ALBEDO)	MEAN VALUE (SURFACE ALBEDO)	SURFACE ALBEDO VALUE (%)	DIGITAL PHOTO	THERMAL IMAGERY	TEMPERATURE (°C)
	WALL		242.209	108.869	0.292164		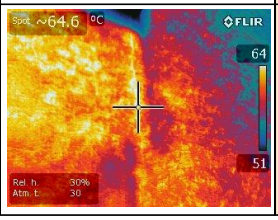	64.6

Table B.6. Data of Building Facade in Eryaman 2

ERYAMAN 2	28.07.2021 - (30°C)	ALBEDO PHOTOGRAPHY	MEAN VALUE (PAPER ALBEDO)	MEAN VALUE (SURFACE ALBEDO)	SURFACE ALBEDO VALUE (%)	DIGITAL PHOTO	THERMAL IMAGERY	TEMPERATURE (°C)
	WALL		189.803	154.196	0.528060		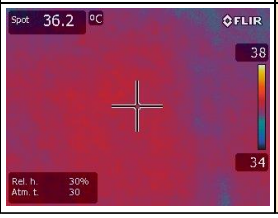	36.2

Table B.7. Data of Building Facade in Eskişehir Yolu

ESKİŞEHİR YOLU	GLASS		
DIGITAL PHOTO			
THERMAL IMAGERY	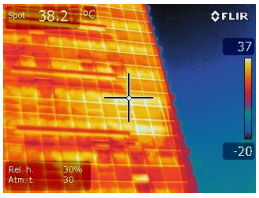		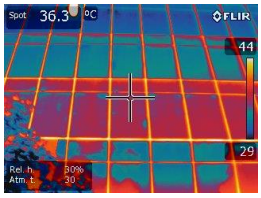
TEMPERATURE (°C)	38.2	37.5	36.3

Table B.8. Data of Building Facade in Gölbaşı

GÖLBAŞI	26.07.2021 - (28°C)	ALBEDO PHOTOGRAPHY	MEAN VALUE (PAPER ALBEDO)	MEAN VALUE (SURFACE ALBEDO)	SURFACE ALBEDO VALUE (%)	DIGITAL PHOTO	THERMAL IMAGERY	TEMPERATURE (°C)
	WALL		218.000	148.108	0.441606		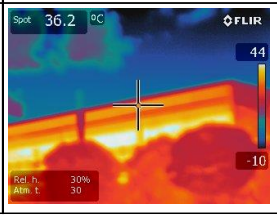	36.2

Table B.9. Data of Building Facade in Hamamönü

HAMAMÖNÜ	22.07.2021 - (29°C)	ALBEDO PHOTOGRAPHY	MEAN VALUE (PAPER ALBEDO)	MEAN VALUE (SURFACE ALBEDO)	SURFACE ALBEDO VALUE (%)	DIGITAL PHOTO	THERMAL IMAGERY	TEMPERATURE (°C)
	WALL		192.116	159.050	0.538125		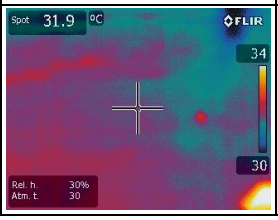	31.9

Table B.10. Data of Building Facade in İşçi Blokları

İŞÇİ BLOKLARI	22.07.2021 - (28°C)	ALBEDO PHOTOGRAPHY	MEAN VALUE (PAPER ALBEDO)	MEAN VALUE (SURFACE ALBEDO)	SURFACE ALBEDO VALUE (%)	DIGITAL PHOTO	THERMAL IMAGERY	TEMPERATURE (°C)
	WALL	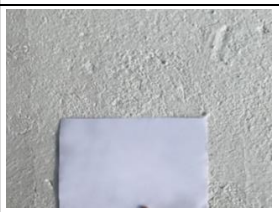	201.718	185.261	0.596970		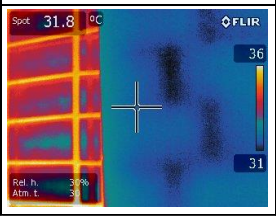	31.8

Table B.11. Data of Building Facade in İvedik

İVEDİK	24.07.2021 - (28°C)	ALBEDO PHOTOGRAPHY	MEAN VALUE (PAPER ALBEDO)	MEAN VALUE (SURFACE ALBEDO)	SURFACE ALBEDO VALUE (%)	DIGITAL PHOTO	THERMAL IMAGERY	TEMPERATURE (°C)
	WALL	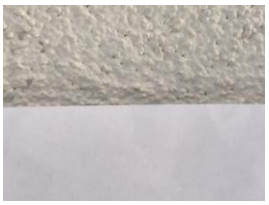	199.174	175.516	0.572793		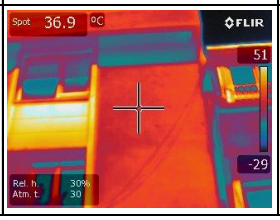	36.9

Table B.12. Data of Building Facade in Kızılay

KIZILAY	23.07.2021 - (28°C)	ALBEDO PHOTOGRAPHY	MEAN VALUE (PAPER ALBEDO)	MEAN VALUE (SURFACE ALBEDO)	SURFACE ALBEDO VALUE (%)	DIGITAL PHOTO	THERMAL IMAGERY	TEMPERATURE (°C)
	WALL		228.996	107.172	0.304205		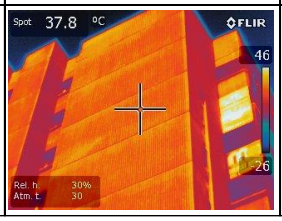	37.8

Table B.13. Data of Building Facade in Mevlana Bulvarı

MEVLANA BULVARI	GLASS		
DIGITAL PHOTO			
THERMAL IMAGERY		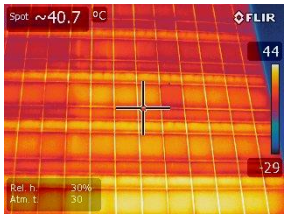	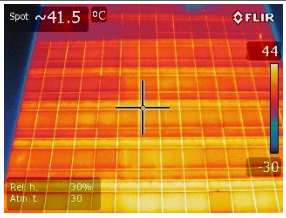
TEMPERATURE (°C)	35.4	40.7	41.5

Table B.14. Data of Building Facade in Sincan

SİNCAN	28.07.2021 - (31°C)	ALBEDO PHOTOGRAPHY	MEAN VALUE (PAPER ALBEDO)	MEAN VALUE (SURFACE ALBEDO)	SURFACE ALBEDO VALUE (%)	DIGITAL PHOTO	THERMAL IMAGERY	TEMPERATURE (°C)
	WALL		191.221	148.971	0.506383		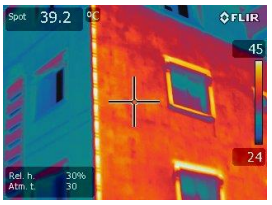	39.2

Table B.15. Data of Building Facade in Tulumtaş

TULUMTAŞ	26.07.2021 - (28°C)	ALBEDO PHOTOGRAPHY	MEAN VALUE (PAPER ALBEDO)	MEAN VALUE (SURFACE ALBEDO)	SURFACE ALBEDO VALUE (%)	DIGITAL PHOTO	THERMAL IMAGERY	TEMPERATURE (°C)
	WALL		221.743	118.121	0.346251			30

Table B.16. Data of Building Facade in Tunus Caddesi

TUNUS	23.07.2021 - (28°C)	ALBEDO PHOTOGRAPHY	MEAN VALUE (PAPER ALBEDO)	MEAN VALUE (SURFACE ALBEDO)	SURFACE ALBEDO VALUE (%)	DIGITAL PHOTO	THERMAL IMAGERY	TEMPERATURE (°C)
	WALL	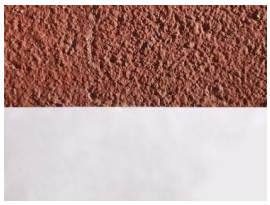	228.717	96.177	0.273329		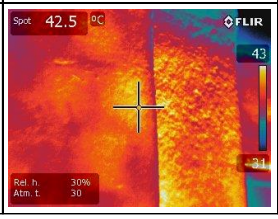	42.5

C. Charts for Surface Albedo and Temperature

Table C.17. Albedo and Temperature Values for Horizontal Surfaces

URBAN BLOCK		SURFACE	SURFACE ALBEDO (%)	SURFACE TEMPERATURE (°C)
1	***BAHÇELİEVLER***	ASPHALT	0.269881	51.7
		PAVEMENT	0.274865	50.7
2	***ÇUKURAMBAR 1***	ASPHALT	0.333377	50.9
		PAVEMENT	0.359344	48.7
		GRASS	0.196716	36.4
3	***ÇUKURAMBAR 2***	ASPHALT	0.335247	50.7
		PAVEMENT	0.350183	52.5
4	***DEMETEVLER***	ASPHALT	0.305435	48.1
		PAVEMENT	0.302289	51.6
		PAVEMENT 2	0.385880	46.6
5	***ERYAMAN 1***	ASPHALT	0.316456	52.5
		GRASS	0.206576	30.3
		BASKETBALL FIELD	0.324980	53.3
		PAVEMENT	0.328973	45.9
		PAVEMENT 2	0.421946	47.6
		PAVEMENT 3	0.233234	52.5
6	***ERYAMAN 2***	GRASS	0.198046	36.1
		GRASS 2	0.247880	57.1
		HIKING TRAIL	0.333108	50.4
		PLAYGROUND	0.240565	72.9
		ASPHALT	0.317233	51.7
		PAVEMENT	0.378528	50.4
		PAVEMENT 2	0.340137	39.6
7	***ESKİŞEHİR YOLU***	ASPHALT	0.262332	62.3
		PAVEMENT	0.380206	46.7
8	***GÖLBAŞI***	ASPHALT	0.333395	53.5
		PAVEMENT	0.303981	44.1
		GRASS	0.196716	33.8
		SOIL	0.333631	45.9
9	***HAMAMÖNÜ***	ASPHALT	0.283442	52.5
		PAVEMENT	0.358976	28.9
		PAVEMENT	0.358976	31.9
		GRASS	0.205187	24.0

Table C.18. (Continued)

10	***İŞÇİ BLOKLARI***	ASPHALT	0.286080	49.9
		PAVEMENT	0.271431	49.2
		PAVEMENT 2	0.234365	58.7
		GRASS	0.206576	33.5
11	***İVEDİK***	ASPHALT	0.310002	52.9
		PAVEMENT	0.299953	49.7
		PAVEMENT 2	0.296186	54.5
12	***KIZILAY***	ASPHALT	0.278743	52.9
		PAVEMENT	0.264794	43.2
13	***MEVLANA BULVARI***	ASPHALT	0.308779	50.7
		PAVEMENT	0.308705	53.4
14	***SİNCAN***	ASPHALT	0.334327	55.3
		PAVEMENT	0.336675	55.4
15	***TULUMTAŞ***	ASPHALT	0.298390	47.1
		PAVEMENT (DARK)	0.280798	45.1
		PAVEMENT (LIGHT)	0.339553	36.0
		GRASS	0.255984	36.5
16	***TUNUS CADDESİ***	ASPHALT	0.290316	51.5
		PAVEMENT	0.280191	52.5
		PAVEMENT 2	0.293751	54.0
		PAVEMENT 3	0.294791	51.1

Table C.19 Albedo and Temperature Values for Vertical Surfaces

URBAN BLOCK		SURFACE	SURFACE ALBEDO (%)	SURFACE TEMPERATURE (°C)
1	***BAHÇELİEVLER***	WALL	0.392083	32.5
2	***ÇUKURAMBAR 1***	WALL	0.333377	35.7
3	***ÇUKURAMBAR 2***	GLASS	-	32.9
4	***DEMETEVLER***	WALL	0.269870	42.7
5	***ERYAMAN 1***	WALL	0.292164	64.6
6	***ERYAMAN 2***	WALL	0.528060	36.2
7	***ESKİŞEHİR YOLU***	GLASS	-	38.2
8	***GÖLBAŞI***	WALL	0.441606	36.2
9	***HAMAMÖNÜ***	WALL	0.538125	31.9
10	***İŞÇİ BLOKLARI***	WALL	0.596970	31.8
11	***İVEDİK***	WALL	0.572793	36.9
12	***KIZILAY***	WALL	0.304205	37.8
13	***MEVLANA BULVARI***	GLASS	-	40.7
14	***SİNCAN***	WALL	0.506383	39.2
15	***TULUMTAŞ***	WALL	0.346251	30.0
16	***TUNUS CADDESİ***	WALL	0.273329	42.5

D. ENVI-met Microclimate Simulation Results

a) T Surface Temperature

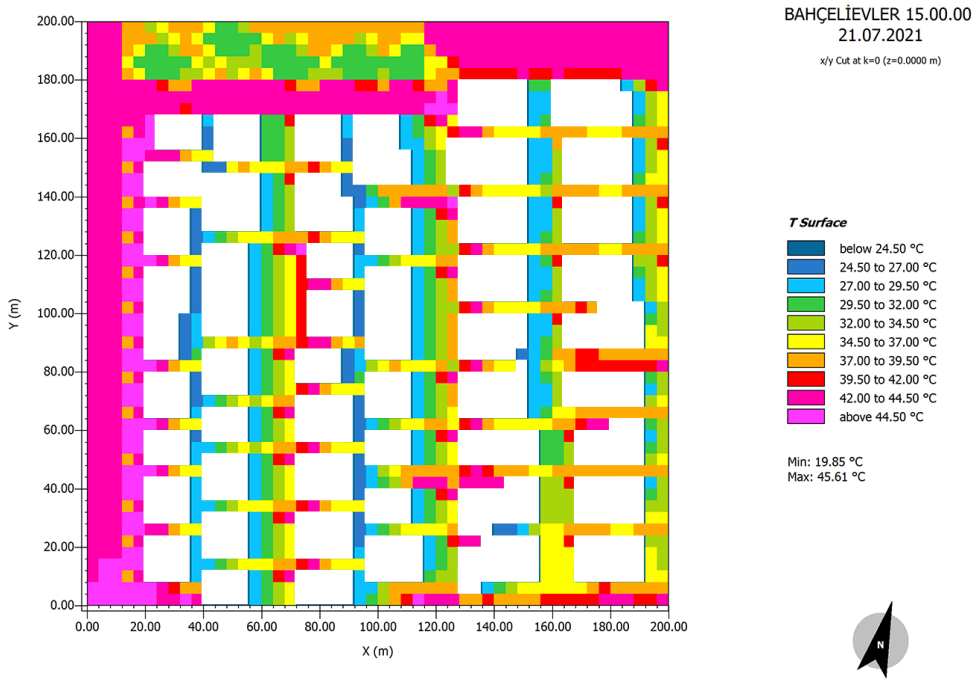

Figure D.1. T Surface Temperature (°C) of Urban Block 1 - Bahçelivler

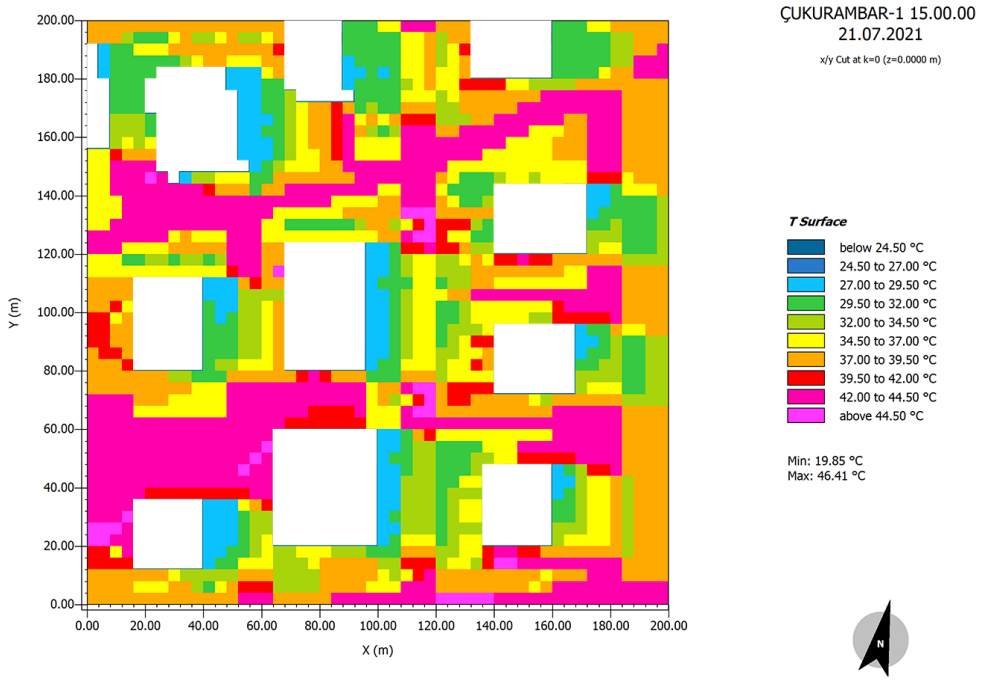

Figure D.2. T Surface Temperature (°C) of Urban Block 2 - Çukurambar 1

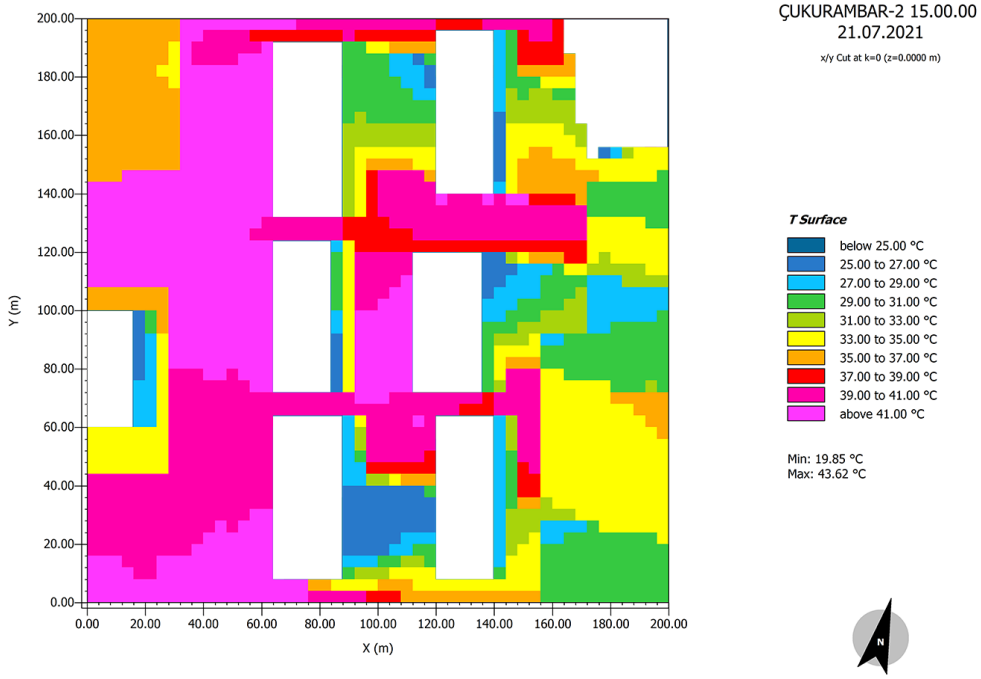

Figure D.3. T Surface Temperature (°C) of Urban Block 3 - Çukurambar 2

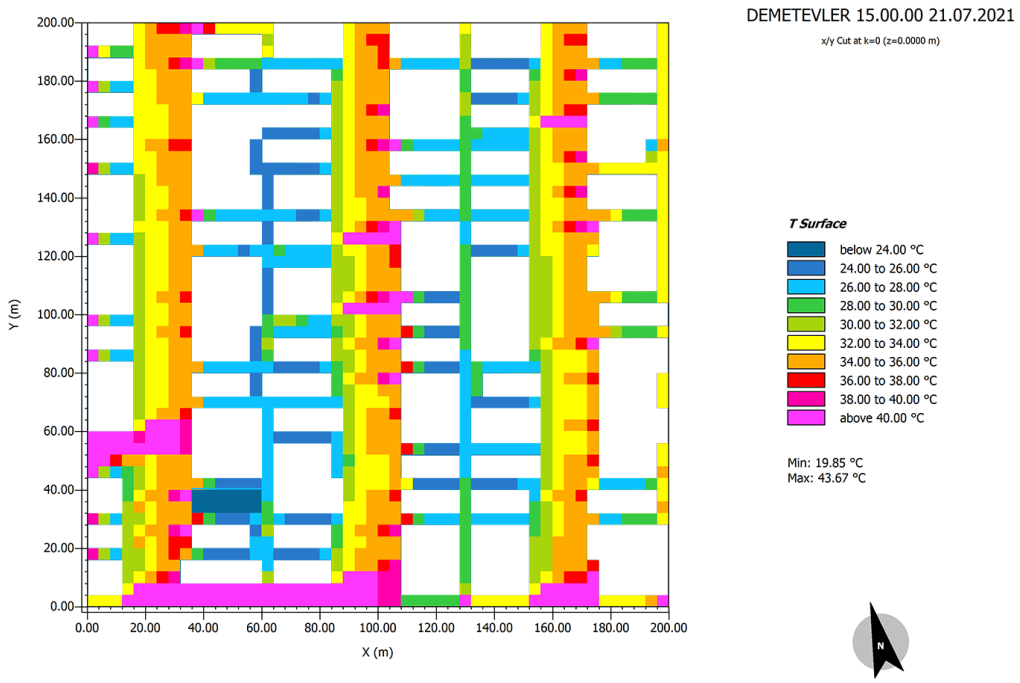

Figure D.4. T Surface Temperature (°C) of Urban Block 4 - Demetevler

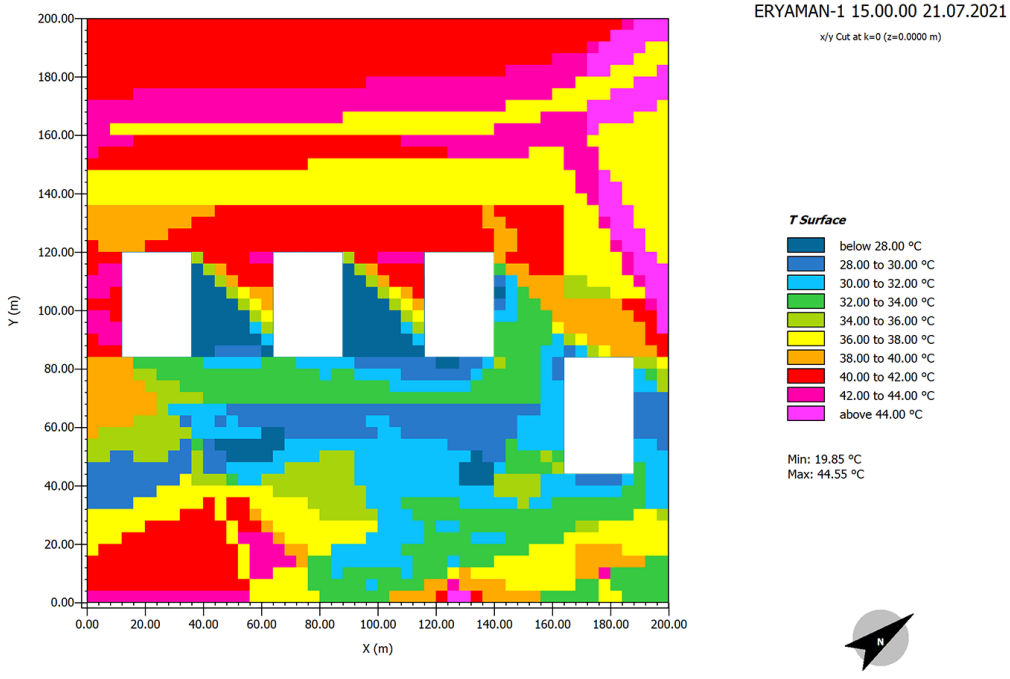

Figure D.5. T Surface Temperature (°C) of Urban Block 5 - Eryaman 1

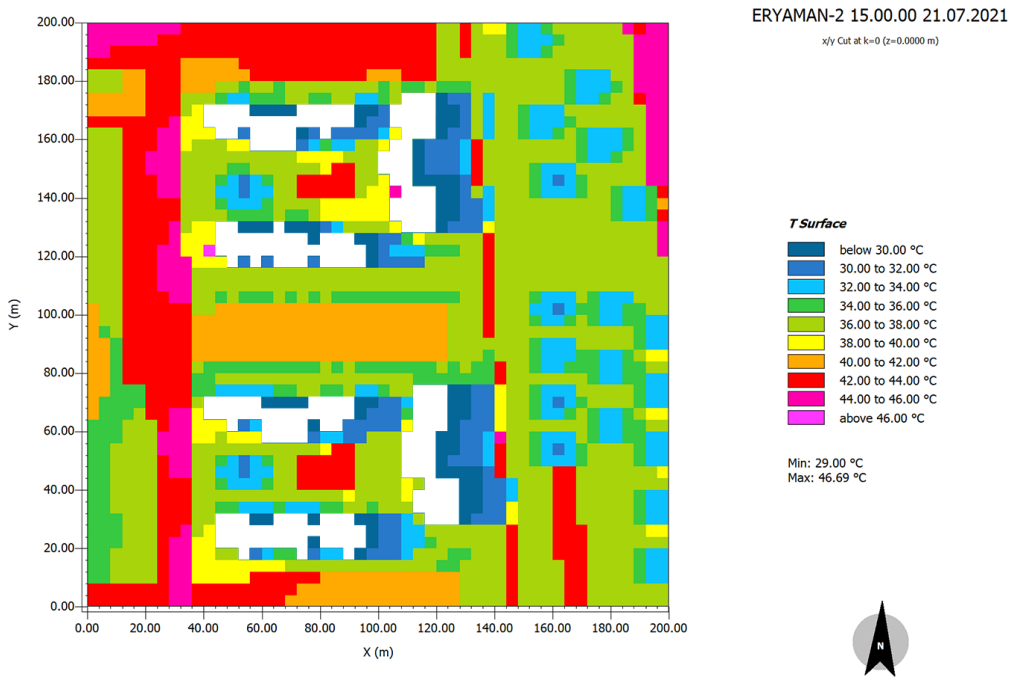

Figure D.6. T Surface Temperature (°C) of Urban Block 6 - Eryaman 2

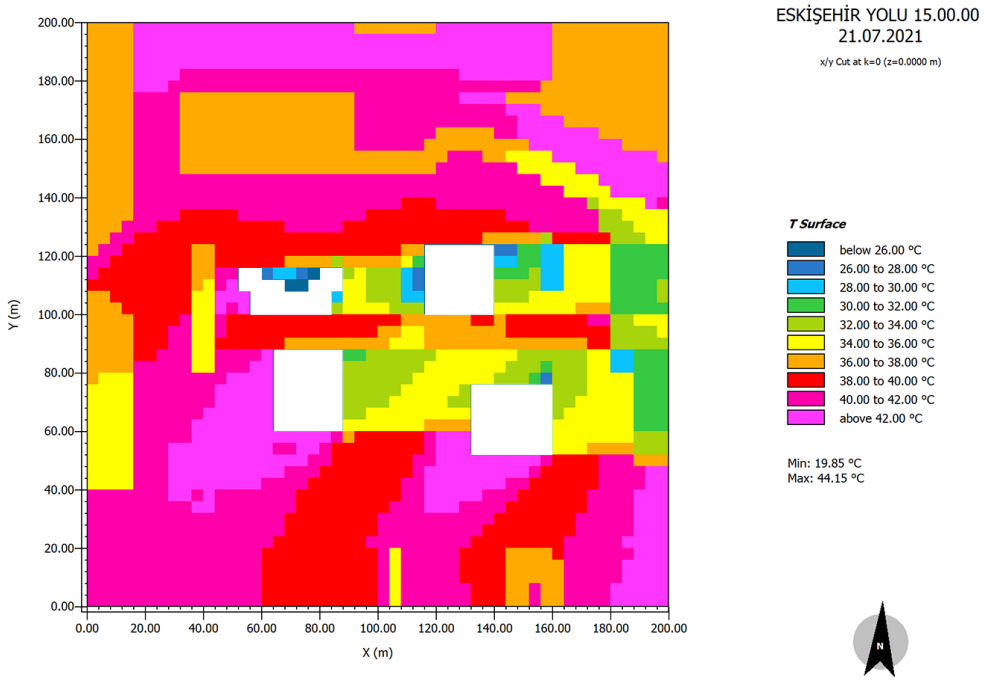

Figure D.7. T Surface Temperature (°C) of Urban Block 7 - Eskişehir Yolu

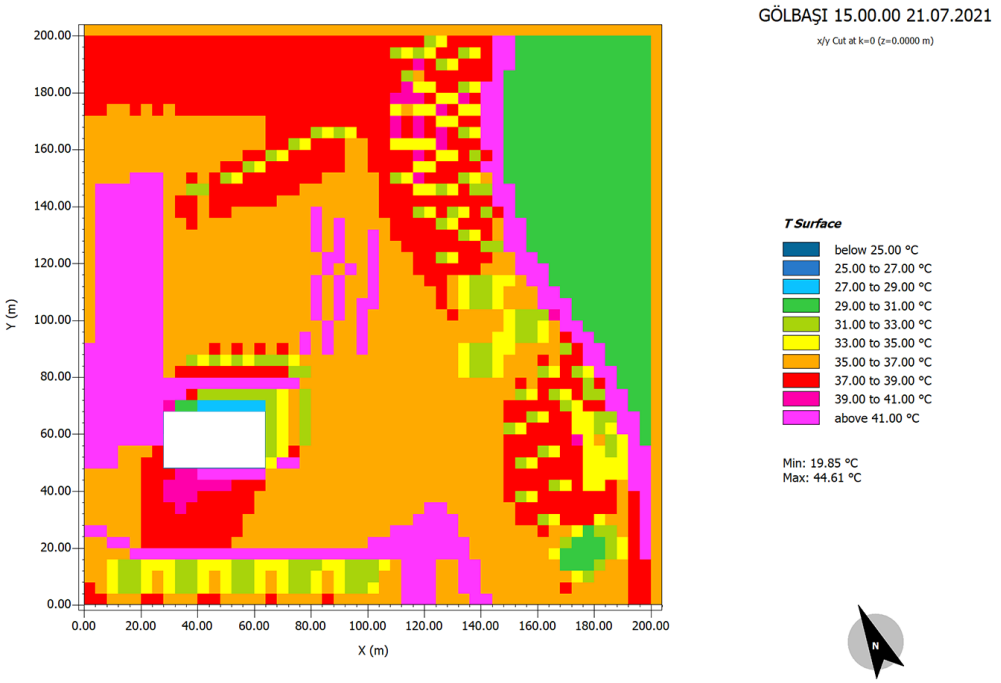

Figure D.8. T Surface Temperature (°C) of Urban Block 8 – Gölbaşı

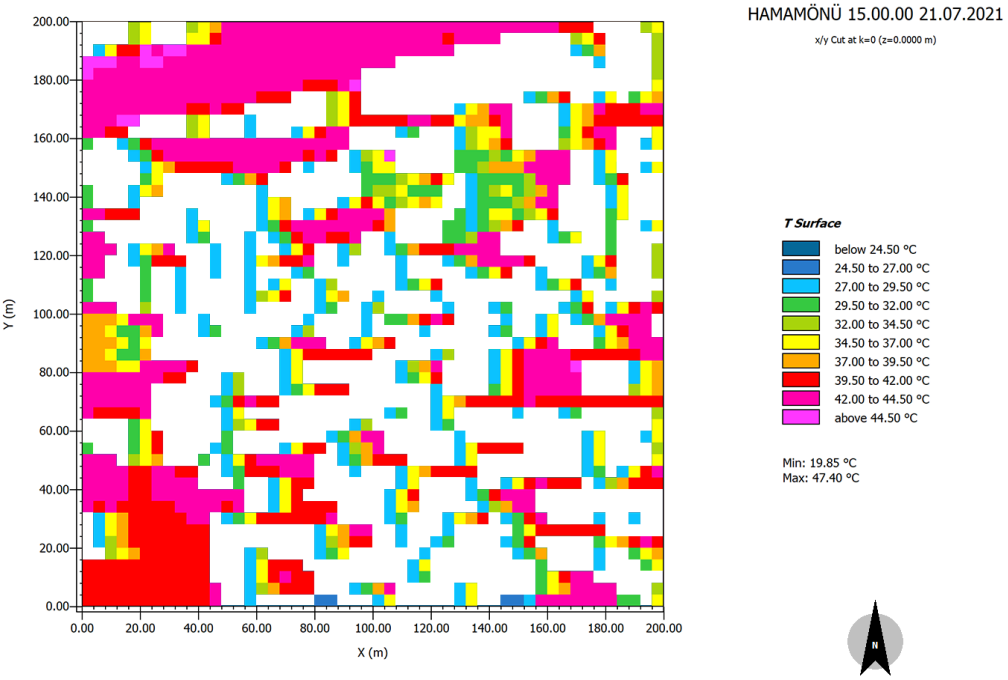

Figure D.9. T Surface Temperature (°C) of Urban Block 9 - Hamamönü

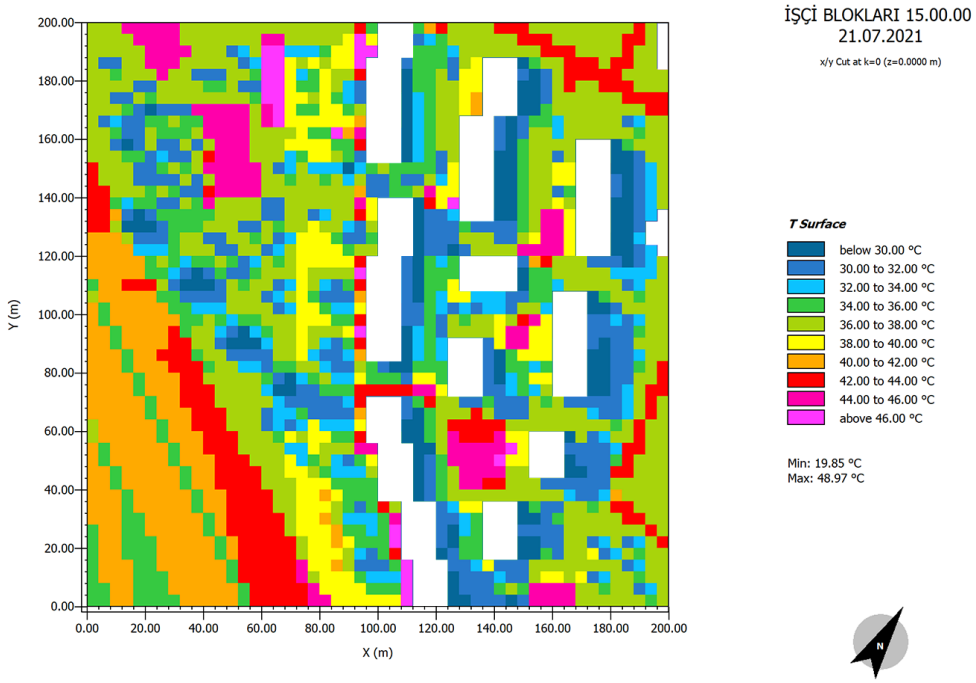

Figure D.10. T Surface Temperature (°C) of Urban Block 10 - İşçi Blokları

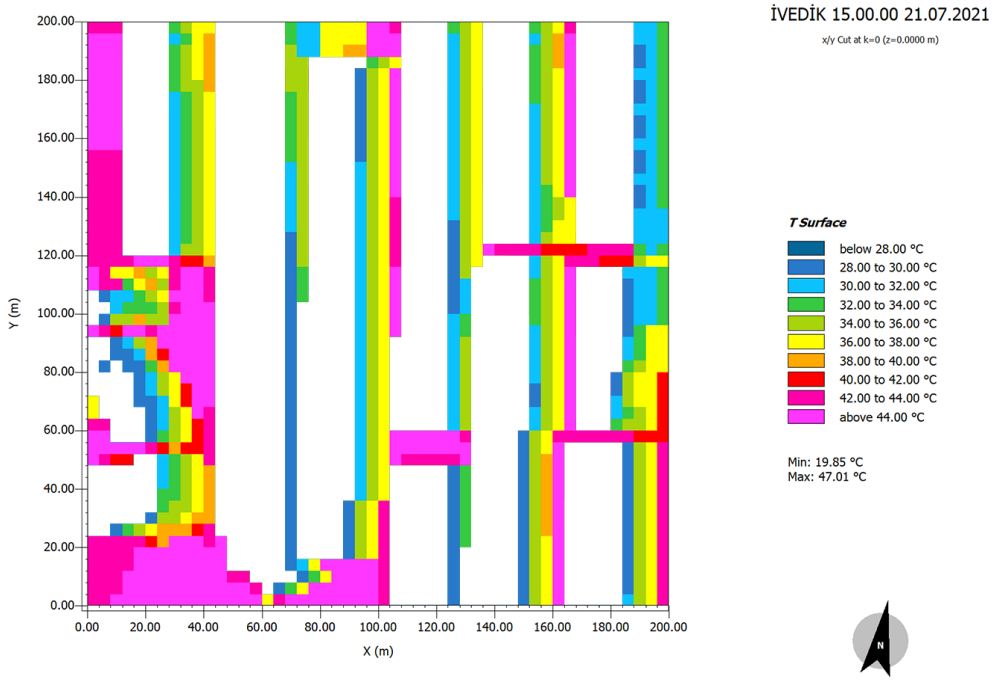

Figure D.11. T Surface Temperature (°C) of Urban Block 11 - İvedik

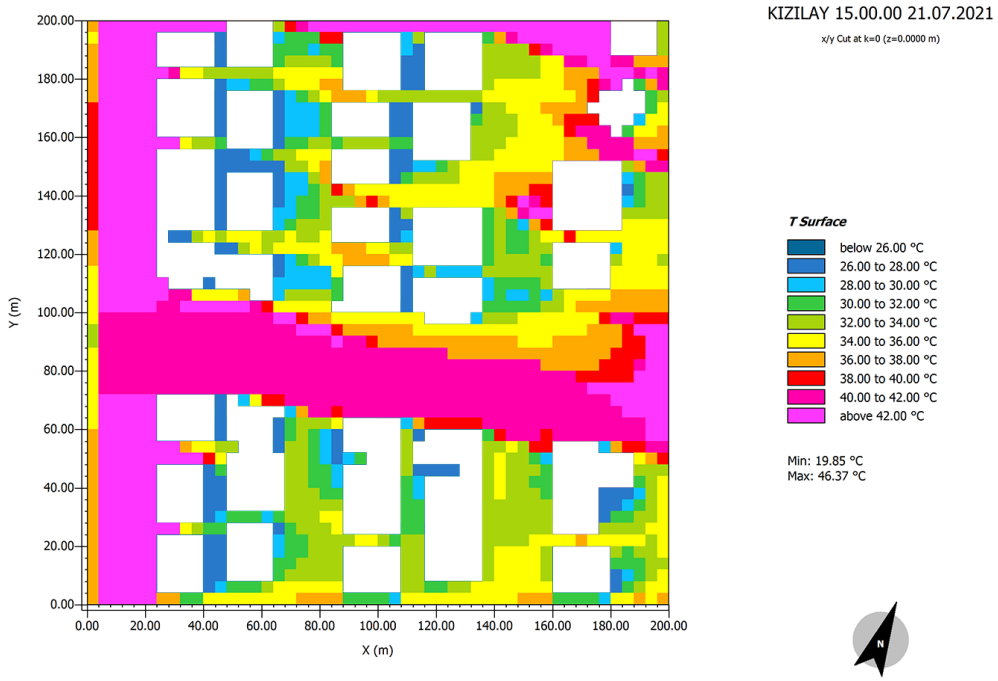

Figure D.12. T Surface Temperature (°C) of Urban Block 12 - Kızılay

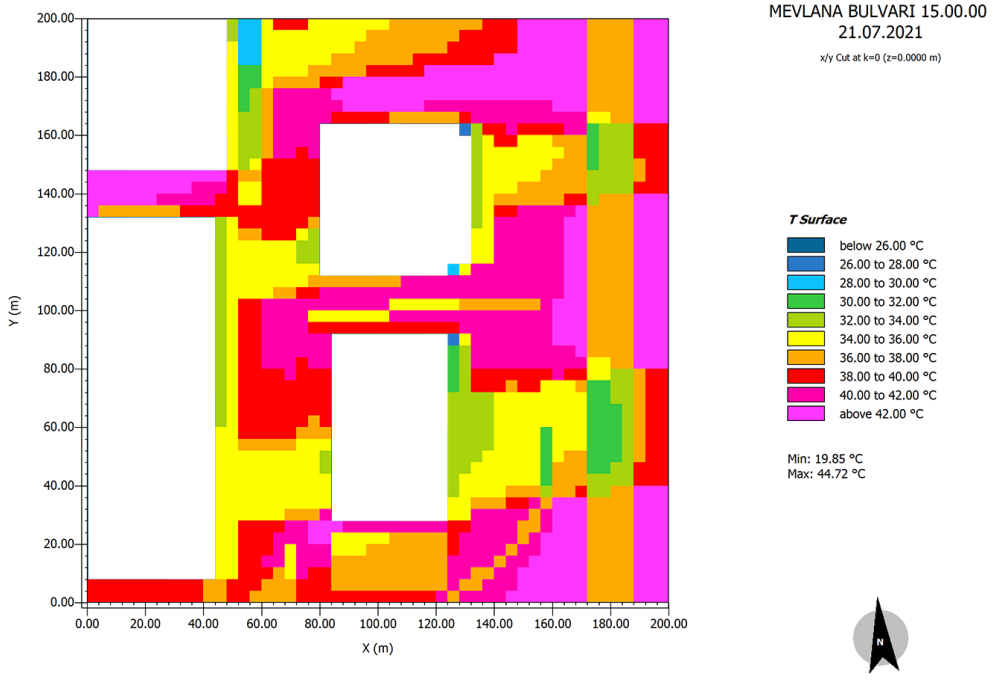

Figure D.13. T Surface Temperature (°C) of Urban Block 13 - Mevlana Bulvarı

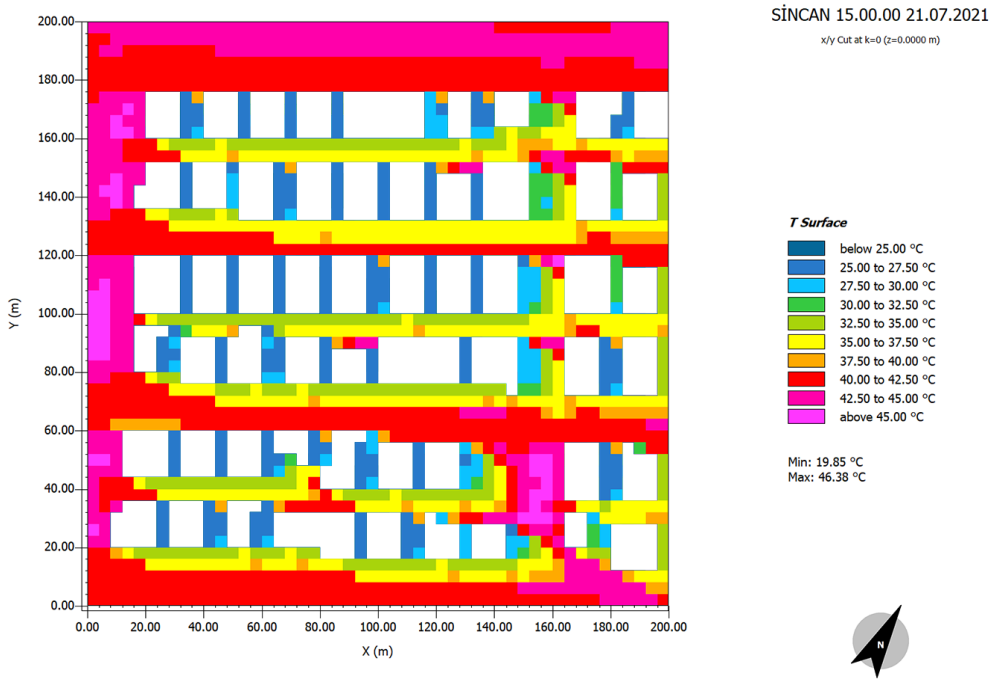

Figure D.14. T Surface Temperature (°C) of Urban Block 14 - Sincan

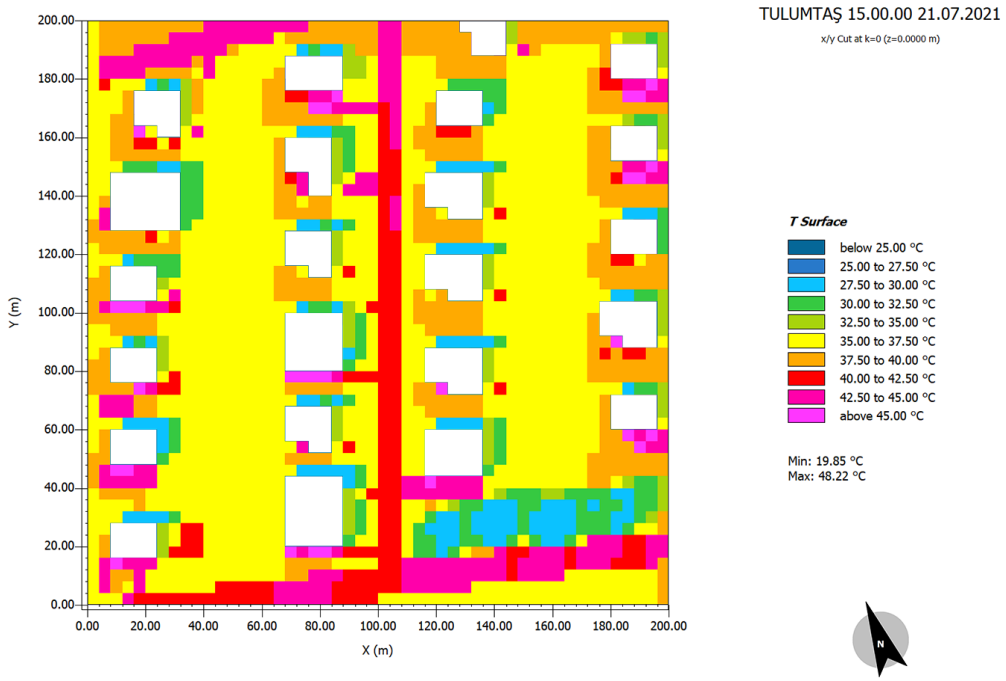

Figure D.15. T Surface Temperature (°C) of Urban Block 15 - Tulumtaş

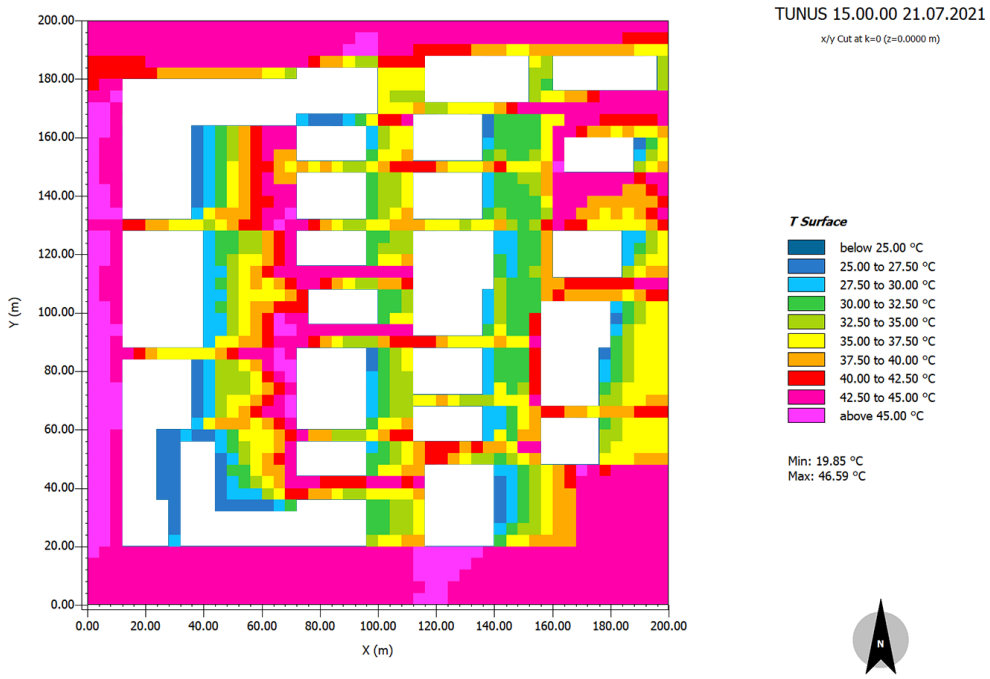

Figure D.16. T Surface Temperature (°C) of Urban Block 16 -Tunus Caddesi

b) Potential Air Temperature

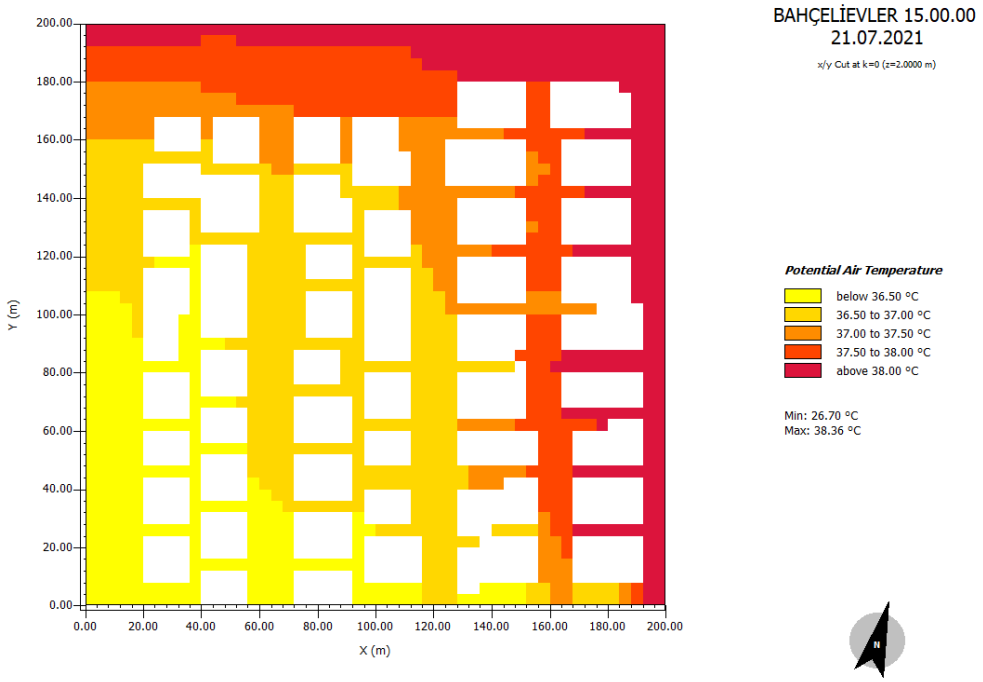

Figure D.17. Potential Air Temperature (°C) of Urban Block 1 - Bahçelievler

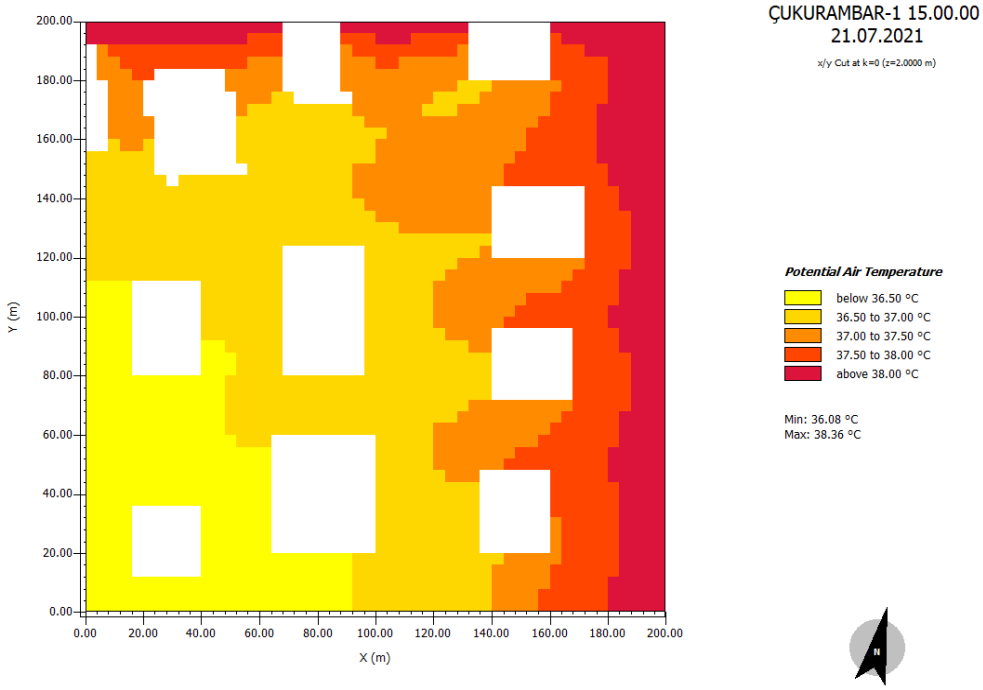

Figure D.18. Potential Air Temperature (°C) of Urban Block 2 - Çukurambar 1

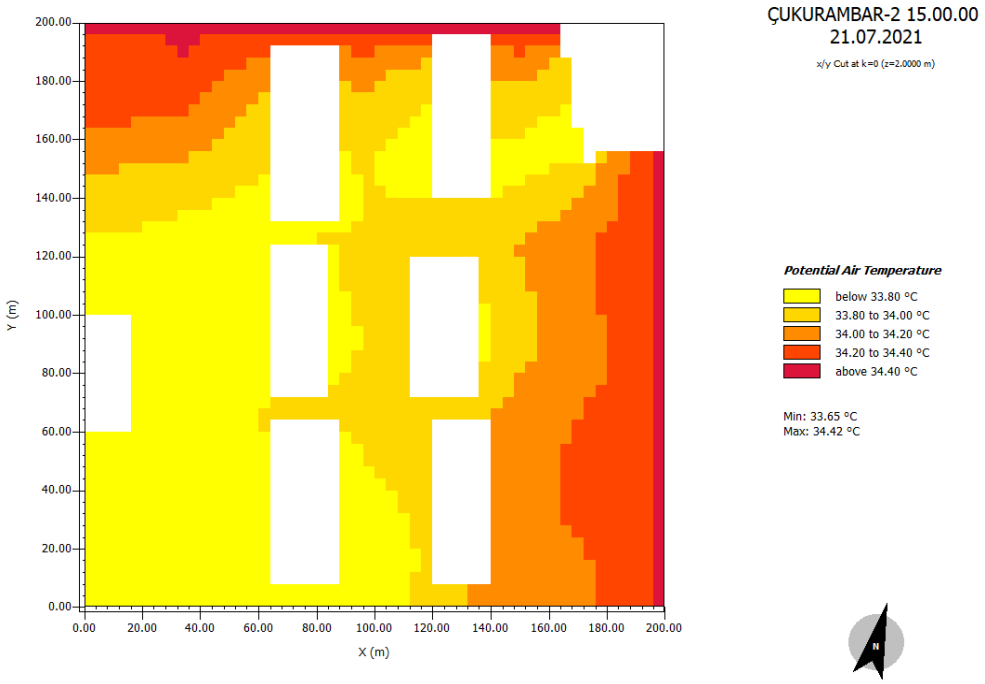

Figure D.19. Potential Air Temperature (°C) of Urban Block 3 - Çukurambar 2

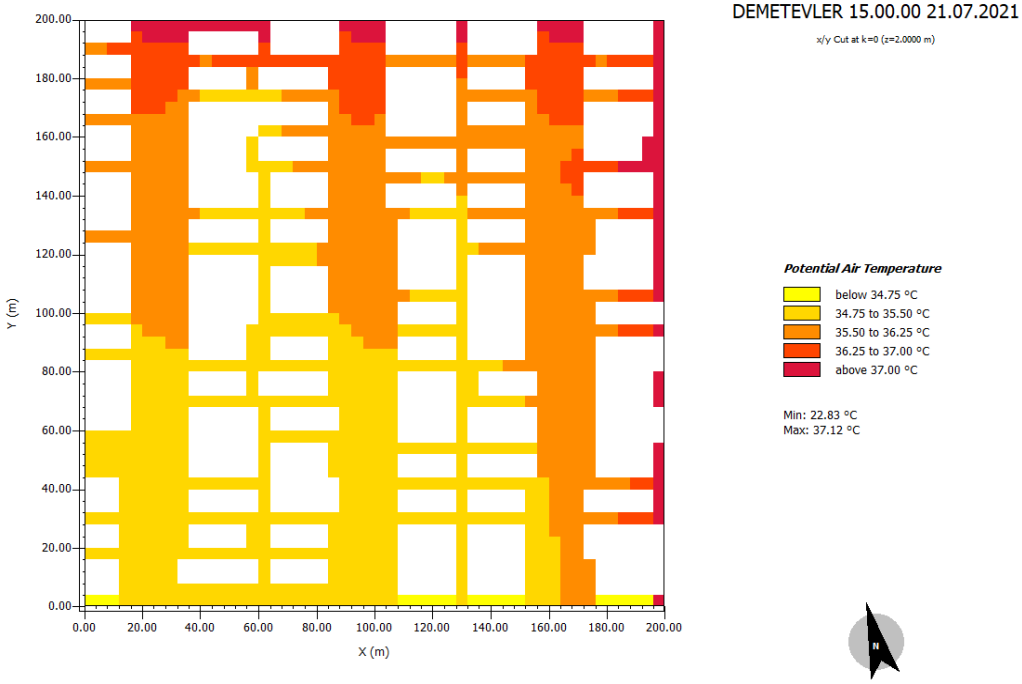

Figure D.20. Potential Air Temperature (°C) of Urban Block 4 - Demetevler

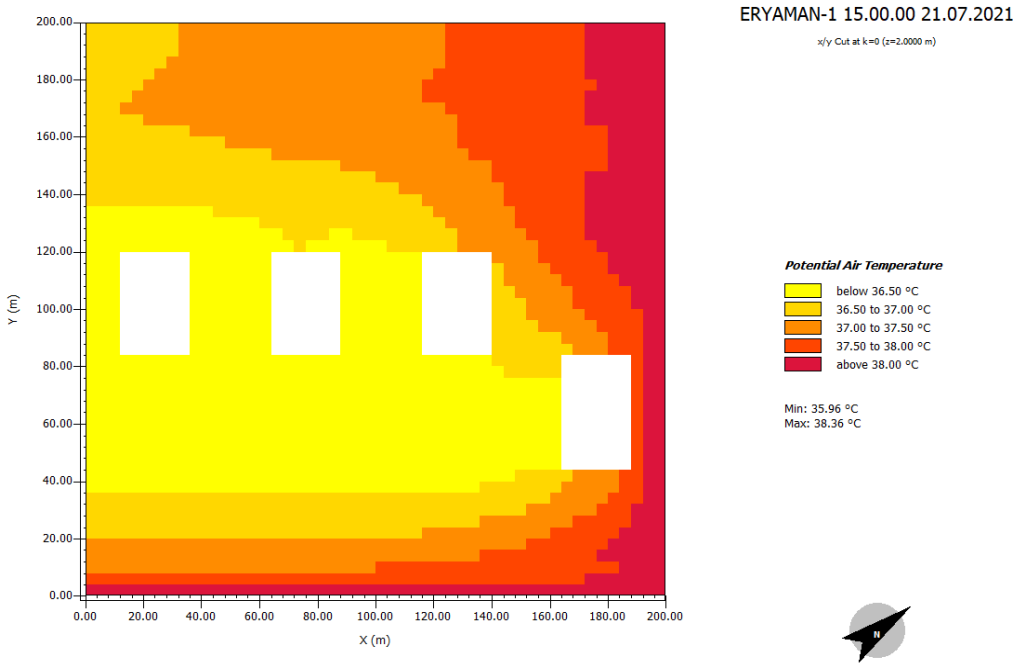

Figure D.21. Potential Air Temperature (°C) of Urban Block 5 - Eryaman 1

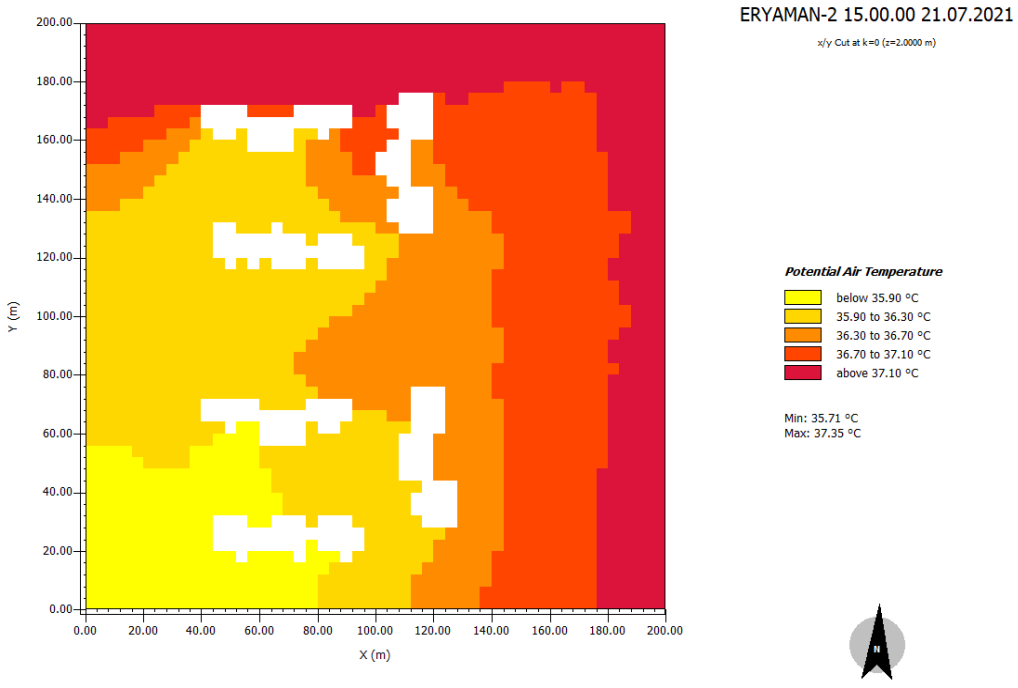

Figure D.22. Potential Air Temperature (°C) of Urban Block 6 -Eryaman 2

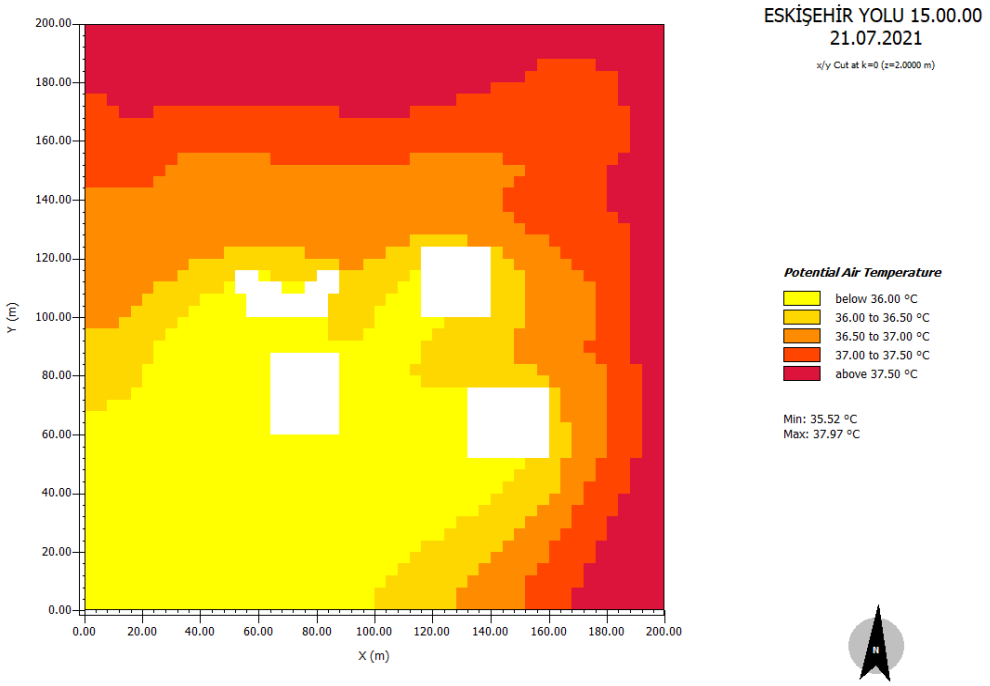

Figure D.23. Potential Air Temperature (°C) of Urban Block 7 - Eskişehir Yolu

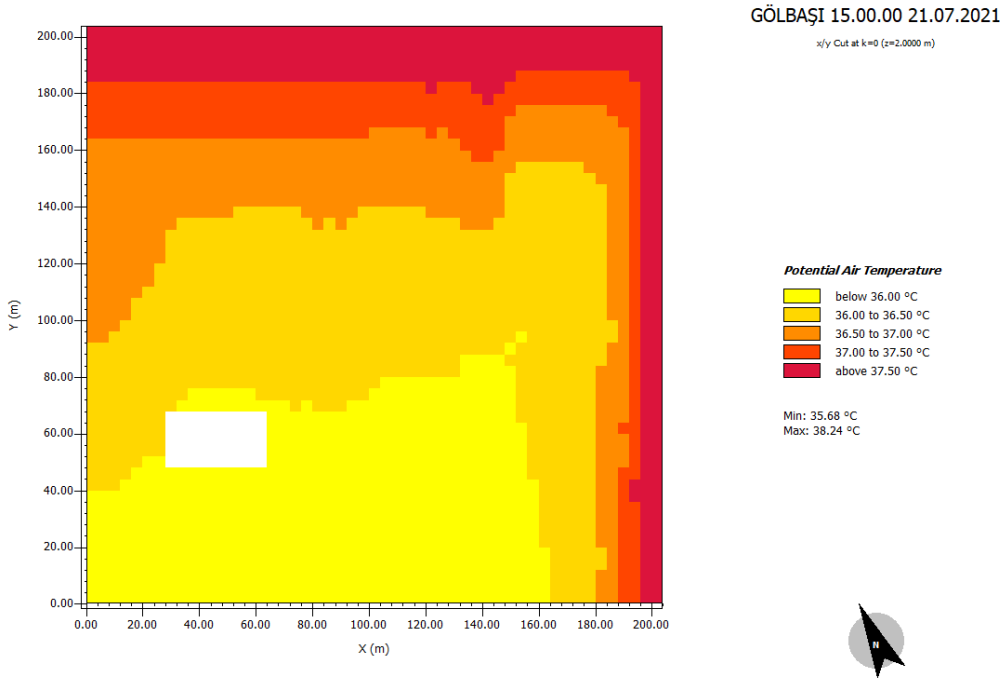

Figure D.24. Potential Air Temperature (°C) of Urban Block 8 -Gölbaşı

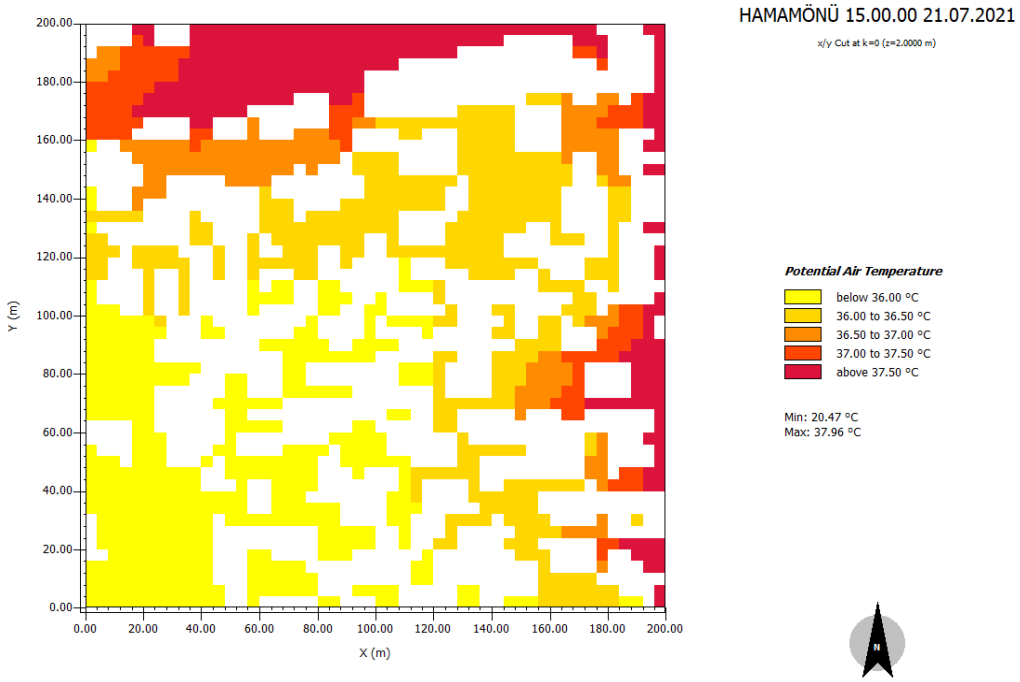

Figure D.25. Potential Air Temperature (°C) of Urban Block 9 - Hamamönü

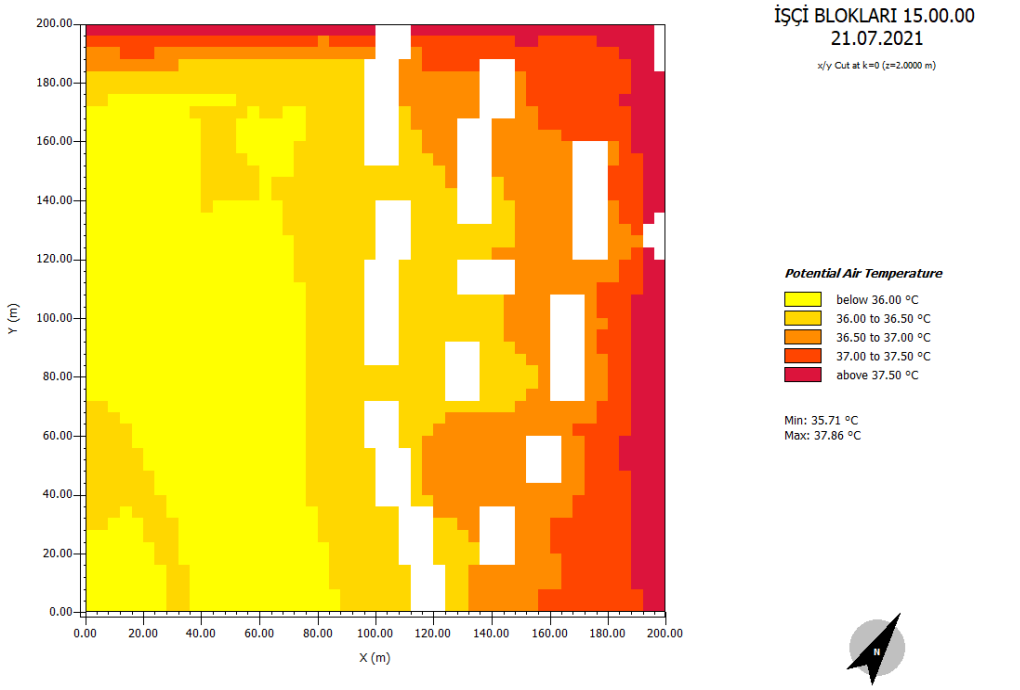

Figure D.26. Potential Air Temperature (°C) of Urban Block 10 - İşçi Blokları

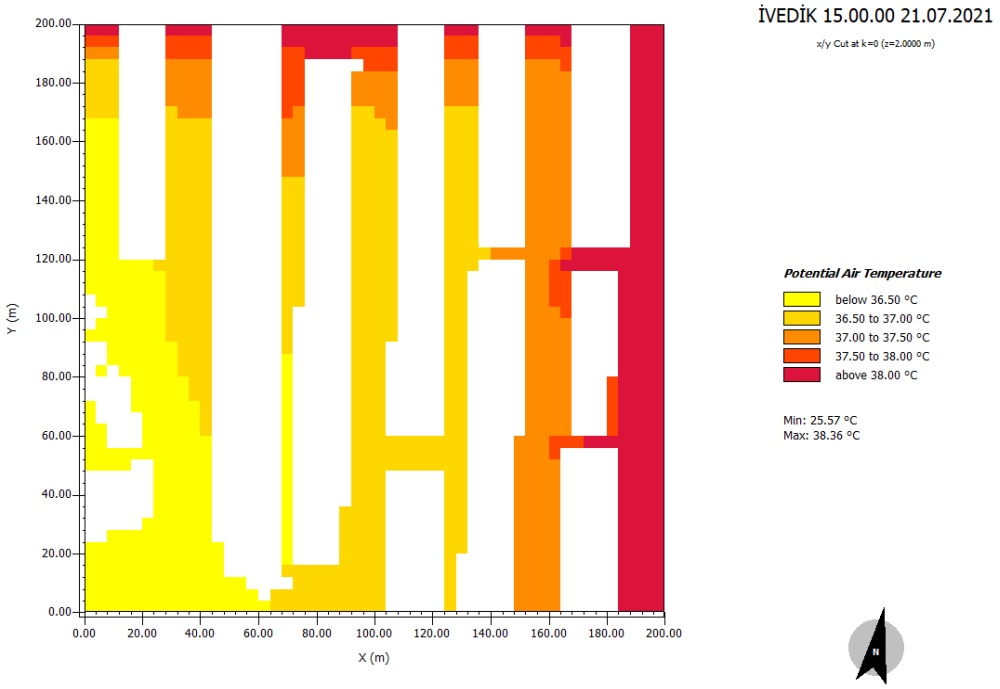

Figure D.27. Potential Air Temperature (°C) of Urban Block 11 - İvedik

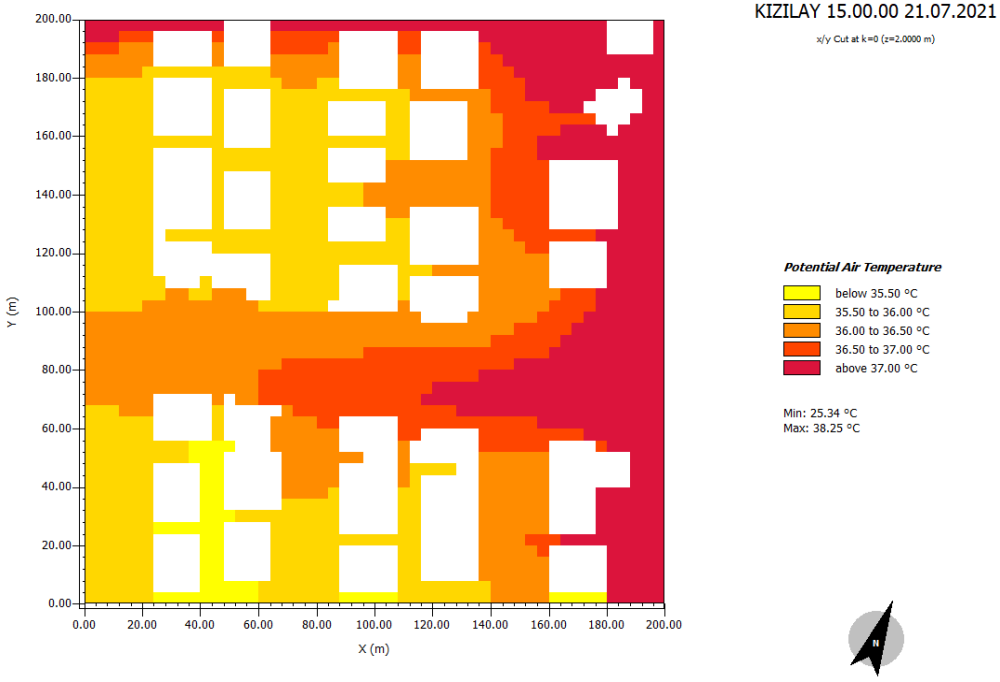

Figure D.28. Potential Air Temperature (°C) of Urban Block 12 - Kızılay

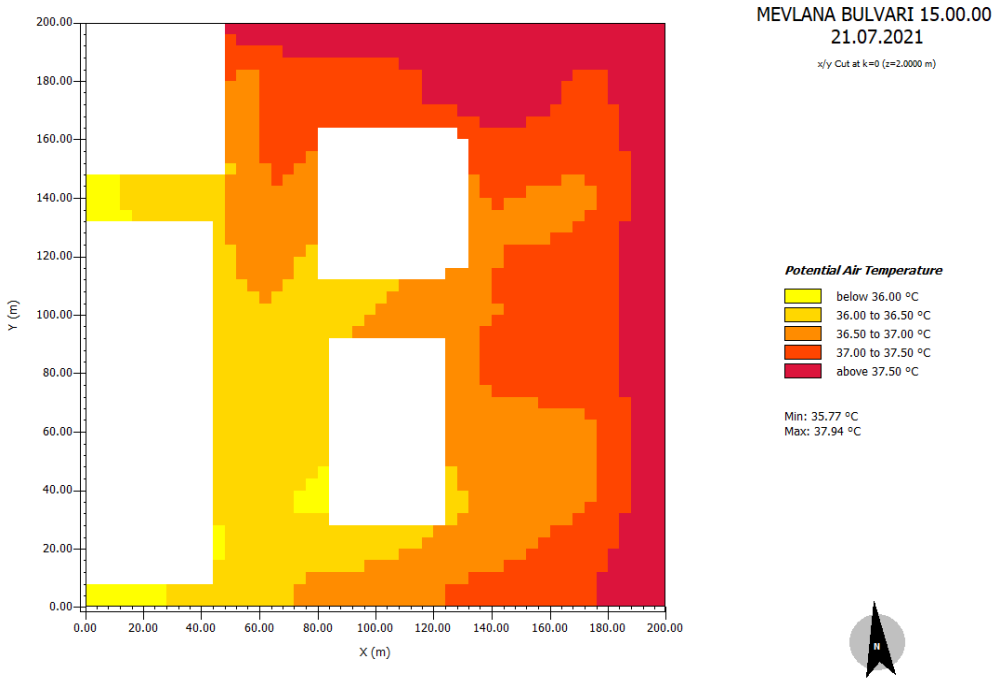

Figure D.29. Potential Air Temperature (°C) of Urban Block 13 - Mevlana

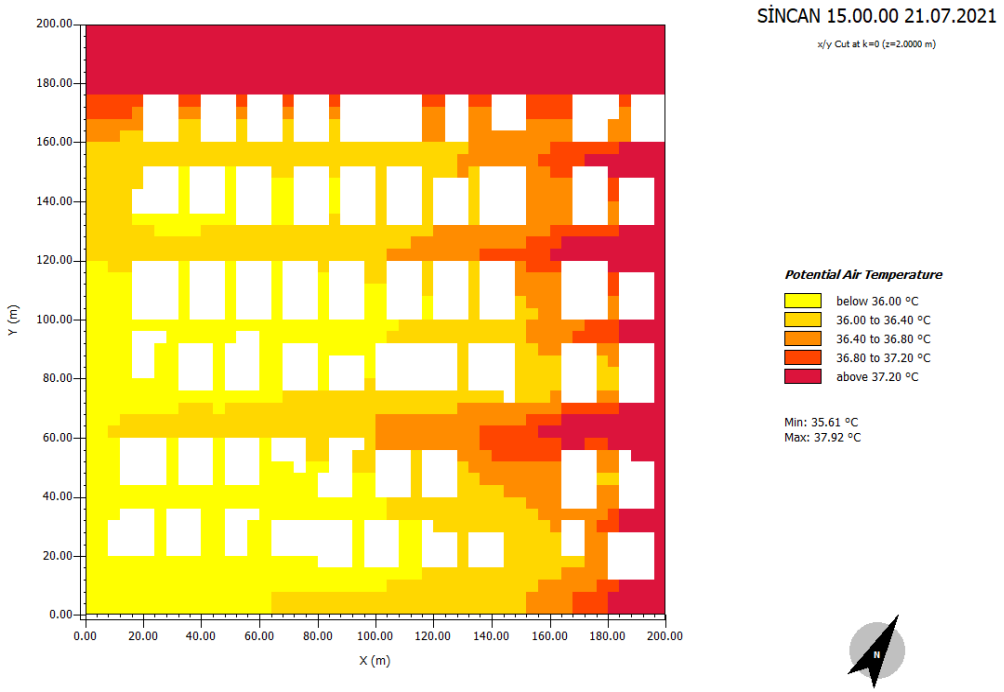

Figure D.30. Potential Air Temperature (°C) of Urban Block 14 - Sincan

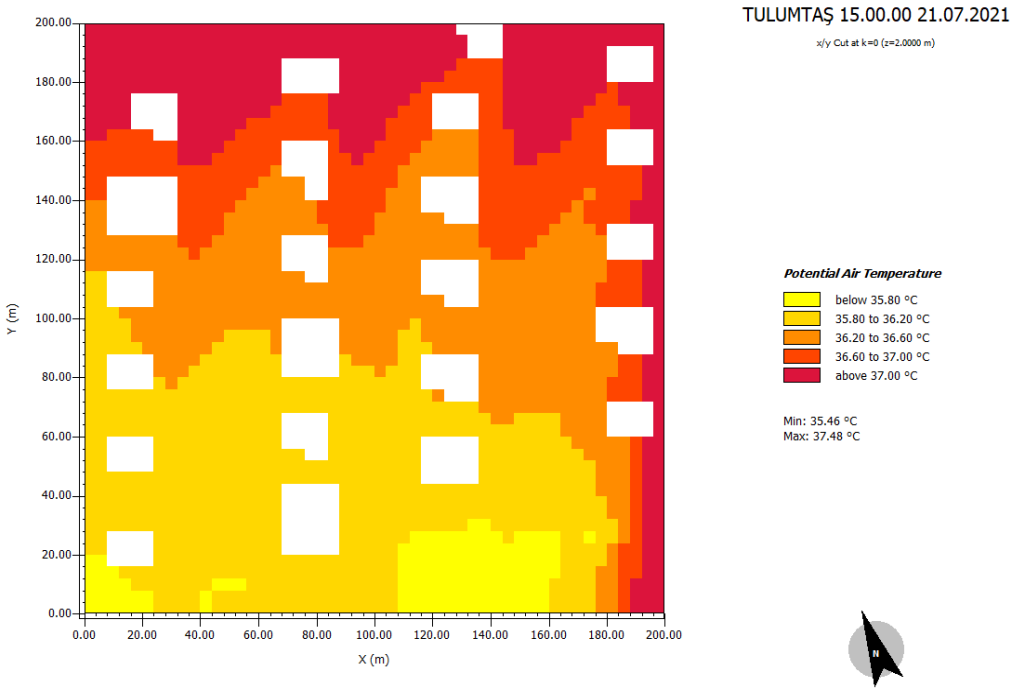

Figure D.31. Potential Air Temperature (°C) of Urban Block 15 - Tulumtaş

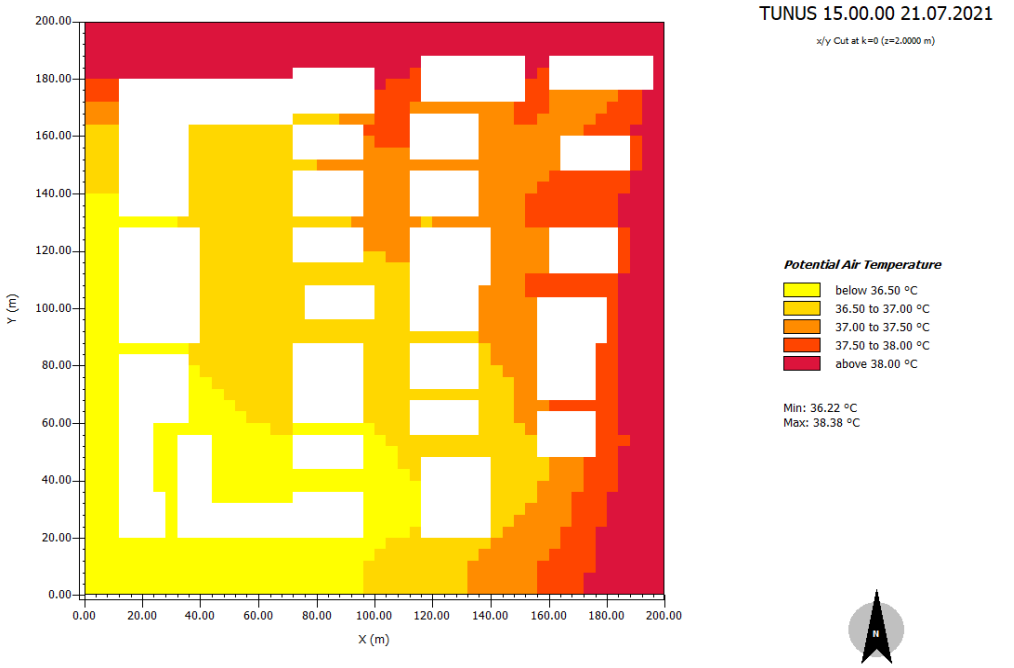

Figure D.32. Potential Air Temperature (°C) of Urban Block 16 - Tunus Caddesi

c) Wind Speed

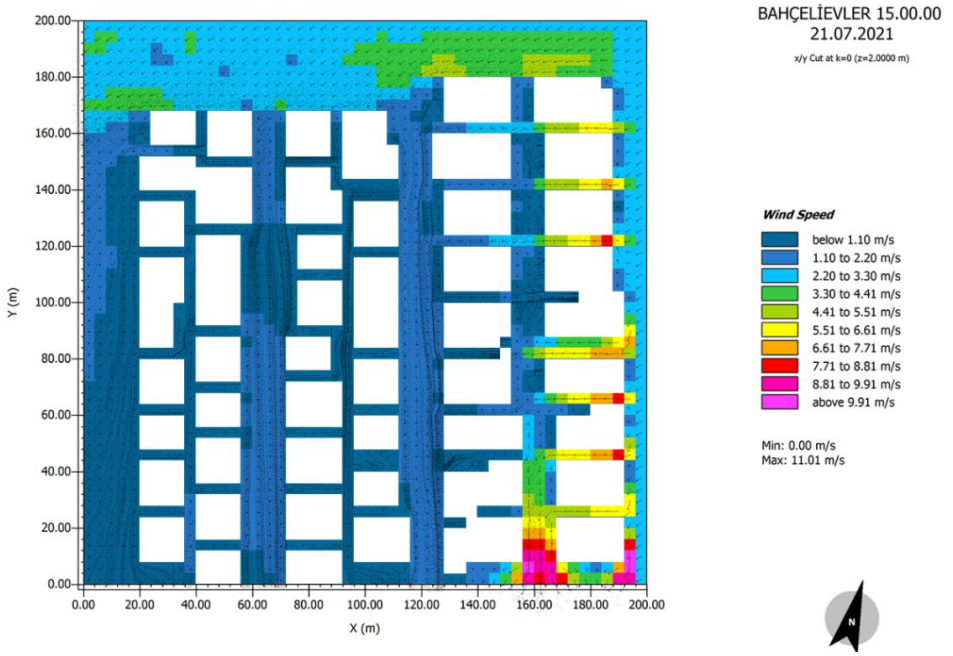

Figure D.33. Wind Speed (m/s) of Urban Block 1 - Bahçelievler

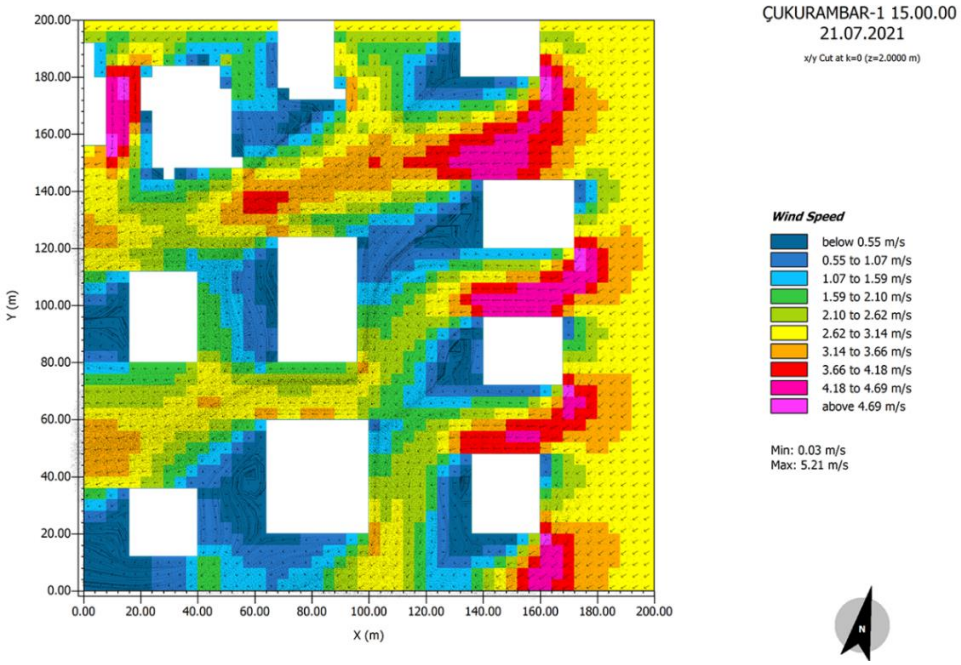

Figure D.34. Wind Speed (m/s) of Urban Block 2 - Çukurambar 1

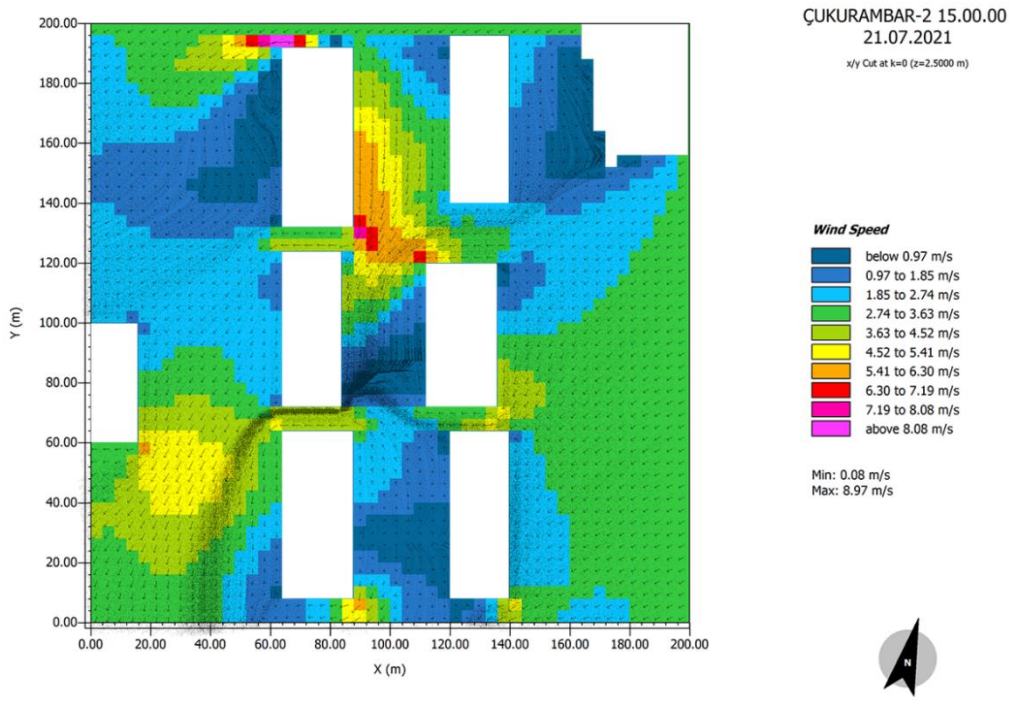

Figure D.35. Wind Speed (m/s) of Urban Block 3 - Çukurambar 2

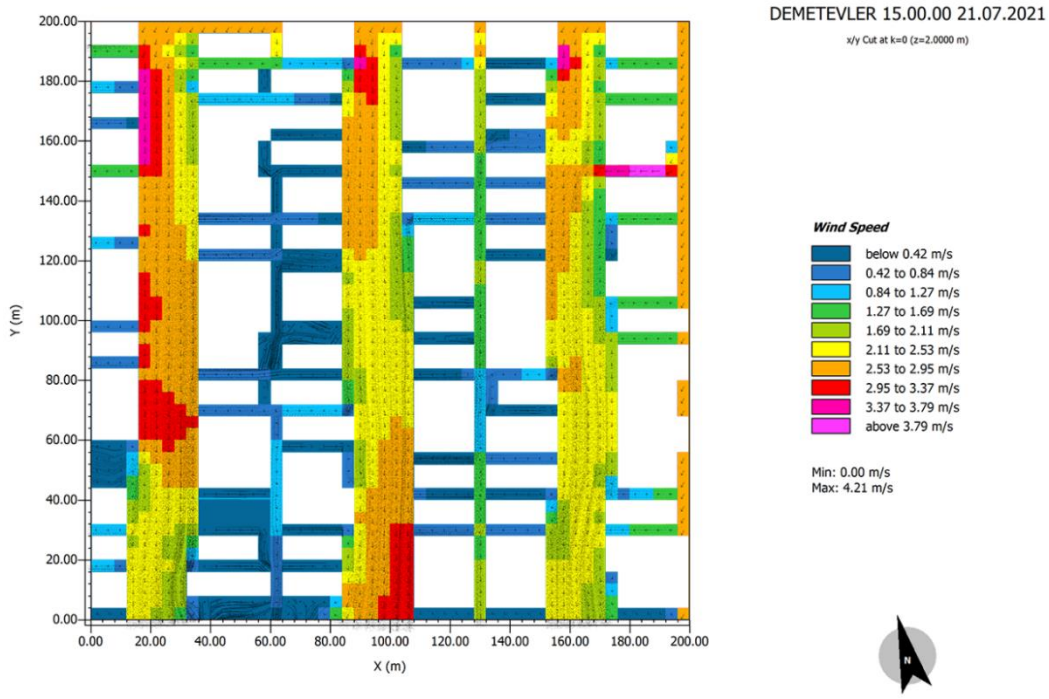

Figure D.36. Wind Speed (m/s) of Urban Block 4 - Demetevler

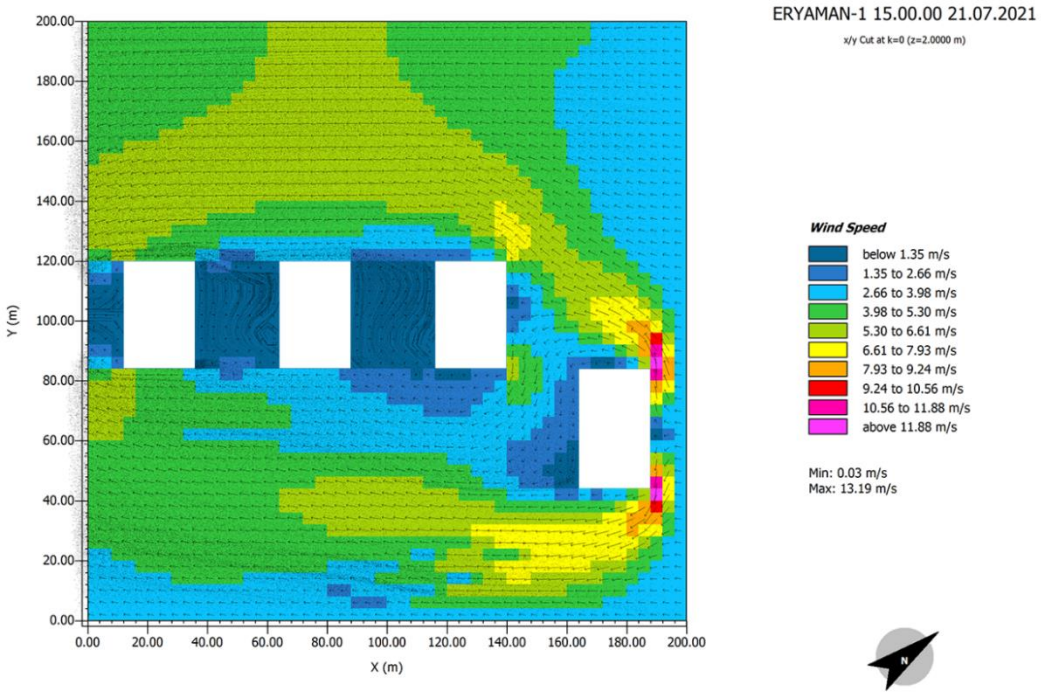

Figure D.37. Wind Speed (m/s) of Urban Block 5 - Eryaman 1

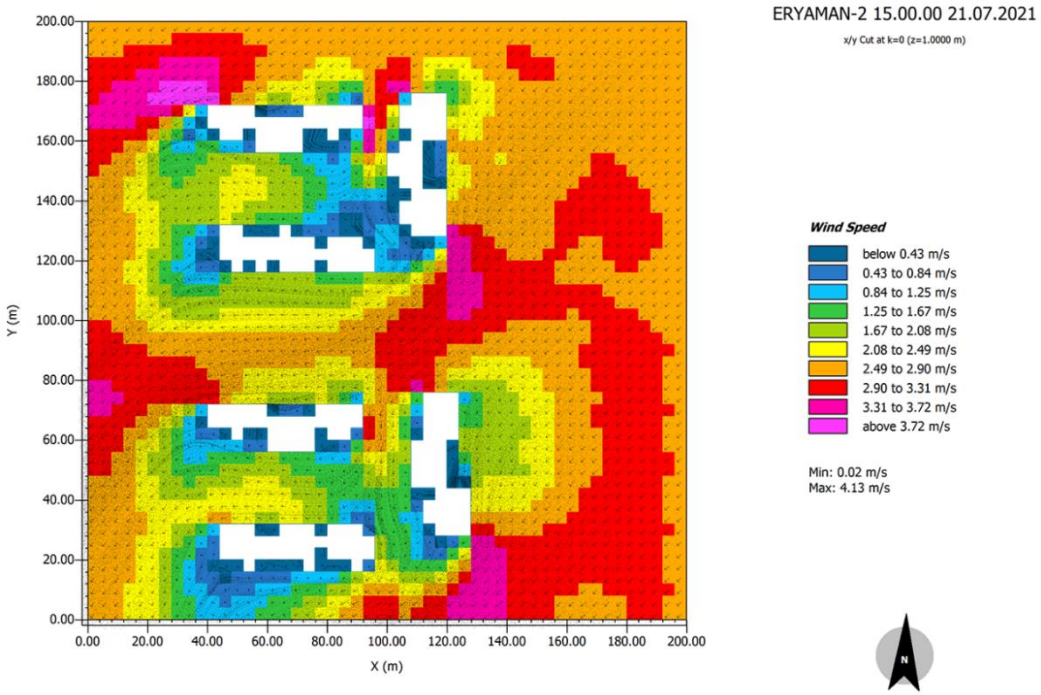

Figure D.38. Wind Speed (m/s) of Urban Block 6 - Eryaman 2

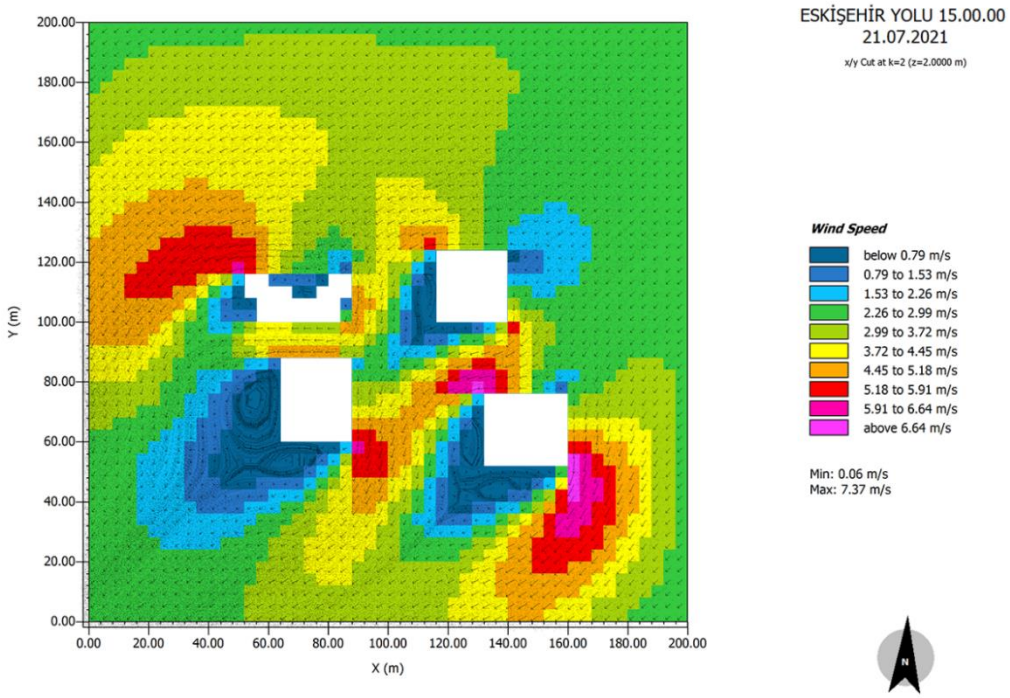

Figure D.39. Wind Speed (m/s) of Urban Block 7 - Eskişehir Yolu

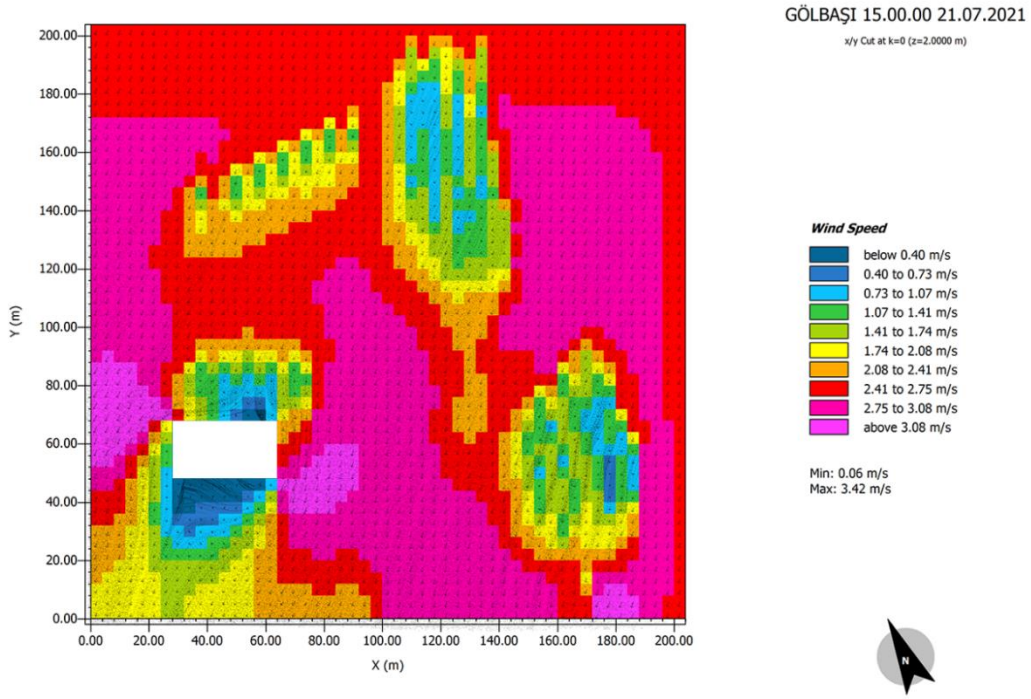

Figure D.40. Wind Speed (m/s) of Urban Block 8 - Gölbaşı

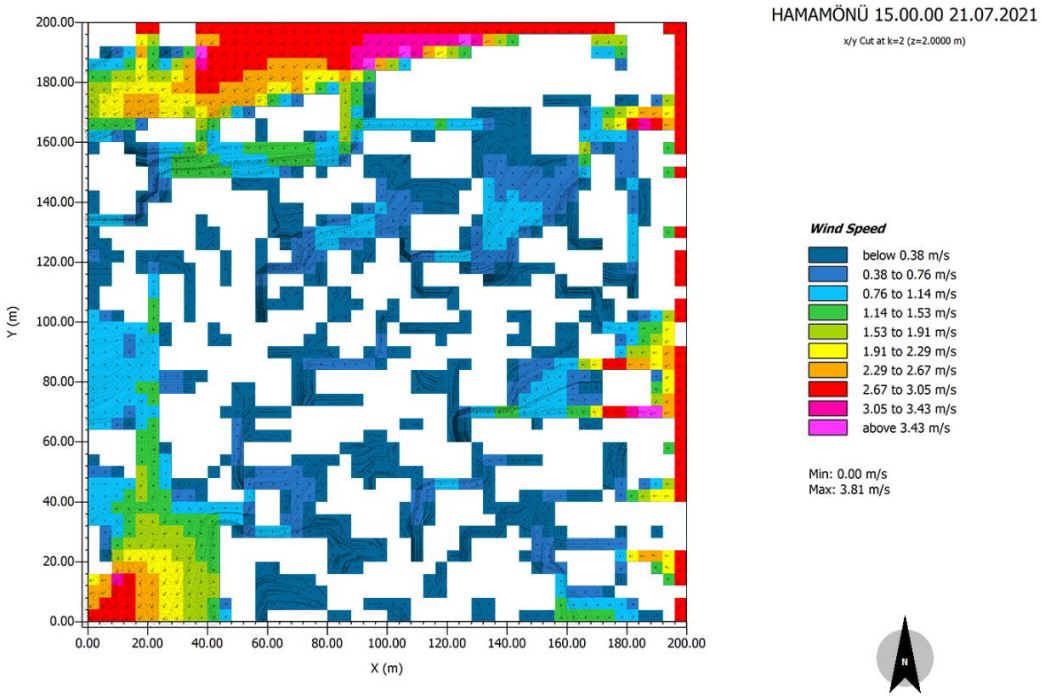

Figure D.41. Wind Speed (m/s) of Urban Block 9 - Hamamönü

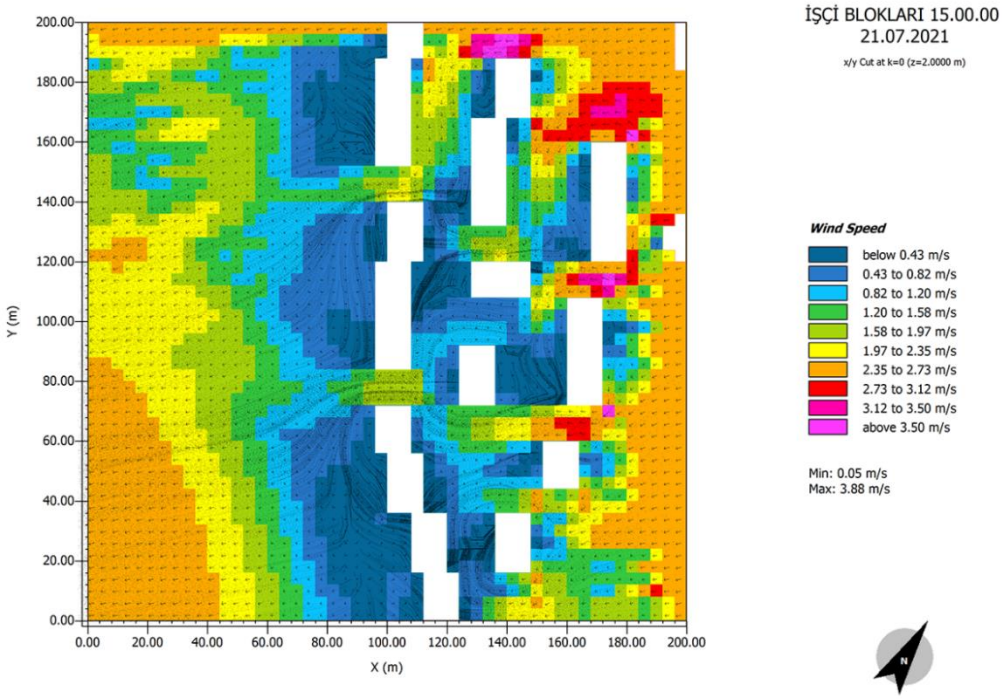

Figure D.42. Wind Speed (m/s) of Urban Block 10 - İşçi Blokları

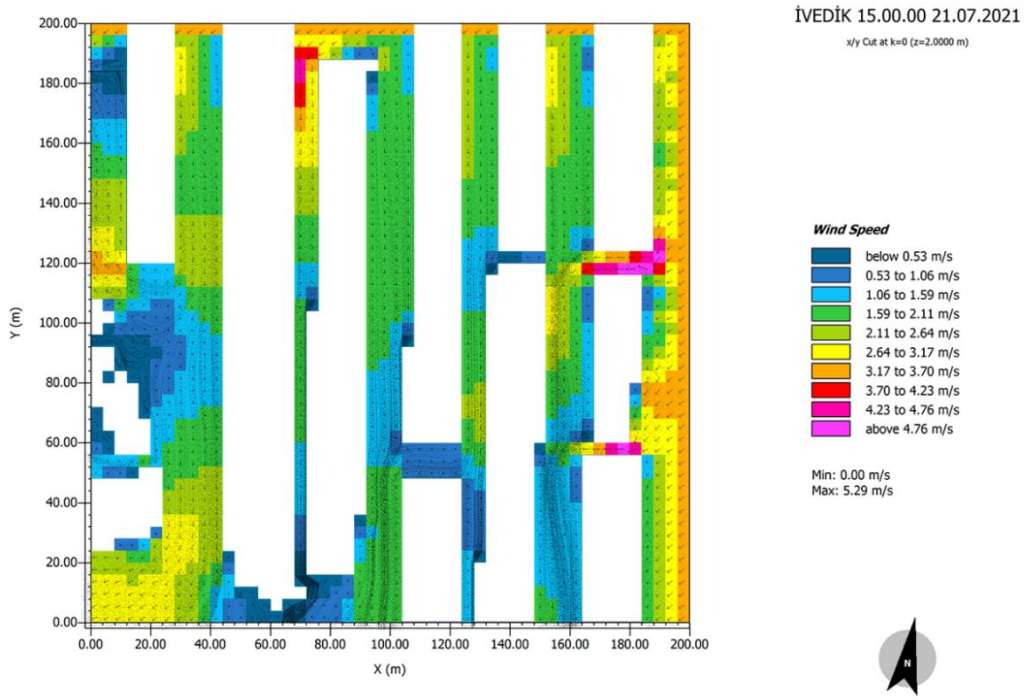

Figure D.43. Wind Speed (m/s) of Urban Block 11 - İvedik

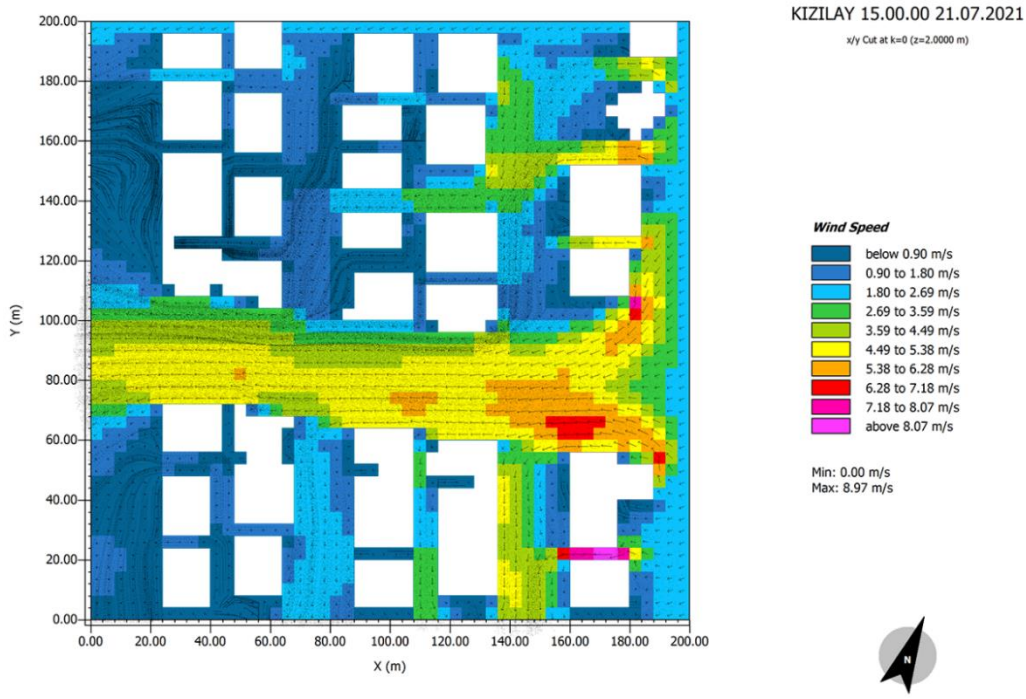

Figure D.44. Wind Speed (m/s) of Urban Block 12 - Kızılay

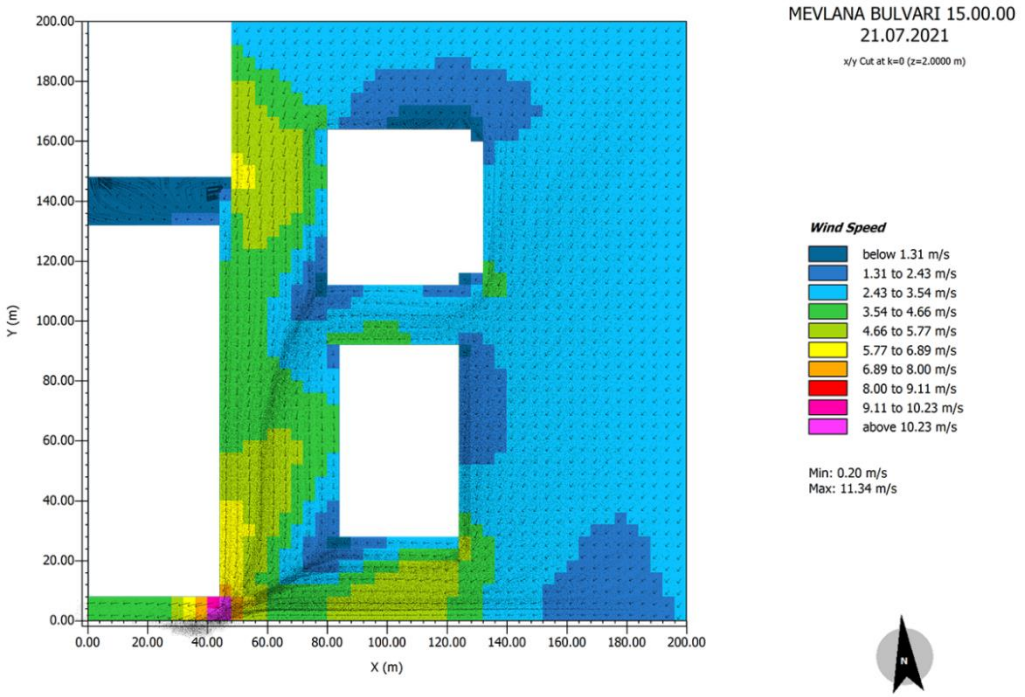

Figure D.45. Wind Speed (m/s) of Urban Block 13 - Mevlana Bulvarı

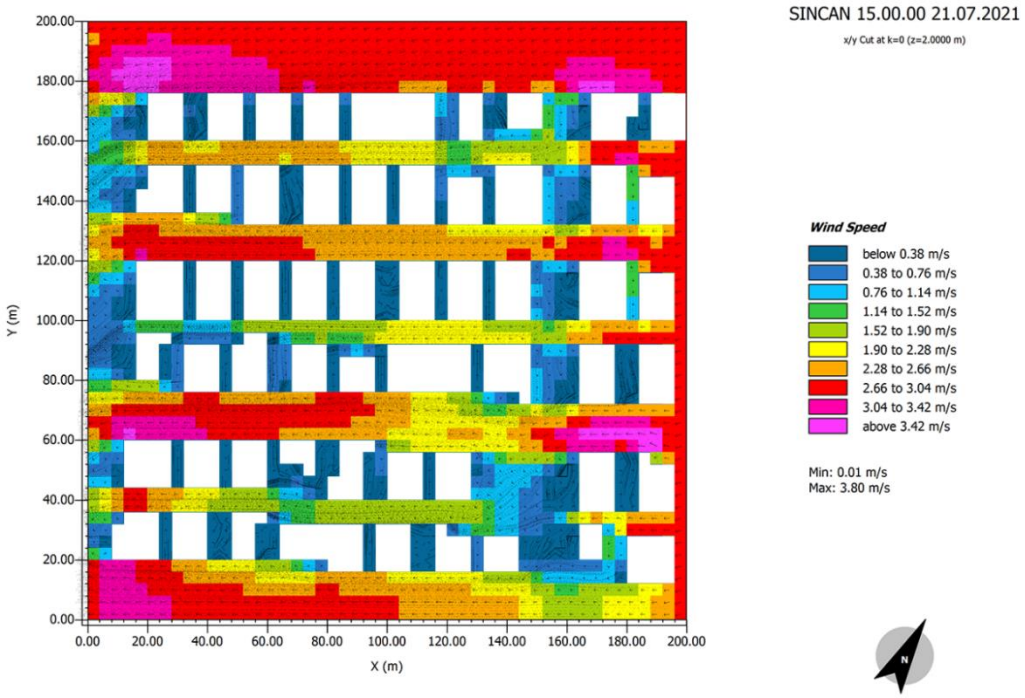

Figure D.46. Wind Speed (m/s) of Urban Block 14 - Sincan

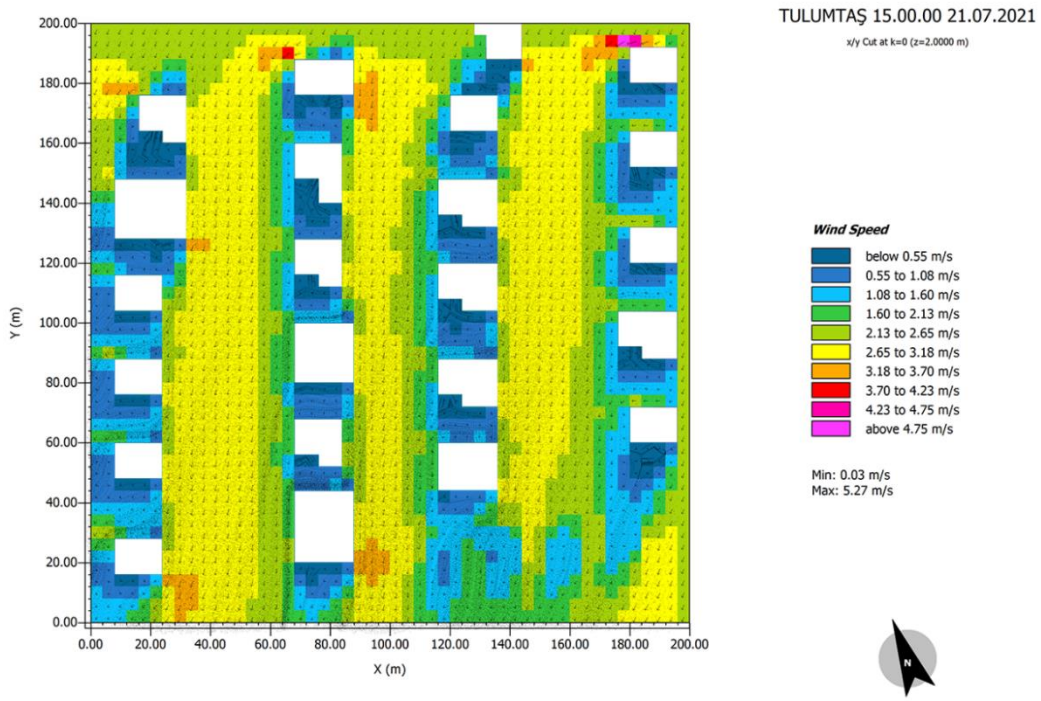

Figure D.47. Wind Speed (m/s) of Urban Block 15 - Tulumtaş

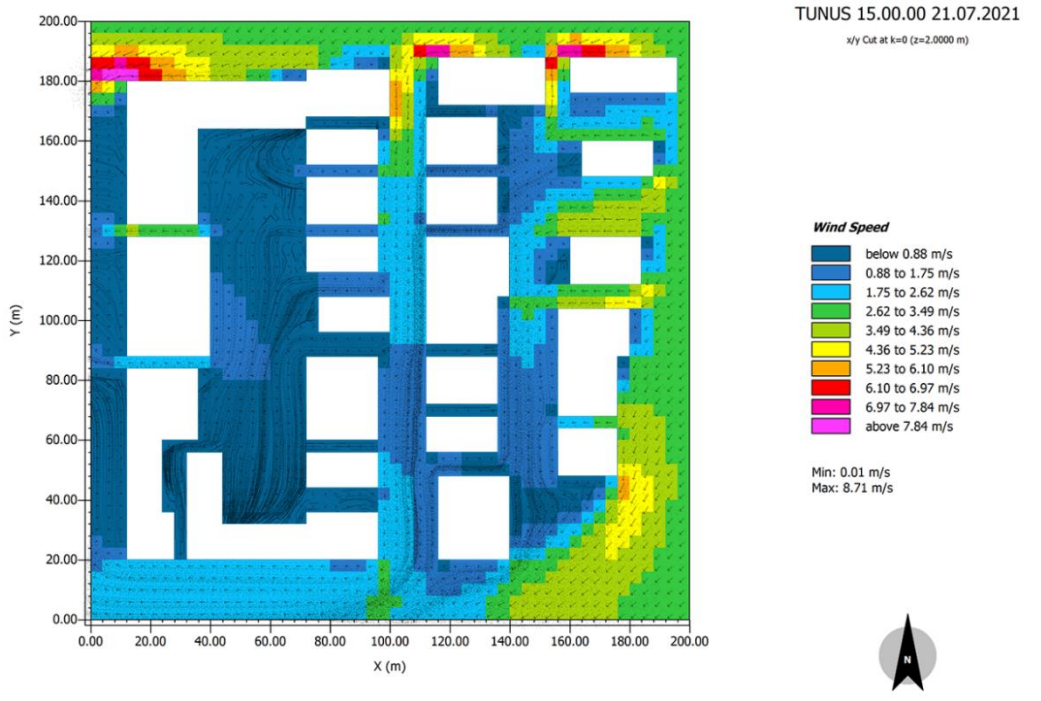

Figure D.48. Wind Speed (m/s) of Urban Block 16 – Tunus Caddesi

d) Reflected Shortwave Radiation

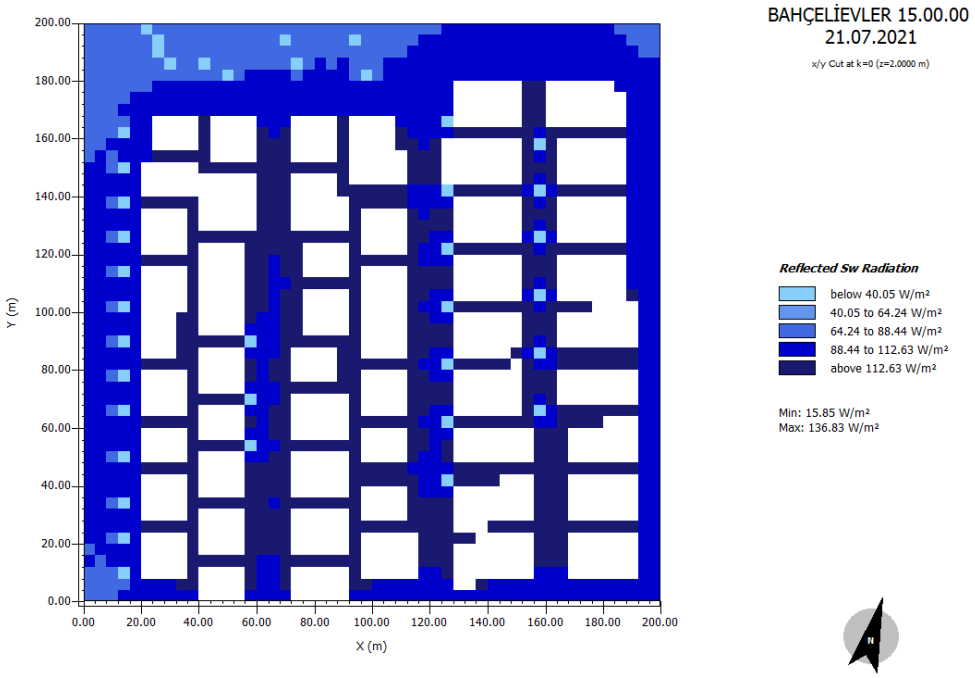

Figure D.49. Reflected Shortwave Radiation (W/m²) of Urban Block 1 –Bahçelievler

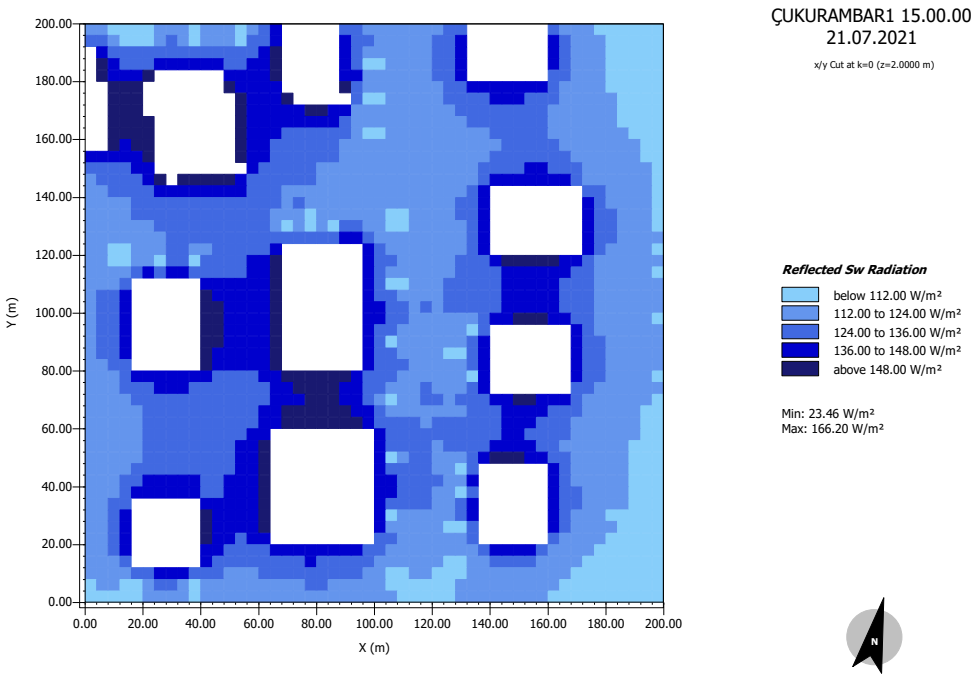

Figure D.50. Reflected Shortwave Radiation (W/m²) of Urban Block 2 - Çukurambar 1

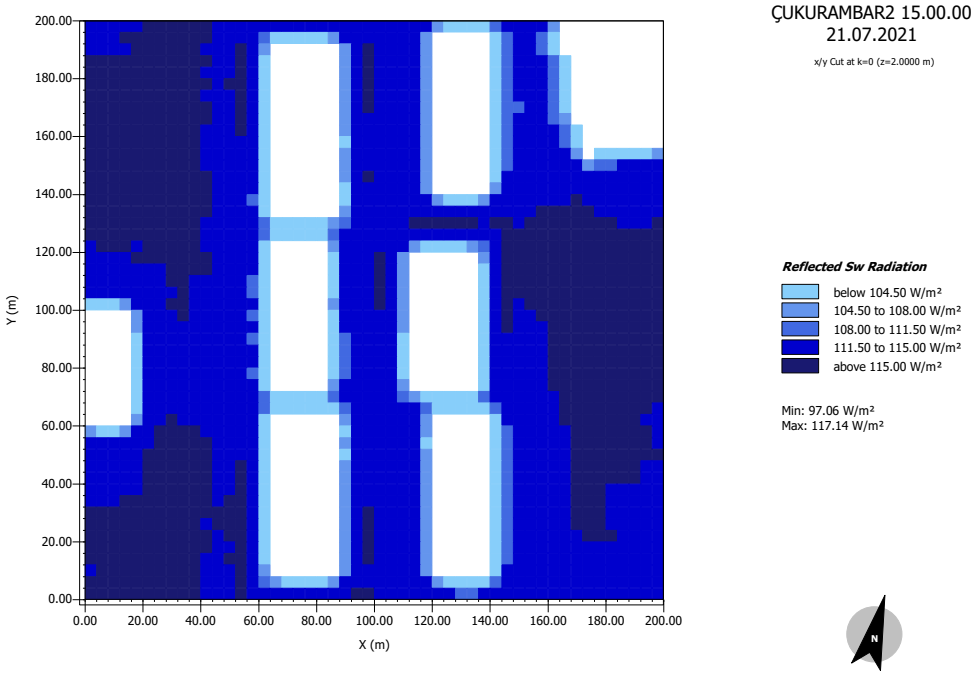

Figure D.51. Reflected Shortwave Radiation (W/m²) of Urban Block 3 – Çukurambar 2

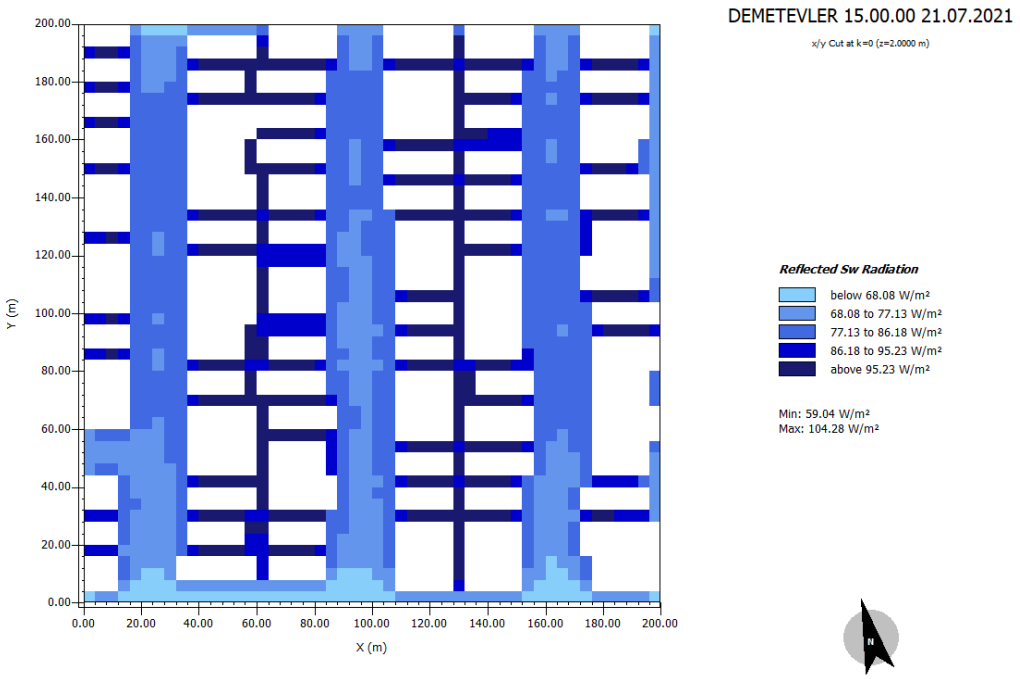

Figure D.52. Reflected Shortwave Radiation (W/m²) of Urban Block 4 – Demetevler

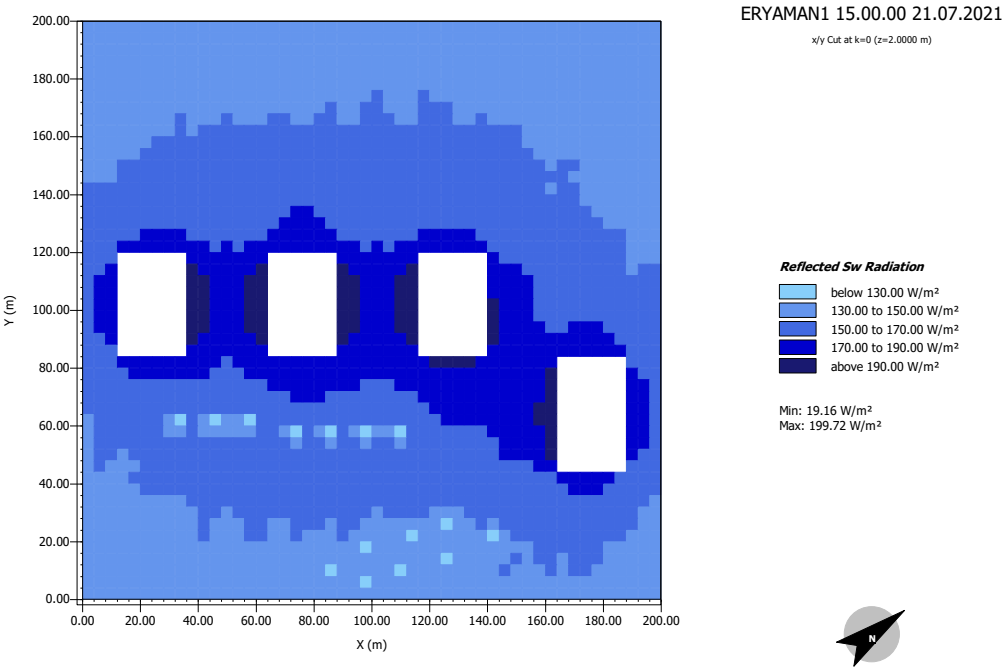

Figure D.53. Reflected Shortwave Radiation (W/m²) of Urban Block 5 - Eryaman 1

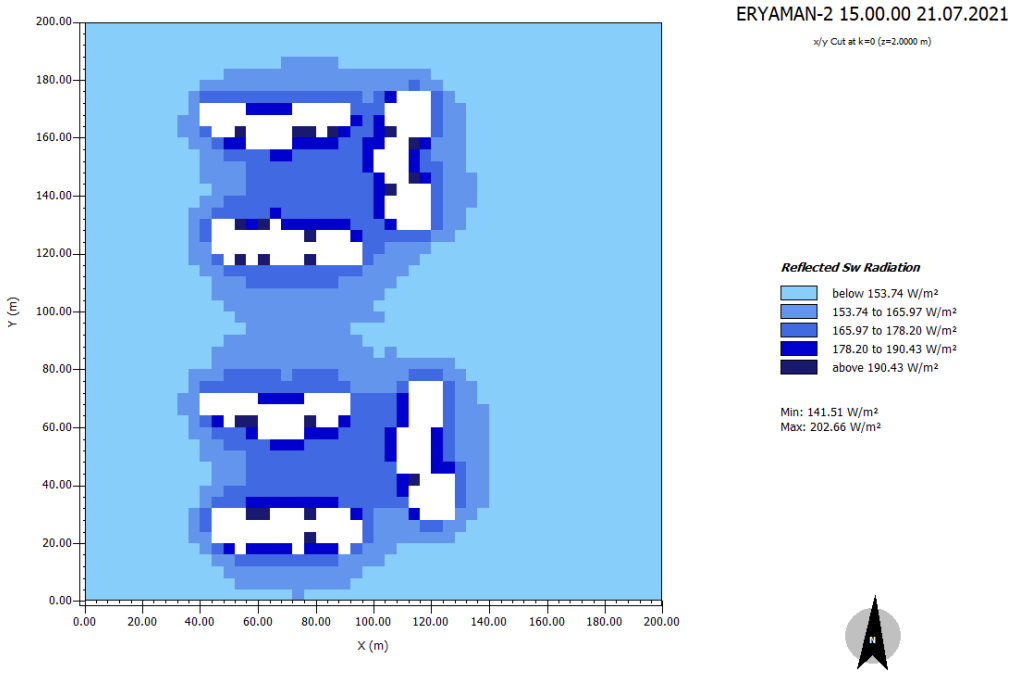

Figure D.54. Reflected Shortwave Radiation (W/m²) of Urban Block 6 - Eryaman 2

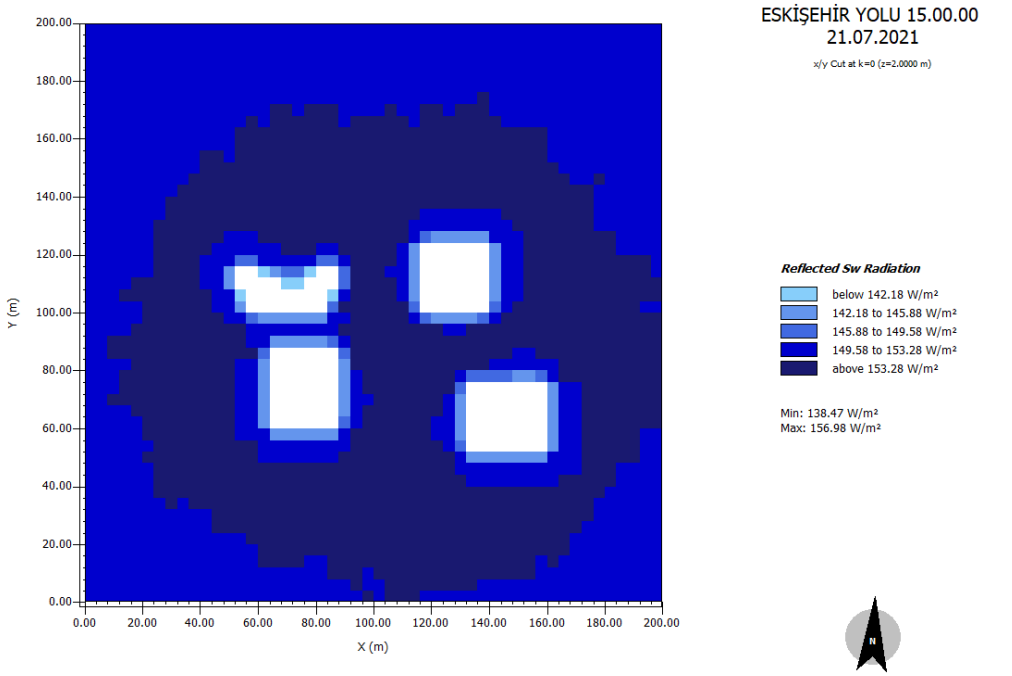

Figure D.55. Reflected Shortwave Radiation (W/m²) of Urban Block 7 - Eskişehir Yolu

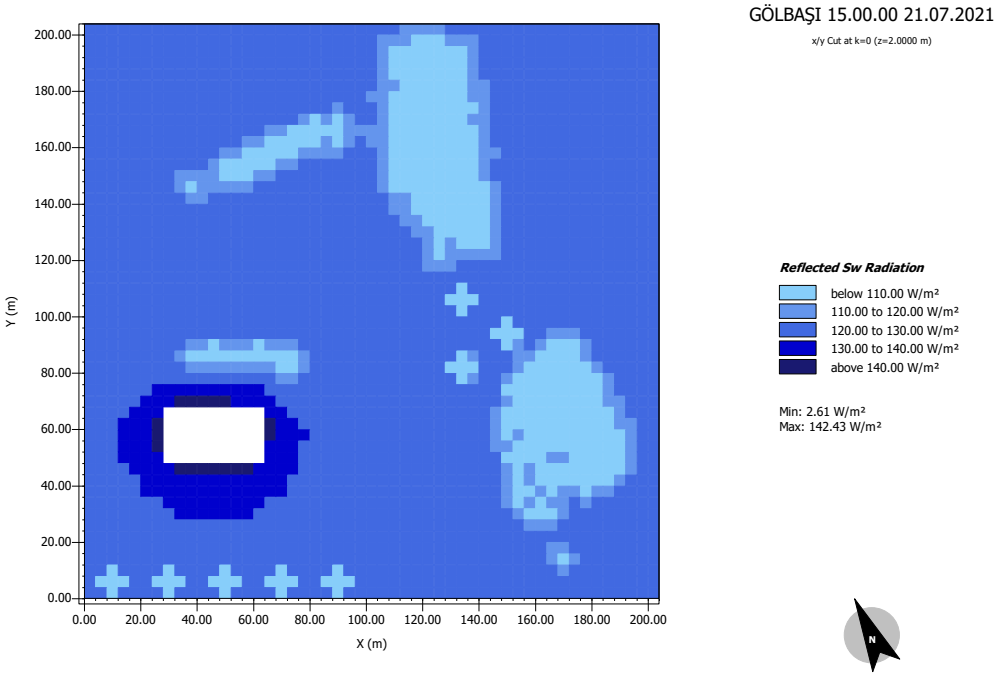

Figure D.56. Reflected Shortwave Radiation (W/m²) of Urban Block 8 - Gölbaşı

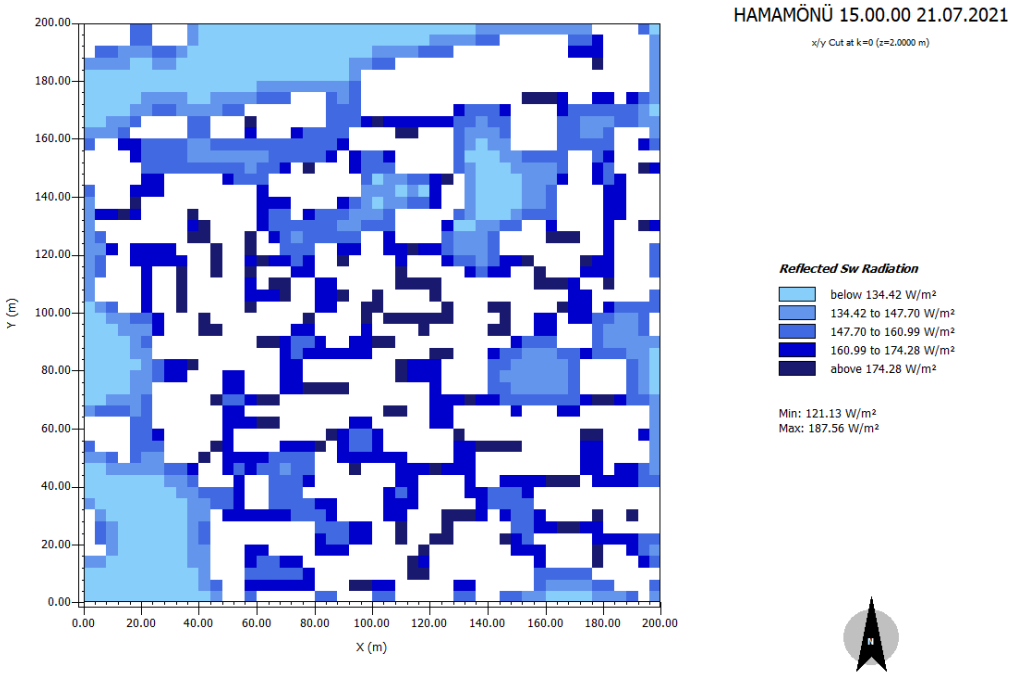

Figure D.57. Reflected Shortwave Radiation (W/m²) of Urban Block 9 - Hamamönü

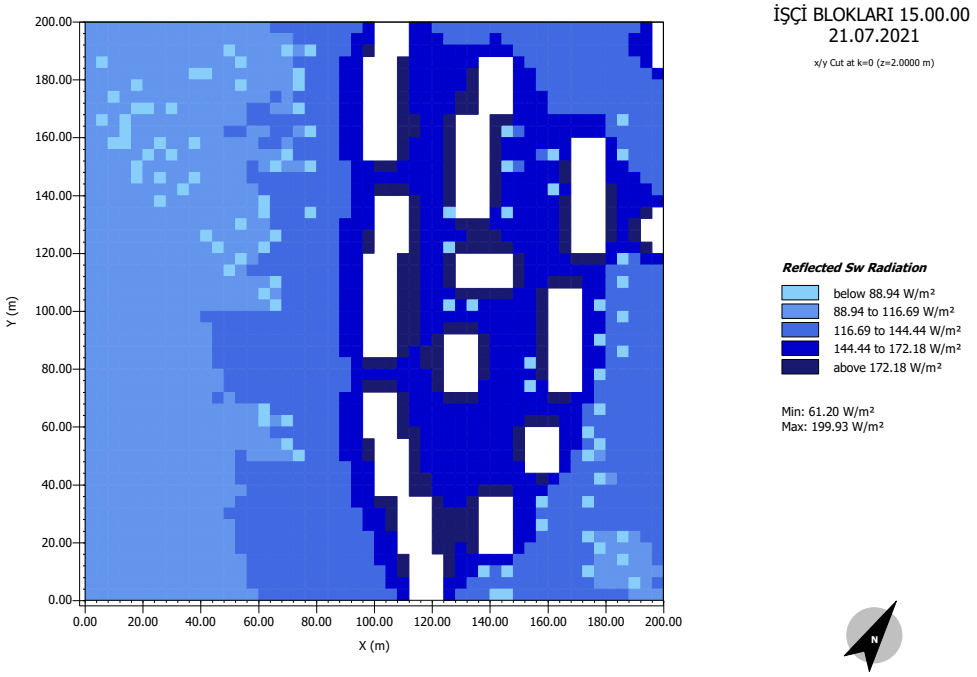

Figure D.58. Reflected Shortwave Radiation (W/m²) of Urban Block 10 - İşçi Blokları

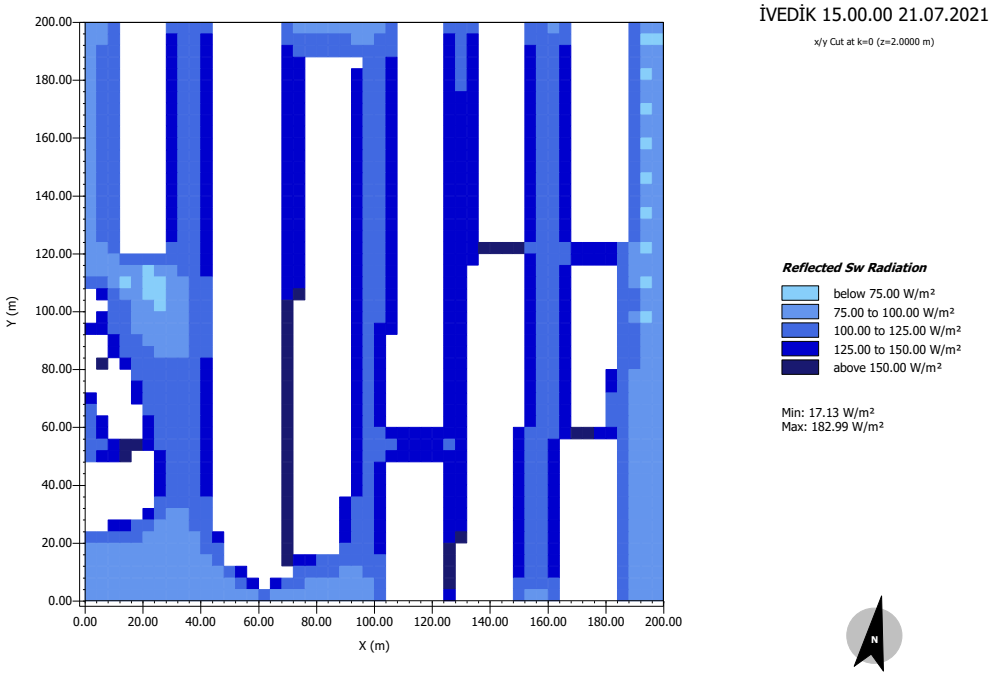

Figure D.59. Reflected Shortwave Radiation (W/m²) of Urban Block 11 - İvedik

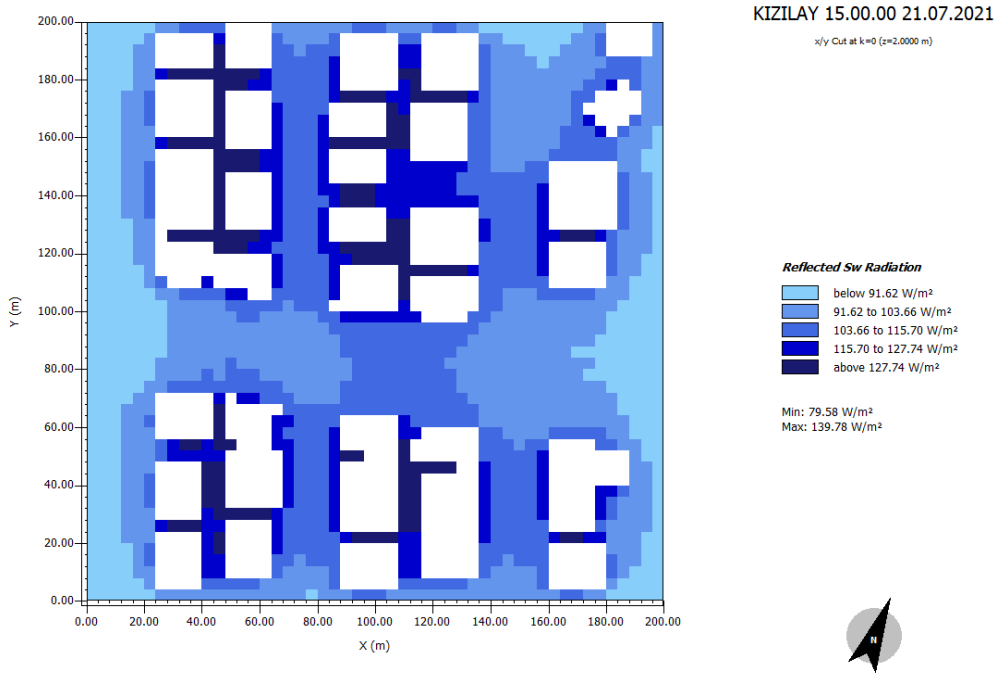

Figure D.60. Reflected Shortwave Radiation (W/m²) of Urban Block 12 - Kızılay

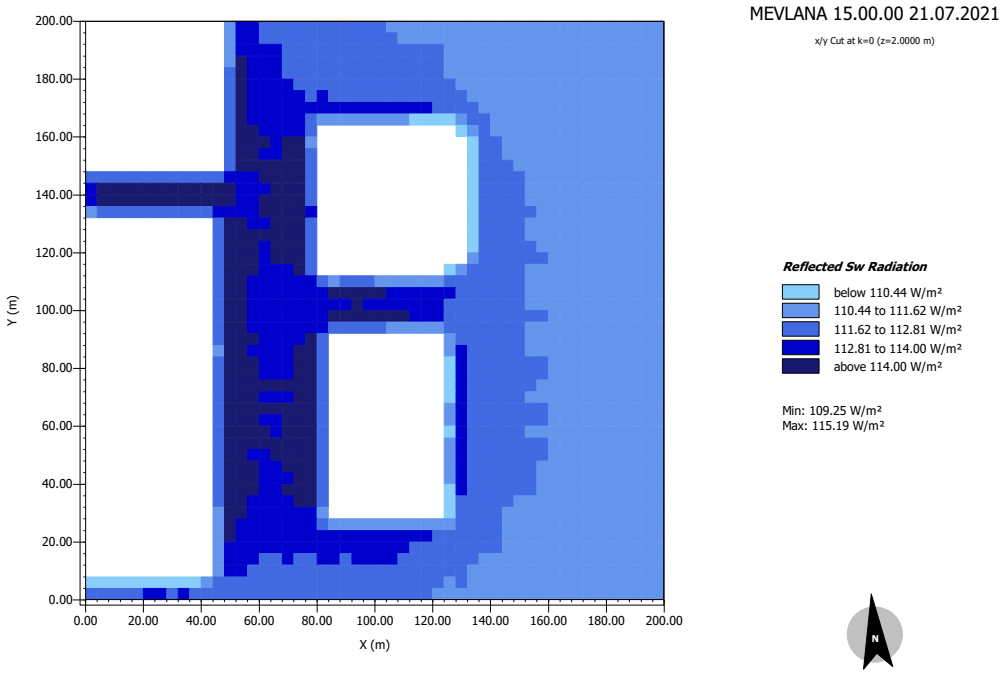

Figure D.61. Reflected Shortwave Radiation (W/m²) of Urban Block 13 – Mevlana Bulvarı

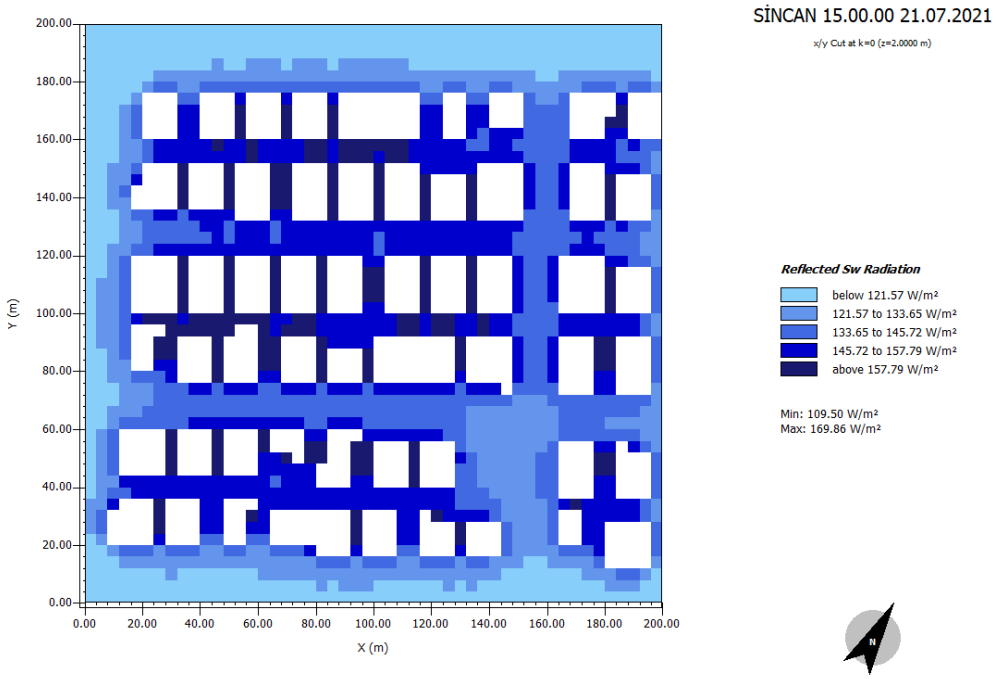

Figure D.62. Reflected Shortwave Radiation (W/m²) of Urban Block 14 - Sincan

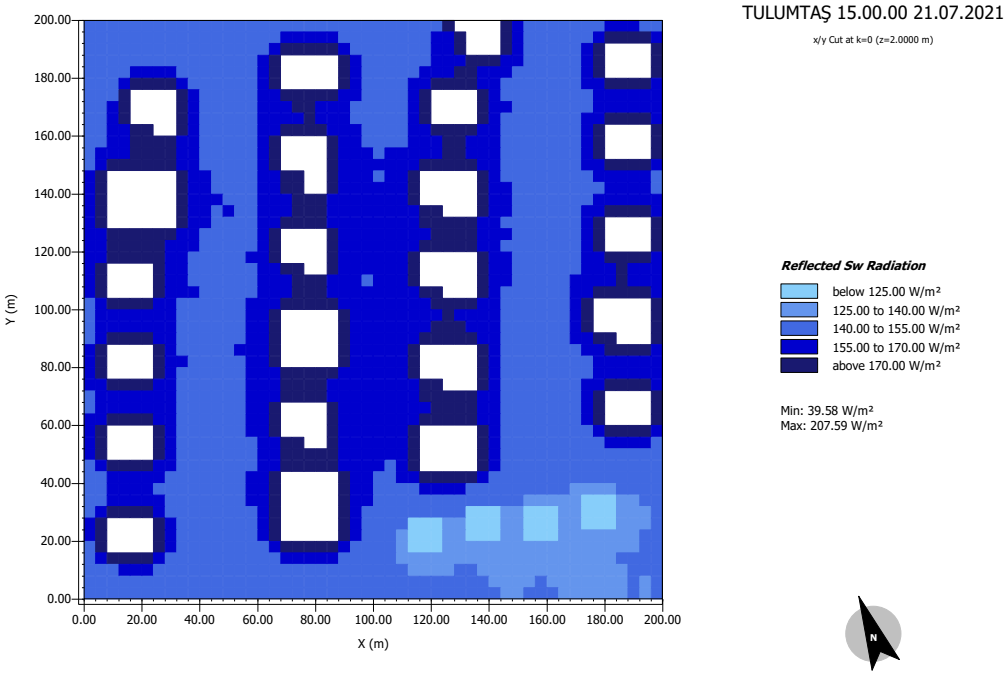

Figure D.63. Reflected Shortwave Radiation (W/m²) of Urban Block 15 - Tulumtaş

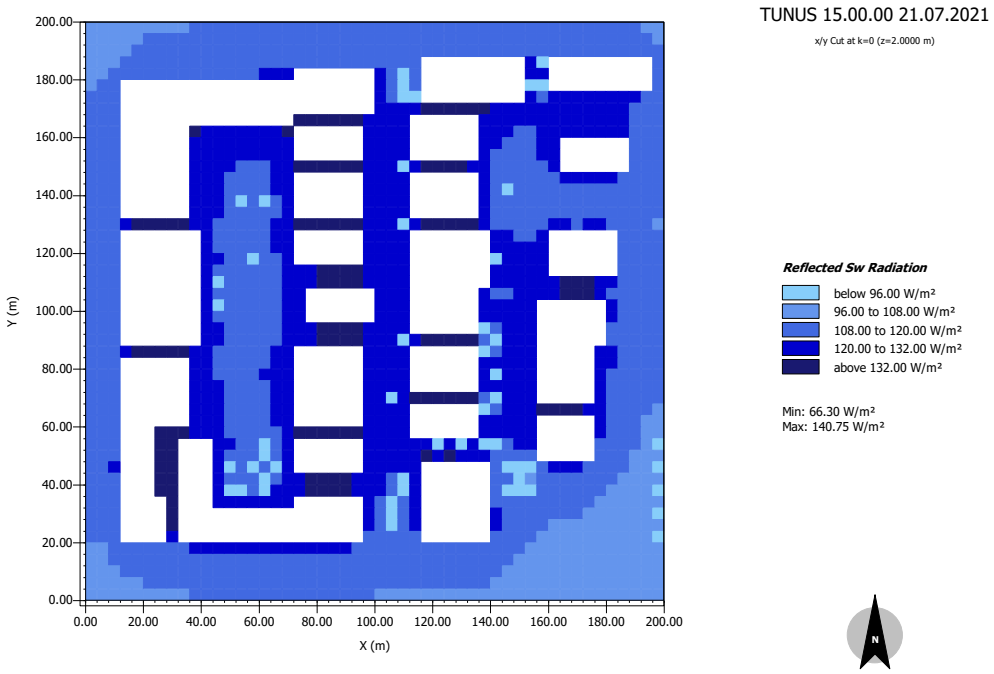

Figure D.64. Reflected Shortwave Radiation (W/m²) of Urban Block 16 - Tunus Caddesi